THE ROLE OF HYPOXIA IN IDIOPATHIC PULMONARY FIBROSIS

by

LAUREN CATHERINE DAVIS

A thesis submitted to the University of Birmingham for the degree of

DOCTOR OF PHILOSOPHY

Supervisors:

Dr Aaron Scott, Professor Elizabeth Sapey & Professor David Thickett.

Institute of Inflammation and Ageing
Collage of Medical and Dental Sciences
University of Birmingham
May 2023

Dedicated to Grandad and Grandad Rob

ACKNOWLEDGEMENTS

Thank you to David and Liz for supervising my project, and for your oversight and leadership. Aaron, thank you for supporting me in pursuing a project of my own design and allowing me the independence to grow as a scientist along the way. I'm very grateful for the opportunity to work with the group. Also, thank you to the Wellcome Trust for funding this project and to the organisers of the MIDAS program, especially Vikki Harrison, for your support throughout.

I would like to acknowledge all the patients who donated tissue for my research. This work would be impossible without the support of patients in a time of personal stress. Additionally, I'm hugely grateful to the team of people who have supported the complex task of patient recruitment. Special thanks to Emma and Di for being our first port of call for recruitment. Thank you to all the clinicians who spent their valuable time consenting patients for our study and thank you to Celine for valiantly taking on the task of screening and consenting in recent months. I am so, so grateful for all your help.

There are so many people to thank in Team Respiratory. I could never have anticipated the bonds I would build when I first joined the group. I feel so lucky to have such a supportive network at work.

Michael and Helena, you made me feel so welcome as a baby PhD student. Thank you for making the time for so many Costa trips and for passing down all your wisdom. Seb and Rahul, thank you for blazing a path for the macrophage massiv. Thank you for driving to Heartlands so many times, I will never stop being grateful that theatres are now just downstairs!

Louise, I could not have made the rapid transition to into the fibrosis family without you. Thank you for encouraging me to pursue my dream project and staying invested as my

significance stars came and went! You have been there for all the ups (Sky Lagoon!) and downs and I'm so, so glad you were. Alice, thank you for promoting me from colleague to housemate and friend. Our DMCs have kept me sane and reminded me of the value of life outside of work. I'm so lucky to have had you to look up throughout my PhD.

Dani, thank you for being my rock in the last few months. Thanks for eating vegetarian paella with me and making me walk up so many flights of stairs. Also thank you for stopping talking about sputum as soon as I pull a face.

Alba and Frances, thank you both for being my work big sisters and the ultimate mentors. Your wisdom and support have made the end of my PhD so much easier. Frances, thank you for the rocky roads and cooked dinners. Alba, thank you for the burrrrrrrrritos. Without both of you I might have succumb to scurvy by this point…

Robyn, you have brought a slice of Luton to Birmingham. Thank you for joining me in wrangling the lung tissue supply in the last couple of years. You've been so generous with your time and energy, and you've made the journey much more fun.

Adura and Kylie- thank you for being such supportive post docs. Adura, thanks for keeping it so real-your laugh never fails to make me see the funny side. Kylie, thank you for being the best social sec and for being a fount of macrophage knowledge. Shaun and Andrew, thank you both for your positivity and support. Shaun thank you for setting me up at my first international conference and making it 10x less scary, Andrew thanks for being my loyal mocha buddy through it all.

To the whole of Team Respiratory- THANK YOU. This PhD has been the ultimate escape room I couldn't have picked a better group to get me through it!

To my friends. Thank you to my voice note cheerleader, Becky, for providing the soundtrack to my mornings and empathizing with the PhD rollercoaster. Emily, thanks for keeping me going with holiday dreams and showing me how to cram in preparation for the last few months! Hannah, thank you so much for always being my cheerleader on the other end of the phone and for moving in with me when Saul moved back. My time in Birmingham has been a series of SpareRoom love stories. I couldn't have survived the COVID lockdowns without Fiona, Charlie, Jodie and Anna, or the PhD write up journey without Alice, Izzy and Juliet.

Saul, I'm so glad I had you by my side this year (even if it was mainly on facetime). You've taught me how to dream big and keep chipping away at the rock. Thanks for backing me 100%. Seeing you go through this journey before me set the bar so high and you've helped me reach it. This document would also have about 50 extra unnecessary commas without you. No jerseys but we make quite a team! #whynotus

To my family, thank you, thank you, thank you! Grandma thank you for reminding me to take breaks and have early nights- I will tomorrow I promise! Thank you for believing in me and trying to keep track of what on earth is going on with all my studies. To my sister, Bean, I couldn't have done this without you. Thank you for custom making me figures before I discovered Biorender (yours were better). You're my best friend and the best cheerleader I could possibly ask for. Mum and Dad. Thank goodness you bribed me to take triple science at GCSE! You've been there in every way I could possibly have asked for. Thanks for reading so many essays over the years and learning the names of so many new colleagues. Thanks for asking how my cells are doing and being the only people as invested in them as I am. I am so lucky to have parents like you who believe in me when I don't believe in myself.

COVID-19 IMPACT STATEMENT

The COVID-19 pandemic had a marked impact on my PhD. I was in my first year when the laboratory was shut down on the 20th March 2020, remaining closed until the 22nd June 2020. I was focused on validating techniques using human lung tissue at this point of my studies. During the first lockdown, I produced a literature review which has since been published in European Respiratory Review (ERR) (DOI: 10.1183/16000617.0121-2021) and contributed to a peer-reviewed paper outlining guidelines for safe return to clinical research during the COVID-19 pandemic (DOI:10.2196/22570).

After working from home for 3 months of my first year, the laboratories reopened in June 2020 with strict restrictions. Laboratory time was halved, to allow for bubble-based working. This 50% laboratory time limit continued until June 2021, severely limiting my laboratory time for 12 months at the end of my first year and most of the second year of my PhD.

Compounding limited laboratory time was the limited access to human tissue that my thesis depended on, due to effects of the pandemic. All research studies were closed during the first wave and were only reinstated after considerable interruption. Our first patient to be recruited after the emergence of COVID-19 was consented in October 2020. Due to the early validation stage I was in when the pandemic hit, I was yet to accumulate stored samples to work with during this delay. Therefore, although I pursued every possible opportunity during this time, work towards my thesis was halted for 7 months.

Even after recruitment resumed, pressures on the NHS remained high through the second and third COVID waves. This resulted in the frequent cancellation of thoracic cases, due to a backlog of medical admissions and limited intensive care unit capacity. This severely affected

the reliability and frequency of tissue supply and continued to limit my progress well into my final year.

The Wellcome Trust and the Institute of Inflammation and Ageing recognised the severe impact of the COVID-19 pandemic on my research, and generously funded a 6-month extension, to compensate for some of the time lost to the pandemic. During this time, I worked hard to maximise the limited tissue supply available to me, by working flexibly across evenings and weekends. However, some sections of this work are limited in biological replication, due to the prolonged effects of the pandemic.

Despite these delays, I believe I have presented a convincing and novel body of work, which contributes to the field and advances our understanding of the effects of hypoxia in human lung tissue in the context of idiopathic pulmonary fibrosis.

OUTPUTS ASSOCIATED WITH THIS THESIS

2021 British Association of Lung Research Summer Meeting (Poster Presentation- awarded Best Poster Prize)- Does hypoxia drive alveolar macrophages to potentiate fibrosis in idiopathic pulmonary fibrosis?

2022 International Colloquium on Lung and Airway Fibrosis (Poster Presentation)- Does hypoxia drive alveolar macrophages to potentiate fibrosis in idiopathic pulmonary fibrosis?

2022 European Respiratory Society Summer Meeting (Poster Presentation)- Does hypoxia drive alveolar macrophages to potentiate fibrosis in idiopathic pulmonary fibrosis?

2019 Mechanisms of Inflammation Symposium (Poster Presentation)- Does hypoxia drive alveolar macrophages to potentiate fibrosis in idiopathic pulmonary fibrosis?

MANUSCRIPTS UNDER PREPARATION

Literature review:

An overview of the role of hypoxia in lung fibrosis

Primary data:

Hypoxia selectively impairs alveolar macrophage efferocytosis by reducing PPARγ expression

Hypoxia increases collagen deposition in a human precision cut lung slice model

ABSTRACT

Idiopathic pulmonary fibrosis (IPF) is a devastating condition of unknown cause that results in progressive, irreversible scarring of the lung. Resultant lung function decline is currently poorly controlled by antifibrotic therapies. The mechanisms driving pathology remain poorly understood. Current evidence suggests that repetitive epithelial injury, in genetically susceptible individuals, escalates to an aberrant wound healing response. Positive feedback potentiates fibroblast ECM secretion. Lung resident macrophages are implicated as the link between injury and fibroblast activation, as key orchestrators of normal wound healing.

Various genetic and environmental factors likely contribute to disease progression. Evidence indicates that some patients' lung tissue contains areas of hypoxia. Nocturnal hypoxemia correlates with worse outcomes in IPF patients, suggesting a pathological role for hypoxia in IPF. Accordingly, hypoxia drives fibrotic changes in human stromal cells *in vitro*.

This thesis hypothesises that hypoxia can cause and/or potentiate profibrotic effects in the IPF lung, altering alveolar macrophage (AM) phenotype and function and causing multi-cellular effects in precision cut lung slices (PCLS). This hypothesis is assessed in using cells and PCLS derived from human lung tissue.

A 48-hour 1% oxygen hypoxic exposure was validated in AMs, to assess phenotypic and functional effects. After demonstrating HIF1α induced transcriptional responses, key mediators implicated in AM contribution to fibrosis were assessed, detecting increased matrix metalloproteinase (MMP)-7 secretion and a trend towards increased MMP-1 secretion. Additionally, hypoxia impaired AM efferocytosis of apoptotic neutrophils, but not phagocytosis of heat-killed *Streptococcus pneumoniae*. No changes in pro-efferocytic (CD163 and CD260) or anti-efferocytic (SIRPα) receptor levels corresponded to this difference.

As efferocytosis introduces more complex cargo than phagocytosis, differences in metabolic demand were a possible distinguishing factor. The role of HIF1α was assessed, given its role in glycolytic shift in hypoxia. Artificial HIF1α stabilisation did not alter efferocytosis, however trends indicate it increased phagocytosis. This distinction suggests that HIF1α activation has distinct effects on the two processes. Further work is required to delineate this difference.

AMs underutilise glycolysis due to adaptation to the lung environment. Therefore, glycolysis was assessed by measuring lactate release in hypoxia with and without lipopolysaccharide (LPS) stimulation. Lactate secretion was increased in hypoxia, although LPS and hypoxia did not have additive effects. This preliminary data on AM glycolytic capacity in hypoxia provides the rationale for real-time analysis of AM metabolism in hypoxia and during efferocytosis.

A 48-hour 1% oxygen challenge was also validated in PCLS, to assess whether profibrotic effects extended beyond effects on human monocultures. HIF1α signalling was again activated and fibrotic markers collagen I and α smooth muscle actin were assessed. Although no changes could be detected at the RNA level, collagen I protein was increased by hypoxia after 48 hours. There was no additive effect of a previously published profibrotic cocktail on changes induced by hypoxia. Future work should explore these findings using spatial techniques to discern cellular contributions.

Overall, this data shows that AMs may contribute to the profibrotic effects of hypoxia, as hypoxia causes increased release of damaging MMP enzymes and reduces efferocytic capacity. Additionally, a human PCLS model supports previous literature describing increased collagen secretion in hypoxia.

CONTENTS

LIST OF FIGURES

LIST OF TABLES

TABLE OF ABBREVIATIONS

AECI	Type I Alveolar Epithelial Cell
AECII	Type I Alveolar Epithelial Cell
AM	Alveolar Macrophage
ARDS	Acute Respiratory Distress Syndrome
BAL,	Bronchoalveolar Lavage
BLM	Bleomycin
CCL	CC-Chemokine Ligand
CCR	CC-Chemokine Receptor
CD	Cytochalasin D
CFTR	Cystic Fibrosis Transmembrane Receptor
CHI3L1	Chitinase 3 Like 1
CT	Computed Tomography
CTGF	Connective Tissue Growth Factor
DAMP	Damage Associated Molecular Pattern
DC	Dendritic Cell
ECM	Extracellular Matrix
EGF	Epithelial Growth Factor
EMT	Epithelial Mesenchymal Transition
ER	Endoplasmic Reticulum
FGFR	Fibroblast Growth Factor
FVC	Forced Vital Capacity
GMCSF	Granulocyte Macrophage Colony Stimulating Factor
GWAS	Genome Wide Association Study
HDAC3	Histone Deacetylase 3
HIF	Hypoxia Inducible Factor
HLA	Human Leukocyte Antigen
HP	Hypersensitivity Pneumonitis
HRE	HIF Response Element
ICAM	Intercellular Adhesion Molecule
IFN	Interferon
IGF	Insulin Like Growth Factor
IH	Intermittent Hypoxia
IIP	Idiopathic Interstitial Pneumonia
IL	Interleukin
ILD	Interstitial Lung Disease
IM	Interstitial Macrophage
IPF	Idiopathic Pulmonary Fibrosis
ITAM	Immunoreceptor Tyrosine-Based Activation Motif
KDM	Lysine Demethylase
LAP	Latency Associated Protein

LLC	Large Latent Complex
LOXL2	Lysyl Oxidase Like 2
LPS	Lipopolysaccharide
LTBP	Latency Binding Protein
LXR	Liver X Receptor
MAPK	Mitogen-Activated Protein Kinase
MARCO	Macrophage Receptor with Collagenous Structure
MCP	Monocyte Chemoattractant Protein
MCSF	Macrophage Colony Stimulating Factor
MDM	Monocyte Derived Macrophage
MMP	Matrix Metalloproteinase
MTOR	Mammalian Target of Rapamycin
MUC	Mucin
NFAT	Nuclear Factor of Activated T-cells
NICE	National Institute for Health and Care Excellence
NOS	Nitric Oxide Synthase
NSIP	Non-Specific Interstitial Pneumonia
OSA	Obstructive Sleep Apnoea
OXPHOS	Oxidative Phosphorylation
PAMP	Pathogen Associated Molecular Pattern
PCLS	Precision Cut Lung Slice
PDGFA	Platelet Derived Growth Factor
PGE_2	Prostaglandin 2
PHD	Prolylhydroxylase
PI3K	Phosphatidylinositol-3-kinase
PLOD2	Procollagen-Lysine,2-Oxoglutarate 5-Dioxygenase 2
PPAR	Peroxisome Proliferator-Activated Receptor
PRR	Pattern Recognition Receptor
RAGE	Receptor for Advanced Glycation End-Product
RALDH	Retinaldehyde Dehydrogenase
ROCK	Rho Kinase
ROS	Reactive Oxygen Species
RXR	Retinoic X Receptor
SFTP	Surfactant Protein
DC-SIGN	dendritic cell-specific ICAM-3-grabbing nonintegrin
SIRP	Signal Regulatory Protein
αSMA	α Smooth Muscle Actin
SMAD	suppressor of mothers against decapentaplegic Protein
TGF	Transforming Growth Factor
TIM	T-cell immunoglobulin mucin protein
TNF	Tumour Necrosis Factor
TSP	Thrombospondin

TUDCA	Tauroursodexycholic Acid
UIP	Usual Interstitial Pneumonia
VEGFA	Vascular Endothelial Growth Factor
VHL	Von Hipple-Lindau Protein
WASP	Wiskott-Aldrich Syndrome Protein

CHAPTER 1: INTRODUCTION

1.1 OVERVIEW

Idiopathic pulmonary fibrosis is the most common interstitial lung disease, with a prevalence of 50 per 100,000 people in the UK (Snell et al., 2016). Unfortunately, therapeutic options are limited, and patient outcomes remain poor (Raghu et al., 2014). Disease mechanism is understood to involve an aberrant wound healing cascade resulting in excessive extracellular matrix deposition in the lung. Macrophages are implicated in disease progression, linking repetitive epithelial injury to fibroblast activation. Further delineation of the IPF disease mechanism is crucial to identifying novel drug targets for future therapy. Various lines of evidence indicate that hypoxia plays a contributing role in IPF disease initiation and/or potentiation. Investigation of the effects of hypoxia on lung stromal cells and murine models has begun to demonstrate profibrotic effects. However, characterisation has not investigated effects on lung macrophages or complex models of human lung tissue.

1.2 IPF AND ILDS

Interstitial lung diseases (ILDs) are a group of diseases in which the lung parenchyma is the focus of dysregulation and loss of function, secondary to variable degrees of inflammation and /or fibrosis dependent on disease type (Figure 1.1). There are numerous types of ILD, including some with a known aetiology such as autoimmune ILDs, drug induced ILDs, environmental exposure ILDs (including asbestosis and silicosis), and chronic hypersensitivity pneumonitis. Idiopathic interstitial pneumonia (IIP) encompasses ILDs that have no identifiable cause, the most common being idiopathic pulmonary fibrosis (IPF). IPF is characterised by a particularly progressive course, with patients developing self-sustaining lung fibrosis culminating in

worsening shortness of breath, forced vital capacity (FVC), quality of life and early mortality (Raghu et al. 2018). However, this is not limited to IPF. Recent consensus has described progressive pulmonary fibrosis (Raghu et al. 2022), which encompasses non-IPF ILDs that follow a similarly progressive phenotype, supporting the notion that perhaps there are underlying shared pathobiological mechanisms (Cottin et al. 2019). Despite these similarities, this thesis will focus on IPF as the most common ILD with the most well characterised patient samples.

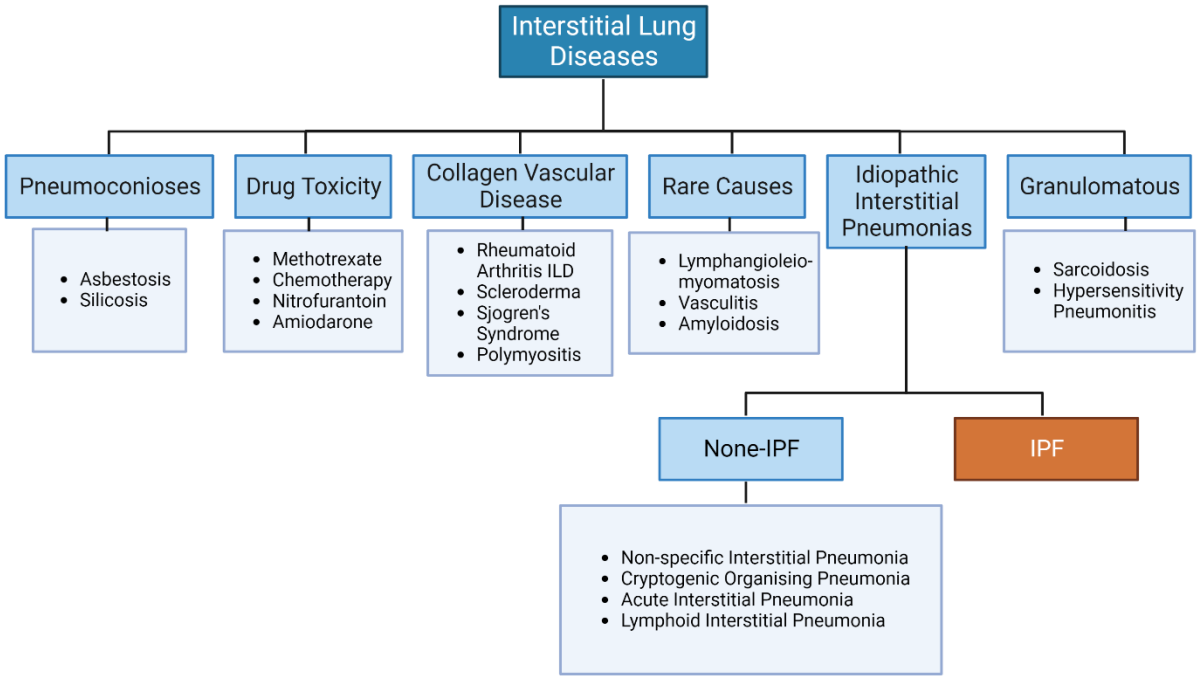

Figure 1.1 Types of ILD. *Interstitial lung diseases are an expansive group of diseases which can be differentiated by radiological and/or histopathological features, exposure history and additional immunological tests* (Travis et al., 2012).

IPF has a very poor median survival rate of 2-5 years (Raghu et al. 2014). The chronic fibrosing nature of the disease results in uncontrolled extracellular matrix deposition, which restricts gas exchange and distends airways, causing honeycombing that eventually results in respiratory failure. IPF appears histologically with a usual interstitial pneumonia (UIP) pattern, with heterogenous fibrotic lesions throughout tissue. Disease course varies between patients, with

some showing steady fibrotic decline, whilst others experience acute exacerbations during which fibrosis worsens rapidly (Figure 1.2)(Raghu et al. 2018).

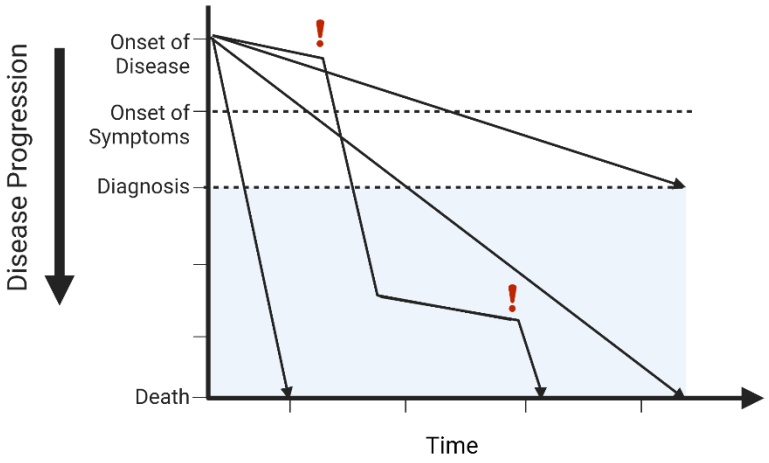

Figure 1.2 IPF Disease Progression. *Schematic adapted from Ley et al.* (2012) *reflecting the varying disease courses IPF progression can follow in different patients. Some patients have constant decline, which can proceed quickly or more slowly. Some patients have periods of relatively stable disease, followed by rapid progression, highlighted by an exclamation mark. These disease courses reflect those seen in patient groups in observational studies* (Veit et al. 2020).

Current treatment strategies combine pharmacological (anti-fibrotic therapies and supplementary oxygen therapy) and non-pharmacological therapies, such as pulmonary rehabilitation. There are only two approved antifibrotic therapies for IPF: Nintedanib and Pirfenidone. Pirfenidone was approved for use by the National Institute for Health and Care Excellence (NICE) in 2013 (NICE 2018), as clinical trials demonstrated the drug reduced FVC decline and improved mortality in patients (T. E. King et al. 2014). The exact mechanism of Pirfenidone is unknown, although it is demonstrated to be anti-inflammatory and antifibrotic (Hughes et al. 2016). NICE subsequently approved Nintedanib for use in IPF in 2016 (Hayton and Chaudhuri 2016). This specific tyrosine kinase inhibitor inhibits vascular endothelial growth factor receptor (VEGFR), platelet derived growth factor receptor (PDGFR) and fibroblast derived

growth factor receptor (FGFR). Clinical trials showed reduced FVC decline and reduced acute exacerbations (Hughes et al. 2016).

No trials have directly compared Nintedanib and Pirfenidone, however a recent retrospective study found no difference in outcomes such as progression and mortality between the patients treated with the two different drugs (Marijic et al. 2021). Although Nintedanib and Pirfenidone slow disease progression in IPF patients, no interventions thus far can stop or reverse fibrosis with lung transplantation remaining the only cure. There is a clear unmet need for more treatment options for IPF patients. In order to identify novel drug targets in the disease, an improved understanding of the disease mechanism and contributing risk factors is required.

1.3 Pathology of IPF

During homeostasis, alveoli make up most of the lung surface. Lined by thin type 1 alveolar epithelial cells (AECI), with occasional cuboidal type 2 alveolar epithelial cells (AECII), these cells sit on a flexible basement membrane, closely interfaced with capillaries for efficient gas exchange. The minimal interstitium between alveolar sacs is comprised of fibroblasts and stromal cells (Travaglini et al. 2020). The gas exchange surface is lined with a hydrophobic mixture of lipids and proteins known as surfactant, produced by AECII cells. Surfactant hydrophobicity prevents alveolar collapse and serves homeostatic immune functions (discussed in section 1.7.2.5) (A. Nayak et al. 2012).

In the lung parenchyma, innate immunity quickly and non-specifically responds to potentially damaging stimuli. Given the constant exposure of the lung to foreign inhaled particles, it is particularly important that innate immunity neutralises and removes stimuli quickly, preventing prolonged damage and inflammation where possible and thereby protecting the delicate

structure of the alveolar sacs (Puttur et al. 2019). Alveolar macrophages (AMs) patrol the alveolar spaces, whilst interstitial macrophages (IMs) patrol the interstitial lung tissue. AMs are responsible for immunosuppression in the alveoli, by phagocytosing foreign bodies, releasing reactive oxygen species to quickly remove pathogens and processing surfactant (Gu et al. 2022). Meanwhile IMs are activated when the epithelium is breached and are more capable of co-ordinating an immune response, whilst maintaining a tolerogenic cytokine environment in the tissue (Hoppstädter et al., 2010).

There is a consensus that IPF is triggered by epithelial damage and apoptosis or necrosis in the alveoli (Kuhn et al., 1989; Kuhn and McDonald, 1991). In genetically susceptible, aged individuals, this escalates to an aberrant wound healing response, where epithelial injury is repetitive and unresolved, resulting in fibrotic escalation (Figure 1.3) (Phan et al., 2020; Betensley et al., 2016; Hewitt and Maher, 2019; Maher et al., 2007; Chambers and Mercer, 2015).

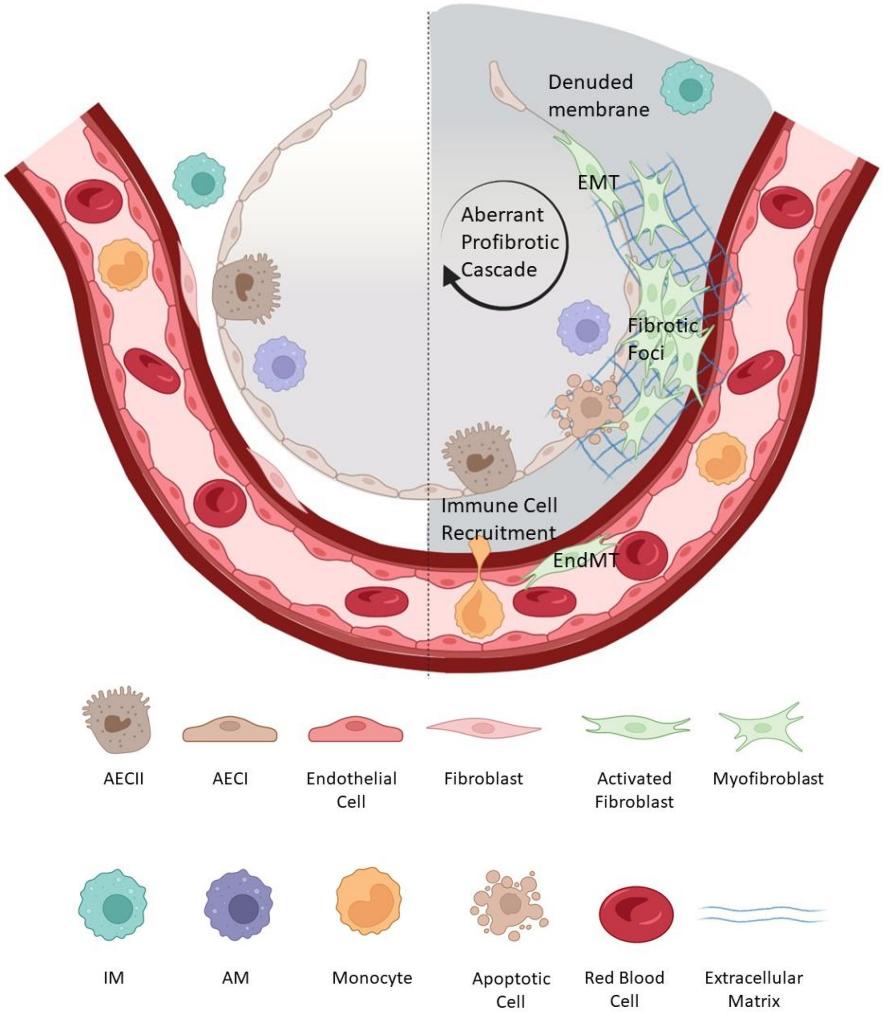

Figure 1.3 Proposed model of aberrant wound healing response in IPF. *A cross sectional diagram of an alveoli, with adjacent capillary. LEFT side shows the alveoli during homeostasis. AECIs line the alveoli, with occasional AECIIs for surfactant secretion. Alveolar macrophages patrol the airspaces, while interstitial macrophages are resident in the parenchyma beneath the epithelial barrier. The parenchyma is made up of stromal cells, including fibroblasts. RIGHT side shows the proposed mechanism by which IPF escalates. Epithelial cells undergo frequent apoptosis, due to repeated microinjuries. Inefficient reepithelialisation, insufficient apoptotic cell clearance and inappropriate cellular signalling causes continued tissue damage and membrane denudation. Fibroblasts become activated and some differentiate into contractile myofibroblasts. Epithelial cells and endothelial cells undergo transdifferentiation into fibroblasts. This response generates excessive extracellular matrix, particularly at fibrotic foci, resulting in impaired gas exchange and loss of lung function. EMT: epithelial mesenchymal transition. EndMT: endothelial mesenchymal transition. AEC: alveolar epithelial cell. IM: interstitial macrophage. AM: alveolar macrophage.*

1.3.1 Normal Wound Healing

In a normal wound healing response, where epithelial cells take the brunt of the injury, wound repair and immune response happen alongside each other. Resident AMs, activated when

damage-associated molecular patterns (DAMPs) or pathogen associated molecular patterns (PAMPs) bind pattern recognition receptors (PRRs), attempt to 'silently' phagocytose or efferocytose pathogens or apoptotic cells respectively (Dahl et al. 2007). If overwhelmed, they escalate the immune response by releasing inflammatory mediators (Cheng, Li and Chen, 2021). This signal is mirrored by epithelial cells, which respond to similar DAMPs and PAMPs by shifting from releasing anti-inflammatory mediators, to pro-inflammatory cytokines and DAMPs (Lucchini et al. 2021). The resultant environment is high in tumour necrosis factor α (TNFα), interleukin (IL)-6, IL-8 and prostaglandins, which activates the endothelium to maximise recruitment of circulating innate immune cells neutrophils and monocytes, as well as adaptive immune cells if required.

The initial positive feedback loop drives a rapid response to the injury. Debris is cleared by phagocytosis and efferocytosis, resulting in removal of inflammatory molecular patterns. Apoptotic immune cells are also subsequently cleared by efferocytosis. Efferocytosis drives a pro-resolution, anti-inflammatory phenotype, with secretion of IL-10 and transforming growth factor β (TGF-β). This signal halts the recruitment of neutrophils and monocytes and contributes to the shift of the whole environment to a pro-resolution one, when no further DAMPs or PAMPs are present (Bosurgi et al. 2017). This switch must be especially efficient in the lung, which is constantly exposed to potentially immunogenic material, as continuous inflammation risks switching from resolution to scar based repair, or loss of tolerance to self-antigens. The tolerogenic properties of AMs must return in this case to neutralise immune responses (Puttur et al. 2019).

Whether or not AMs have the capacity to clear debris, or escalate an immune response to clear it, a wound healing cascade is also activated to repair epithelial damage. Growth factors drive the dedifferentiation of epithelial cells, allowing them to spread, migrate and proliferate to cover the denuded area of basement membrane (Crosby and Waters 2010). These growth factors, including epithelial growth factor (EGF), vascular endothelial growth factor A (VEGFA), insulin like growth factor (IGF) and TGF-β are released by epithelial cells, macrophages, and exposed basement membrane (Crosby and Waters, 2010; Lloyd and Snelgrove, 2018). Cytokines and chemical mediators stemming from the immune response, including CC chemokine ligand (CCL)11, IL-4, IL-13 and reactive oxygen species (ROS), also drive epithelial cell proliferation and migration (Lucchini et al. 2021). The progenitor cells during this re-epithelialisation are surfactant producing, cuboid AECIIs, which subsequently differentiate into AECIs (Lucchini et al. 2021).

Where needed, activated fibroblasts and macrophages deposit extracellular matrix, such as collagen and fibrinogen, to provide support to the migrating epithelium. When necessary, epithelial cells can also undergo epithelial mesenchymal transition (EMT) to become mesenchymal cells with increased contractile and migratory properties. Further, fibroblasts can be activated to become myofibroblasts, that deposit larger amounts of extracellular matrix (ECM) and have highly contractile capacity, facilitated by α smooth muscle actin (αSMA) expression, which enables wound closure. This process is largely driven by TGF-β, as well as other growth factors like connective tissue growth factor (CTGF). Expansion is held under control by macrophage derived matrix metalloproteinases (MMPs), which digest excess ECM, and by timely apoptosis of wound healing cells after resolution for clearance by efferocytosis (Lucchini et al. 2021).

1.3.2 Aberrant Wound Healing

Evidence from human IPF tissue and animal models provides some understanding into how the aberrant fibrotic response escalates. Repetitive damage causes epithelial cell apoptosis and necrosis; in IPF patient samples, necrotic epithelial cells surround areas of denuded membrane (Kuhn et al., 1989; Fukuda et al., 1995; Visscher and Myers, 2006). This results in continuous release of DAMPs, which potentiate the inflammatory response. MMPs and other immune mediators therefore cause more extensive tissue damage. This may be exacerbated by ineffective or overwhelmed efferocytosis of apoptotic cells. Continuous tissue damage is poorly compensated for by AECI hyperplasia. The loss of functional progenitor cells and basement membranes required for successful regeneration of tissue increase the likelihood of a profibrotic response to fill the gaps. Indeed, in the IPF lung, denuded basement membranes (Kuhn and McDonald 1991) and apoptotic epithelial cells (Lappi-Blanco, Soini and Pääkkö, 1999; Maher et al., 2012) overlie fibrotic foci, where highly synthetic myofibroblasts increase proliferation and ECM deposition, indicating this is a consequence of insufficient epithelial repair.

Myofibroblasts are traditionally thought to be derived from lung resident fibroblasts, however bone marrow derived circulating fibrocytes have recently been implicated for recruitment into the tissue during this process (Strieter et al. 2009; Heukels et al. 2018). Furthermore, uncontrolled EMT and endothelial mesenchymal transition (EndMT) is implicated in pulmonary fibrosis. Studies have previously indicated that EMT contributes to the highly synthetic myofibroblast pool, however recent consensus suggests that the fibrogenic properties of EMT stem from its role in dysregulated cross talk and cytokine release (Kage and Borok 2012).

Increased expression of growth factors, TGF-β, IGF, PDGF and CTGF drive these excessive responses in fibroblasts and epithelial cells (Phan et al. 2020).

Intense paracrine interactions in fibroblastic foci result in excessive ECM deposition, laden with highly cross-linked collagen, which stimulates positive feedback in myofibroblasts, and resists digestion by MMPs. In this situation, IPF fibroblasts have been compared to a cancer, as whilst fibrotic foci are not driven by malignancy, their reactive phenotype is highly synthetic and invasive (Chambers and Mercer 2015). With fibrotic foci at the leading edge, fibrosis spreads and destroys lung tissue, leaving it unable to regenerate due to lost alveolar structures, basement membranes and progenitor cells (Ahluwalia, Shea and Tager, 2014).

1.3.3 TGF-β Signalling Pathways

Many signals that have purposes in normal homeostasis can also potentiate fibrosis when uncontrolled. A prolific example is TGF-β. In homeostasis, TGF-β is produced by AMs with IL-10 to maintain epithelial homeostasis and tolerance. However, if continuous, it also establishes a cascade of fibrotic differentiation.

TGF-β is released non-covalently bound to latency associated protein (LAP), which holds it inactive. Once secreted, TGF-β and LAP form a complex with latency binding protein (LTBP) to form a complex named the large latent complex (LLC) (Figure 1.4). LTBP is largely found in the extracellular matrix, resulting in storage of TGF-β extracellularly (Kanzaki et al. 1990).

Latent TGF-β can be released and activated rapidly in response to a range of stimuli, including ROS, proteolysis, and acidification (Miyazono and Heldin 1989; Daniel et al. 2004). Integrins, namely αVβ6 expressed by AECs, can also release TGF-β by binding an integrin recognition

sequence within LAP, which releases TGF-β in a mechanosensitive way, responding to contractile forces within the ECM (M. Shi et al. 2011).

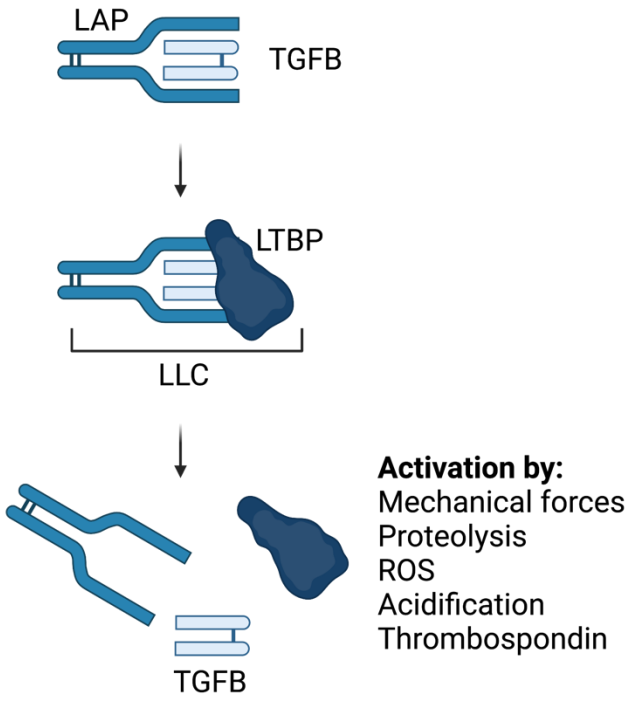

Figure 1.4 TGF-β activation. *Transforming growth factor (TGF-β) is released associated with latency associated peptide (LAP), this holds TGF-β in its latent form. Extracellularly, the TGF-β/LAP complex binds to latency binding protein (LTBP) in the extracellular to form the large latency complex (LLC). TGF-β can be released by a variety of stimuli. Mechanical forces can release TGF-β, due to an integrin binding site of LAP. Additionally, proteolysis, reactive oxygen species (ROS), acidification and thrombospondin can trigger the disassembly of the LLC and TGF-β release.*

When activated, downstream signalling occurs via the heterodimeric TGF-βR1 and TGF-βR2 receptors (Figure 1.5). Upon dimerization initiated by a ligand, TGF-βR2 phosphorylates TGF-βR1. TGF-βR1 subsequently phosphorylates suppressor of mothers against decapentaplegic (SMAD)2 and SMAD3, which form a complex with SMAD4 and translocates to the nucleus. In the nucleus, transcriptional regulators interact with SMAD complexes to regulate gene expression. SMAD driven effects of TGF-β are known as canonical signalling (Frangogiannis

2020). TGF-β also triggers non-canonical signalling, including mitogen-activated protein kinase (MAPK) and mammalian target of rapamycin (MTOR) signalling (Y. E. Zhang 2008).

Cell and environment specific responses to TGF-β are regulated in a variety of ways. The three TGF-β isoforms are differentially expressed and have different effects. Downstream signalling molecules, such as SMAD proteins, are differentially expressed, degraded and post-transcriptionally modified. Beyond this, transcription factors that direct SMAD proteins to the relevant binding sites are differentially expressed across varying cell types and environments, resulting in differential cell responses to TGF-β stimulation (Saito, Horie and Nagase, 2018).

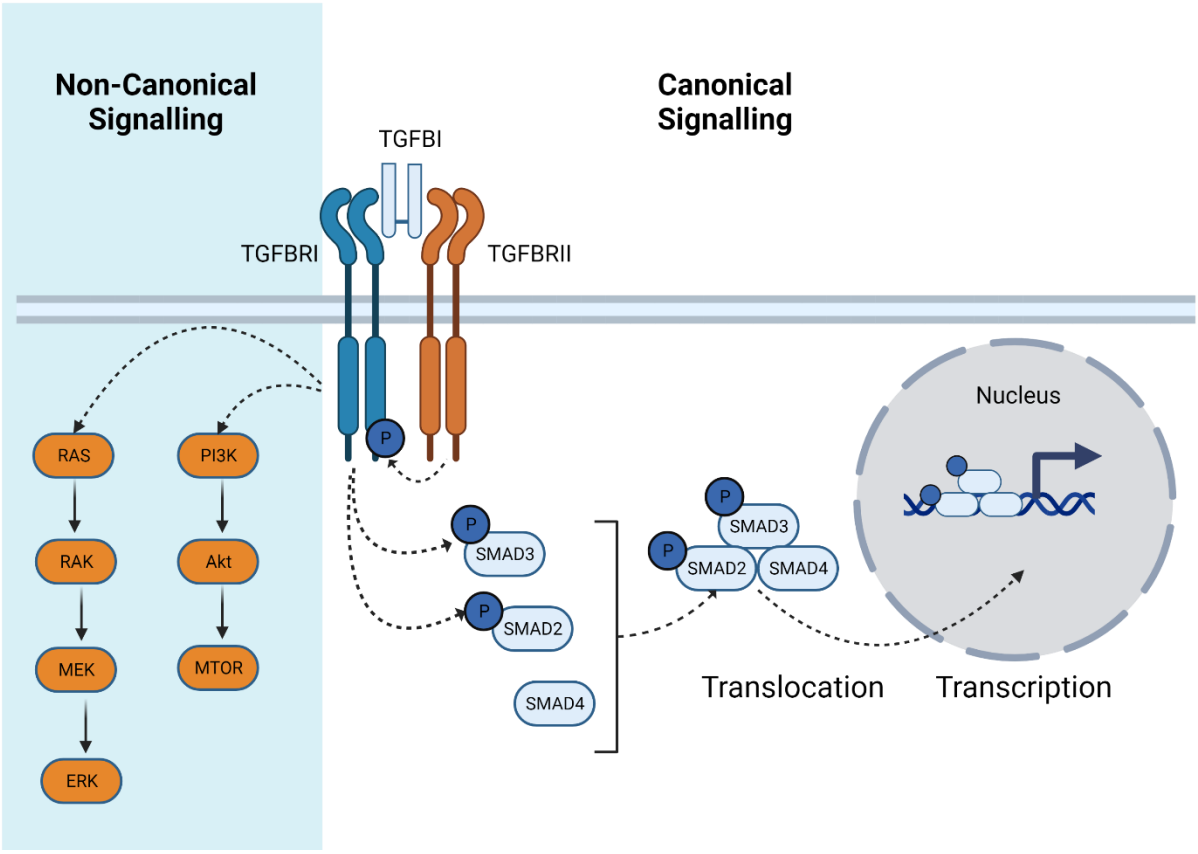

Figure 1.5 TGF-β signalling pathways. *During canonical signalling, when TGFβ binds its heterodimeric receptors TGF-βRI and TGF-βRII, TGF-βRII transphosphorylates and activates TGF-βRI. TGF-βRI subsequently phosphorylates SMAD3 and SMAD2. These SMAD proteins assemble with SMAD4 and translocate into the nucleus. Here, the SMAD proteins act as transcription factors for TGFβ response genes. Non-canonical signalling from the TGFβRI and TGFβRII receptors can also activate RAS/RAK/MEK/ERK signalling and PI3K/Akt/MTOR signalling.*

1.4 Risk Factors

Given the idiopathic nature of IPF, multiple risk factors with overlapping mechanisms must converge to initiate and potentiate disease. As such, it is proposed that IPF effects genetically susceptible people with relevant environmental exposure and comorbidities. Risk factors described below have been used alongside patient tissue, *in vivo,* and *in vitro* work to derive the aberrant wound healing model described in IPF (Phan, Thị Hằng Giang 2021).

1.4.1 Genetic Risk Factors

Familial history of IPF is one of the strongest risk factors of IPF, indicating a marked genetic component to susceptibility (García-Sancho et al. 2011). As such, large scale genome wide association studies (GWAS) have identified genetic polymorphisms that associate with increased risk, both in sporadic cases of IPF and familial IPF (Noth et al., 2013; Fingerlin et al., 2013). The most well characterised genetic risk factors are associated with the *MUC5B* gene, encoding mucin 5B. Variants associated with IPF cause mucous hypersecretion (Seibold et al. 2011; Peljto et al. 2013). One such variant is the rs35705950 variant in the *MUC5B* promoter. Although the rs35705950 variant in the *MUC5B* gene is enriched in the IPF population (38%), the variant is also present in the healthy population (9%) (Seibold et al., 2011; Peljto et al., 2013; Yang et al., 2015). This confirms that further risk factors come together to cause IPF in at risk individuals.

Other genetic risk variants associated with IPF development, spanning common and rare frequencies, include variants in mucins (*MUC2*), telomere maintenance component genes (*TERT, TERC, OBFC1, RTEL1*), surfactant proteins (*SFTPC, SFTPA1, SFTPA2, ABCA3*), cell-cell adhesion (*DPP9, DSP*), and cell cycle regulation genes (*KIF15, MAD1L, CDKN1A, TP53*) (Fingerlin et al., 2013; Noth et al., 2013; Michalski and Schwartz, 2020).

1.4.2 Physiological Risk Factors

Several conditions are enriched in IPF patient cohorts, indicating potential causal links. These include gastroesophageal reflux (Gribbin, Hubbard and Smith, 2009; García-Sancho et al., 2011) and diabetes (Enomoto et al., 2003; Gribbin, Hubbard and Smith, 2009; García-Sancho Figueroa et al., 2010).

Obstructive sleep apnoea (OSA) is also more prevalent in IPF populations (76% in IPF patients versus 16% in control cohorts according to meta-analysis by Karuga et al (2022)). Emerging evidence indicates a causal contribution of OSA. A study demonstrated that people with OSA had increased markers of subclinical ILD, as assessed by computed tomography (CT) and serum markers, compared to healthy controls (J. S. Kim et al. 2017). Furthermore, IPF patients with OSA had worse lung function and survival, indicating that OSA may potentiate IPF progression (Bosi et al. 2017).

Finally, increased age is a major risk factor for the development of IPF. The median age of IPF patients is 65, with the highest prevalence in those over 75 years old. Cases in young adults are very rare (Collard 2012; Nalysnyk et al. 2012).

1.4.3 Environmental Risk Factors

Finally, environmental exposures increase risk of IPF development. Smoking is the most common risk factor (Baumgartner et al., 2000; García-Sancho Figueroa et al., 2010; García-Sancho et al., 2011). A meta-analysis of studies investigating environmental exposures in IPF found smoking increased IPF risk (odds ratio 1.6)(Park, Ahn and Kim, 2021). Additionally, viral infection (Folcik et al., 2013; Sheng et al., 2020; Mostafaei et al., 2021), bacterial colonisation (Molyneaux et al. 2014; Mostafaei et al. 2021), and occupational dust exposure (García-Sancho Figueroa et al., 2010; García-Sancho et al., 2011; Park, Ahn and Kim, 2021) have been established as risk factors for IPF development.

1.4.4 Contribution of Risk Factors

Many risk factors have clear links to continuous epithelial damage. For example, gastroesophageal reflux causes microinjury to the epithelium, as micro-aspirations of stomach

acid inappropriately contact the epithelial lining of the lung (Tobin et al. 2012). Meanwhile, OSA is proposed to cause microinjury due to tractional changes in the tissue and by causing oxidative stress (Lederer et al. 2012; Leslie 2012). Additionally, genetic polymorphisms causing increased epithelial cell senescence, like those impairing telomerase function or DNA repair, or polymorphisms causing surfactant protein misfolding, like those in SFTPC (Thurm et al), increase ER stress and death in the epithelial barrier layer. Ageing worsens this situation, as telomere shortening causes epithelial cell senescence and apoptosis (Naik and Moore, 2014; Zhang, Xu and Cong, 2021).

The capacity of risk factors to impair wound healing, or exacerbate wound healing into a profibrotic response are less obvious. Shortened telomeres and cell senescence impair the ability of epithelial cells to proliferate and regenerate (Zhang, Xu and Cong, 2021). Smoking and OSA cause oxidative stress, which impairs immune cell functions that are crucial for wound healing (Gille et al., 2017a; di Vincenzo et al., 2022; Thimmulappa et al., 2019). Further understanding is required to fully characterise the contribution of risk factors to disease progression.

1.5 Modelling Progressive Fibrosing ILDs

A range of *in vivo* and *in vitro* models have thus far been employed to delineate IPF disease mechanisms.

1.5.1 *In Vivo* Models

1.5.1.1 Spontaneous Animal Models

Some animals develop spontaneous disease which closely resembles IPF. West highland terriers, cats, horses, and donkeys all develop disease that has been historically described as

IPF. It has been argued that these models are useful for understanding the mechanism of spontaneous disease. However, these models have marked histological differences to human disease (Moore et al., 2013; Tashiro et al., 2017). For example, spontaneous lung fibrosis in West Highland terriers appears with a non-specific interstitial pneumonia (NSIP) pattern, as opposed to the UIP pattern on CT required for human diagnosis (Syrjä et al. 2013). Furthermore, the complex genetic and environmental influences that may contribute to animal disease is likely to markedly differ from human influences. For example, equine herpesvirus 5 has been frequently identified in the lung tissue of horses with lung fibrosis and is thus suggested as the causative factor. This virus is distinct from those implicated as risk factors in human disease, although the model may provide useful insights into viral risk factors in general (Williams et al. 2013).

Overall, spontaneous animal models provide an insight into spontaneous disease, that may help the field in understanding some shared risk factors in human IPF. They may also be useful models for testing therapeutics to slow and reverse fibrosis. However, the models are likely to be insufficient for complete mechanistic understanding, or for testing preventative or early interventional therapies, as the causes of disease, although largely idiopathic, are distinct from humans.

1.5.1.2 Murine Models

Murine models are the most heavily used in understanding IPF. The major models are described in Table 1.1. Bleomycin exposure is the most frequently used trigger of lung fibrosis in mice. Intratracheal bleomycin causes DNA damage in proliferating cells in the lungs, causing the development of fibrosis (Reinert et al. 2013). Although this model is low cost, consistent and

the best characterised murine model of pulmonary fibrosis (R. G. Jenkins et al. 2017), important differences exist between bleomycin exposed mice and humans with IPF. Bleomycin induced fibrosis begins with a profound inflammatory phase much more significant than any seen in human IPF (Izbicki et al. 2002). A large proportion of therapeutic studies (61% between 2008 and 2019) give interventions preventatively in bleomycin treated mice (during the inflammatory phase before day 7), rather than during a therapeutic window after the establishment of fibrosis (Kolb et al. 2020). The fibrosis induced by bleomycin is also resolving, unless repeat bleomycin doses are administered (Peng et al. 2013). Other significant differences include the known, singular trigger of fibrosis, the none UIP histological pattern and young mice lacking age and exposure risk factors. Aged mice show worsened fibrosis and impaired resolution (Stout-Delgado et al. 2016), however a recent American Thoracic Society report advised against using aged mice in most circumstances, due to the increased complexity of the model (R. G. Jenkins et al. 2017).

All the murine models outlined in Table 1.1 rely on a known trigger of fibrosis, which inherently makes these models different from idiopathic human disease. The benefits and drawbacks of these models are outlined in Table 1.1. It is clear that no one model alone can represent the complexities of human disease. Although a combination of models can be used to provide better representation of disease, the lack of appropriate preclinical animal models is emphasised by the unusually high failure rate of IPF drugs following transition into patients due to poor efficacy (Jenkins et al., 2017; Kolb et al., 2020).

Model	Pros	Cons
Exposures		
Bleomycin (single dose) Intratracheal administration of antibiotic known to cause lung fibrosis, via DNA damage in proliferative cells. Best used after inflammatory phase (d1-7) in fibrotic stage (d8-21), to understand therapeutic potential.	• Similar early molecular signal to humans • Well characterised • Quick • Low cost	• Resolving fibrosis • Non-UIP histological pattern • Usually in young mice (not representative of ageing patients) • Patchy fibrosis • Not idiopathic
Bleomycin (repeated dosing) Intratracheal administration of antibiotic known to cause lung fibrosis, via DNA damage in proliferative cells.	• Continuous fibrosis	• Expensive • Time consuming • Not idiopathic • Non-UIP histological pattern
Silicosis/ Asbestosis Repeated inhalation of silica particles or asbestos.	• Clinically relevant stimuli of human lung fibrosis • Unresolving and progressive	• Not reproducible fibrotic patterns • Non-UIP pattern • Slow to develop • Not idiopathic
Fluorescein isothiocyanate (FITC) exposure Inhalation or i.t. administration of FITC results in protein conjugates, alveolar injury, and vascular leakage.	• Fluorescent tracking of inhaled particles • Persistent up to 24 weeks	• Variable response • Non-UIP histological pattern • Marked inflammatory infiltrate
Radiation Focussed radiation injury to lungs in shielded animals.	• Clinically relevant stimuli	• Slow- fibrosis develops over 24 weeks • Not idiopathic
Cytokine Overexpression		
TGF-β Adenovirus Intratracheal administration of adenovirus for the overexpression of constitutively active TGF-β.	• Better replicates fibrosis patterns • Persistent fibrosis up to 64 days • Vascular remodelling	• Incompletely characterised • Focussed on one specific signalling pathway • Higher than physiological TGF-β levels • Include adenovirus immune response
Genetically Modified		
Mice with common or rare genetic variants from familial or idiopathic pulmonary fibrosis cohorts respectively. Including variants in surfactant protein genes (*SFTP-C, SFTP-A*), telomerase related genes (*TERT and TERC*) and mucous glycoprotein gene MUC5B. Either	• Represent relevant genetic risk alleles • Mice with I73 T SP-C in type II AECs develop	• Expensive • Incompletely characterised • Most require addition of bleomycin • Limited relevance to other genetic risk alleles or

induce spontaneous fibrosis or increased fibrotic response to bleomycin.	spontaneous disease	combinations of risk alleles

Table 1.1 Murine models of IPF. *Table shows a summary of the more widely used murine models of lung fibrosis, highlighting the mechanism behind fibrotic induction and the costs and benefits of each model for use in investigating IPF* (Yanagihara et al. 2020)*. UIP: usual interstitial pneumonia, TGF-β: transforming growth factor β,*

1.5.2 *In vitro* Models

The difficulties preclinical models have caused in the drug development pathway in IPF emphasise the need for representative human-derived *in vitro* models, which may narrow down successful drug candidates. Additionally, these models may be used to further our understanding of disease triggers, disease progression, and potential new drug targets.

1.5.2.1 Single Cell Cultures

Single cell cultures have long formed the mainstay of pre-clinical human models. These tools are useful in a reductionist approach, understanding the contribution of various mechanistic factors. Although cell lines are often practical and well characterised, primary human cell lines offer the best replication of human cells (Humbert et al. 2022). Epithelial cells and fibroblasts can be isolated from bronchial brushing or human lung tissue sections taken from biopsy or lobectomy procedures (Humbert et al. 2022). AMs can be isolated from BAL fluid or lung tissue sections, while IMs must be isolated from lung tissue using tissue dissociation and sorting procedures (Humbert et al. 2022; E. M. King et al. 2022). AMs are largely considered non-proliferative and are used fresh, although some protocols have been proposed for long term culture of these cells (Nayak et al., 2018; Subramanian et al., 2022a). Other immune cells can be isolated directly from blood of patients and controls, or derived from bloodborne progenitors, such as neutrophils and monocyte derived macrophages respectively (Humbert et al. 2022).

Single cell cultures have provided huge insight into the cellular mechanism of IPF. However, there are major flaws that prevent the results of single cell work from being directly applicable. Most relevant to the study of IPF is the stiffness of tissue culture plastic (10^6 kPa), which is far greater than that of the lung parenchyma (1-15 kPa) (F. Liu et al. 2010; Booth et al. 2012). This has been demonstrated to affect cell phenotype (Marinković, Liu and Tschumperlin, 2013; Asano et al., 2017; Blokland et al., 2022). Additionally, without the complex intracellular interactions and polarisation, single cell cultures cannot encapsulate the escalating interactions seen in pulmonary fibrosis (Birgersdotter, Sandberg and Ernberg, 2005).

1.5.2.2 3D Culture Models

To address the limitations of single cell cultures, various 3D models have been generated to investigate specific aspects of the disease. 3D hydrogels are used to model the mechanical effects of stiffness and ECM interactions, by seeding cells within the hydrogel. Although traditionally produced using an artificial ECM mixture (e.g. Matrigel), hydrogels produced using ECM from diseased tissue have been developed to account for disease specific differences in ECM composition (de Hilster et al., 2020; Nizamoglu et al., 2022; Saleh et al., 2022). Further still, ECM can be decellularised to provide disease-specific 3D scaffolds to model IPF ECM (Booth et al., 2012; Burgstaller et al., 2021).

In addition, lung organoids are used to investigate specific elements of IPF disease. Derived from human fresh or induced pluripotent stem cells, these self-assembling structures recapitulate the cell-cell interactions of lung stromal cells (Strikoudis et al. 2019). Although they have benefits, including the representation of patient specific genetic polymorphisms for

personalised medicine approaches (Surolia et al. 2017), the simplicity of organoid systems limits them to the study of specific elements of the disease (Yanagihara et al. 2020).

Thin slices of lung tissue, termed precision cut lung slices (PCLS), can also be maintained in culture, for the study of human and animal lung tissue in its multicellular form (G. Liu et al. 2019). This model benefits from maintaining the extracellular matrix and cellular contacts of real lung tissue, maximising the physiological relevance of the model. PCLS can be derived from IPF tissue to model the later stages of disease (Mercer et al. 2016; Tatler et al. 2016; Wei et al. 2021), or from explants from none-IPF tissue, to model the early stages of IPF disease progression (Alsafadi et al. 2017). Despite benefits, this model lacks certain relevant elements of the lung tissue, such as circulation and an air interface.

1.6 Innate Immunology in IPF

Interpretation of early evidence in IPF dictated that the disease did not have a strong immune component (Gauldie, 2002; Blackwell et al., 2014). Infiltrating immune cell numbers are lower than other ILDs (Desai et al. 2018). Treatment with low dose steroids worsened disease outcome (Raghu et al., 2012), and anti-inflammatory biologics had no benefit (Raghu et al. 2008; T. E. King et al. 2009). Additionally, for diagnosis, ground glass opacities indicating inflammation must be largely absent from CT scans (Devaraj 2014) and autoimmune markers should be absent in serum and upon examination (Balestro et al., 2016; Raghu et al., 2011). However, as understanding of inflammation grows, we can identify ways that immune cells are likely involved in pulmonary fibrosis, without the presence of a conventional inflammatory cascade (Desai et al. 2018). Therefore, recent research has begun to analyse immune cell function and polarisation in IPF.

1.7 MACROPHAGES IN IPF

As highlighted in section 1.3, macrophages are an integral cell type in control of the wound healing response. As a major focus of this thesis, a thorough understanding of the macrophage populations and functions within the lung is required.

1.7.1 Macrophage Subsets and Heterogeneity

Macrophages are sentinel innate immune cells, responsible for the removal of harmful pathogens and substances, and orchestrating wider immune responses (Hussell and Bell 2014). Pulmonary macrophages are transcriptionally distinct from tissue resident macrophages in other tissues (Lavin et al. 2015). Recent research has demonstrated that these changes are epigenetically controlled by histone modifications, which recruit a unique combination of transcription factors, resulting in the unique macrophage gene expression signals identified in the lung (Ebina-Shibuya et al. 2016). These signatures are being identified with increasing clarity as single cell RNA and proteomic analysis improves (Mould et al., 2019; Qie et al., 2022).

1.7.1.1 Location

Macrophages in the lung are characterised by their location, where AMs patrol the alveoli and IMs patrol the parenchyma beneath the epithelial barrier (Hussell and Bell 2014). To date, two spatially distinct populations of IMs have been characterised in mice, which localise differently within the parenchyma (Schyns et al., 2019; Gibbings et al., 2017; Chakarov et al., 2019). This work has yet to be replicated or confirmed in human lung tissue. Cell specific markers have been identified to differentiate AMs and IMs, which differ in murine and human cells. Human pulmonary macrophages all express cluster of differentiation (CD)68, CD141, CD14, CD163, CC chemokine receptor (CCR)-7 and human leukocyte antigen (HLA)-DR, whilst AMs express more CD11c and IMs express more CD11b. AMs also express more CD206 and exclusively express

CD169. There are also reported populations of CD163 low and CD163 high AMs (Lugg et al., 2022; Byrne et al., 2016). In mice, all pulmonary macrophages express Mer tyrosine kinase (MerTK). IMs express more CD11b and CD64, whilst AMs express more CD11c and CD206. AMs also exclusively express CD200 receptor (CD200R), CD68 and Siglec F (Misharin et al., 2013; Byrne, Maher and Lloyd, 2016). AMs and IMs are also functionally distinct, which is unsurprising given their different locations. IMs are relatively better at antigen presentation, but less efficient at phagocytosis (Bedoret et al., 2009; Franke-Ullmann et al., 1996; Gu et al., 2022; Byrne et al., 2016).

1.7.1.2 Source

Pulmonary macrophages are also classified by their source. Tissue resident macrophages across several organs originate from varying combinations of progenitors. Some tissue resident macrophages originate from embryonic derived progenitors and persist via self-renewal within the tissue. By contrast, monocyte derived macrophages develop as infiltrating monocytes differentiate within the tissue (Gomez Perdiguero et al., 2015; Hoeffel et al., 2015).

In the lung, ongoing research is dissecting the contribution of embryonically derived, self-renewing macrophages and monocyte derived macrophages. Bone marrow chimeras in thoracically shielded mice and parabiosis studies indicate that AM self-renewal largely maintains AMs during homeostasis in germ free mice, for at least 5 to 8 months (Janssen et al., 2011; Hashimoto et al., 2013; Soucie et al., 2016; McQuattie-Pimentel et al., 2021). Establishment and self-renewal rely on granulocyte-macrophage colony-stimulating factor (GMCSF) (Guilliams et al., 2013) and TGF-β (Yu et al. 2017) among other factors and is possible due to temporary changes, such as transcription factor levels (Soucie et al., 2016; Rauschmeier

et al., 2019) and epigenetic changes (Yao et al. 2020) in these cells. Some studies have demonstrated that there is a constant low level of monocyte derived macrophage infiltration and differentiation at steady state in mice, which maintains the AM pool (Liu et al, 2019).

Some murine studies have demonstrated that tissue resident AMs can persist through infection or injury and maintain the AM pool independent of monocyte infiltration (Janssen et al., 2011; Hashimoto et al., 2013). However other studies, likely involving more severe disruption to tissue resident AMs, demonstrated that monocyte derived macrophages infiltrate the tissue and replenish the AM pool. At first, these cells are substantially different to tissue resident AMs, both phenotypically and metabolically (Woods et al., 2020a; Mould et al., 2017; Gibbings et al., 2015). Monocyte derived AMs retain increased functional plasticity, contrasting to the hyporesponsive state of tissue resident AMs, making them more likely to be shaped by pro-inflammatory or pro-fibrotic stimuli in the tissue (Kulikauskaite and Wack 2020). After several weeks, monocyte derived AMs acquire similar functions and self-renewal capacity to tissue-resident AMs (van de Laar et al. 2016; McQuattie-Pimentel et al. 2021), however some transcriptional differences persist with unknown functional consequences (Gibbings et al., 2015; Aegerter et al., 2020).

In humans, the increased complexity and individuality of exposures over a lifetime is likely to dramatically increase the heterogeneity of AMs. The variety of infections and chronic exposures experienced from a young age increases the likelihood that monocyte derived AMs have been recruited to replenish the AM pool. Indeed, evidence from lung transplant patients has been used to understand the contribution of AM self-renewal and monocyte macrophage replenishment across life. In sex mismatched lung transplants, donor AMs were largely replaced

by recipient AMs within a year. This indicates that human lungs, exposed to a higher level of daily insults, rely more heavily on monocyte derived macrophages to replenish the tissue resident AM pool. These monocyte derived AMs were mature after 1 year (Byrne et al. 2020). Although this could be limited to the transplant setting, Mould et al. (2021) used pseudotime single cell RNA sequencing analysis of blood monocytes and bronchoalveolar lavage (BAL) cells in healthy participants, to provide strong evidence that monocytes infiltrate the tissue and differentiate into AM cells in steady state in humans. To add further complexity to the human AM pool, each event that causes depletion of pulmonary AMs creates a unique inflammatory environment, with the potential to influence monocyte differentiation in a variety of ways. This escalates the development of a heterogenous population of AMs across the human lifespan (Morales-Nebreda et al. 2015).

The ontogeny of IMs is less well understood, due to limited surface marker differentiation from dendritic cells. Emerging single cell analysis suggests that IMs initially originate from yolk sac and foetal monocyte derived cells (Schyns et al., 2019). Parabiosis studies in mice suggest that some (Tan and Krasnow, 2016; Schyns et al., 2019) or even all IMs (Chakarov et al. 2019) are replaced by monocyte derived IMs after birth, with one study suggesting that self-renewal capacity is limited to IMs within certain niches (e.g. nerve fibre associated) (Ural et al. 2020).

1.7.1.3 M1/M2 Paradigm

Macrophages derived from monocytes have traditionally been described as M1 (classically activated) and M2 (alternatively activated) phenotypes. There have been various landmark papers with overlapping but distinct definitions of these macrophage groups, summarised by Xue et al. (2014). Typically, M1 macrophages are proinflammatory cells induced by

lipopolysaccharide (LPS), interferon γ (IFN-γ) or GMCSF, expressing inducible nitric oxide synthase (iNOS) for nitric oxide production, IL-1β, IL-12B, and TNFα. Surface markers used to identify these cells include HLA-DR, CD80, CD14 and CD38. By contrast, M2 macrophages differentiate in response to stimuli including TGF-β, IL-4, IL-10, or macrophage colony-stimulating factor (MCSF), and are anti-inflammatory and profibrotic, expressing IL-10, TGF-β, and arginase 1, which competes with iNOS, to convert arginine into the precursor for collagen, ornithine. Associated surface markers defining this phenotype are CD36, CD206 and CD163.

It has been widely acknowledged that although differentiation of monocytes *in vitro* with specific cytokines produces these phenotypes, the tissue specific reality that monocytes are exposed to are much more complex, and therefore yield much more varied and plastic macrophage phenotypes (Xue et al. 2014). For this reason, the field reached a consensus to describe monocytes derived *in vitro* with reference to the stimulus used for their differentiation (for example, M(IFN-γ), M(LPS), M(IL-10), M(IL-4))(P. J. Murray et al. 2014) Although this nomenclature clarifies the source of *in vitro* monocyte derived macrophages, *in vitro* studies still cannot recapitulate tissue specific complexity.

Evidence from tissue resident and monocyte derived macrophages *in vivo* consolidates this. It has been demonstrated that AMs co-express M1 and M2 markers in a homeostatic state (Hussell and Bell 2014; Mitsi et al. 2018), and in various chronic diseases (Anthony et al. 2014). Although AMs can be skewed to express more classic M1 markers with IFN-γ stimulation and more M2 markers with IL-4 and IL-13 stimulation (Shaykhiev et al. 2009), it is important to note that they maintain functional plasticity after the event (Herold, Mayer and Lohmeyer, 2011).

1.7.2 AM Functions

1.7.2.1 Tolerogenic Capacity

At baseline, AMs produce large amounts of TGF-β and IL-10. TGF-β is required for the maintenance of the AM population. These cytokines are strongly anti-inflammatory, supressing the activation of immune responses at rest in the lung (Byrne, Maher and Lloyd, 2016). TGF-β, alongside retinaldehyde dehydrogenase (RALDH) 1 and 2 (Bazewicz et al. 2019) released by AMs also contributes to the differentiation of regulatory T cells, capable of establishing tolerance in the lungs (Soroosh et al. 2013). Epithelial cells are strong promoters of the tolerogenic environment of the lung at baseline. Beyond producing tolerogenic and neutralising surfactant, they produce IL-10 and activate TGF-β by expressing αvβ6 integrins. They also express CD200, which ligates CD200R on macrophages to block inflammatory signalling in AMs (Woo, Jeong and Chung, 2021).

1.7.2.2 Inflammatory Capacity

When AMs are activated and the anti-inflammatory properties of unstimulated epithelial cells are removed (Fernandez et al., 2004; Bissonnette et al., 2020), AMs switch to a pro-inflammatory state. NFκB signalling triggers an inflammatory cascade, which triggers chemokine release for the recruitment of further innate immune cells (Dorrington and Fraser 2019). Neutrophil extracellular traps (NETs) can further activate AMs to escalate inflammation (Song et al., 2019). Activated inflammatory AMs have a higher capacity for phagocytosis and increase reactive oxygen species and protease release (Woo, Jeong and Chung, 2021).

1.7.2.3 Phagocytosis

Phagocytosis is the process of engulfment and digestion of large particles, such as pathogens and foreign bodies (Figure 1.6). Professional phagocytes, including macrophages and dendritic cells, are best equipped to do this efficiently, although nonprofessional phagocytes, such as epithelial cells and fibroblasts, can phagocytose in certain circumstances (Arango Duque and Descoteaux 2016; Gordon and Plüddemann 2017).

Macrophages rely upon phagocytosis to maintain homeostasis and remove pathogens. Foreign particles and pathogens attract macrophages in a variety of ways. Namely PAMPs introduced by a pathogen itself, or DAMPs released by damage caused by the pathogen or foreign substance upon its interaction with the body. These PAMPs and DAMPs bind PRRs on local immune cells triggering a cascade of immune signalling for phagocyte migration and activation (Gordon and Plüddemann 2017).

Macrophages express an array of PRRs, which orchestrate recruitment, tethering, and uptake of foreign bodies. Non-opsonic receptors bind directly to repetitive patterns on the surface of pathogens (K. Li and Underhill 2020). These include Dectin 1, Mincle and dendritic cell-specific ICAM-3-grabbing nonintegrin (DC-SIGN), which bind yeast beta glucan, mycobacterium cell wall and specific pathogen glycans respectively (Herre et al., 2004; van Liempt et al., 2006; Ishikawa et al., 2009). By contrast, opsonic receptors bind host molecules, which are released into circulation to coat and label foreign invaders for removal (Uribe-Querol and Rosales 2020). For example, Fc receptors bind the constant end of antibodies generated by the adaptive immune response against specific antigens (Nimmerjahn and Ravetch 2006; Rosales and Uribe-Querol 2013). Meanwhile, complement receptors bind activated complement molecules, after they

non-specifically coat and tag the outside of invaders, in an antibody, lectin or positive feedback driven way (Brown, 1992; Tohyama and Yamamura, 2006; van Lookeren Campagne, Wiesmann and Brown, 2007; Dustin, 2017).

These receptors work in concert to orchestrate phagocytosis. Some receptors have been demonstrated as *bona fide* phagocytosis receptors, capable of triggering the start of phagocytosis. These include Fc receptors (Rosales and Uribe-Querol 2013), complement receptors (van Lookeren Campagne, Wiesmann and Brown, 2007; Dustin, 2017), Dectin 1 (Brown and Gordon, 2001; Herre et al., 2004), Mincle ((Lobato-Pascual et al. 2013) and DC-SIGN (Azad, Torrelles and Schlesinger, 2008). Additional non opsonic receptors known to bind pathogens, including CD-14 (LPS binding protein receptor)(Schiff et al. 1997), class A scavenger receptor (SR-A) (LPS receptor)(Peiser et al. 2000), and macrophage receptor with collagenous structure (MARCO) (bacterial receptor)(van der Laan et al. 1999), have an undetermined role. It is not clear whether they simply tether the phagocyte to pathogen, tether and prime the cell for phagocytosis, or induce phagocytosis themselves (Doyle et al. 2004).

The convergence of receptors activates the cellular machinery in the cell to facilitate invagination and extravaginiation of the membrane around foreign particles (Uribe-Querol and Rosales 2020). Cytoskeletal changes begin at the site of phagocytic receptor clustering and activation. Receptors have overlapping but distinct signalling pathways to achieve the initiation and extension of pseudopodia. Overall, the cortical cytoskeleton is disrupted, allowing actin filament establishment by nucleation at the front of the pseudopodia. Actin is also depolymerised at the base of the phagocytic cup (Freeman and Grinstein 2014).

Specific mechanisms for some receptors are well understood. For example, Fc receptors cluster when activated, causing immunoreceptor tyrosine-based activation motif (ITAM) phosphorylation and Src family kinase recruitment. These kinases trigger phosphatidylinositol-3-kinase (PI3K) activation on the membrane. Resultant phosphatidylinositol 3,4,5-trisphosphate (PIP3) activates small GTPase Rac1, which causes actin polymerisation, initiating the formation of actin patches at the phagocytic cup (Rosales 2007). Additional GTPase cell division control protein 42 (Cdc42) is then activated to trigger actin related protein (Arp)2/3 mediated actin filament nucleation, via Wiskott-Aldrich Syndrome protein (WASP) (H. Park and Cox 2009). Filament extension is given direction by F-actin debranching proteins (coronins) activated in the nascent phagosome by phosphoinositides such as PI(4,5)P2 transiently appearing in the membrane (Yan et al. 2005).

By contrast, complement receptors activate distinct pathways for engulfment. Complement receptors activate rho GTPases but not Rac or CDC42 GTPases (Allen and Aderem, 1996; May et al., 2000). Rho GTPase activates myosin II via Rho kinase. Myosin II activates Arp2/3 for branched actin assembly at the phagocytic cup (Olazabal et al. 2002). Rho GTPase also activates Mammalian diaphanous-related formin (mDia1), causing long, straight actin accumulation in the phagocytic cup and establishing a microtubuole link to the phagosome via cytoplasmic linker protein-170 (CLIP-170) (Lewkowicz et al. 2008). This form of phagocytosis appears distinct visually, as the particle sinks into the membrane, rather than being engulfed by extensive pseudopodia (Aderem and Underhill 1999).

To complete phagocytosis, the membrane must fuse and surround an internalised phagosome. Filamentous actin dissociates, due to PI3K dependent inactivation of GTPases (Beemiller et al.

2010). Actin bound myosins work to contract in rings around the phagosome, eventually squeezing out excess liquid (myosin II) (Araki et al. 2003), and pulling the extensions closed around the particle (myosin Ic)(Swanson et al., 1999; Diakonova, Bokoch and Swanson, 2002).

The phagosome then undergoes maturation, to break down and/or recycle its contents (Levin, Grinstein and Canton, 2016). Ras-related protein (Rab)5 on the phagosome triggers fusion with early endosomes (Christoforidis et al. 1999; Kitano et al. 2008), causing an increase in Rab7 on the membrane (Vieira et al. 2003). As Rab5 is lost, Rab7 triggers fusion with late endosomes (Rink et al. 2005). The late endosome introduces proteases like cathepsins (Fairn and Grinstein 2012), along with a V-ATPase proton pump, which reduces internal pH to 5.5-6.0 (Marshansky and Futai 2008). Finally, lysosomes fuse with the phagosome, to create the phagolysosome. This reduces the pH further (Marshansky and Futai 2008), and exposes contents to ROS, H_2O_2 and further hydrolytic enzymes including lysozymes and lipases. Progressive acidification and digestive enzymes reduce the contents of the phagolysosome to harmless components which can be recycled or excreted (Minakami and Sumimoto 2006).

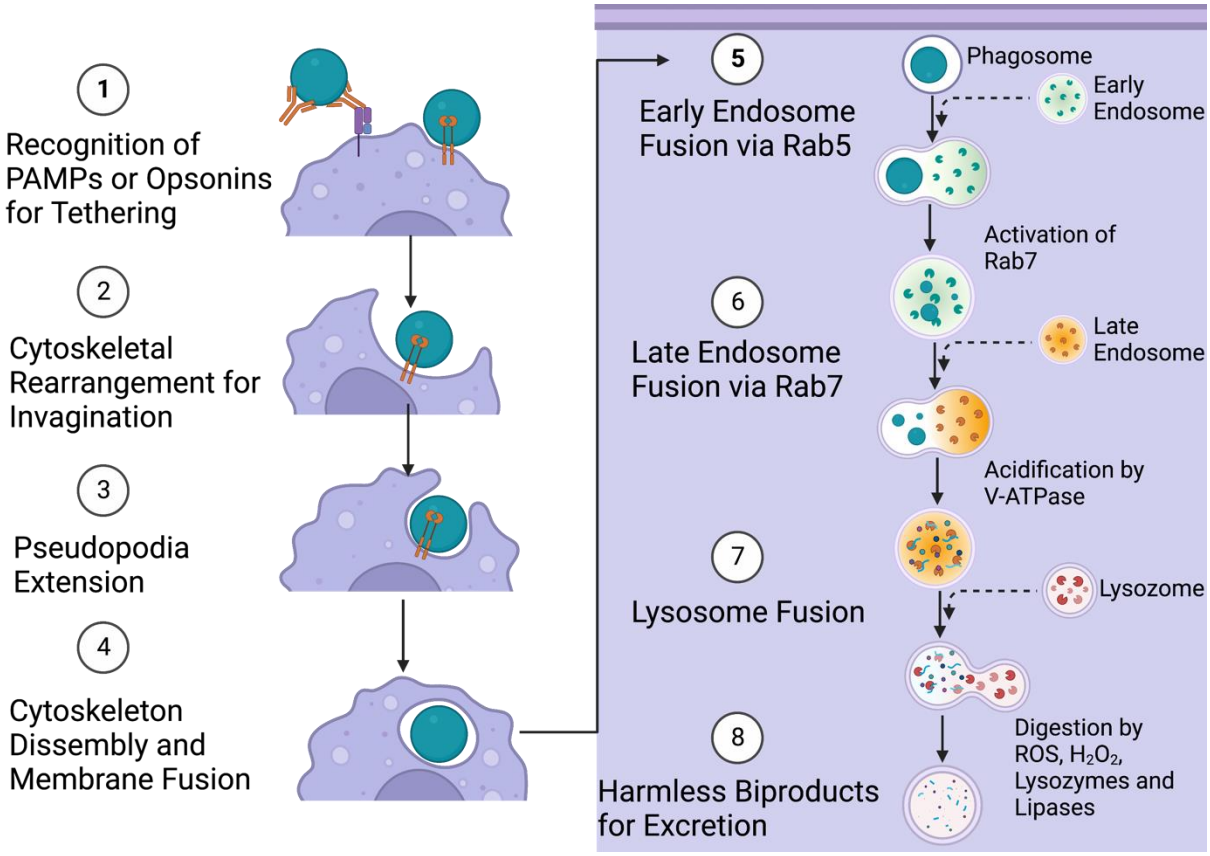

Figure 1.6 Macrophage phagocytosis. (1) Macrophages bind to pathogens via non opsonic receptors (direct binding to pathogenic product) and/or opsonic receptors (binding via opsonins non-specifically coating pathogenic products). (2) Downstream signalling results in cytoskeletal rearrangements, allowing for invagination of the membrane at the point of binding and (3) extension of pseudopodia around the pathogenic particle. Exact signalling mechanisms are receptor dependent. (4) Membranes eventually fuse, via contractile myosin rings, closing the phagosome. The phagosome progressively matures to digest its contents. (5) Firstly, the phagosome expresses Rab5, allowing for fusion with the early endosome. (6) This triggers Rab7 expression, facilitating fusion with late endosomes. This introduces digestive enzymes and V-ATPase, which progressively acidifies the phagosome. (7) Finally, the phagosome fuses with lysosomes, creating the phagolysosome. This further reduces pH and introduces reactive oxygen species and digestive enzymes. (8) Eventually, there is complete digestion of the pathogen into harmless products for recycling and excretion.

1.7.2.4 Efferocytosis

Efferocytosis is a type of phagocytosis where apoptotic cells are engulfed by phagocytes. Although there are many overlapping mechanisms with phagocytosis, they must remain reasonably distinct, as efferocytosis is a reaction to self-cells, so immunoreactivity must be

avoided. Due to the different environments where phagocytosis versus efferocytosis occur, the long-lasting effect of efferocytosis on phagocyte function also differentiates it from phagocytosis (Doran, Yurdagul and Tabas, 2019).

Apoptosis is a type of programmed cell death that thousands of cells across the body undergo every day. The process is crucial during development, and to maintain homeostasis, but is also important for contraction of responsive cells during inflammation and wound healing. The ordered process of apoptosis is highly conserved, and is marked by cell shrinkage and chromatin condensation, followed by blebbing of the cells into smaller apoptotic bodies densely packed with organelles. In this way, apoptosis prevents the release of DAMPs, such as cell free DNA, which could result in inflammation and even autoimmunity (Fink and Cookson, 2005; Elmore, 2007; Nagata, 2018).

Apoptotic bodies must be removed by professional or non-professional phagocytes, to avoid breakdown of apoptotic bodies by secondary necrosis (Grabiec and Hussell 2016; Rogers et al. 2017). Professional phagocytes, namely AMs in the airways, migrate to the site of apoptosis, as apoptotic cells release 'find me' signals, including ATP, UTP, and chemokine (C-X3-C motif) ligand 1 (CX3CL1) (Medina and Ravichandran 2016). Phagocytes subsequently bind 'eat me' signals on the apoptotic membrane, via a range of receptors found on the phagocyte surface (Arandjelovic and Ravichandran 2015; Medina and Ravichandran 2016).

The best studied 'eat me' signal is phosphatidylserine. Phosphatidylserine is usually hidden on the inner leaflet of the plasma membrane, held there by a balance of flippase and scramblase enzyme activity. Apoptotic signalling inactivates these enzymes, causing phosphatidyl serine externalisation on the outer leaflet of the membrane (Segawa et al. 2014). Phosphatidylserine

is required but not always sufficient for efferocytosis (Arandjelovic and Ravichandran 2015). Evidence suggests that in some settings, it works in concert with further 'eat me' signals, to meet the threshold for engulfment. Other 'eat me' signals include thrombospondin 1 (TSP-1), intercellular adhesion molecule (ICAM)3 and altered sugars (Arandjelovic and Ravichandran 2015). There are also 'don't eat me' signals expressed by live cells, including CD47 (Oldenborg et al. 2000) and CD31 (S. Brown et al. 2002), which decrease the efferocytic activity of phagocytes upon ligation of receptors including signal-regulatory protein α (SIRPα).

Phosphatidylserine and other 'eat me' signals can bind a wide range of receptors, both directly (including triggering receptor expressed on myeloid cells (TREM2), CD300, Receptor for advanced glycation end-product (RAGE), brain angiogenesis inhibitor (BAI)1 and T-cell immunoglobulin mucin protein (TIM) 4) and via bridging molecules (including αvβ3 and αvβ 5 via Milk-fat globule EGF factor-8 (MFG-E8), and Axl and MerTK via protein S or Gas6) (Grabiec and Hussell 2016; Nagata 2018). The contribution and redundancy of these receptors is incompletely understood. It is likely that the type of receptors engaged varies across efferocytosis stage and location, with some acting as tethering only (such as TIM-4 (Park, Hochreiter-Hufford and Ravichandran, 2009)), while others have signalling roles (Grabiec and Hussell 2016).

The signals downstream of 'eat me' receptors result in the cytoskeletal rearrangement required for efferocytosis. Receptors converge to activate Rac1 GTPase (Boada-Romero et al. 2020). For example, the tyrosine kinase receptor MerTK binds phosphatidylserine via adaptors. Autophosphorylation of its cytoplasmic domains results in Rac1 recruitment and activation (van der Meer, van der Poll and Van't Veer, 2014). Like FcR driven phagocytosis, Rac1 GTPase

triggers actin polymerisation, developing actin patches to establish localised invagination and extravagination. WASP proteins recruit the ARP2/3 complex, triggering actin filament nucleation and extension (Boada-Romero et al., 2020). When the phagocytic cup has closed around the apoptotic body, Rho GTPases stop Rac1 driven polymerisation and the myosins work in a similar way to contract and close the phagosome. The phagosome matures in a similar way to conventional phagocytosis, including fusion to early and late endosomes, then fusion with lysosomes, resulting in progressive acidification (Nagata, 2018; et al., 2020). Although largely similar, emerging evidence outlines how phagosome maturation differs between phagocytosis and efferocytosis, preventing antigenic presentation following efferocytosis (Canton et al., 2014; Yin et al., 2016).

In addition to cytoskeletal changes, efferocytosis alters the phenotype of the phagocytic cell. Firstly, efferocytosis promotes an anti-inflammatory response in phagocytes. For example, macrophages increase TGF-β, prostaglandin E2 (PGE_2) and IL-10 output following efferocytosis, whilst decreasing inflammatory TNFα, IL-1 and IL-8 release (Fadok et al., 1998; Chung et al., 2007; Ariel and Serhan, 2012; Pashover-Schallinger et al., 2012). As such, efferocytosis is a tolerogenic process, likely evolved to prevent any immunogenic response to apoptosis, which could trigger autoimmunity and chronic inflammation, and to promote wound healing in areas of extensive cell death. Secondly, phagocytes respond to initial efferocytic event by increasing their capacity to continually efferocytose. For example, efferocytosis triggers an increase in expression of efferocytic receptors, such as MerTK (Schilperoort et al. 2023).

The mechanisms behind these phenotypic changes have not been completely delineated. Rac1 activation likely drives some of the changes in mediator release following efferocytosis (Fond

et al. 2015). The influx of new metabolites from apoptotic cell engulfment, including a large amount of lipids, has also been suggested to necessitate and drive a metabolic shift due to increased fatty acid oxidation, a metabolic driver of M2 macrophage polarisation, and demonstrated to increase IL-10 release (Zhang et al., 2019a). Finally, nuclear receptors liver X receptor (LXR), peroxisome proliferator-activated receptor (PPAR) δ, PPARγ and retinoic X receptor (RXR) responding to the phagolysosome can confer changes to gene expression after efferocytosis. For example, evidence indicates that these nuclear receptors are responsible for increased efferocytic receptor expression (A-Gonzalez et al., 2009a; Mukundan et al., 2009; Rőszer et al., 2011).

Much of our understanding of efferocytosis mechanisms is derived from macrophages differentiated *in vitro*. Given the differences between macrophages derived *in vitro* and lung resident macrophages highlighted in section 1.7.1, it cannot be presumed that the efferocytic mechanisms described in the literature are utilised in the same way by lung resident macrophages. Mahida et al (2021) demonstrated a role for Rac1 in the cytoskeletal rearrangement required for efferocytosis of apoptotic neutrophils in human AMs. The study also identified a role for Rho kinase (ROCK) in inhibiting Rac1 upon ligation of 'don't eat me' signal receptor SIRPα. In addition to ligation by CD47, in the alveolar space SIRPα is also ligated by surfactant proteins A and D, which are highly expressed in this environment as described in section 1.7.2.5. In murine AMs, efferocytosis *in vitro* induces TGF-β and arginase expression, while reducing iNOS expression (K. K. Kim et al. 2018). Additional studies show induction of PGE_2 in murine AMs after efferocytosis (Medeiros et al. 2009).

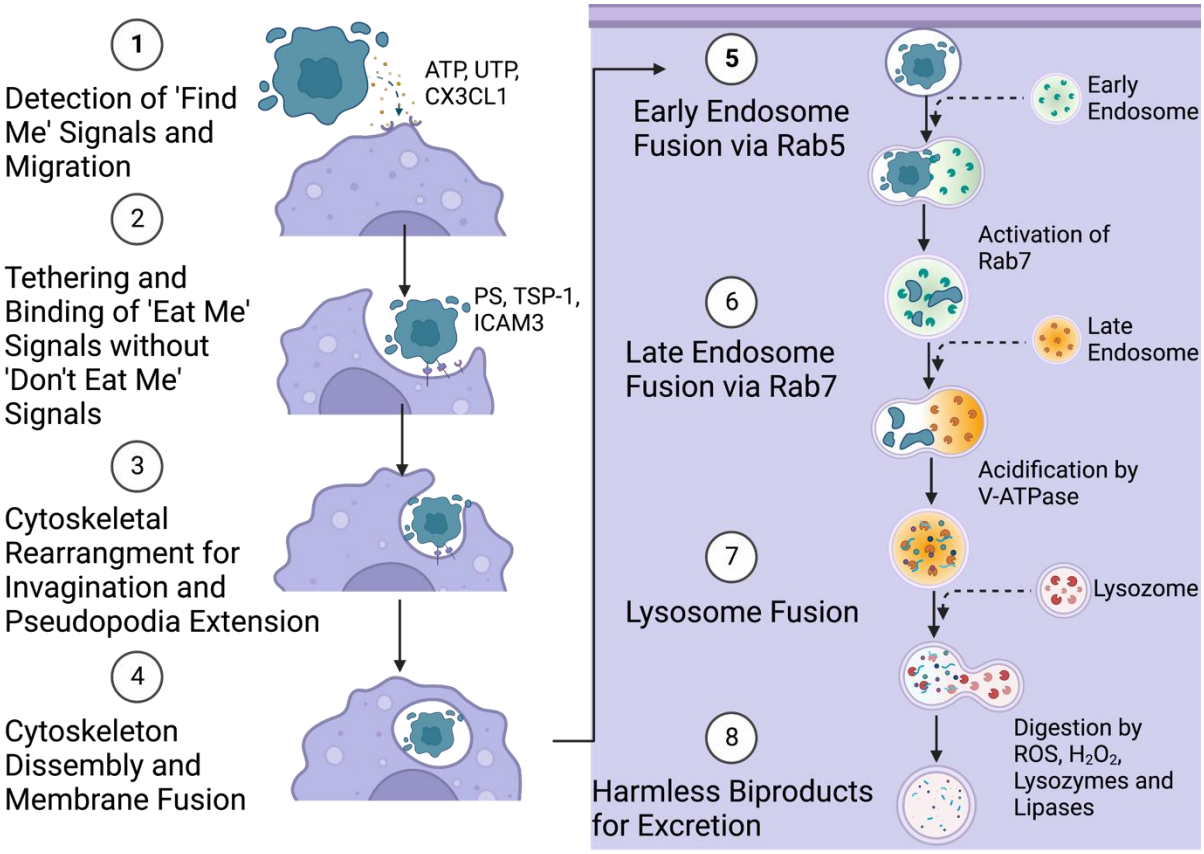

Figure 1.7 Macrophage Efferocytosis. (1) Macrophages are attracted to apoptotic cells via soluble 'find me' signals, including ATP and CX3CL-1. (2) Once in proximity, macrophages bind 'eat me' signals on the surface of apoptotic cells. Phosphatidyl serine (PS) is a major 'eat me' signal. (3) When macrophages bind these signals, and don't bind any 'don't me signals' such as CD-47, cytoskeletal rearrangement is triggered, causing invagination of the membrane and pseudopodia extension. (4) Subsequently, membranes fuse around the apoptotic cell, facilitated by further cytoskeletal rearrangements, to enclose the phagosome. The phagosome progressively matures to digest its contents. (5) Firstly, the phagosome expresses Rab5, allowing for fusion with the early endosome. (6) This triggers Rab7 expression, facilitating fusion with late endosomes. This introduces digestive enzymes and V-ATPase, which progressively acidifies the phagosome. (7) Finally, the phagosome fuses with lysosomes, creating the phagolysosome. This further reduces pH and introduces reactive oxygen species and digestive enzymes. (8) Eventually, there is complete digestion of the apoptotic cell into harmless products for recycling and excretion.

1.7.2.5 Surfactant Recycling

As previously described, pulmonary surfactant is a hydrophobic mixture of phospholipids and proteins produced by AECII cells, which lines the alveoli preventing collapse. Lipids, including cholesterol, triglycerides and free fatty acids, make up 90% of surfactant, and are associated

with surfactant protein (SP) -A, -B, -C and -D (Pattle 1955). SP-B and SP-C increase the hydrophobicity of surfactant. Meanwhile, SP-A and SP-D have dual roles in innate immune regulation (Watson, Madsen and Clark, 2021). These proteins act as powerful scavenger receptors, agglutinating pathogens, coating and improving removal of apoptotic and necrotic cells, binding free cell and bacterial DNA for clearance and collecting noxious particles for clearance (Hartshorn et al., 1998; LeVine et al., 2000; Nayak et al., 2012; Carreto-Binaghi, Aliouat and Taylor, 2016). SP-A and SP-D also actively neutralise viruses, preventing cellular attachment (Watson et al. 2019).

Beyond this, SP-A and SP-D have modulatory roles in innate and adaptive immune cell function. On myeloid cells, including AMs, the proteins neutralise inflammatory responses in homeostasis by binding SIRPα. However, when a pathogen is bound, the proteins orientation changes and they bind calrecticulin/CD91 receptor complex, boosting anti-pathogen responses (Gardai et al., 2003). SP-A and SP-D have been shown to reduce cytokine responses to stimuli including LPS and PAMPs (Yoshida, Korfhagen and Whitsett, 2001). This creates a relatively tolerogenic environment in response to usually inflammatory DAMPs. A similar role occurs in dendritic cells, whereby SP-A and -D reduce antigen presentation in response to pathogens, while meanwhile improving phagocytosis of the pathogen, maintaining an anti-inflammatory response to pathogens (Brinker, Garner and Wright, 2003; Hortobágyi et al., 2008).

When GMCSF signalling is prevented by rare autoimmune antibodies against GMCSF, humans develop pulmonary alveolar proteinosis (PAP). In exploring this, it was determined that AMs are the key cell in surfactant clearing and catabolism, and that local GMCSF signalling is crucial in mediating catabolism of surfactant proteins and lipids, via PPARγ signalling, which gives AMs

their unique receptors and functions (Yoshida et al., 2001). Indeed, in PAP patients, AMs develop large lipid bodies and are unable to catabolise surfactant successfully, leading to the extracellular build-up of surfactant (Iyonaga et al., no date).

1.7.2.6 Iron Metabolism

To maintain homeostasis, AMs must metabolise and store excess iron which builds up in the lung. This function is crucial to prevent harmful pathogen colonisation and impaired immune cell function (Recalcati and Cairo 2021). A major source of iron is from haem groups in red blood cells. Macrophages take up this iron via erythrophagocytosis, or after haemolysis or injury, when it is bound by scavenger receptors (Tolosano et al., 2010; White et al., 2013; Muckenthaler et al., 2017). Additional iron enters via transferrin receptors and metal transporters (Khadem Ali et al. 2020). Excess iron is stored in macrophages as ferritin, and export occurs through ferroportin transporters (Arosio, Ingrassia and Cavadini, 2009). Iron is a key component for enzymes involved in catalysis of oxidant and antioxidant generation performed by macrophages. Macrophages are also comparatively resistant to ferroptosis (iron driven apoptosis), unlike cells that only take up iron when required for function (Cui et al., 2021b; Recalcati and Cairo, 2021). Iron regulation has not been thoroughly analysed in AMs specifically, however some disease related changes in AMs have been identified in the lung. For example, ferroptosis is increased during AM *Mycobacterium tuberculosis* (mTB) infection, due to increased autophagy and ferritin breakdown (Amaral et al. 2019). Additionally, in cystic fibrosis patients, the loss of cystic fibrosis transmembrane conductance regulator (CFTR) is responsible for iron transport dysregulation in macrophages (Hazlett et al. 2020).

1.7.3 Changes in IPF

Resident macrophages are one of the most studied immune cell types in IPF, due to their presence regardless of inflammation. In IPF tissue, macrophages are often identified in areas enriched for myofibroblast development (Byrne, Maher and Lloyd, 2016). Initial studies in a bleomycin (BLM) induced murine model of IPF showed that liposomal clodronate depletion of macrophages in the fibrotic phase of a BLM model limited fibrosis, whilst depletion in the resolution phase delayed resolution (Gibbons et al. 2012). This emphasises the complex role of macrophages temporally across the course of fibrosis and normal resolution.

Although the M1/M2 macrophage paradigm is an oversimplification, the sliding scale of polarisation is relevant in IPF. In homeostasis, the antifibrotic and antimicrobial properties typical of an M1 macrophage must be balanced against their potentially damaging inflammatory functions, whilst the wound healing and anti-inflammatory properties associated with an M2 phenotype must be balanced against their profibrotic potential. Aberrant polarisation and functional deficits in macrophages in the lung have been implicated as the link between initial epithelial injury and continuous fibroblast differentiation in IPF. Table 1.2 summarises the changes identified in AMs and IMs from patients with IPF and murine models of IPF and describes their potential relevance to the fibrotic cascade. Most evidence from the fibrotic lung focusses on AMs, due to their accessibility in humans, assessing changes in their output and function. By contrast, there is a dearth of data on IMs in IPF, despite their location within the parenchyma, which would enable them to influence fibrosis (Byrne, Maher and Lloyd, 2016).

1.7.3.1 Markers

Unsurprisingly, macrophages from IPF patients and animal models do not polarise to look like any of the *in vitro* MDM classes described. Although they are more enriched for traditional M2 markers, they co express markers of M1 activation (Byrne, Maher and Lloyd, 2016). CD206, a scavenger receptor with key roles in supressing inflammatory cytokine release, is an established marker of pro-resolution macrophages, and is enhanced in IPF AMs (Pechkovsky et al. 2010; Y. Zhou et al. 2014) and mouse models (Ji et al. 2014). CD206 is also increased on IMs in bleomycin treated animals (Ji et al. 2014). CD163 is a scavenger receptor associated with pro-resolution macrophage polarisation, which more frequently and at a higher intensity in AMs from IPF patients (Gibbons et al., 2012; Vasarmidi et al., 2019). Classic marker of pro-resolution macrophage polarisation arginase 1 is also increased in IPF AMs (Mora et al. 2006) and in AMs from bleomycin treated mice (Endo et al. 2003; Kitowska et al. 2008). In a murine model of radiation induced fibrosis, arginase 1 was increased in IMs to a greater extent than AMs, both at baseline and in fibrosis (Meziani et al. 2018). However, mice with selective arginase 1 deletion are vulnerable to liver fibrosis in some instances, so its role in fibrosis is not entirely consistent (Pesce et al. 2009).

1.7.3.2 Secretion of Growth Factors

AMs are prolific secretors of growth factors, to maintain tolerogenic homeostasis in the lung. Changes in these mediators have been studied widely in IPF. TGF-β is one of the most implicated profibrotic mediators in lung fibrosis. It is increased in BAL in IPF, as well as other profibrotic diseases (Khalil et al. 1989; Jagirdar et al. 1996). As previously mentioned, AMs are a major source of TGF-β for tolerance and self-renewal, and TGF-β expression is increased in AMs from patients with IPF and other fibrotic lung diseases, as well as in AMs from murine

models of lung fibrosis (Murray et al., 2011; Larson-Casey et al., 2016). TGF-β signalling is proposed to trigger EMT and fibroblast activation via galectin-3, which is also increased in IPF AMs (Nishi et al. 2007).

1.7.3.3 Secretion of Cytokines

As key innate immune regulators, macrophages release many chemokines and cytokines. IL-10, an anti-inflammatory mediator released with TGFβ to maintain homeostasis, is increased in IPF AMs (Freeburn, Armstrong and Millar, 2005; Larson-Casey et al., 2016). Whilst some models show IL-10 is protective against lung fibrosis (Nakagome et al. 2006), others show knockout is protective (Barbarin et al. 2004). This exemplifies the temporal and cell specific nature of the role of cytokines in disease progression.

CCL18 is a potent driver of myofibroblast differentiation, secreted by classically differentiated M2 macrophages. This marker is also increased in IPF AMs (Prasse et al., 2006; Schupp et al., 2015), and levels in BAL are inversely correlated with lung function (Prasse et al. 2006). A downstream signalling molecule from CCL18, Chintinase 3-like 1 (CHI3L1) is also increased in IPF AMs and BAL levels inversely correlate with survival time (Y. Zhou et al. 2014). This is therefore likely to be part of the axis through which CCL18 is involved in fibrosis.

1.7.3.4 Secretion of ECM and ECM Modifying Enzymes

ECM maintenance is controlled in part by AMs, which are capable of secreting both ECM components such as collagen, and proteinases for their breakdown such as MMPs, as well as taking up ECM components. The gene encoding collagen I (*Col1a1*) is increased in IPF AMs (Tsitoura et al. 2019; 2021). The excess release of collagen is likely to stiffen ECM and worsen fibrosis.

IPF AMs also express increased MMPs including MMP-8 (Craig et al. 2014a), MMP-9 (Henry et al. 2002), MMP-3 (Yamashita et al. 2011) and MMP-1 (Selman et al. 2000; Zuo et al. 2002). MMP-7, which is expressed by AMs and epithelial cells, is also significantly increased in IPF BAL, although upregulated production has only been identified in epithelial cells in IPF tissue (Zuo et al. 2002).

MMPs have diverse, overlapping, and contrasting roles in fibrosis. For example, MMP-1, also known as collagenase, is strongly upregulated in IPF patient BAL and correlates with worse disease outcomes. However, at a molecular level, MMP-1 breaks down fibrillar collagen in fibroblasts thereby reducing tissue rigidity. This contrast reflects the intricate balance of ECM degrading enzymes that is upset in IPF, causing more damage than repair (Chuliá-Peris et al. 2022).

Similarly, MMP-7 can degrade decorin, a proteoglycan responsible for TGFβ inactivation (Imai et al., 1997; Zhang et al., 2009). This function contrasts with the MMP-7 increase in IPF BAL, and the protective nature of MMP7 knock out in murine bleomycin induced fibrosis (Zuo et al. 2002). Another example of this fine balance is MMP-9. MMP-9 deletion in mice does not protect against bleomycin induced fibrosis (Betsuyaku et al. 2000), despite its increase in IPF BAL and the capacity of MMP-9 to proteolytically activate latent TGFβ (G. Jenkins 2008; Kobayashi et al. 2014). Instead, overexpression of MMP-9 by AMs in mice was protective against fibrosis (Cabrera et al. 2007).

This data shows that AM expression of MMPs must be interpreted very carefully, to differentiate causal and reactive outputs. This is likely due to the dual role of many MMPs in

breaking down ECM and activating growth factors and other proteinases that potentiate fibrosis.

1.7.3.5 Functional Changes

The function of IPF macrophages is less well studied than their profibrotic outputs. However, efferocytosis and phagocytosis remain crucial to homeostatic maintenance in the lung, meaning function is crucial to avoid aberrant wound healing. Morimoto et al. (2012) demonstrated an increased number of apoptotic cells in the BAL from IPF patients. It is not clear whether this is due to increased apoptotic cell burden in the airways, decreased efferocytic capacity, or both. As efferocytosis polarises macrophages towards a pro-resolution phenotype (Freire-de-Lima et al. 2006), continuous efferocytosis may drive aberrant macrophage polarisation in IPF. Alternatively, if AM efferocytosis is impaired in these patients, increased secondary necrosis and DAMP release may drive repetitive epithelial injury (Henson and Tuder, 2008; Morimoto, Janssen and Terada, 2012). It is possible that both these pathways contribute as IPF progresses. Delivery of apoptotic AECIIs intratracheally in mice is sufficient to drive lung fibrosis via macrophage profibrotic mediator release, emphasising the relevance of the pathway (K. K. Kim et al. 2018).

Impaired phagocytosis of *Staphylococcus aureus* was demonstrated in murine AMs following bleomycin exposure (Warheit-Niemi et al. 2022). Although there is some evidence implicating unresolved infections in IPF disease mechanism, in the current paradigm of aberrant wound healing, it is hard to determine what the effect of impaired phagocytosis may be in normal progression of IPF. However, impaired phagocytic capacity likely increases the risk of infection driven acute exacerbations in IPF patients.

Dysregulated lipid metabolism has been identified in the whole IPF lung (Suryadevara et al. 2020), in fibroblasts, epithelial cells and AMs. Specifically, lipid laiden AMs are described in some IPF animal models (Yasuda et al., 1994; Azuma et al., 2005). AMs partake in lipid metabolism in the lung through their uptake and recycling of surfactant. There are several genetic loci linked with IPF risk located in genes related to surfactant proteins, highlighting this pathway as one with possible mechanistic involvement, however the precise mechanism remains unclear. AMs also metabolise lipids during efferocytosis, which introduces an increased lipid burden in the cell. This efferocytosis and lipid processing axis has been implicated in pulmonary fibrosis in murine models (Romero et al. 2015).

Category	Marker	References	AMs		IMs		Relevance
			H	M	H	M	
Profibrotic Markers	Arginase	(Mora et al., 2006, Endo et al., 2003; Kitowska et al., 2008, Meziani et al., 2018)	↑	↑		↑	Competes with iNOS to convert arginine into collagen precursor, causing polarisation to pro-resolution phenotype.
	CD206	(Pechkovsky et al., 2010; Zhou et al., 2014, Ji et al., 2014)	↑	↑		↑	Scavenger receptor with role in suppressing inflammatory response. Classic marker of pro-resolution macrophages.
	CD163	(Gibbons et al., 2012; Vasarmidi et al., 2019)	↑				Scavenger receptor associated with pro-resolution macrophage polarisation.
Growth Factors	TGFβ	(Murray et al., 2011; Larson-Casey et al., 2016)	↑	↑			Key growth factor implicated in mediating fibrosis via effects on fibroblasts and epithelial cells.
	Galectin 3	(Nishi et al. 2007)	↑				Downstream signalling molecule from TGFβ.
	PDGFA	(Martinet et al. 1987)	↑				Growth factor implicated in fibrotic responses; receptor inhibited by Nintedanib.
Cytokines	IL-10	(Freeburn, Armstrong and Millar, 2005; Larson-Casey et al., 2016)	↑				Cytokine responsible for anti-inflammatory environment in the lungs, induces pro-resolution macrophages.
	CCL-18 CHI3L1	(Schupp et al., 2015; Prasse et al., 2006) (Zhou et al., 2014)	↑				Potent activator of myofibroblast differentiation secreted by pro-resolution macrophages and its downstream signalling molecule, both inversely correlated with disease severity.
	IL1β	(Nagai et al. 1991; Kline et al. 1993)	↑				IL1β-IL-17 signalling axis highlighted in murine fibrosis models (Wilson et al. 2010).
	IL-13	(Hancock et al. 2012)	↑				Induces TGFβ expression via the IL13α2 receptor (Fichtner-Feigl et al., 2005).
ECM	Collagen 1A1	(Tsitoura et al. 2019; 2021)	↑				Key cytoskeletal protein associated with scar deposition as IPF progresses.
	Osteopontin	(Tsitoura et al. 2019; 2021)	↑				Cytoskeletal component associated with increased stiffness in the ECM. Expression correlates with disease severity.
	MMP8	(Craig et al., 2015, 2014)	↑				Collagen I break down. Increased in IPF BAL.
	MMP9	(Henry et al. 2002)	↑				TGFβ activation. Increased in IPF BAL. Overexpression protective and deletion not protective in murine fibrosis.
	MMP3	(Yamashita et al. 2011)	↑				Pro-MMP activation and ECM breakdown. Increased in IPF BAL.
	MMP1	(Selman et al. 2000; Zuo et al. 2002)	↑				Collagen breakdown. Upregulated in IPF BAL and correlates with worse disease outcomes.

	MMP7	(Zuo et al. 2002)	↑ ?				Degrades decorin, which is responsible for TGFβ degradation (Imai et al., 1997; Zhang et al., 2009). *Increased in IPF BAL. Expression demonstrated in AMs at baseline, although increased expression so far demonstrated in IPF epithelial cells only* (Zuo et al. 2002). Knockout protective in murine lung fibrosis (Zuo et al. 2002).
Function	Efferocytosis	(Morimoto, Janssen and Terada, 2012)	↓ ?				Increased apoptotic cells in BAL from IPF patients. *Increased burden or impairment in efferocytosis or both.*
	Phagocytosis	(Warheit Niemi et al., 2022)		↓			Impaired phagocytosis of *Staphylococcus aureus* in AMs from bleomycin induced murine model.
	Iron processing	(Puxeddu et al., 2014, Allden et al., 2019)	↓				Iron laden macrophages and increased transferrin identified in IPF BAL (Puxeddu et al., 2014). Subset of IPF AMs express no CD71 iron uptake receptor and therefore cannot take up iron. Frequency of $CD71^-$ AMs correlate with disease severity (Allden et al. 2019).
	Lipid processing	(Suryadevara et al., 2020, Azuma et al., 2005; Yasuda et al., 1994).		↓			Lipid laden macrophages in IPF animal models.

Table 1.2 Summary of the changes observed in lung resident macrophages in IPF (H) and murine models of IPF (M). *CD: cluster of differentiation. TGFβ: transforming growth factor β. VEGFA: vascular endothelial growth factor A. iNOS: inducible nitric oxide synthase. PDGFA: platelet derived growth factor A. IL: interleukin. CCL: CHI3L1: MMP: matrix metalloproteinase. BAL: bronchoalveolar lavage. IPF: idiopathic pulmonary fibrosis. AM: alveolar macrophage. IM: interstitial macrophage. H: human. M: murine. ? indicates indeterminate evidence, evidence highlighted using italics in the relevance column.*

1.8 HYPOXIA

Oxygen availability differs greatly between organs, often present at a gradient decreasing with increased distance from oxygenated blood supply. As such, oxygen acts as an environmental factor key to the organ specific specialisation of different cell types. Different organs adapt to maintain homeostasis at different physiologic oxygen levels.

Organs with limited blood supply and high metabolic demand operate in constant and expected hypoxia, known as physiologic hypoxia. These organs include the spleen and bone marrow (Caldwell et al., 2001; Carreau et al., 2011). Organs such as the liver or kidneys have more blood supply, and thereby have higher oxygen availability, although this remains much lower than normal air (Jagannathan, Cuddapah and Costa, 2016). The lung has one of the highest oxygen availabilities of all organs. Oxygen is present across a gradient, highest in the airways, dropping towards the alveoli and further reducing across the alveolar membrane and towards the interstitium (Carreau et al. 2011).

When homeostasis is disrupted, organs can experience abnormally low oxygen and/or variable oxygen levels. For example, this occurs during inflammation, when dilated blood vessels impair oxygen supply and metabolically active immune cells invade and use available oxygen (Eltzschig and Carmeliet 2011). It can also occur in solid tumours and in areas of occluded blood flow (Begg and Tavassoli 2020). This is known as pathological hypoxia, as it can act as a pathological stimulus to further disrupt homeostasis.

1.8.1 Hypoxia in IPF

It has been suggested by multiple studies that the lungs of IPF patients are subjected to extended periods of hypoxia. IPF patients have an increased burden of nocturnal hypoxaemia,

which correlates with decreased lung function and poor outcomes (Myall et al. 2022). Specifically, there is an established association between OSA and IPF (Bosi et al. 2017), as outlined in section 1.4.2, with OSA likely to cause hypoxic periods in the lung tissue. As fibrosis progresses and airflow is restricted, it stands to reason that this causes further hypoxia in areas of the tissue. Supporting this theory is evidence of stabilisation of the oxygen sensitive transcription factor components hypoxia inducible factor 1α (HIF1α), HIF2α and carbonic anhydrase-XI (CA-XI) in IPF lung tissue (Burman et al. 2018; Khawaja et al. 2020). Brereton et al (2022) have also recently published a cross tissue HIF signalling signature, which predicts clinical outcomes.

It is unclear whether hypoxia plays an initiating role in IPF or a potentiating role in fibrosis once established. This may differ between patient subtypes. For example, those with OSA may suffer epithelial injury due to initial hypoxic insults (due to endoplasmic reticulum (ER) stress and AECI death (Burman et al. 2018)), while other patients may see tissue hypoxia as fibrosis progresses.

1.8.2 Hypoxia Signalling

In general, hypoxia responses have evolved to cope with or combat hypoxia, by driving angiogenesis and metabolic adaptation (Majmundar, Wong and Simon, 2010). Many cellular responses to hypoxia are driven by a family of hypoxia inducible factors (HIF) (Figure 8). HIF isoforms -1, -2 and -3 are all heterodimers of HIFα and HIFβ subunits. HIFβ subunits are constitutively expressed, whilst HIFα subunits are degraded in the presence of oxygen. When oxygen is sufficient, prolyl hydroxylase domain (PHD) enzymes use oxygen to hydroxylate proline residues in HIFα, causing subsequent ubiquitination and proteasomal degradation. Factor inhibiting HIF (FIH) also uses oxygen to inhibit HIF activity. When oxygen is insufficient

to permit degradation, HIFα subunits dimerise with HIFβ and translocate to the nucleus, to act as transcription factors at HIF response elements (HREs) within the genome. HIF isoforms target a range of genetic targets, with some redundancy. Typically, HIF-1 and HIF-2 control expression of genes for the adaptation to low oxygen tensions, such as angiogenic factors and anaerobic metabolic enzymes, whilst HIF-3 acts to negatively regulate these feedback loops. HIF-1 acts more acutely than HIF-2, which persists longer in hypoxic tissue (Majmundar, Wong and Simon, 2010).

There are additional HIF independent hypoxic signalling cascades. For example, PHD enzymes can target other substrates in the presence of oxygen (Webb, Coleman and Pugh, 2009). Additionally, jumonji C domain histone lysine demethylases (JmjC-KDMs) demethylate proteins in hypoxia, although the consequences of these posttranscriptional modifications remain largely unknown (Chopra et al. 2020).

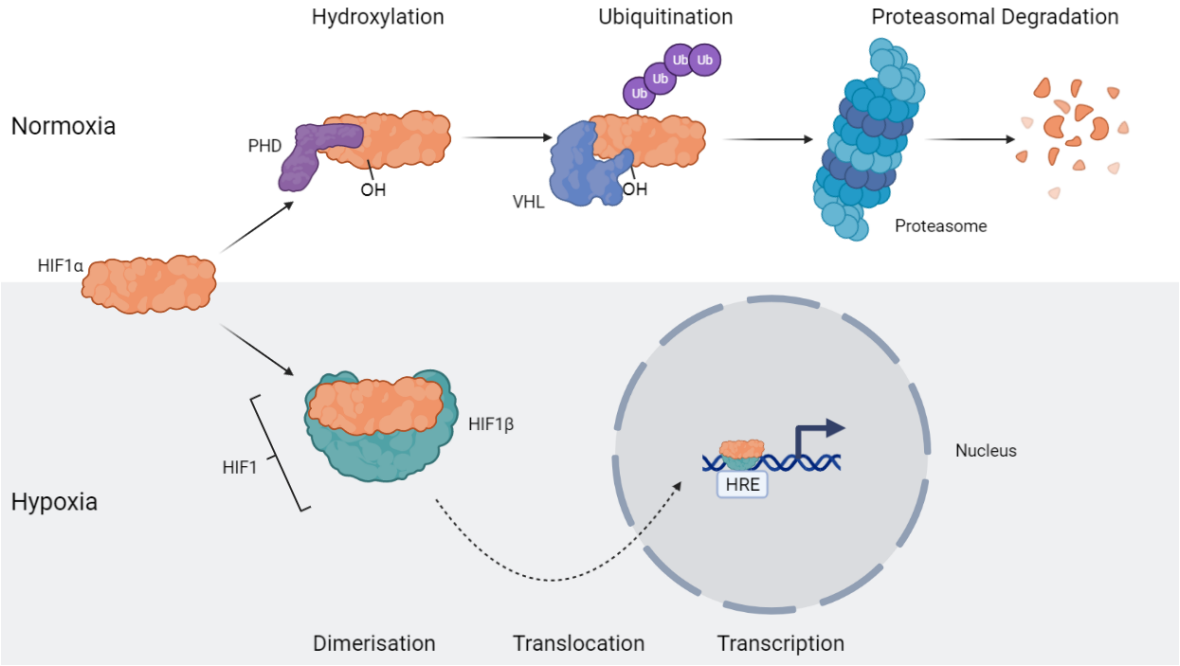

Figure 8 HIF signalling. *In normoxia (white) PHD enzymes bind to HIF1α and add hydroxyl groups in an oxygen dependent way. This tags HIF1α for ubiquitination by Von Hippel–Lindau (VHL) enzyme. Ubiquitination tags the protein for proteosomal digestion, causing the HIF1α to be digested in normoxia, preventing downstream signalling. Meanwhile, in hypoxia (grey) PHD enzymes are inactive due to lack of oxygen, preventing HIF1α digestion. Instead HIF1α dimerises with HIF1B and translocates to the nucleus, where it binds to HIF1 response elements within the DNA, to act as a transcription factor for gene expression. HIF1 is used for an example in this figure, however HIF2 and HIF3 are regulated in the same way, although with different expression patterns and stability, and different target genes. HIF: hypoxia inducible factor, HRE: HIF response element, PHD: prolyl hydroxylase domain, VHL: Von Hippel–Lindau.*

1.8.3 *In Vivo* Evidence for the Role of Hypoxia

In a murine repeated tracheal bleomycin model of lung fibrosis, pimonidazole adducts indicate areas of extreme hypoxia (<1% O_2), particularly focused in AECIIs (Burman et al. 2018). These adducts demonstrate that hypoxia is present in frequently used murine models of pulmonary fibrosis and begins to characterise the degree of hypoxia in the fibrotic lung.

Various studies have extended this work to demonstrate that continuous (14%) and intermittent hypoxia (30-60 second cycles between 21% O_2 and 5-10% O_2 over 8-12 hours) worsen single dose bleomycin induced lung fibrosis following medium term exposure (2-4

weeks) (Table 1.3). The lungs of mice treated with hypoxia and intratracheal bleomycin over several studies showed increased fibrotic area by Masson's Trichrome staining (Burman et al. 2018; Kang et al. 2020), increased fibrotic gene expression (for example *TGFB* and *Col1a1*)(Gille et al., 2018; Xiong et al., 2021), increased collagen deposition (Braun et al., 2018; Burman et al., 2018; Gille et al., 2018; Kang et al., 2020) and increased wet/dry lung weight ratios (Gille et al. 2018), when compared to mice treated with bleomycin alone.

In most studies, fibrosis was not detected in animals exposed to intermittent hypoxia without bleomycin. However, these studies were powered to detect changes after bleomycin and hypoxia challenge. Two studies investigating hypoxia alone saw some changes. Shi et al (2020) demonstrated worsened fibrosis by Masson's Trichrome staining and *TGFB* mRNA expression in animals after intermittent hypoxia exposure (8 hours/day, 4 weeks). Additionally, while Wu et al (2021) reported no histological changes after intermittent hypoxia (12 hours/day, 9 days), gene expression changes in the lung after exposure included pathways of interest in pulmonary fibrosis, such as genes encoding targets of antifibrotic drug Nintedanib, as well as immune pathways and circadian signalling. These studies strengthen the proposal that periods of intermittent hypoxia have the capacity to potentiate pulmonary fibrosis. Further studies are required to understand how hypoxia may act as an initiating factor in disease. Limitations of current studies include relatively short-term periods of intermittent hypoxia, which may be insufficient to detect the accumulation of alveolar damage from intermittent hypoxia alone.

Author	Year	Hypoxia Regime	Hypoxia Effect	Bleomycin Regime	Hypoxia + Bleomycin Effect
Wu	(2021)	21% → 6% → 21% Over 100s. 12h/day. 9 days.	No histologic changes. Changes in circadian rhythm and immune pathway gene expression in lungs.	N/A	N/A
Shi	(2020)	21% → 5% → 21% Over 90s. 8h/day. 28 days.	Increased Masson's Trichrome staining. Increased *TGFB* and *TSP1* expression.	N/A	N/A
Burman	(2018)	14% constant. 14 days.	No effect of hypoxia alone	Single dose (0.04 U) 7 days before hypoxia	Increased Masson's Trichrome staining. Increased total collagen deposition.
Braun	(2018)	21% → 10% → 21% Over 120s. 10h/day. 30 days.	No effect of IH alone	Single dose (1.5 U/kg) 5 days before hypoxia	Increased total collagen deposition.
Kang	(2020)	21% → 7% → 21% Over 60s. 8 h/day. 14 days before BLM, 28 days after BLM.	Increased immune cell count in BAL. Alveolar damage detected.	Single dose (0.01 U) after 2 weeks of hypoxia	Increased Masson's Trichrome staining. Increased total collagen deposition.
Xiong	(2021)	21% → 10% → 21% Over 90s. 8 h/day. 4-21 days.	No effect of IH alone	Single dose (3.0 mg/kg) 24h before hypoxia	Increased C*ol1a1* and *TGFB* expression (d8). Increased ashcroft score (d21). Increased hydroxyproline (d21).
Gille	(2018)	21%-->6%-->21% Over 90s. 8 hours/day. 21 days.	No effect of IH alone	Single dose (3.5 unit/g) 24h before hypoxia	Increased BAL cell count. Increased wet/dry lung weight ratio. Increased C*ol1a1*, *TGFB*, *FIN*, *CTGF* expression. Increased total collagen deposition.

Table 1.3 In vivo effects of hypoxia with and without bleomycin. *Table summarising studies which investigate the effect of hypoxic exposures on murine lung fibrosis markers with and without bleomycin treatment. s: seconds. h: hours. IH: intermittent hypoxia. BAL: bronchoalveolar lavage fluid. TGFB encodes TGFβ, TSP-1 encodes thrombospondin 1, Col1a1 encodes collagen I, Fin encodes fibronectin, CTGF encodes connective tissue growth factor.*

Some murine studies explored the mechanism by which hypoxia causes reported profibrotic effects. Burman et al (2018) demonstrate that hypoxic AECIIs colocalise with areas of endoplasmic reticulum stress, marked by C/EBP homologous protein (CHOP) activation. CHOP knockout proved protective against hypoxic worsening of bleomycin driven fibrosis, implicating epithelial ER stress and apoptosis in fibrosis. Corroborating this finding, Shi et al (2020) demonstrated that ER stress attenuator tauroursodexycholic acid (TUDCA) was able to rescue the hypoxic worsening of bleomycin induced fibrosis.

To elucidate the role of fibroblast HIF1α signalling in bleomycin induced fibrosis, Goodwin et al (2018) exposed fibroblast specific HIF1α knockout mice to bleomycin and reported a partial rescue of fibrotic progression. Inhibition of glycolysis in these animals also rescued fibrotic development, implicating HIF1α mediated fibroblast glycolysis in bleomycin induced fibrosis. In contrast to this, epithelial cell specific HIF1 and HIF2 knockout was not protective against exaggerated bleomycin fibrosis following continuous hypoxia (Burman et al. 2018). This evidence demonstrates the cell specific complexity of the role of hypoxia, and hypoxia dependent and independent HIF signalling, in the development and potentiation of fibrosis.

1.8.4 The Effects of Hypoxia on Stromal Cells and Extracellular Matrix

Several studies have examined the effects of hypoxia on lung stromal cells *in vitro*. This corroborates *in vivo* evidence for the profibrotic potential of hypoxia, translates it into human cells and allows for mechanistic investigation.

1.8.4.1 Profibrotic Effects of Hypoxia on Pulmonary Fibroblasts

In vitro evidence demonstrates the profibrotic capacity of hypoxia on lung fibroblasts and epithelial cells. Hypoxia exposure (between 1-3% O_2 in the studies described) *in vitro* drives

myofibroblast differentiation (demonstrated by αSMA fibre development) (Robinson et al., 2012; Aquino-Gálvez et al., 2019), proliferation (Mizuno et al., 2009; Bodempudi et al., 2014; Senavirathna et al., 2018), collagen production (Robinson et al. 2012), migration (S. H. Jeong et al. 2022), and invasion (S. H. Jeong et al. 2022).

Several overlapping mechanisms have been suggested for these changes in fibroblasts. HIF2α has been implicated in increased proliferation, both by increasing nuclear factor of activated T-cells (NFAT) signalling driving G1/S cell cycle stage (in normal and IPF fibroblasts in response to hypoxia) (Senavirathna et al. 2018), and by increasing hypoxamir micro RNA (miR)210 expression, resulting in repression of downstream MAX Network Transcriptional Repressor (Mnt), an inhibitor of c-Myc driven cell proliferation mediator in IPF fibroblasts (Bodempudi et al. 2014). Meanwhile, HIF1α siRNA knockdown reduces hypoxia-augmented myofibroblast differentiation in response to TGF-β, implicating it in this process (Goodwin et al. 2018). HIF1α has also been implicated in increased expression of collagen modifying enzymes Lysyl Oxidase Like 2 (LOXL2) and Procollagen-Lysine,2-Oxoglutarate 5-Dioxygenase 2 (PLOD2) in fibroblasts in hypoxia and pseudohypoxia, resulting in increased pathologic pyridinlone collagen crosslinking and increased ECM stiffness (Brereton et al. 2022).

Histone deacetylase 3 (HDAC3) has been implicated in mediating the increased migratory responses of fibroblasts in hypoxia (S. H. Jeong et al. 2022) and global DNA hypermethylation has also been identified in myofibroblasts differentiated in hypoxia (Robinson et al. 2012), indicating an epigenetic element in the control of this response.

1.8.4.2 Profibrotic Effects of Hypoxia on Pulmonary Epithelial and Endothelial Cells

As epithelial cell injury and apoptosis is a key proposed disease mechanism, it is crucial to note that Burman et al (2018) demonstrated that hypoxia mediates epithelial cell apoptosis *in vitro* due to ER stress and subsequent CHOP signalling. Additionally, primary AECIs in hypoxia expressed increased cytoskeletal and fibroblast markers *in vitro*, indicating that hypoxia drives EMT. HDAC3 was implicated in facilitating EMT via Akt signalling in hypoxia (S. H. Jeong et al. 2022).

Some work has also explored the effects of hypoxia on lung endothelial cells. One study comparing endothelial cells from control and bleomycin treated mice demonstrated that some markers of endothelial injury, pro-fibrotic mediators, including PDGF, and collagen synthesis were increased by hypoxia in all endothelial cells. However, bleomycin exaggerated this effect, predisposing endothelial cells to release pro-fibrotic mediators, synthesise collagen and αSMA and express mesenchymal transition markers in hypoxia. Some of these changes, including αSMA generation, were colocalised with HIF2α stabilisation, implicating its transcriptional programs in the response (Akahori et al. 2022).

1.8.5 Hypoxia Effects on Immune Cells

The effects of hypoxia on immune cells have been investigated in many organs. Whilst physiological hypoxia helps regulate proper immune cell functions in areas like germinal centres (S. H. Cho et al. 2016), the effects of pathological, confused hypoxia has organ specific and sometimes detrimental effects. Immune cell function has been best studied in the pathologically hypoxic tumour microenvironment (Begg and Tavassoli 2020). Additional studies have interrogated the effects of 'inflammatory hypoxia' surrounding areas of immune cell

infiltration (Eltzschig and Carmeliet 2011). Studies emphasise a strongly tissue specific effect of hypoxia. In some contexts hypoxia drives immunosuppression, while in others it drives immune activation.

This is unsurprising when considering the complex relationship between hypoxia and inflammation (Cramer et al. 2003). Hypoxia and immune signalling pathways overlap. For example, the PI3K/Akt and MAPK/ERK pathways can drive HIFα stabilisation and nuclear accumulation respectively (Sang et al. 2003; Zhen Zhang et al. 2018), whilst ROS can negatively regulate PHD enzymes, causing HIFα stabilisation (Cash, Pan and Simon, 2007). Additionally, PHDs hydroxylate other targets, such as IKKB when oxygen is present, causing oxygen dependent inhibition of the NFκB inflammatory signalling cascade (Scholz et al. 2013). Reciprocally, NFκB is key for transcription of HIF1α and therefore accumulation in hypoxia (Rius et al. 2008).

1.8.5.1 Macrophages

Very few studies have investigated the effects of hypoxia on lung macrophages, particularly in the context of fibrosis. However, studies of macrophages in other contexts can help to understand the potential effects of hypoxia and hypoxic responses in lung macrophages. Most of this literature investigates hypoxia in tumour associated macrophages.

Takeda et al (2010) were the first to identify differential roles of HIF1 and HIF2 signalling in macrophage polarisation and plasticity in normoxia. Independent of hypoxia, HIF1α accumulation drives iNOS activation and inflammatory polarisation of monocyte derived macrophages, whilst HIF2α accumulation causes arginase expression and polarisation towards a pro-resolving phenotype. Given that hypoxia induces HIF1 and HIF2 response gene expression

changes, hypoxia likely contributes to macrophage polarisation. Indeed, similar roles for HIF1α and HIF2α stabilisation in macrophage polarisation have been identified across various hypoxic disease states, such as the RA joint and solid tumour (Tazzyman et al. 2014). The sequential stabilisation of HIF1α followed by HIF2α has been shown to progress macrophage function from proinflammatory to immunosuppressive over time in some contexts. However, given the tissue specific complexity of macrophage differentiation, physiological vs pathological hypoxia and macrophage function, it is difficult to predict the outcome of hypoxic challenge in pulmonary macrophages.

1.9 Hypothesis and Aims

There is a strong body of evidence demonstrating the role of hypoxia in the potentiation of IPF. Most work has characterised the effects of hypoxia on animal models and single cell models of human stromal cells. This work is yet to be translated into a complex model of human lung tissue. Additionally, whilst macrophages are strongly implicated in IPF disease progression, and hypoxia signalling can induce macrophage polarisation, the effects of hypoxia on lung resident macrophages in the context of fibrosis has not been investigated. Therefore, I hypothesise that:

Hypoxia can cause and/or potentiate profibrotic effects in the IPF lung, directly altering AM phenotype and function and causing multi-cellular effects in precision cut lung slices.

In investigating this hypothesis, the thesis aimed to:

(1) Characterise human AM phenotype and function in hypoxia,

(2) Define the role of HIF1 transcriptional programs on AM function in hypoxia,

(3) Characterise AM metabolic capacity in normoxia and hypoxia,

(4) Characterise the effects of hypoxia on markers of fibrosis in human precision cut lung slices (PCLS)

(5) Demonstrate the role of HIF1 in the profibrotic effects of hypoxia in PCLS.

CHAPTER 2: METHODS

2.1 ETHICAL APPROVAL, RECRUITMENT AND SAMPLES

2.1.1 Lung Tissue

Lung tissue samples were obtained from patients who were having lung tissue removed during a lobectomy, pneumonectomy, or wedge resection at the Queen Elizabeth Hospital in Birmingham. Most patients received these surgeries as part of their clinical treatment for lung cancer.

Adult patients undergoing the applicable lung resection surgeries were eligible for consent under ethical approval granted by the Regional Ethical Approval Committee (REC: 17/WM/0272). Patients provided written, informed consent prior to surgery, and demographic data such as smoking status and lung function were recorded. Following removal, tissue beyond the tumour margins that was surplus to histopathological examination was obtained for laboratory research. This tissue was stored in 0.9% saline at 4°C until processing within 18 hours.

For this study, patients were excluded if they were current or recent ex-smokers (quit within 4 years of surgery), or if they suffered from chronic obstructive pulmonary disease. Additional exclusion criteria included the use of immunomodulatory drugs and recent exposure to chemotherapy or immunotherapy.

2.1.2 Blood

Blood was obtained under ethical approval from the University of Birmingham Ethical Approval Committee (approval number: ERN 12-1185R2). Healthy volunteer participants were

employees of the University of Birmingham and provided written consent prior to donating blood. Donors were aged 19-65 and self-reported to be in good health.

Phlebotomy was performed by a trained phlebotomist. Peripheral venous blood was collected into 6ml vacutainer tubes (BD Biosciences. Catalogue number: 367886) containing sodium heparin (95 United States Pharmacopeia units).

2.2 Tissue Culture

Tissue culture was performed using aseptic technique with a class II biological safety cabinet. Unless otherwise stated incubations were performed at 37°C, 5% CO_2.

2.2.1 Primary Cell Isolation and Culture

2.2.1.1 Alveolar Macrophage Isolation

Lung tissue sections were stored at 4°C in 0.9% saline until use, for maximum 18 hours. AMs were isolated as summarised in Figure 2.1. Tissue was lavaged by flushing 0.9% saline through visible airways using a 25-gauge needle and intravenous giving set. Lavage continued until the saline ran clear. Cells from lavage fluid were collected by centrifugation (500 x g, 5 minutes, 4°C) and resuspended in 0.9% saline. Up to 18 ml saline mixture was gently layered on 12 ml Lymphoprep™ (STEMCELL. Catalogue number: 07861) in a 50 ml Falcon tube, and gradients were centrifuged to isolate a buffy coat (800 x g, 30 minutes, 4°C, 0 break and 1 acceleration). Buffy coat was isolated using a Pasteur pipette, and cells were washed in PBS (500 x g, 10 minutes, 4°C).

Cells were counted on a fast counter slide, using trypan blue staining to exclude dead cells. These AMs were then plated in supplemented RPMI (Roswell Park Memorial Institute Medium (RPMI) 1640 media supplemented with 10% FBS, 100 U/mL penicillin, 100 µg/mL streptomycin

and 2 mM L-glutamine (Sigma-Aldrich)). AMs were seeded at $1x10^6$/well in 6 well plates, $2.5x10^5$/well in 24 well plates or $5x10^4$/well in 96 well plates. Cells were left to adhere overnight, before fresh supplemented RPMI was added to remove debris. AMs were used as soon as possible, and not beyond 2 days after tissue processing.

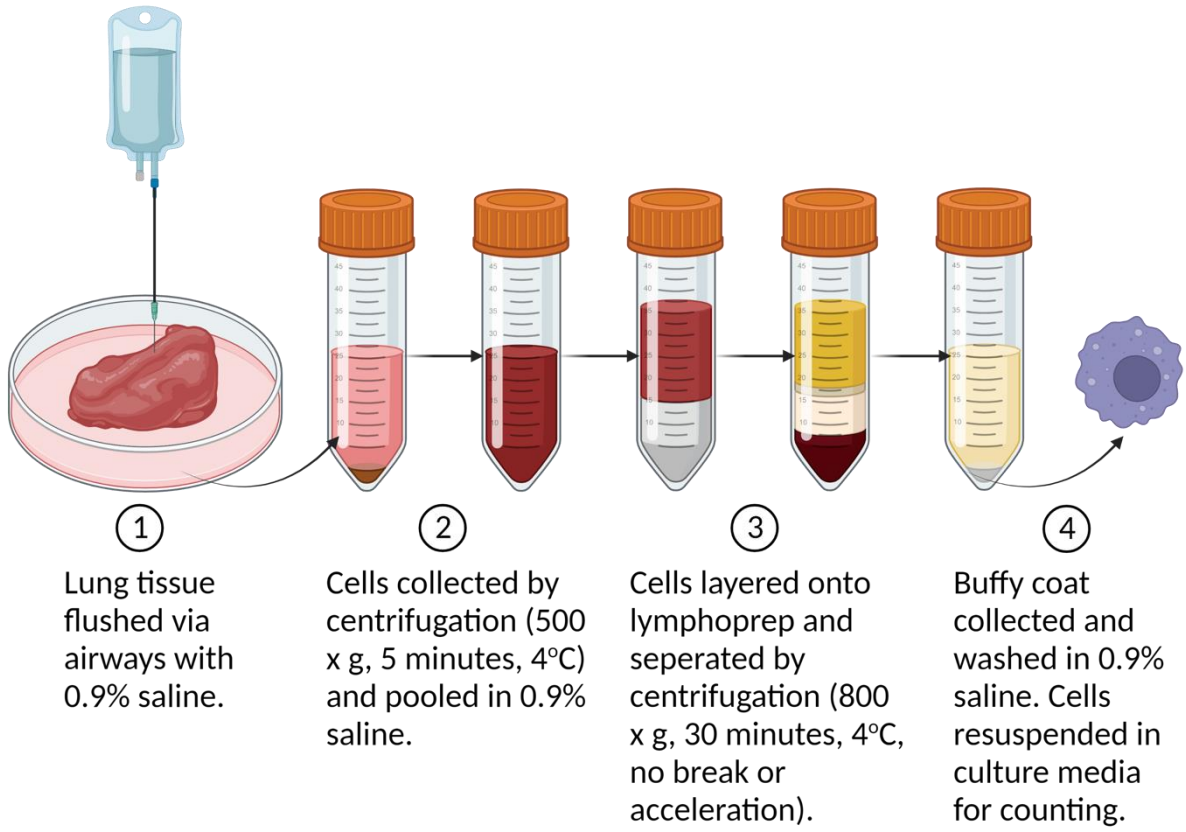

Figure 2.1 Alveolar macrophage isolation from human lung tissue. *(1) Lung tissue was transferred into a petri dish and flushed with 0.9% saline, using a saline bag, giving set and 25-gauge needle. Saline was flushed through visible airways in the tissue. (2) Cell pellets were pooled by centrifugation (500 x g, 5 minutes, 4°C) and resuspended in saline. (3) Up to 18 ml cell suspension was layered over 12 ml lymphoprep, and gradients were separated by centrifugation (800 x g, 30 minutes, 4°C). (4) Buffy coat was isolated using a Pasteur pipette and cells were washed in saline. Cells were then resuspended in culture media and counted.*

2.2.1.2 Neutrophil Isolation

Neutrophils were isolated from the whole blood of healthy volunteers, as described in section 2.1.2. 2% dextran in 0.9% saline was added to blood at a ratio of 1:6, resulting in a final dextran

concentration of 0.33%. The blood/dextran mixture was gently mixed and allowed to sediment for 30-40 minutes, until a clear buffy coat layer became visible.

For neutrophil separation from PBMCs, biphasic Percol gradients were generated, as depicted in Figure 2.2. Percol (Sigma-Aldrich. Catalogue number: P4937) was diluted to 90% using 9% saline to generate stock Percol. Stock Percol was then diluted in 0.9% saline, to generate 80% stock Percol (1 stock Percol : 3 0.9% saline) and 56% stock Percol (7 stock Percol : 6 0.9% saline). 5 ml 56% stock Percol was layered into a 15 ml falcon tube, then 2.5 ml 80% stock Percol was slowly layered under 56% Percol layer, using a Pasteur pipette.

Buffy coat from sedimented blood was slowly layered onto the top of the 56% stock Percol layer, held at a 45^{o} angle, using a Pasteur pipette. When all buffy coat was layered over the gradient, tubes were centrifuged (470 x g, 20 minutes, 0 brake, 0 acceleration). This resulted in a peripheral blood mononuclear cells (PBMCs) band at the 56% interface, and a neutrophil band at the 80% interface, with remaining blood cells pelleted at the bottom of the tube. (Figure 2.2) To maximise purity, PBMCs and plasma were removed first using a Pasteur pipette. Using a fresh pipette, neutrophils were next isolated into sterile phosphate buffered saline (PBS) and topped up to 15 ml with PBS. Cells were pelleted (250 x g, 10 minutes) and gently resuspended in serum-free RPMI (RPMI 1640 media supplemented with 100 U/mL penicillin, 100 µg/mL streptomycin and 2 mM L-glutamine) for counting.

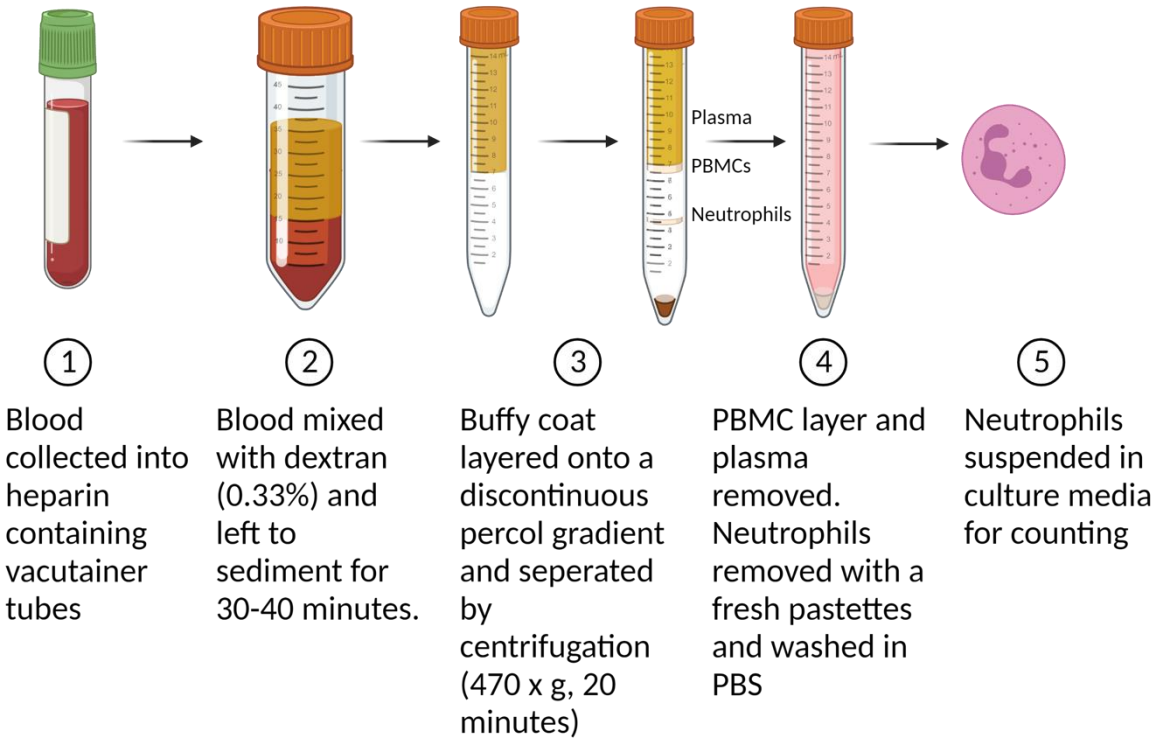

Figure 2.2 Neutrophil isolation from heparinised whole human blood. (1) Human blood was isolated into a heparin containing vacutainer (95 United States Pharmacopeia Units) by a trained phlebotomist. (2) Blood was mixed with dextran (0.33%), gently mixed and allowed to sediment until a defined buffy coat layer appeared. (3) Buffy coat was isolated and transferred gently onto a discontinuous Percol gradient in a 15 ml Falcon tube. PBMCs and neutrophils formed distinct bands in the gradient following centrifugation (470 x g, 20 minutes, room temperature). (4) The PBMC and plasma layers were removed using a Pasteur pipette to avoid contamination. Subsequently, the neutrophil layer was isolated with a fresh pipette, and neutrophils were washed in PBS (250 x g, 10 minutes, room temperature). (5) Cells were gently resuspended in cell culture media and counted. PBMC: peripheral blood mononuclear cells. PBS: phosphate buffered saline.

2.2.1.3 Differential Cell Counts by Cytospin

Purity of primary cell isolations was assessed by cytospin. Cells were loaded into a cytospin cassette (a funnel, filter paper and frosted glass slide, held by a cassette case), $2x10^5$ AMs or $5x10^5$ neutrophils in 200 µl media. Cytospin cassettes were spun (300 rotations per minute, 5 minutes) in the Shandon Mk II cyto-centrifuge (Thermo Electron Corporation.). Slides were then fixed in 100% methanol for 30 seconds and stained using the RESTAIN® Quick-Diff Kit

(REAGENA. Catalogue number: 102164). Slides were submerged in the cytoplasmic dye (pink) for 30 seconds, then the nuclear dye (purple) for 15 seconds. After washing in ddH_2O, slides were left to dry. Cells were imaged on a light microscope (45x), with 4 fields of view captured for cell counting. Cell types were differentiated by morphology and size.

2.3 Hypoxia Exposure

Cultures were incubated in a hypoxic environment within a Whitley H35 HypoxyStation (Don Whitley Scientific Ltd.). Gas concentrations within the chamber were 1% O_2, 5% CO_2 and 94% N_2. The chamber was maintained at 37°C and 85% humidity. Plates were transferred into the airlock chamber, where gas concentrations were adjusted. This allowed plates to be transferred into the main workstation, using the attached air-tight sleeves and portholes. After transfer into the hypoxystation, the lid of the tissue culture plate was briefly removed to exchange the air within the plate. Plates were left, protected from light where necessary, until they were retrieved for final analysis immediately before use. Some assays were performed within the hypoxystation as specified. Normoxic conditions for comparison were maintained in a normal cell culture incubator, with 5% CO_2 at 37^{o}C. Although these conditions were referred to as 21% oxygen throughout the thesis in accordance with existing literature, approximate oxygen levels are 18.6% in these conditions, when controlling for temperature and humidity (Place, Domann and Case, 2017).

2.4 Bacterial Culture

Streptococcus pneumoniae (SP) (Serotype 14 (NCTC 11902, National Collection of Type Cultures)) was cultured in anaerobic conditions, generated in an anaerogen jar containing an Oxoid™ AnaeroGen™ 2.5 L Sachet (Thermo Scientific. Catalogue number: 10269582). 50 µl live

broth stock was initially cultured in 25 ml Brain Heart Infusion broth (BHI) (Thermo Scientific. Cataolgue number: 53286) for at least 8 hours (shaking 150 rotations per minute, 37°C). This culture was transferred to 500 ml BHI for 16 hours incubation in the same conditions. Bacterial concentrations were established by serial dilution of broth (10^{-1}, 10^{-3}, 10^{-5} and 10^{-7}) onto Oxoid X10 Columbia agar with horse blood (Thermo Scientific. Catalogue number: 12917158) for overnight culture. Colony forming units (CFU) were calculated by counting colonies at the dilution with 2-20 colonies. Once CFU was established, bacteria were heat killed for 2 hours at 70°C. Killing was confirmed by streaking on a fresh Columbia agar with horse blood.

Heat killed bacteria were stained with 10 µg/ml Alexa Fluor 647 NHS Ester molecular probe (Invitrogen. Catalogue number: A37573) in $NaHCO_3$ buffer for 18 hours in the dark. Bacteria were then washed (14000 x g, 3 minutes) 3 times in PBS, for storage at -20°C until use.

2.5 PHAGOCYTOSIS

Phagocytosis was performed by addition of heat killed bacteria to macrophages at a ratio of 10:1, in 24 well plates or chamber well slides. A negative control well was treated with cytoskeleton depolymerising agent Cytochalasin D (Sigma-Aldrich. Catalogue number: PHZ1063) (10 µM) for 30 minutes prior to the addition of bacteria, to control background fluorescence and variability between samples. Following incubation at 37°C, 5% CO_2 for various time points, cells were rinsed with PBS, before harvest for flow cytometry or fixing for immunofluorescent staining.

2.6 EFFEROCYTOSIS

Neutrophils isolated from whole blood as described in Section 2.2.1.2 were suspended at $4x10^6$/ml in serum free RPMI with 5 µM Molecular Probes™ CellTracker™ Deep Red Dye

(Invitrogen. Catalogue number: C34565) dissolved in 20 µl DMSO (Sigma-Aldrich. Catalogue number: D1435). Incubation for 45 minutes allowed for intracellular uptake and metabolism of the dye to a deep red colour (excitation/emission 630/650 nm). Neutrophils were then washed twice in serum free RPMI with high-speed centrifugation (1500 x g, 5 minutes). Stained neutrophils were resuspended at $2x10^6$/ml in serum free RPMI left to enter apoptosis during 24-hour incubation (37°C) in a sealed falcon tube.

Apoptotic neutrophils, resuspended at $2x10^6$/ml in supplemented RPMI, were added to macrophages at a ratio of 4:1 in 24 well plates or microscope chamber well slides. A negative control well was treated with Cytochalasin D (10 µM) for 30 minutes prior to the addition of neutrophils, to control for the adherence of neutrophils to the outside of the cell and autofluorescence of the sample. Following incubation, cells were rinsed twice with ice cold PBS to remove loosely adherent neutrophils before harvest for flow cytometry or fixing for immunofluorescent staining.

2.7 Flow Cytometry

2.7.1 Viability Analysis by Flow Cytometry

For viability analysis, adherent cells were rinsed with PBS. Cells were then incubated with TrypLE™ Express trypsin (ThermoFisher Scientific. Catalogue number: 12605028) for 5 minutes (37°C, 5% CO_2). Trypsin was neutralised with supplemented RPMI and cells were transferred to flow cytometry tubes by vigorous pipetting.

For staining with propidium iodide and annexin V, cells were washed twice in annexin V buffer (ddH_2O containing: 10 mM 4-(2-hydroxyethyl)-1-piperazineethanesulfonic acid (HEPES) (pH7.4), 140 mM NaCl and 2.5 mM $CaCl_2$, filter sterilised at 0.2 µM) (400 x g, 5 minutes, 4°C),

for optimal annexin V binding. AMs were resuspended with Annexin V BV421 (BioLegend. Catalogue number: 640924) (1:50) in annexin buffer, for 15 minutes on ice. Cells were washed twice in annexin buffer (400 x g, 5 minutes, 4°C). For analysis, cells were resuspended in 200 µl annexin buffer. Immediately before sampling, 1% propidium iodide (Sigma-Aldrich. Catalogue number: P4864) was added to each tube.

Flow cytometry was performed on the MACSQuant 10 cytometer (Miltenyi Biotech). Data was analysed on FlowJo software v10 (BD Biosciences). The gating strategy in Figure 2.4 shows how AMs and single cells were identified using forward and side scatter. Subsequently, unstained and single colour controls were used to position quadrants separating double negative, single positive and double positive cells. Beyond this, gates were not changed and 10,000 events were collected in the AM gate for future analysis.

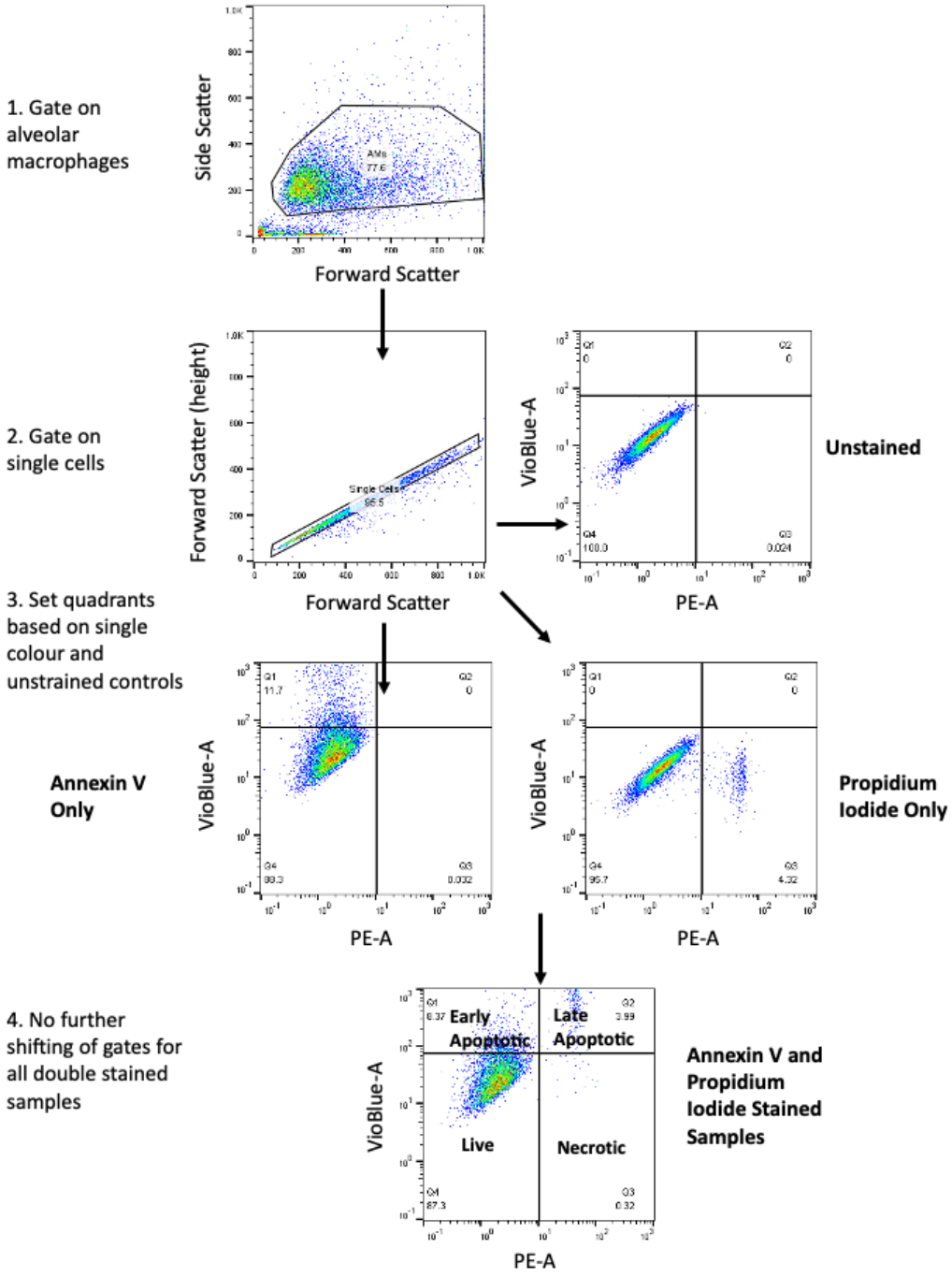

Figure 2.3 Gating strategy to assess alveolar macrophage viability. Events were collected on the MACSQuant 10 flow cytometer. Events of the appropriate size (forward scatter) and granularity (side scatter) for alveolar macrophages were selected for further analysis. Single cells were selected by plotting forward scatter (area) against forward scatter (height), to exclude doublets where these two measures were not proportional. Quadrants dividing stained cells into single and double stained populations were set using unstained cells, assumed to be all double negative on VioBlue and PE staining. These quadrants were adjusted based on single stained controls, to ensure correct placement. These gates were not adjusted between samples.

2.7.2 Functional Assessment by Flow Cytometry

For functional analysis, cells were incubated with TrypLE™ Express trypsin for 5 minutes (37°C, 5% CO_2). Trypsin was neutralised with supplemented RPMI and cells were transferred to flow cytometry tubes by vigorous pipetting. Cells were washed twice in FACS buffer (PBS, 1% BSA (w/v), 1% EDTA (v/v)) (400 x g, 5 minutes, 4°C). $2x10^6$ CFU *Streptococcus pneumoniae* or $2x10^5$ neutrophils respectively were also washed for gating. For analysis, cells were resuspended in 200 µl FACS buffer.

Flow cytometry was performed on the MACSQuant 10 cytometer. Data was analysed on FlowJo software v10. The gating strategies in Figures 2.5 and 2.6 show how AMs and single cells were identified using forward and side scatter. Subsequently, cytochalasin D controls were used to set a gate for phagocytic (Figure 2.5) or efferocytic cells (Figure 2.6). Beyond this point, gates were not changed and 10,000 events were collected in the AM gate for future analysis.

Phagocytosis and efferocytosis results were expressed as median fluorescence intensity (MFI) (calculated on the single cell gate) and as percentages of positive cells. Values were normalised by expressing as a fold change from the cytochalasin D control to account patient variability.

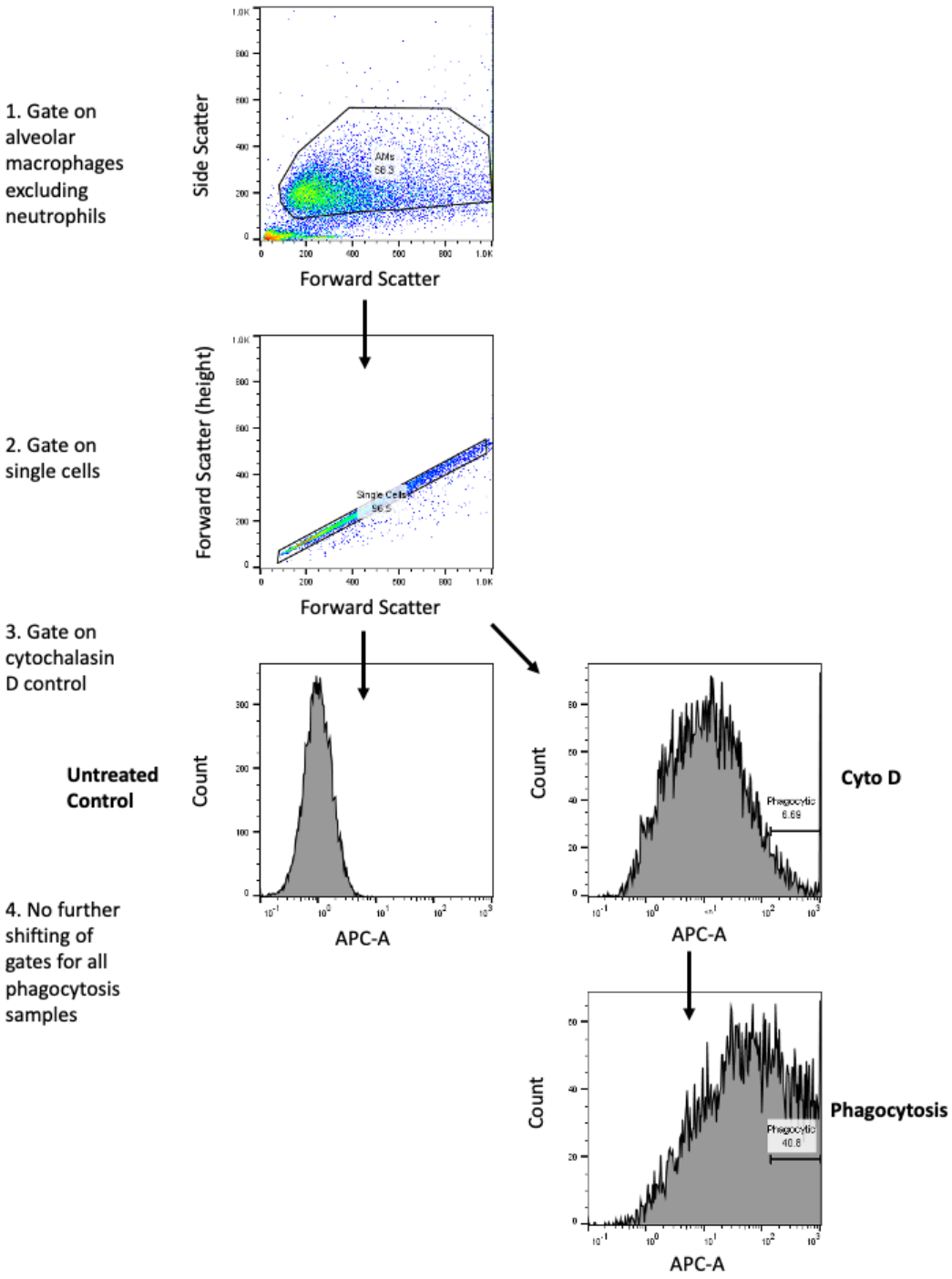

Figure 2.4 Gating strategy to assess alveolar macrophage phagocytosis. Events were collected on the MACSQuant 10 flow cytometer. Events of the appropriate size (forward scatter) and granularity (side scatter) for alveolar macrophages were selected for further analysis. Single cells were selected by plotting forward scatter (area) against forward scatter (height), to exclude doublets where these two measures were not proportional. A histogram of APC staining intensity was used to identify phagocytic cells. A positive gate was set using the cytochalasin D treated control cells. After the gating strategy was set, gates were not moved.

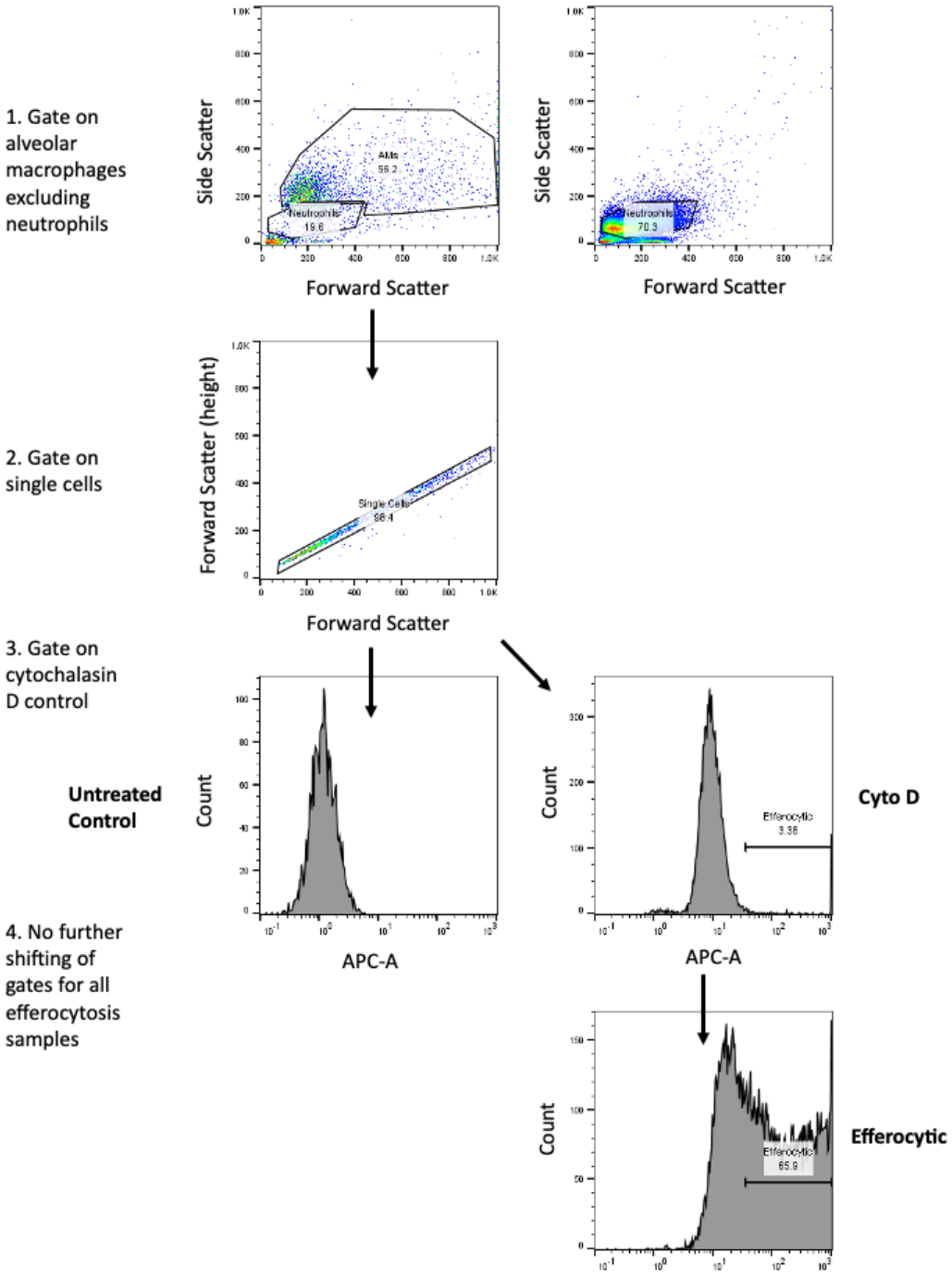

Figure 2.5 Gating strategy to assess alveolar macrophage efferocytosis. Events were collected on the MACSQuant 10 flow cytometer. Alveolar macrophages and apoptotic neutrophils were sampled individually, and gates were drawn around both populations based on size (forward scatter) and granularity (side scatter). The alveolar macrophage gate was adjusted to ensure minimal overlap with the apoptotic neutrophil population. Single cells were selected by plotting forward scatter (area) against forward scatter (height), to exclude doublets where these two measures were not proportional. A histogram of APC staining intensity was used to identify efferocytic cells. A positive gate was set using the cytochalasin D treated control cells. After the gating strategy was set, gates were not moved.

2.8 MOLECULAR BIOLOGY TECHNIQUES

2.8.1 Protein and RNA extraction from cell cultures

2.8.1.1 Protein Extraction from Cells

Following rinsing with PBS, $2.5x10^5$ cells were lysed directly in 400 µl Laemmli buffer (Sigma Aldrich), using manual disruption with a cell scraper. This isolation was performed in the hypoxystation for hypoxia treated cells, to avoid the breakdown of hypoxia dependent proteins before storage. Protein was stored at -80°C until further use.

2.8.1.2 RNA Extraction from Cells

RNA was extracted from cell cultures using the Nucleospin RNA II Kit (Machery Nagel. Catalogue number: 740955.50) according to manufacturer's instructions. Briefly, cells were lysed in 350 µl lysis buffer containing 3.5 µl 2-mercaptoethanol, using a cell scraper for mechanical cell lysis. Lysate was mixed 1:1 with 100% ethanol, before transfer to RNA binding columns. Columns were spun at 11,000 x g for 30 seconds at 4°C. Membrane desalting buffer was then run through the column (350 µl, 11,000 x g, 60 seconds, 4°C). DNA was digested using 95 µl DNAse reaction mixture, added directly to the silica membrane for 15 minutes at room temperature. The membrane was washed first in 200 µl RAW2 buffer, to inactivate DNAse, then twice in RA3 buffer (all 11,000 x g, 4°C). A 2-minute centrifugation at 11,000 x g was performed to dry the silica membrane. Finally, RNA was eluted in 60 µl RNAse free water (11,000 x g, 1 minute, 4°C), into an RNAse free Eppendorf tube. RNA was quantified on the NanoDrop™ 2000 Spectrophotometer (ThermoFisher Scientific. Catalogue number: ND-2000). After calibration with RNAse-free water as a blank, 2 µl samples were loaded onto the stage for assessment of RNA quantity (ng/µl) and 260/280 ratio.

2.8.2 SDS-Page and Western Blotting

2.8.2.1 Gel electrophoresis

SDS- polyacrylamide gel electrophoresis (PAGE) gels were poured into the 1 mm Dual Mini Gel Cast (Atto. AE-6401) for gel dimensions 90 mm (W), 80 mm (H). 10% acrylamide separating gel (10% acrylamide in ddH_2O containing 1% SDS and 20% 1.5 M Trizma (pH 8.8)) was created and crosslinking was activated by the addition of 100 µl 10% ammonium persulfate (APS) and 10ul tetramethylethylenediamine (TEMED). Gels were immediately poured and allowed to set in the mould, topped with isopropanol to ensure level set. Isopropanol was removed and gels were rinsed with ddH_2O.

Stacking gel (4% acrylamide in ddH_2O containing 1% SDS and 20% 0.5 M Trizma (pH 6.8)) was prepared and crosslinking was activated by the addition of 200 µl 10% APS and 15 µl TEMED. Stacking gel was poured into the mould, followed by the addition of a 12-well comb. Gels were allowed to set and kept moist at 4°C until use.

Gels were loaded into the Mini-Slab electrophoresis tank (Atto. Catalogue number: WSE-1165), with running buffer (25 mM Trizma, 192 mM glycine, 0.1% (w/v) SDS in ddH_2O) filling the side and central reservoirs.

Protein samples isolated via trizol extraction, that did not already contain Lamelli buffer, were mixed with 5 µl Lamelli buffer. All samples were boiled at 100°C for 5 minutes and allowed to cool. Combs were gently removed, and wells were rinsed with running buffer using a syringe and needle, to flush out excess gel. End wells were left empty on either side of the gel. 10 µl Colour Pre-stained Protein Standard (New England Bioscience. Catalogue number: P7719S) was loaded where required. 25 µl samples were loaded into subsequent wells.

The Mini-Slab unit was connected to an electrophoresis power supply (Consort). Gels were run at 35 mA (or 70 mA for two gels), maximum 100 V for approximately 1 hour, until proteins were separated across the gel.

2.8.2.2 Western Blot

Gel casts were dismantled gently and the gel was cut free using a scalpel. Gels were carefully transferred into a blotting stack, assembled in a PoweredBLOT ACE semi-dry transfer system (Atto. Catalogue number: WSE-4115). Filter paper, Amersham™ Protran® Premium Western blotting membrane (GE Healthcare. Catalogue number: 10600008), and gels were all soaked in transfer buffer (25 mM Trizma, 192 mM glycine, 10% SDS in 20% methanol). Once saturated, components were stacked according to manufacturer instructions. The transfer system was set for a standard transfer for 45 minutes (or 1 hour for two gels).

Proteins were initially visualised on the membrane by 15 minutes staining in ponceau red (Sigma-Aldrich. Catalogue number: P7170), with gentle shaking on a horizontal rotary shaker. After washing in PBS-T (0.1% Tween 20), membranes were blocked in 5% non-fat milk (Marvel powdered milk), in PBS-T at room temperature for 1 hour with shaking. Following 3x 15-minute washes in PBS-T with shaking, membranes were incubated with primary antibody in 1% non-fat milk PBS-T (Table 2.1), overnight shaking at 4^{o}C. Following 3 further washes as above, membranes were incubated with secondary antibody in 1% non-fat milk PBS-T (Table 2.2), for 1 hour at room temperature with shaking. Finally, membranes were washed 3 times.

Target	Host Species	Concentration	Manufacturer	Catalogue Number
αSMA	Mouse	1:500	Sigma	A5228
Actin	Mouse	1:1000	Sigma	A4700
Collagen I	Rabbit	1:500	Abcam	ab138492
GAPDH	Rabbit	1:10000	Abcam	ab181602
HIF1α	Mouse	1:500	BD Bioscience	10652614

Table 2.1 Primary antibodies used for western blots.

Target Species	Host Species	Manufacturer	Concentration	Catalogue Number
Mouse	Goat	R&D Systems	1:1000	HAF007
Rabbit	Goat	Dako	1:2000	P0448

Table 2.2 Secondary antibodies used for western blots.

2.8.2.3 Protein visualisation

For visualisation, membranes were incubated at room temperature for 5 minutes in electrochemiluminescence (ECL) substrate (WESTAR® Supernova HRP Detection Substrate (GeneFlow. Catalogue number: K1-0068) for low expression targets or Cytvia ECL Western Blotting Reagents (GE Healthcare. Catalogue number: RPN2106) for high expression targets). Excess liquid was removed, and membranes were transferred into the ChemiDoc MP transilluminator (Bio-Rad.). A colorimetric picture was taken for visualisation of the protein ladder. A chemiluminescent picture was taken, using autoexposure and or signal accumulation to optimise image. Images were saved individually and as a merge image, to confirm band size.

Membranes were stripped by incubation with Restore™ Western Blot Stripping Buffer (Thermo Scientific. Catalogue number: 21059) for 15 minutes at room temperature with shaking. Membranes were washed 3 times as above and subsequently re-blocked for further staining as above.

2.8.2.4 Membrane imaging and densitometry analysis

Western blot densities were calculated using Image J/FIJI (V1.52a). Lanes were plotted and visualised using the Image J >Analyse >Gels function. Optical density curves were enclosed using the straight-line tool and area under the curve was measured using the tracing tool (Figure 2.6). Band densities were normalised to an endogenous control protein as a loading control and expressed as a percentage of the endogenous control band density, or as a percentage of a composite value derived from multiple housekeeper proteins.

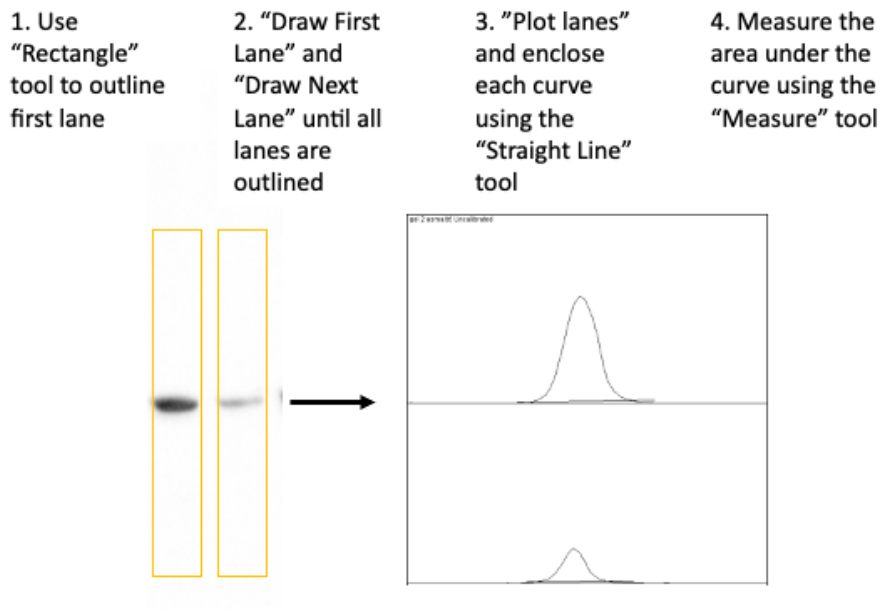

Figure 2.6 Western blot band density assessment using Fiji. *(1) In Fiji, the rectangle tool was used to enclose the first lane of the western blot. (2) The "draw first lane" and "draw next lane" tools were used to replicate this plot across the blot, until all lanes were outlined. (3) The "Plot Lanes" tool was used to plot densitometry across the length of each lane. Peaks, reflecting protein bands, were enclosed using the straight-line tool. (4) The measure tool was used to quantify the area under each curve for further analysis.*

2.8.3 RT-PCR

Reverse transcription polymerase chain reactions (RT-PCR) were run using the QuantiFast Probe RT-PCR Kit (Qiagen. Catalogue number: 204454) according to the manufacturer's

instructions. The eukaryotic 18S rRNA Endogenous Control primer (VIC™/TAMRA™ probe) (Applied Biosystems. Catalogue number: 4310875) was added to each well as a loading control. Target gene primers with FAM probe (TaqMan™, Applied Biosystems. Catalogue number: 4331182) are outlined in Table 2.3.

Target	Catalogue Number	Probe
ACTA2	HS00426835_g1	FAM
Col1A1	HS00164004_m1	FAM
HIF1α	HS00153153_m1	FAM
SLC2A1	HS80892681_m1	FAM
IL1B	HS01555410_m1	FAM
MMP1	Hs00899658_m1	FAM
MMP7	HS01042796_m1	FAM
MMP9	HS00234579_m1	FAM
VEGFA	HS00900055_m1	FAM

Table 2.3 Target primer list for qPCR. *Primers were purchased with the names and assay numbers described above from Applied Biosciences.*

Master mixes were generated for each primer (10.25 µl QuantiFast Probe RT-PCR Master Mix, 0.5 µl target (FAM) primer, 0.5 µl endogenous control primer, 0.25 µl QuantiFast reverse transcriptase mix). 40 ng RNA was loaded in 5 µl RNAse free water. In total, 11.5 µl master mix was loaded per well, along with 5 µl total RNA volume. Plates were briefly spun at 100 x g for 1 minute immediately before running. Plates were loaded into the CFX384 Thermocycler (BioRad). After a 10-minute reverse transcription step at 50°C and 5-minute PCR activation step at 95°C, the following temperature cycles were run 40 times: 10 seconds at 95°C (denaturation) and 30 seconds at 60°C (annealing/extension). Data was analysed using CFX Maestro software (BioRad). Threshold cycles were set for both probes, and Ct values were obtained for each well.

ΔCt values were calculated by subtracting the control Ct value from the treated Ct value. ΔΔCt values were calculated by subtracting the average Ct value of the control from the ΔCt value. ΔΔCt values were expressed as $2^{-\Delta\Delta Ct}$.

2.8.4 ELISA

Supernatants were isolated from cells or PCLS and centrifuged (400 x g, 5 minutes) to remove debris, for assessment by enzyme-linked immunosorbent assays (ELISA). Samples were stored at -80°C until use, with up to 1 freeze thaw cycle on ice acceptable per sample.

VEGF-A was measured using the VEGFA Quantikine ELISA (Biotechne. Catalogue number: DVE00) according to manufacturer's instructions. MMP-7 was measured using the MMP-7 Quantikine ELISA (Biotechne. Catalogue number: DMP700) according to manufacturer's protocol. MMP-1 was measured using the Human Total MMP-1 DuoSet ELISA (Biotechne. Catalogue number: DY901B). TGF-β was measured using the Human TGF-beta 1 DuoSet ELISA (Biotechne. Catalogue number: DY240) according to the manufacturer's protocols. TGF-β was first activated using the Sample Activation Kit (Biotechne. Catalogue number: DY010). 20 µl 1 N HCl was added to 100 µl supernatant, in order to activate TGF-β. After 10 minutes incubation at room temperature, 20 µL of 1.2 N NaOH/0.5 M HEPES was added to neutralise the sample. The subsequent ELISA was run immediately.

For DuoSet ELISA kits, 96 well flat-bottomed ELISA plates were precoated capture antibody at the recommended working concentration in PBS. After overnight incubation, plates were washed in 0.05% PBS-Tween 3 times, before blotting to remove remaining liquid. Subsequently, plates were blocked using the recommended block buffer for 1 hour at room temperature, before washing 3 times. For all ELISAs, standards were diluted to appropriate concentrations

to generate standard curves. Samples and standards were plated, with dilution where necessary, and plates were incubated with gentle shaking for 2 hours. Samples were removed and plates were washed again 3 times. The relevant detection antibody was diluted to the working concentration and added to the plate at 200 µl per well, for a further 2-hour incubation. Plates were washed 3 times. 100 µl of the working concentration Streptavidin-HRP was added to each well for 20 minutes. After 3 final washes, 100 µl substrate solution was added per well. The plate was protected from light for approximately 20 minutes, until the standard curve was sufficiently developed. Finally, 50 µl stop solution was added per well.

Plates were read on the Synergy HT plate reader, to measure absorbance at 450 nm and 570 nm. Standards were used to generate a linear equation, with which to derive the protein content of samples. Background signal detected in media alone was subtracted from all samples.

2.9 Statistical Analysis

Statistical analysis was performed on GraphPad Prism. A statistical decision tree for this thesis is summarised in Figure 2.7. Normality of data was assessed using a Shapiro-Wilk test. Normally distributed data was analysed using a paired or unpaired t-test for two groups or a one-way ANOVA for 3 or more groups. Data that was not normally distributed was analysed using a Wilcoxon matched pairs signed-rank test for paired data, or Mann Whitney test for unpaired data. For 3 or more groups of data that was not normally distributed, a Friedman test followed by Dunn's multiple correction test was performed for matched data, whilst unmatched data was analysed using a Kruskal Wallis test, followed by a Dunn's multiple correction test. A

significance threshold of p<0.05 was used throughout. Graphs were plotted in GraphPad Prism.

Key axis labels are summarised in Table 2.4.

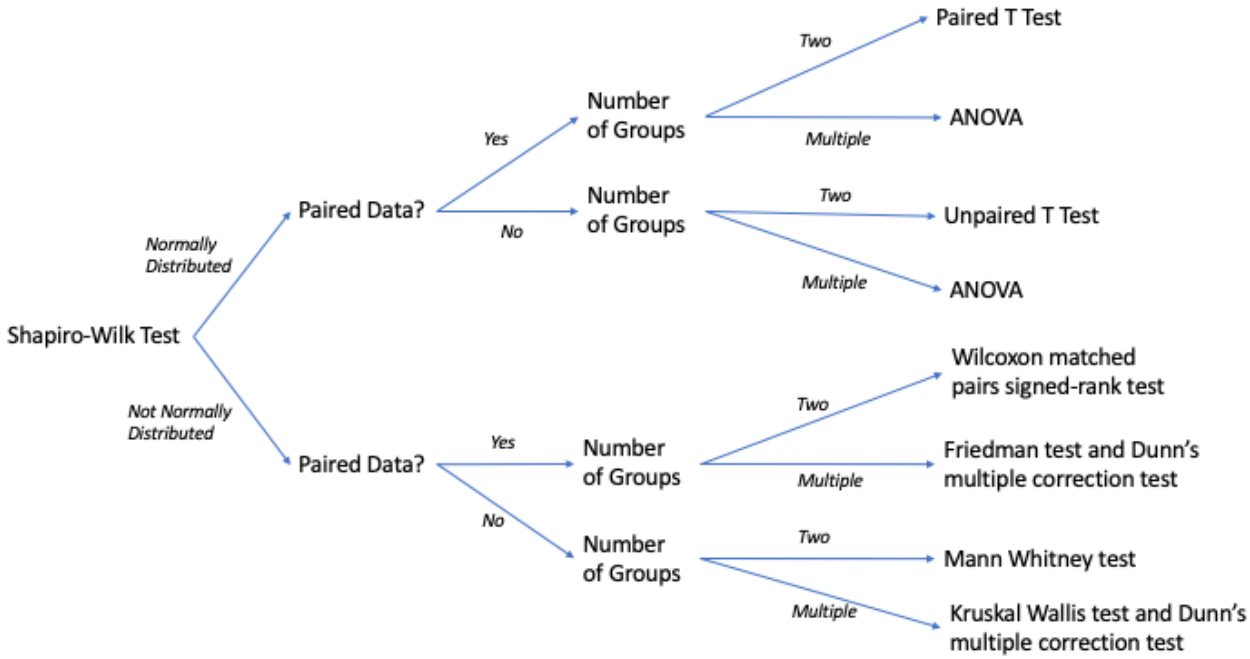

Figure 2.7 Statistical Decision Tree. Statistical decision tree was followed to determine the stats test to be used for each data set. P values ≤0.1 to be included on graphs. All P values and statistical test performed to be included in figure legend.

Label	Treatment
Never	Never Smoker
LT Ex	Long Term Ex-Smoker
UTC	Untreated Control
CD	Cytochalasin D
N	Normoxia
H	Hypoxia
NI	Normoxia with 50 µM IOX-2
NT	Normoxia with 10 ng/ml TGF-β
HT	Hypoxia with 10 ng/ml TGF-β
NFC	Normoxia with Fibrotic Cocktail (Alsafadi et al., 2017)
HFC	Hypoxia with Fibrotic Cocktail (Alsafadi et al., 2017)
HPlo	Hypoxia with 5 µM PX-478
HPm	Hypoxia with 10 µM PX-478
HKlo	Hypoxia with 20 µM KC7F2
HKm	Hypoxia with 40 µM KC7F2

Table 2.4 Graph Axis Key. Graphs throughout the thesis were annotated using these abbreviations on the X axis to define treatment conditions.

CHAPTER 3: MACROPHAGES IN HYPOXIA

3.1 INTRODUCTION

Macrophages in the lung play a crucial role in maintaining tolerance and homeostasis at rest. During infection and injury, they orchestrate infiltration of immune cells, clear pathogens and debris, and promote wound healing and resolution for a return to homeostasis (Hussell and Bell 2014). AMs are the best understood type of macrophages in the lung, due to their accessibility in the tissue. At baseline, these cells produce TGF-β and IL-10 for the maintenance of tolerance (Byrne, Maher and Lloyd, 2016). When required, AMs use phagocytosis to clear pathogens and efferocytosis to clear apoptotic cells and debris. Their additional functions include iron homeostasis and surfactant catabolism (Gu et al. 2022). Due to their key functional plasticity in wound healing, and their propensity to produce profibrotic TGF-β, AMs are frequently identified as the key link between microinjury and fibroblast activation during IPF development (Byrne, Maher and Lloyd, 2016).

Growing evidence demonstrates a potential role for hypoxia in fibrotic progression in the lung during IPF. There is substantial *in vitro* evidence for the profibrotic effect of hypoxia on pulmonary stromal cells (Mizuno et al., 2009; Robinson et al., 2012; Bodempudi et al., 2014; Burman et al., 2018; Senavirathna et al., 2018; Aquino-Gálvez et al., 2019; Akahori et al., 2022; Jeong et al., 2022). Less is known about the effects of hypoxia on pulmonary macrophages. A body of literature has established a role for AMs in systemic release of cytokines, including monocyte chemoattractant protein 1 (MCP-1), following local hypoxic challenge (Chao, Wood and Gonzalez, 2009; Chao et al., 2011). However, the effects of hypoxia on AM polarisation, phenotype and function have been less deeply investigated, particularly in the context of

fibrosis. As such, the effects of hypoxia in addition to profibrotic mediators relevant to the IPF tissue environment, such as TGFβ, have not been characterised.

Extensive work has examined the effects of hypoxia on macrophages more broadly. This work is largely focussed on tumour associated macrophages, where hypoxia drives the accumulation of tumorigenic macrophages (Colegio et al., 2014; Jeong et al., 2019; Vitale et al., 2019; Bai et al., 2022). There is a well-established role for HIF1 responses in inflammatory macrophage polarisation, and a role for HIF2 in pro-resolution macrophage polarisation in murine bone marrow derived macrophages (Takeda et al. 2010). Furthermore, metabolic shifts, like those triggered by hypoxia, are shown to be crucial in macrophage polarisation events. For example, glycolysis is a common hypoxia response associated with inflammatory macrophage polarisation, although in IPF it has been linked to pro-resolution macrophage polarisation (Freemerman et al., 2014; Palsson-Mcdermott et al., 2015; Xie et al., 2017).

The effects of hypoxia on human AMs are likely to be tissue specific due to the unique tissue environment in the lung (Svedberg et al., 2019a). This work hypothesised that hypoxia induces a profibrotic phenotype in AMs and impairs function. The aims of this chapter were to:

(1) establish and validate a model of hypoxia exposure in AMs,

(2) establish and validate tests of AM phagocytosis and efferocytosis,

(3) demonstrate hypoxic response in AMs,

(4) characterise AM phenotype after hypoxia exposure,

(5) characterise AM growth factor and proteinase secretion and gene expression after hypoxia,

(6) characterise AM function in hypoxia, with and without stimulation with TGF-β.

3.2 METHODS

3.2.1 Neutrophil Viability Staining and Flow Cytometry

For assessment of viability, neutrophils were seeded at $1x10^5$ in flow cytometry tubes and washed twice in annexin buffer (300 x g, 5 minutes). Propidium iodide and annexin staining was performed as follows. Neutrophils were stained with 100 µl annexin V (1:100 in annexin buffer) for 15 minutes at room temperature. After 2 washes in annexin buffer, cells were suspended in 200 µl annexin buffer for analysis. Immediately before running on the MACSQuant 10, propidium iodide was added 1:100. A representative gating strategy for neutrophil viability analysis is shown in Figure 3.1.

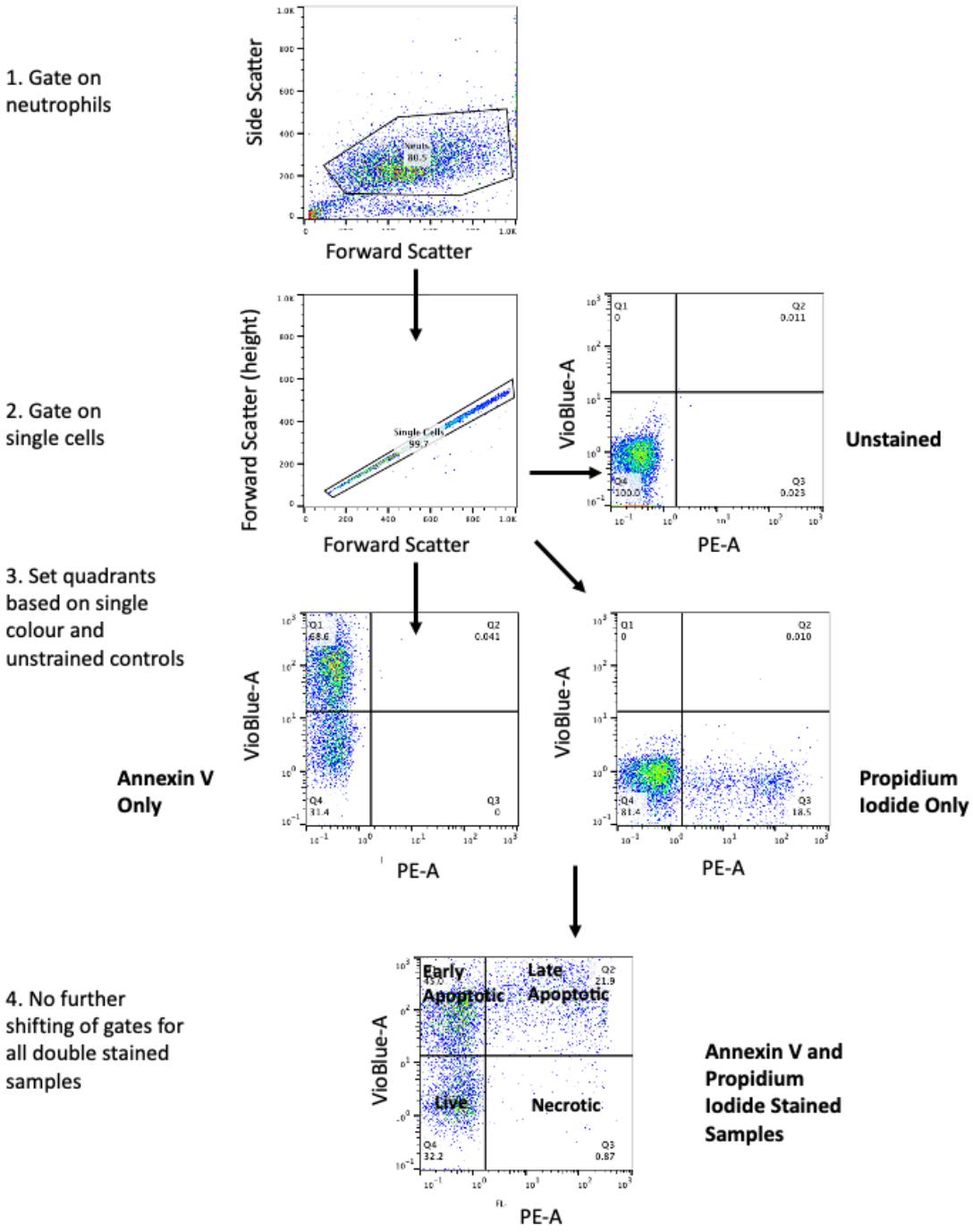

Figure 3.1 Gating strategy to assess neutrophil viability. Events were collected on the MACSQuant 10 flow cytometer. Events of the appropriate size (forward scatter) and granularity (side scatter) for neutrophils were selected for further analysis. Single cells were selected by plotting forward scatter (area) against forward scatter (height), to exclude doublets where these two measures were not proportional. Quadrants dividing stained cells into single and double stained populations were set using unstained cells as double negative events for VioBlue and PE staining. These quadrants were adjusted based on single stained controls, to ensure correct placement. These gates were not adjusted between samples

3.2.2 Immunofluorescent Staining and Imaging of AMs

Human AMs were seeded at $5x10^4$ cells per well, in 8 well ibidi chambered clover-slips (Ibidi. Catalogue number: 80826). For functional assessments, bacteria or apoptotic neutrophils were added at equivalent ratios to those used in functional assays (sections 2.5 and 2.6). Upon the conclusion of functional assays, AMs were washed once with PBS, then fixed for 30 minutes in 4% paraformaldehyde (Thermo Scientific. Catalogue number: J1899) at room temperature. After 2 washes in PBS, chamber well slides were stored with 200 µl PBS per well at 4^{o}C until staining.

For intracellular staining, cells were permeabilised with 0.1% Triton X 100 (Sigma-Aldrich. Catalogue number: T8787) for 30 minutes at room temperature, then washed in FACS buffer. Wells were then blocked using 10% human serum in FACS buffer for 30 minutes at room temperature.

Primary antibodies were added to samples at appropriate concentrations (Table 3.1) in FACS buffer and incubated overnight at 4^{o}C. After washing with FACS buffer twice, secondary antibodies were added where required at relevant concentrations (Table 3.1) in FACS buffer and incubated for 30 minutes at room temperature. For nuclear staining, cells were incubated in DAPI (1 µg/ml) in PBS for 5 minutes at room temperature. Finally, wells were washed in FACS buffer, covered in 200 µl FACS buffer and kept protected from light at 4^{o}C until imaging. Cells were imaged on the Zeiss LSM 780 at 40x magnification using Zen Black software.

Target/Marker	Primary Antibody/Dye	Details	Secondary	Details
CD63	Rabbit Monoclonal 1:100	Thermofisher Scientific. Catalogue number: MA5-30187	Donkey anti-Rabbit IgG Alexa Fluor™ 568	Thermofisher Scientific. Catalogue number: A10042
Nucleus	DAPI 1 µg/ml	Thermofisher Scientific. Catalogue number: 62248	N/A	
Streptococcus pneumoniae	Alexa Fluor™ 647 NHS Ester (Prestained)	Invitrogen. Catalogue number: A37573	N/A	
Apoptotic neutrophils	CellTracker™ Deep Red Dye (Prestained)	Invitrogen. Catalogue number: C34565	N/A	

Table 3.1 Immunofluorescent Staining for Fluorescence Microscopy

3.2.3 AM Surface Staining

For surface staining, $2.5x10^5$ AMs were harvested per condition. To harvest, cells were washed with PBS and incubated with non-enzymatic cell dissociation solution (Sigma-Aldrich. Catalogue number: C5914) after PBS rinse, for 10 minutes (37°C, 5% CO_2). These cells were topped up with supplemented RPMI and harvested gently using a cell lifter.

Cells were incubated with Fc Block in PBS (1:50) (Miltenyi Biotech. Catalogue number: 130-059-901) for 30 minutes at room temperature to block antibody binding receptors. After washing in FACS buffer, cells were incubated with relevant antibodies (Table 3.2) for an hour at room temperature, then washed twice more in FACs buffer. Isotype control panels were added to separate tube of cells, at equivalent concentrations to the associated test antibody (Table 3.2). For compensation, positive and negative Mouse Ig Control Compensation Particles (BD Biosciences. Catalogue number: 552843) were incubated with 1 µl antibody of interest for 20 minutes at room temperature, before washing in FACS buffer. For analysis, cells or beads were resuspended in 200 µl FACS buffer.

Target	Fluorophore	Clone	Manufacturer	Concentration	Isotype Control
CD163	FITC	GHI/61	BD Biosciences	1:20	Mouse IgGκ
CD206	APC	19.2	BD Biosciences	1:20	Mouse IgGκ
CD80	PE	L307.4	BD Biosciences	1:20	Mouse IgGκ
SIRPα	APC	15-414	ThermoFisher	1:20	Mouse IgG2aκ

Table 3.2 Antibodies for AM Surface Marker Staining

Flow cytometry was performed on the MACSQuant 10 cytometer (Miltenyi Biotech). MACSQuant manual compensation was performed using single colour-stained beads. The compensation matrix generated was applied to samples. Figure 3.2 shows a representative gating strategy for this analysis. Isotype controls were used to set positive gates and data was normalised by subtracting isotype control values.

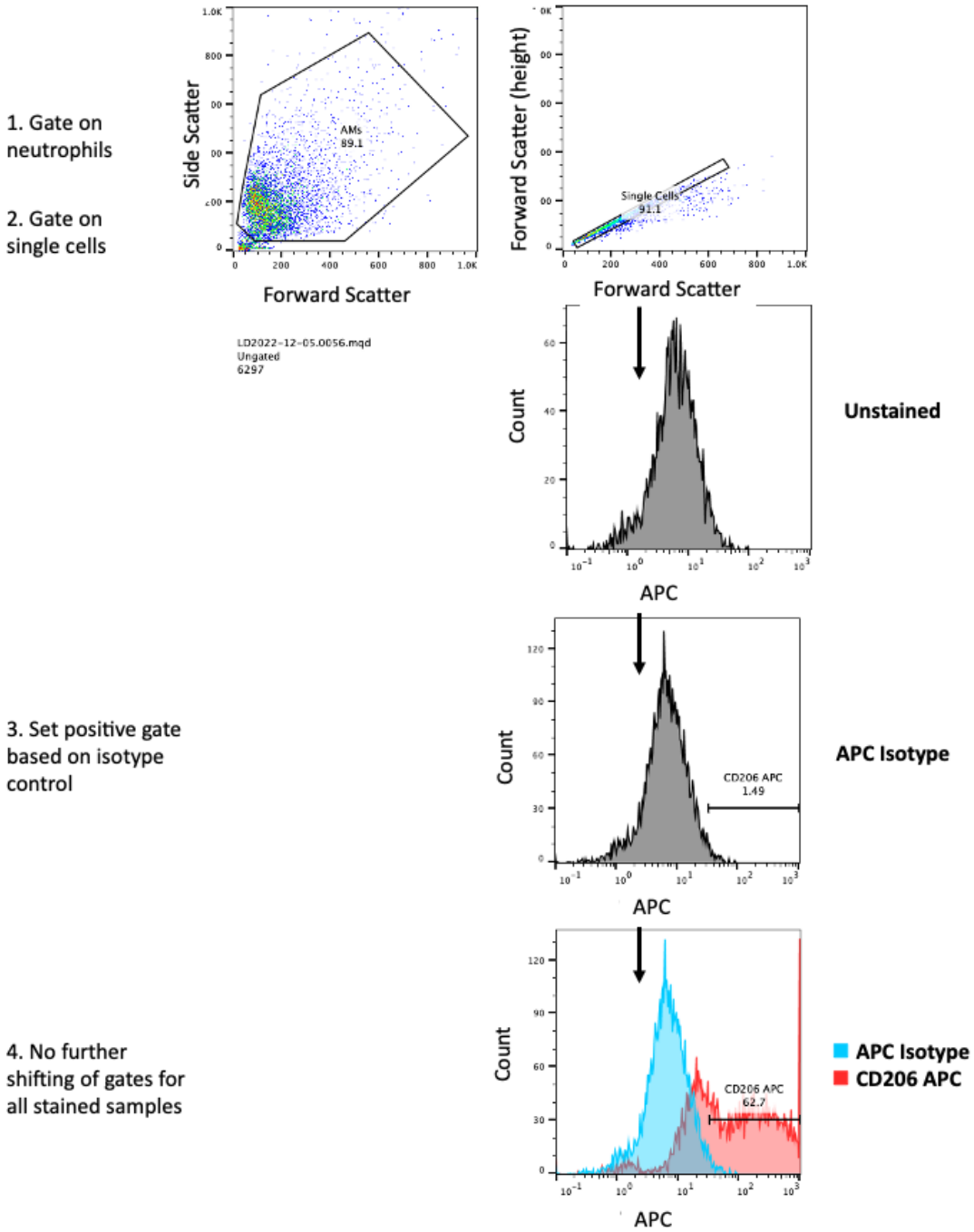

Figure 3.2 Gating Strategy for AM Surface Marker Staining. Events were collected on the MACSQuant 10 flow cytometer. Events of the appropriate size (forward scatter) and granularity (side scatter) for alveolar macrophages were selected for further analysis. Single cells were selected by plotting forward scatter (area) against forward scatter (height), to exclude doublets where these two measures were not proportional. Unstained cells were used to set positive gates, containing <2% of events. Isotype controls were then run, and if required gates were shifted to ensure <2% events fell into the positive gate. Gates remained unchanged and the remainder of samples were analysed to determine the percent of events within the positive gate and the total MFI of the population.

3.3 RESULTS

3.3.1 Validation

3.3.1.1 AM yield

Lung tissue was obtained from 25 donors for AM isolation. 56.5 % were long-term ex-smokers (quit >4 years ago), 43.5 % were never smokers (Table 3.3).

	Summary	Never Smoker 10 (43.5%)	Long Term Ex-Smoker 13 (56.5%)	P Value
Age	73 (IQR 12)	74 (IQR 14)	73 (IQR 12)	*0.5968*
Sex	13 (56.5%) M 10 (43.5%) F	3 (30%) M 7 (70%) F	9 (69%) M 4 (31%) F	*0.0995*

Table 3.3 Donor Details for Lung Tissue Used for AM Isolation. *Age of smoking groups were compared using a Mann-Whitney statistical test. Sex distributions between smoking groups were compared using a Fisher's exact test.*

The median AM yield was $1.42x10^6$ per gram of tissue (IQR: $3.69x10^6$)(Figure 3.3A). When grouped by smoking status, AM yields were not significantly different between long-term ex-smokers and never smokers (Median: $1.58x10^6$ vs $1.15x10^6$, p=0.6)(Figure 3.3B).

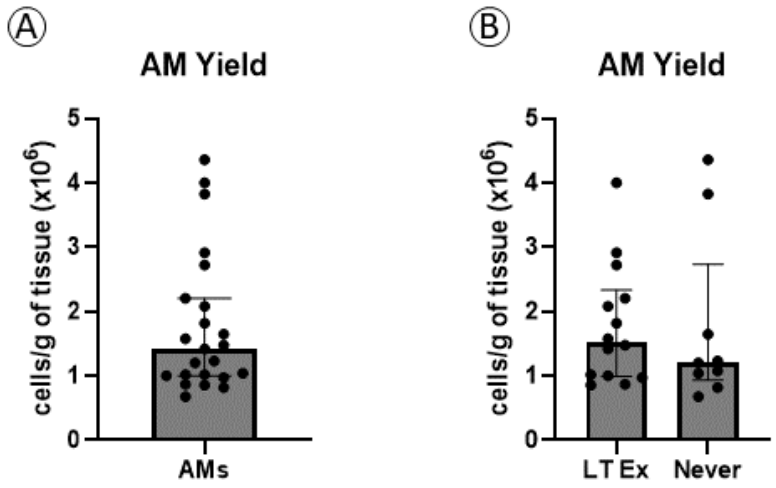

Figure 3.3 AM Yields from Human Lung Tissue. AMs were isolated from human lung tissue by lavage with saline. (A) AM yield per gram of human lung tissue. (B) AM yield per gram, grouped by smoking status. Comparison by Mann-Whitney test, N= 23, LT Ex vs Never p=0.64. Data is presented as a median (±IQR). LT Ex: Long term ex-smoker.

3.3.1.2 Phagocytosis

AMs were incubated with heat killed *Streptococcus pneumoniae*, to investigate their phagocytic function. Extensive validation was required to establish optimal combination of assay conditions, particularly due to batch-to-batch variability when using new batch of heat killed bacteria.

Cytochalasin D treatment was used to prevent phagocytosis, by depolymerisation of the actin cytoskeleton, as a negative control. Our group previously validated the use of 10 µM cytochalasin D in AMs to prevent phagocytosis (Mahida, Scott, Parekh, Lugg, Belchamber, et al., 2021) and efferocytosis (Mahida, Scott, Parekh, Lugg, Belchamber, et al., 2021; Mahida, Scott, Parekh, Lugg, Hardy, et al., 2021). In this study too, cytochalasin D treatment prevented phagocytosis over 4 hours, when assessed as MFI ($p<0.0001$) and as percentage of positive cells ($p<0.0001$)(Figure 3.4). The efficacy of Cytochalasin D in preventing phagocytosis is demonstrated by microscopy in Figure 3.5, where intact *Streptococcus pneumoniae* (pink) are

visible outside of the alveolar macrophage cytoplasm (green) when cytochalasin D is added, while ingested *Streptococcus pneumoniae* within the cytoplasm are visible in AMs not treated with cytochalasin D. 10 µM Cytochalasin D treatment was used as baseline for all phagocytosis assays, to calculate fold change.

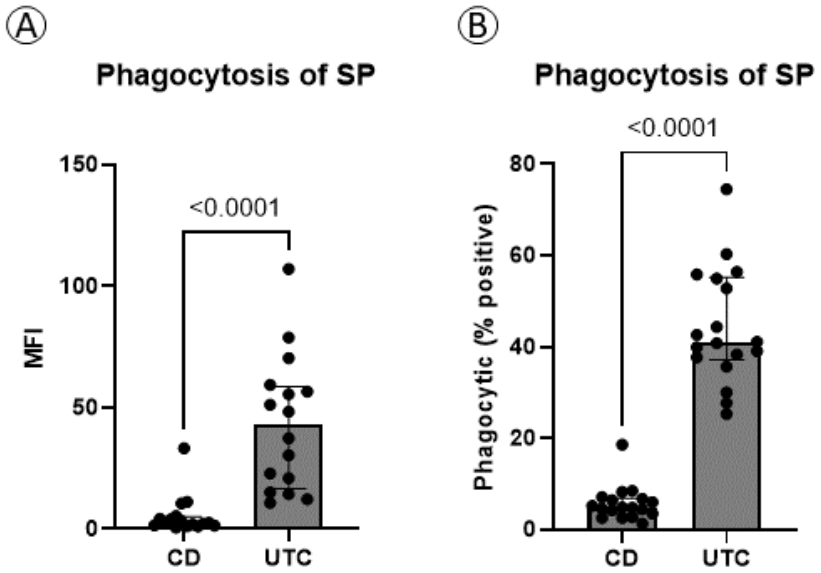

Figure 3.4 The Effects of Cytochalasin D on AM Phagocytosis by Flow Cytometry. *AMs were incubated with heat killed Streptococcus pneumoniae for 4 hours, and phagocytosis was assessed by flow cytometry. (A) Mean fluorescence intensity (MFI) and (B) percentage positive events were presented for AMs pre-treated with cytochalasin D (CD) and untreated control AMs (UTC). Comparisons made using a Wilcoxon's test. N= 17. MFI CD vs UTC p<0.0001. % Positive CD vs UTC p<0.0001. Data is presented as median (±IQR).*

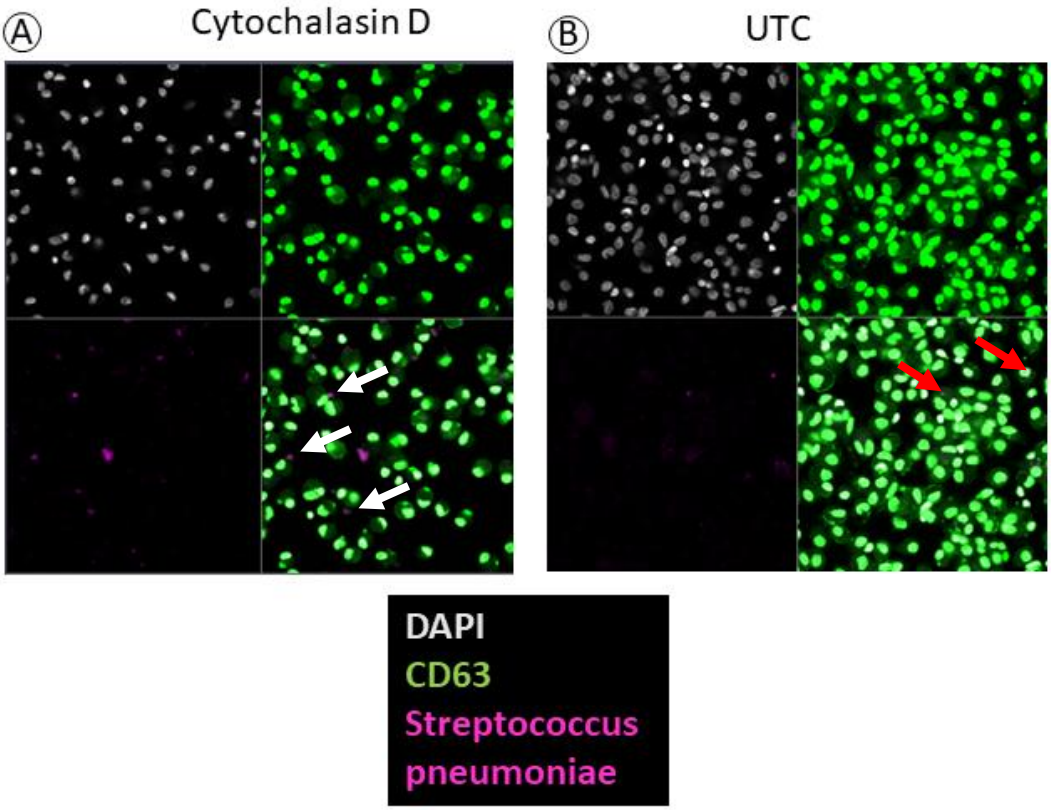

Figure 3.5 The Effects of Cytochalasin D on AM Phagocytosis by Microscopy. *AMs were incubated with heat killed Streptococcus pneumoniae (pink) for 4 hours, and phagocytosis was assessed by microscopy at 40X magnification. (A) AMs pre-treated with cytochalasin D and (B) untreated control AMs were stained for DNA (DAPI-grey) and CD63 (green). White arrows indicate bacteria external to the AM cell membrane, red arrows indicate bacteria internalised within the AMs. Single channel images are overlaid to create composite images (bottom right).*

Belchamber et al (2019) used a 4-hour time point to assess AM phagocytosis of heat killed bacteria. Time points either side of this were assessed in this study, in case of bacterial-batch specific differences in the speed of AM response. Time dependent phagocytic responses were variable between patient samples. Overall, the percent of AMs that phagocytosed and the MFI of AMs were similar across 2, 4 and 6 hours (Figure 3.6A,B). The 4-hour time point was sufficient to provide a marked shift in bacterial uptake, therefore AMs were incubated with *Streptococcus pneumoniae* for 4 hours for all future phagocytosis experiments.

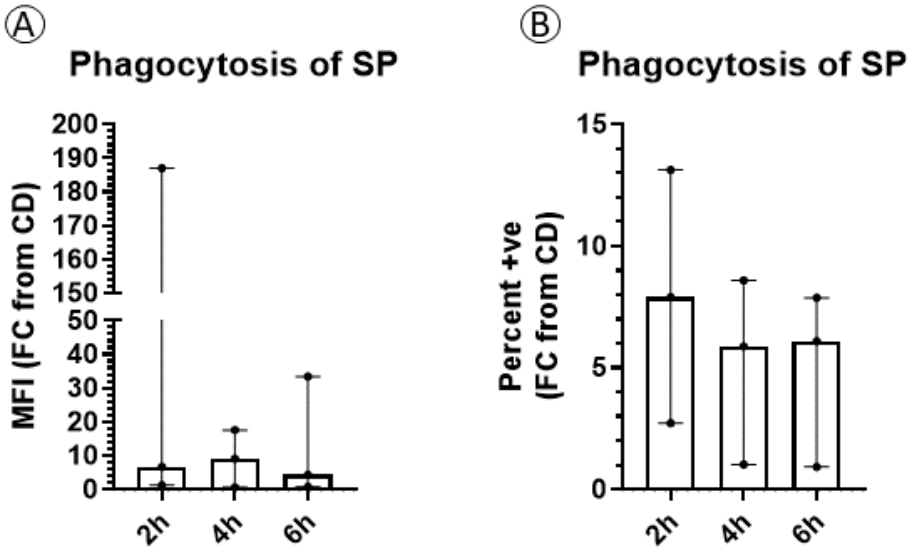

Figure 3.6 AM Phagocytosis Over Time. AMs were incubated with heat killed, fluorescently labelled Streptococcus pneumoniae for 2, 4 and 6 hours, and phagocytosis was assessed by flow cytometry. (A) Mean fluorescence intensity (MFI) and (B) percentage positive events were presented comparing these timepoints. Data is presented as a fold change (FC) from cytochalasin D (CD) control. Graphs show median (±IQR). N=3.

To assess the effect of smoking status on phagocytosis, percentage of phagocytic cells, expressed as a fold change from cytochalasin D control, were presented for long-term ex-smokers and never smokers (Figure 3.7). There was no significant difference in the percentage of phagocytic cells in never smokers when compared to long term ex-smokers ($p>0.9999$).

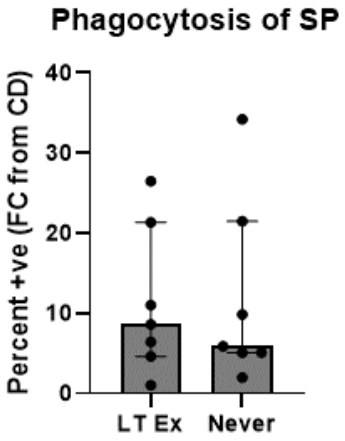

Figure 3.7 AM Phagocytosis by Smoking Status. AMs were incubated with heat killed, fluorescently labelled Streptococcus pneumoniae for 4 hours, and phagocytosis was assessed by flow cytometry. Percentage positive events were presented comparing phagocytosis in never smokers and long-term ex-smokers (LT Ex). Data is presented as a fold change (FC) from cytochalasin D control (CD). Comparison by Mann-Whitney Test, LT Ex vs Never p >0.9999. Graphs show median (±IQR). N=14.

3.3.1.3 Efferocytosis

AMs were incubated with apoptotic neutrophils to investigate their efferocytic function. The assay required robust validation to confirm the best combination of experimental variables.

Overnight serum starvation has previously been demonstrated to consistently induce neutrophil apoptosis (Mahida, Scott, Parekh, Lugg, Belchamber, et al., 2021; Mahida, Scott, Parekh, Lugg, Hardy, et al., 2021). Neutrophil apoptosis was confirmed in this study, using propidium iodide uptake and annexin V binding to differentiate live, early apoptotic, late apoptotic, and necrotic cells by flow cytometry. After overnight starvation, neutrophils were mostly in early or late apoptosis (45% (IQR: 21.4) and 29.9% (IQR: 21.8) respectively) (Figure 3.8).

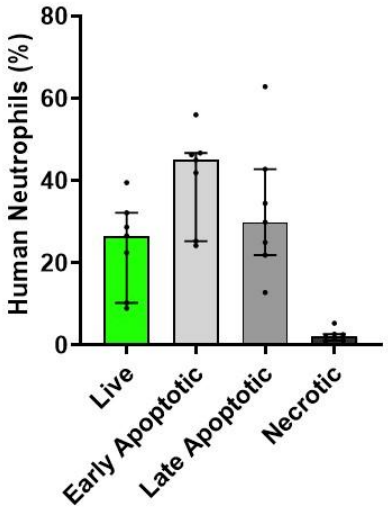

Figure 3.8 Neutrophil Apoptosis after Overnight Serum Starvation. Neutrophil viability was assessed by propidium iodide and annexin V staining after overnight serum starvation. Staining was used to differentiate live, necrotic, late apoptotic and early apoptotic cells. N=7. Graphs show median (±IQR).

Viability of neutrophils treated with overnight starvation followed by 2h hypoxia was also assessed. This exposure was relevant as apoptotic neutrophils added to hypoxically challenged AMs would be exposed to hypoxia for 2 hours. The percentage of live, early apoptotic, late apoptotic, and necrotic neutrophils after overnight starvation followed by 2h hypoxia was not significantly different compared to neutrophils kept in normoxia (Figure 3.9).

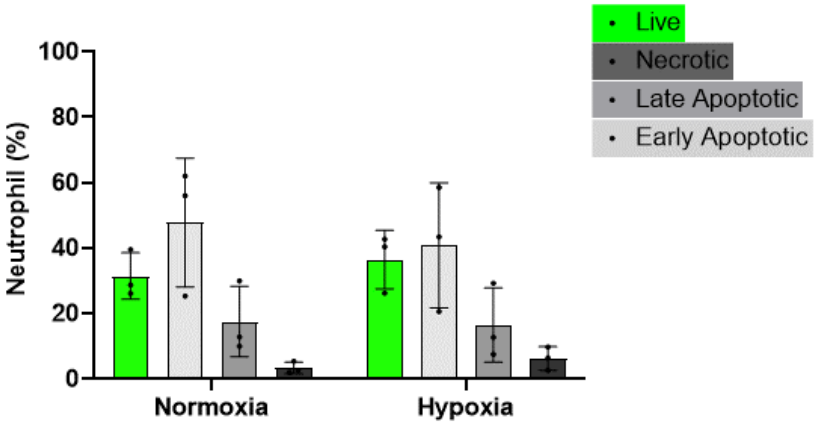

Figure 3.9 Neutrophil Apoptosis after Acute Hypoxia Treatment. *Neutrophil viability was assessed by propidium iodide and annexin V staining after overnight serum starvation, followed by 2 hours normoxia or hypoxia. Staining was used to differentiate live, necrotic, late apoptotic and early apoptotic cells. Comparison using a Two Way ANOVA with Sidak's multiple comparisons test. Normoxia vs hypoxia Live p= 0.9336, Early Apoptotic p=0.9900, Late Apoptotic p>0.999, Necrotic p=0.7509. Data is presented as median (±IQR). N=3.*

Cytochalasin D treatment was used, as described in the phagocytosis assay (section 3.3.1.2), to depolymerise the actin cytoskeleton, thereby preventing efferocytosis. In accordance with Mahida et al. (2021), 10 µM cytochalasin D prevented efferocytosis over 2 hours ($p<0.0001$)(Figure 3.10). The efficacy of Cytochalasin D in preventing efferocytosis is confirmed by microscopy, where whole apoptotic neutrophils (pink) are visible outside of the AM cytoplasm (green) when cytochalasin D is added, while ingested neutrophils within the cytoplasm are visible in AMs not treated with cytochalasin D (Figure 3.11). Cytochalasin D (10 µM) treatment was used as baseline for all phagocytosis assays to calculate fold change.

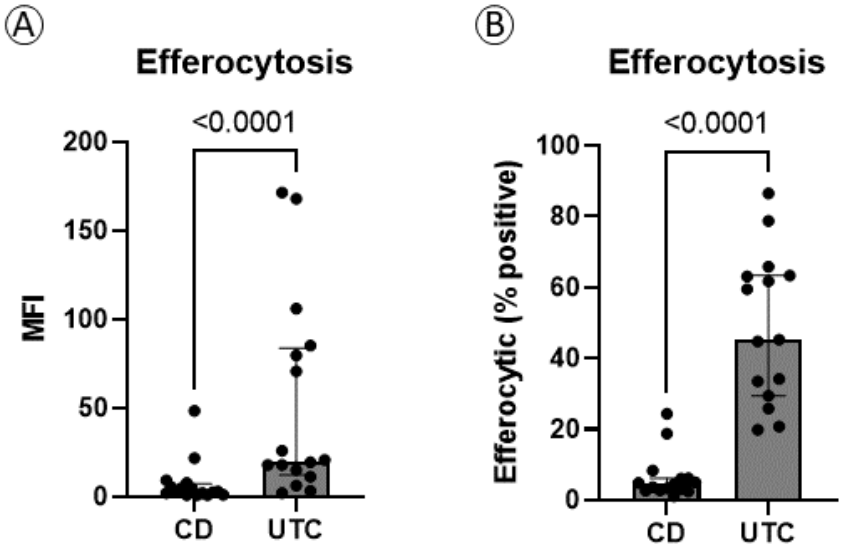

Figure 3.10 The Effects of Cytochalasin D on AM Efferocytosis by Flow Cytometry. AMs were incubated with fluorescently stained apoptotic neutrophils for 4 hours, and efferocytosis was assessed by flow cytometry. (A) Mean fluorescence intensity (MFI) and (B) percentage positive events were presented for AMs pre-treated with cytochalasin D (CD) and untreated control AMs (UTC). Comparison made using Wilcoxon's tests. MFI CD vs UTC p<0.0001. % positive CD vs UTC p<0.0001. Data is presented as median (±IQR). N=16.

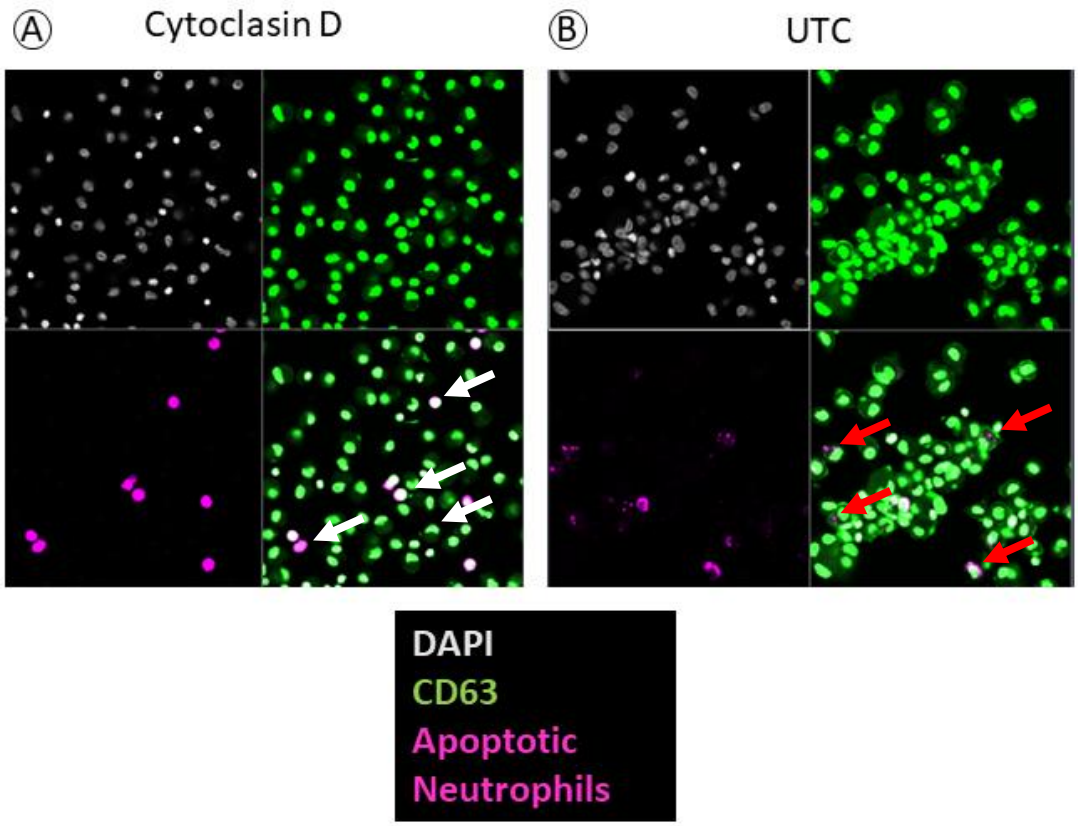

Figure 3.11 The Effects of Cytochalasin D on AM Efferocytosis by Microscopy. *AMs were incubated with fluorescently labelled apoptotic neutrophils (pink) for 4 hours, and efferocytosis was assessed by microscopy at 40X magnification. (A) AMs pre-treated with cytochalasin D and (B) untreated control AMs were stained for DNA (DAPI-grey) and CD63 (green).White arrows indicate neutrophils external to the AM cell membrane, red arrows indicate neutrophils internalised within the AMs. Single channel images are overlaid to create composite images (bottom right).*

Our group has previously demonstrated that 2 hours is sufficient incubation time for the assessment of efferocytosis (Mahida, Scott, Parekh, Lugg, Belchamber, et al., 2021). This study explored further timepoints to determine whether alternative time points could provide further information when examining efferocytic function. The percent of AMs that efferocytosed and MFI of AMs were similar across 2, 4 and 6 hours (Figure 3.12A,B). Given that the 2-hour time point was sufficient to provide a large window of change in percentage of positive AMs and AM MFI, AMs were incubated with apoptotic neutrophils for 2 hours for all future efferocytosis experiments.

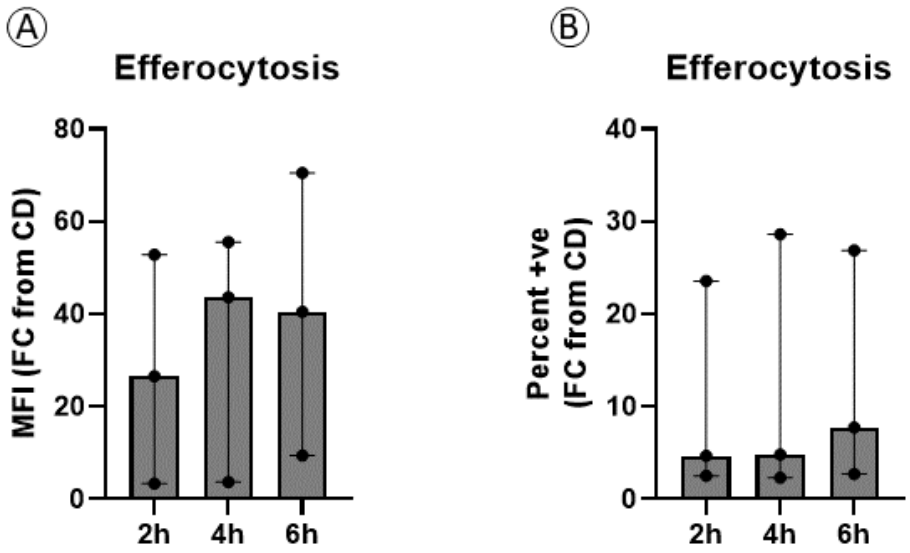

Figure 3.12 AM Efferocytosis Over Time. AMs were incubated with heat killed, fluorescently labelled apoptotic neutrophils for 2, 4 and 6 hours, and efferocytosis was assessed by flow cytometry. (A) Mean fluorescence intensity (MFI) and (B) percentage positive events were presented comparing these timepoints. Data is presented as a fold change (FC) from cytochalasin D (CD) control. Graphs show median (±IQR). N=3.

To compare efferocytic function in never smokers and long-term ex-smokers, the percentage of efferocytic AMs were presented for the two groups, expressed as a fold change from cytochalasin D control. There was no significant difference in efferocytosis in the two populations (p=0.3357)(Figure 3.13).

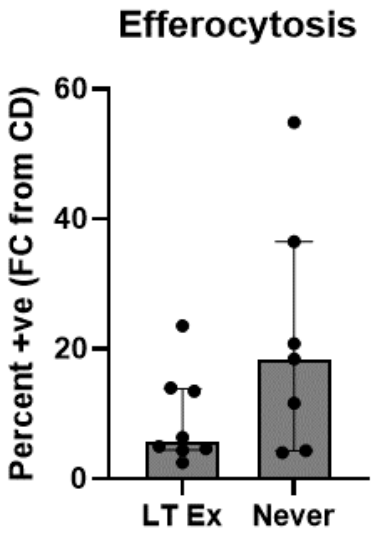

Figure 3.13 AM Efferocytosis by Smoking Status. AMs were incubated with fluorescently labelled apoptotic neutrophils for 2 hours, and efferocytosis was assessed by flow cytometry. Percentage positive events were presented comparing phagocytosis in never smokers and long-term ex-smokers (LT Ex). Comparison using a Mann-Whitney test, LT Ex vs Never p= 0.3357. Data is presented as a fold change (FC) from cytochalasin D control (CD). Graphs show median (±IQR). N=15.

3.3.1.4 AM viability in hypoxia

To demonstrate the feasibility of examining AM response and function after hypoxic challenge, AM viability was first assessed by flow cytometry after 48 hours in normoxia and hypoxia. Annexin V binding and propidium iodide uptake were used to differentiate live, early apoptotic, late apoptotic, and necrotic cells. Figure 3.14 shows the proportion of these cell populations with and without hypoxic challenge. AM viability was unchanged by hypoxia (Figure 3.14).

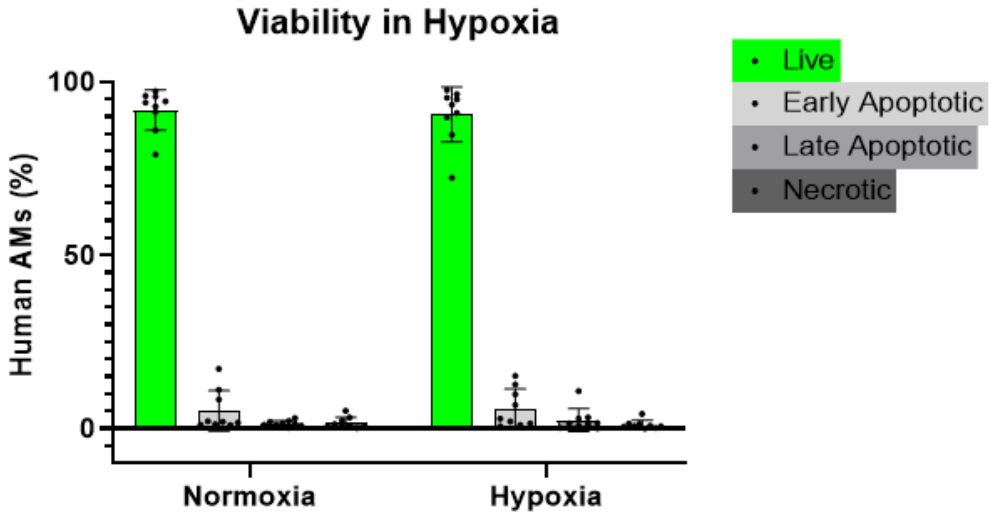

Figure 3.14 AM Viability after 48 Hours Hypoxia. AM viability was assessed by propidium iodide and annexin V staining after 48 hours normoxia (21% O_2, 5% CO_2, 37°C) and hypoxia (1% O_2, 5% CO_2, 37°C). Staining was used to differentiate live, necrotic, late apoptotic, and early apoptotic cells. Comparison using a Two Way ANOVA with Sidak's multiple comparisons test. Normoxia vs hypoxia Live p= 0.9935, Early Apoptotic p=0.9978, Late Apoptotic p=0.8596, Necrotic p=0.8987. Data is presented as median (±IQR). N=9.

3.3.1.5 AM stimulations

TGF-β stimulation was validated in AMs for 48 hours to more closely replicate the profibrotic environment found in the lung during IPF. This exposure was designed to be added alongside hypoxic challenge to better characterise the effects of hypoxia in AMs during IPF progression. AM viability following 48-hour treatment with TGF-β (10 ng/ml) was unchanged as compared to untreated control cells (Figure 3.15). TGF-β treatment for 48 hours increased the percentage of phagocytic AMs (p=0.0156) and the MFI of AMs (p=0.0156) (Figure 3.16A,B). TGF-β treatment did not change the percentage of efferocytic AMs and their MFI (Figure 3.16C,D). This concentration and duration of TGF-β treatment was subsequently included in functional AM assays.

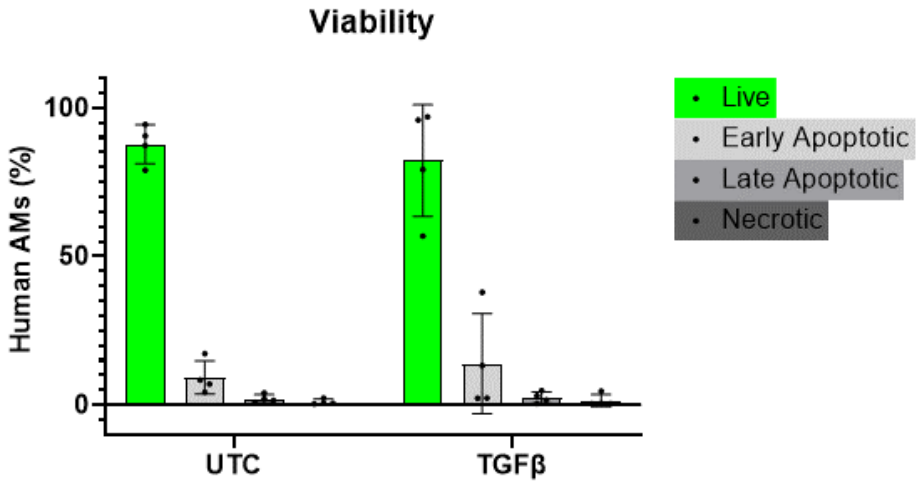

Figure 3.15 AM Viability After 48-hour TGF-β Stimulation. AM viability was assessed by propidium iodide and annexin V staining with and without 48-hour 10 ng/ml TGF-β treatment. Staining was used to differentiate live, necrotic, late apoptotic and early apoptotic cells. Comparison using a Two Way ANOVA with Sidak's multiple comparisons test. UTC vs TGF-β Live p= 0.9760, Early Apoptotic p=0.9807, Late Apoptotic p=0.9960, Necrotic p=0.9875. Data is presented as median (±IQR). N=4.

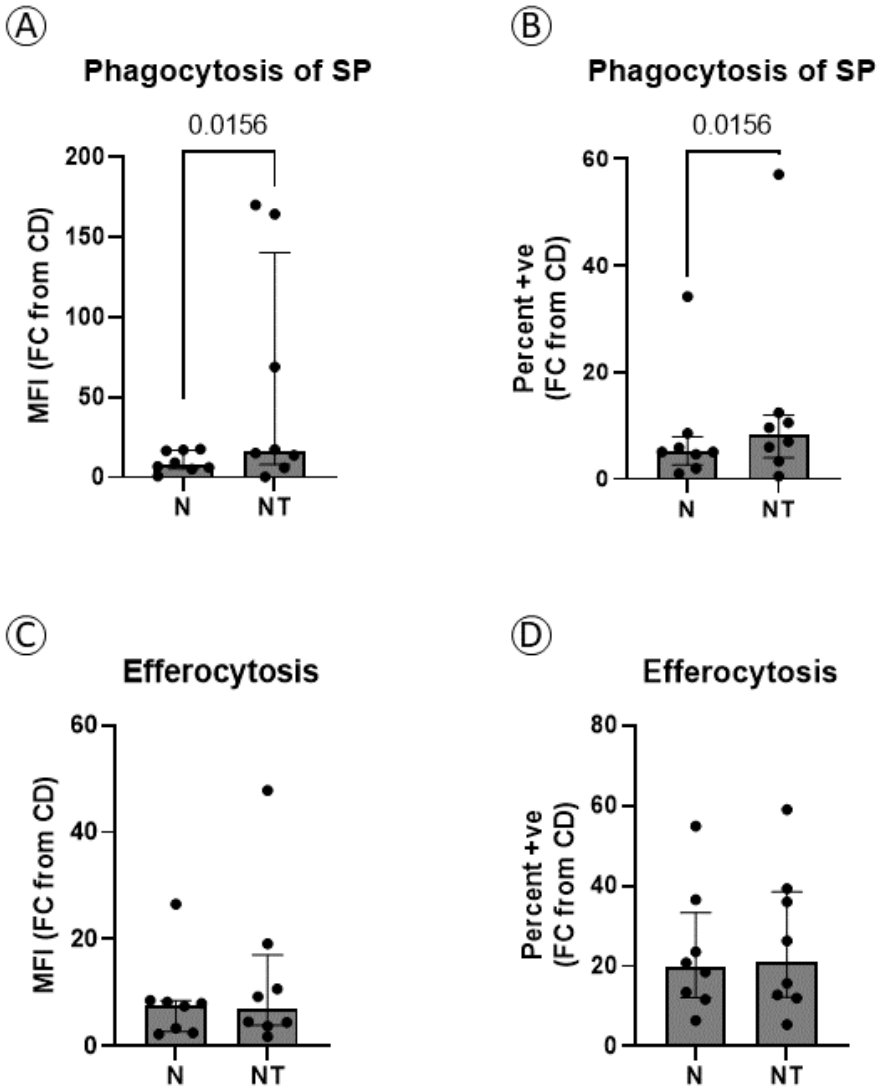

Figure 3.16 AM Function After 48-hour TGF-β Stimulation. AMs were treated with 10 ng/ml TGF-β for 48 hours in normoxia. AMs were incubated with heat killed, fluorescently labelled Streptococcus pneumoniae for 4 hours, and phagocytosis was assessed by flow cytometry. (A) Mean fluorescence intensity (MFI) and (B) percentage positive events were presented comparing phagocytosis with and without TGF-β. MFI N vs NT p=0.0156. % Positive N vs NT p=0.0156. AMs were incubated with fluorescently labelled apoptotic neutrophils for 2 hours, and efferocytosis was assessed by flow cytometry. (C) MFI and (D) percentage positive events were presented comparing efferocytosis with and without TGF-β. MFI N vs NT p=0.1094. % Positive N vs NT p=0.1953. Normoxia (N), Normoxia with TGF-β (NT). Data is presented as a fold change (FC) from cytochalasin D (CD) control. Comparisons were made using a Wilcoxon's Test. Graphs show median (±IQR). N=8.

LPS treatment (10 µg/ml) was validated in AMs for 48 hours, in an attempt to replicate the priming effect previously described of LPS in macrophages (Fujihara et al., 2003; Wu, Chen and

Chen, 2009). These conditions would more closely replicate conditions in the lung during infection, and reflect the combinatorial effect of hypoxia with LPS, with potential implications particularly in phagocytic response.

AM viability following 48-hour treatment with LPS (10 µg/ml) was unchanged as compared to an untreated control (Figure 3.17). LPS treatment for 48 hours did not stimulate phagocytosis or efferocytosis (Figure 3.18A-D), with no differences detected in either function. As the priming effect of LPS previously demonstrated to increase phagocytosis was not demonstrated following this stimulation, LPS stimulation was not included in subsequent functional assays.

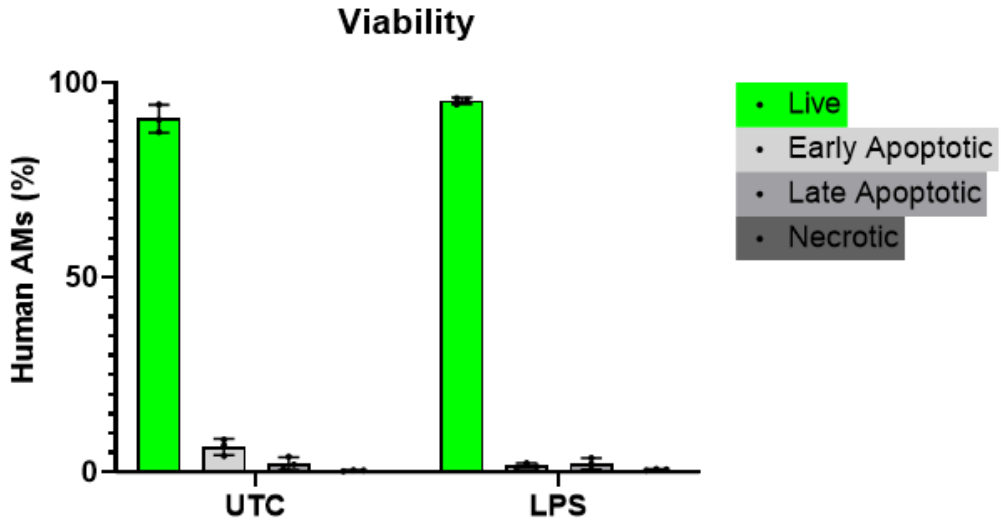

Figure 3.17 AM Viability After LPS Stimulation. AM viability was assessed by propidium iodide and annexin V staining with and without 48-hour treatment with 10 µg/ml LPS. Staining was used to differentiate live, necrotic, late apoptotic and early apoptotic cells. Comparison using a Two Way ANOVA with Sidak's multiple comparisons test. UTC vs LPS Live p= 0.4736, Early Apoptotic p=0.1803, Late Apoptotic p>0.9999, Necrotic p=0.4763. Data is presented as median (±IQR). N=3.

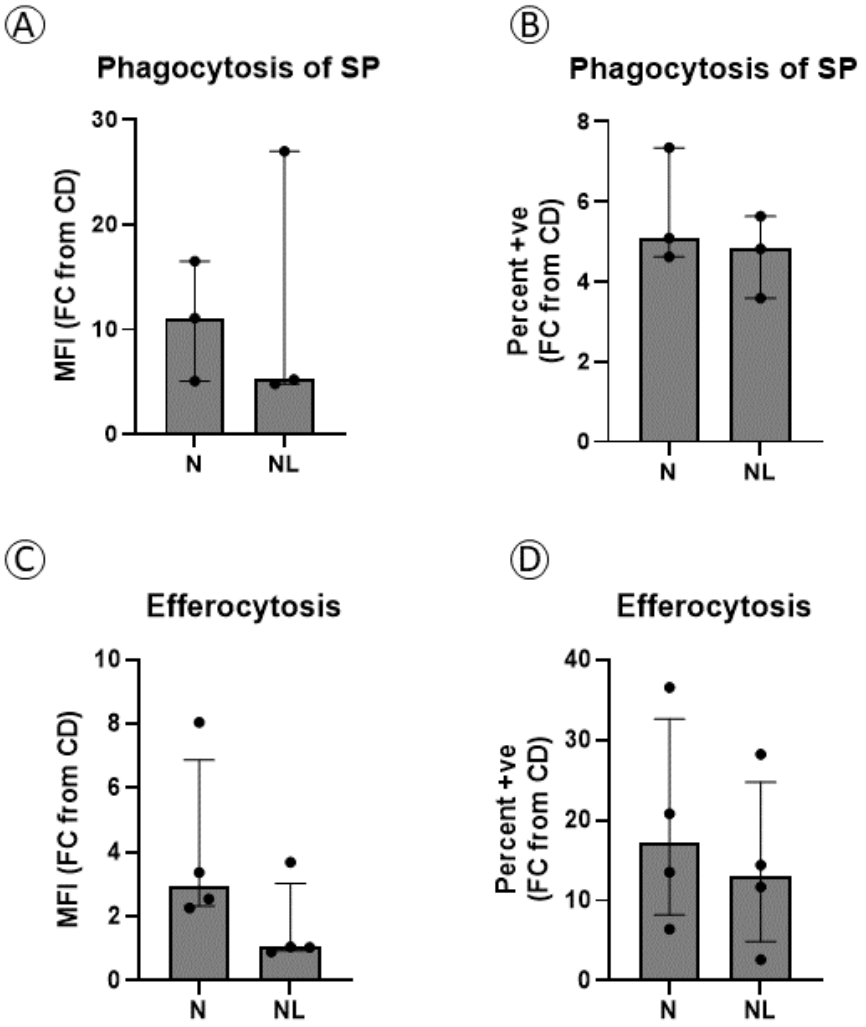

Figure 3.18 AM Function After LPS Stimulation. AMs were treated with 10 µg/ml LPS for 48 hours in normoxia. AMs were incubated with heat killed, fluorescently labelled Streptococcus pneumoniae for 4 hours, and phagocytosis was assessed by flow cytometry. (A) Mean fluorescence intensity (MFI) and (B) percentage positive events were presented comparing phagocytosis with and without LPS. N=3. MFI N vs NL p>0.9999. % Positive N vs NL p=0.7500. AMs were incubated with fluorescently labelled apoptotic neutrophils for 2 hours, and efferocytosis was assessed by flow cytometry. (C) MFI and (D) percentage positive events were presented comparing efferocytosis with and without LPS. N=4. MFI N vs NL p=0.25. % Positive N vs NL p=0.6250. Data is presented as a fold change (FC) from cytochalasin D control (CD). Comparisons were made using a Wilcoxon's test. Graphs show median (±IQR).

3.3.2 AM Hypoxia Response

To demonstrate AM response to hypoxic challenge, HIF1α protein and RNA levels were assessed across a time course, using western blotting and qPCR respectively. Known HIF1α

response genes were measured at the RNA level, by qPCR, and at the protein level, by ELISA or western blotting as appropriate.

HIF1α was not detectable in AMs cultured in normoxia, however HIF1α was stabilised in AMs within 4 hours of hypoxia exposure, when normalised to an actin loading control (p=0.0355) (Figure 3.19A,B). HIF1α was still present after 48 hours hypoxia (p=0.0033), although there was significantly less HIF1α at 48 hours than 4 hours (p=0.0372) (Figure 3.19A,B). Meanwhile, there was a trend towards reduced *hif1a* gene expression after 48 hours exposure (p=0.084) (Figure 3.20).

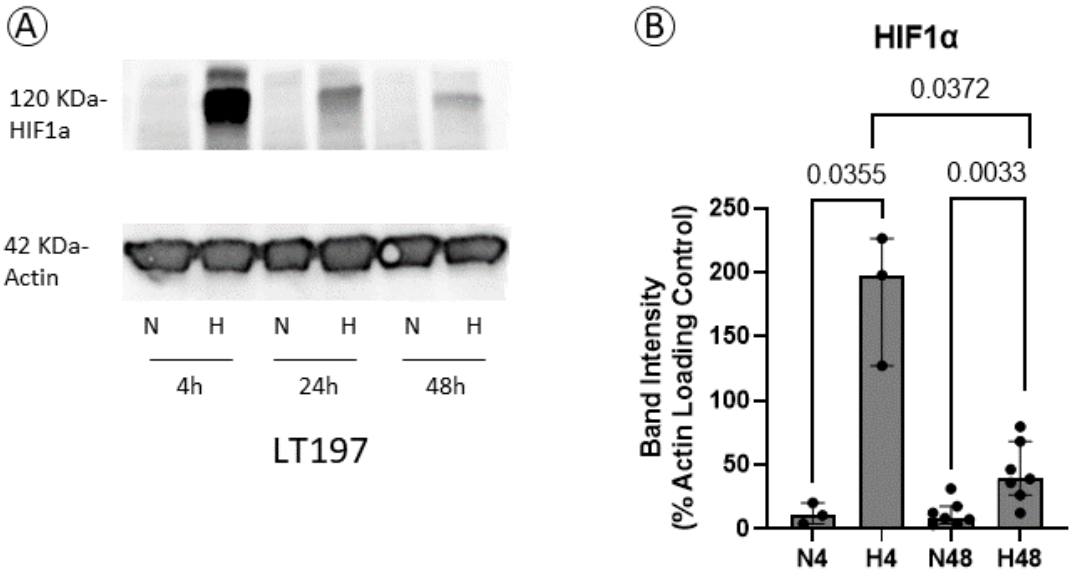

Figure 3.19 HIF1α Protein Stabilisation. *AMs were incubated in normoxia (21% O_2, 5% CO_2, 37°C) or hypoxia (1% O_2, 5% CO_2, 37°C) for 4 hours (N4, H4) (N=3) and 48 hours (N48, H48) (N=7). HIF1α protein levels were subsequently assessed by western blotting, alongside actin as a loading control. Representative western blot (A) showing HIF1α at 120 kDa and actin at 42 kDa. Band densities were assessed using Image J, and (B) HIF1α band intensity was presented as a percentage of actin band intensity. Within a single timepoint, comparisons were made using a paired T Test. N4 vs H4 p=0.0355, N48 vs H48 p=0.0033. Between timepoints, comparisons were made using an unpaired T Test with Welch's Correction. H4 vs H48 p=0.0372. Graphs show median (±IQR).*

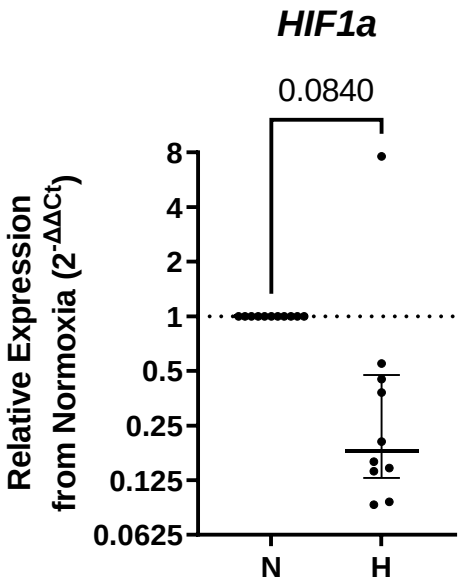

Figure 3.20 Hif1a Gene Expression. AMs were incubated in normoxia (21% O_2, 5% CO_2, 37°C) or hypoxia (1% O_2, 5% CO_2, 37°C) for 48 hours. Hif1a RNA transcript levels were subsequently assessed by qPCR, alongside 18S rRNA expression as a loading control. Data was presented as $2^{-\Delta\Delta Ct}$ relative to normoxic AM expression. Comparisons were made using a Wilcoxon's test. N vs H p=0.0840. Graphs show median (±IQR). N= 10.

HIF1α response gene *VEGFA* showed a statistically significant, 3.5-fold increase in expression after 48 hours (p=0.0039) (Figure 3.21A). VEGFA protein secretion was also increased in supernatants after 48 hours (p=0.0023). Marginal differences were observed in supernatant volume between cells incubated in normoxia and hypoxia. Therefore, total protein content was assessed by BCA analysis, and VEGFA levels were normalised against BCA results. After correction, there was still a significant increase in VEGFA release detected in hypoxic conditions (p=0.0093) (Figure 3.21B,C).

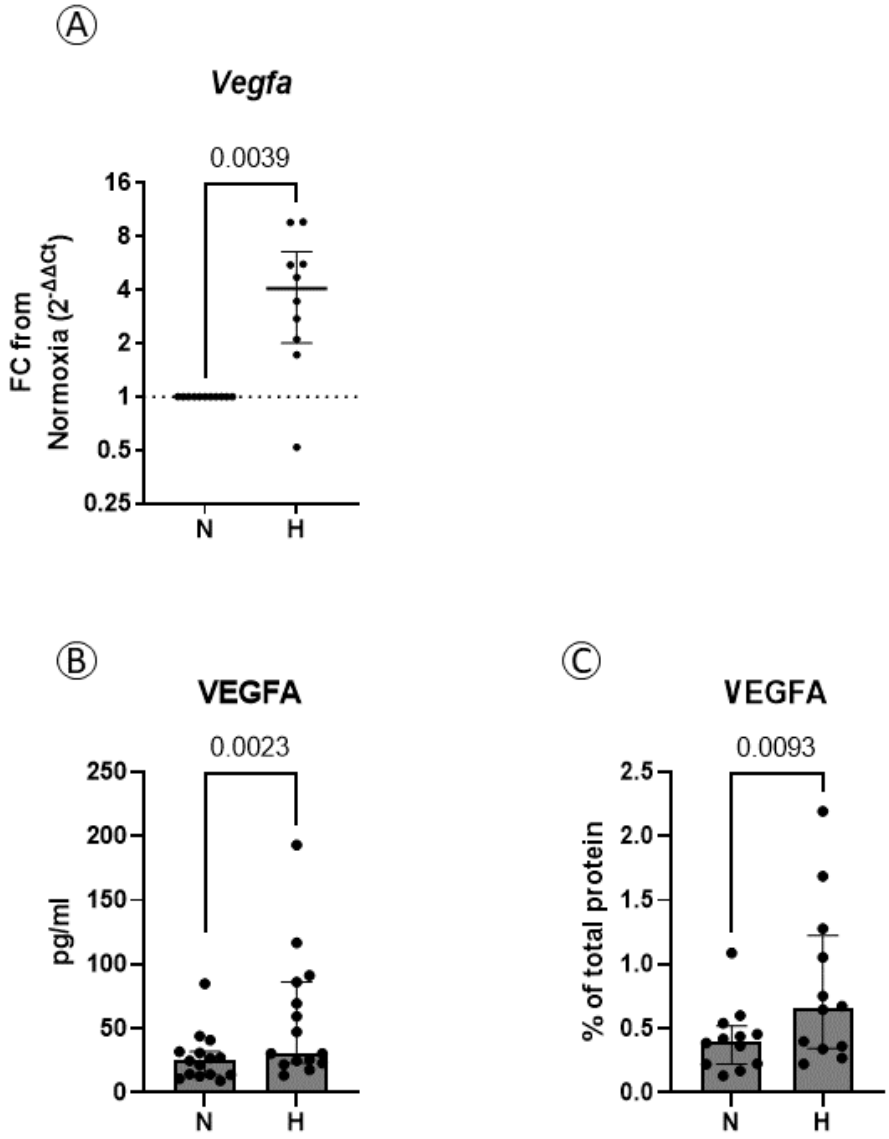

Figure 3.21 VEGFA *Gene and Protein Expression. AMs were incubated in normoxia (21% O_2, 5% CO_2, 37°C) or hypoxia (1% O_2, 5% CO_2, 37°C) for 48 hours. (A) Vegfa RNA transcript levels were subsequently assessed by qPCR, alongside 18S rRNA expression as a loading control. Data was presented as $2^{-\Delta\Delta Ct}$ relative to normoxic AM expression. N=10. N vs H p=0.0023. (B) VEGFA protein secretion into supernatant after 48 hours was assessed by ELISA. N=15. N vs H p=0.0023. (C) VEGF-A protein secretion following normalisation to total protein concentrations, as assessed by BCA analysis. N=15. N vs H p=0.0093. Comparisons were made using Wilcoxon's tests. Graphs show median (±IQR).*

Expression of another HIF1α response gene, *SLC2A1*, was also significantly increased in AMs after 48 hours, when compared to expression normoxia (Figure 3.22). The increase in *SLC2A1* expression was more pronounced than *VEGFA* (7.6 fold increase, p=0.0078).

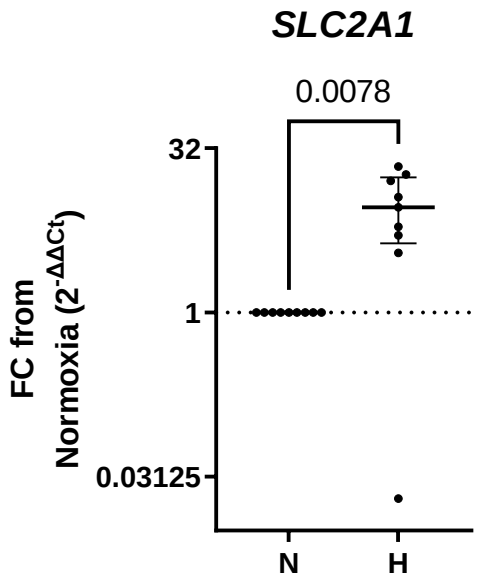

Figure 3.22 SLC2A1 Gene Expression. AMs were incubated in normoxia (21% O_2, 5% CO_2, 37°C) or hypoxia (1% O_2, 5% CO_2, 37°C) for 48 hours. SLC2A1 RNA transcript levels were subsequently assessed by qPCR, alongside 18S rRNA expression as a loading control. Data was presented as $2^{-\Delta\Delta Ct}$ relative to normoxic AM expression. N=9. Comparisons were made using Wilcoxon's test. N vs H p=0.0078. Graphs show median (±IQR).

3.3.3 AM Phenotype

To characterise the phenotype of AMs following hypoxic challenge, the surface expression of various markers was measured using an antibody panel, for assessment by flow cytometry.

Hypoxia did not change the expression of inflammatory macrophage marker CD80 (Figure 3.23 A,E). Furthermore, hypoxia did not modulate expression of scavenger receptors, CD206 and CD163 (Figure 3.23 B,C,F,G). SIRPα expression on AMs was also unchanged by 48 hours hypoxia (Figure 3.23 D,H).

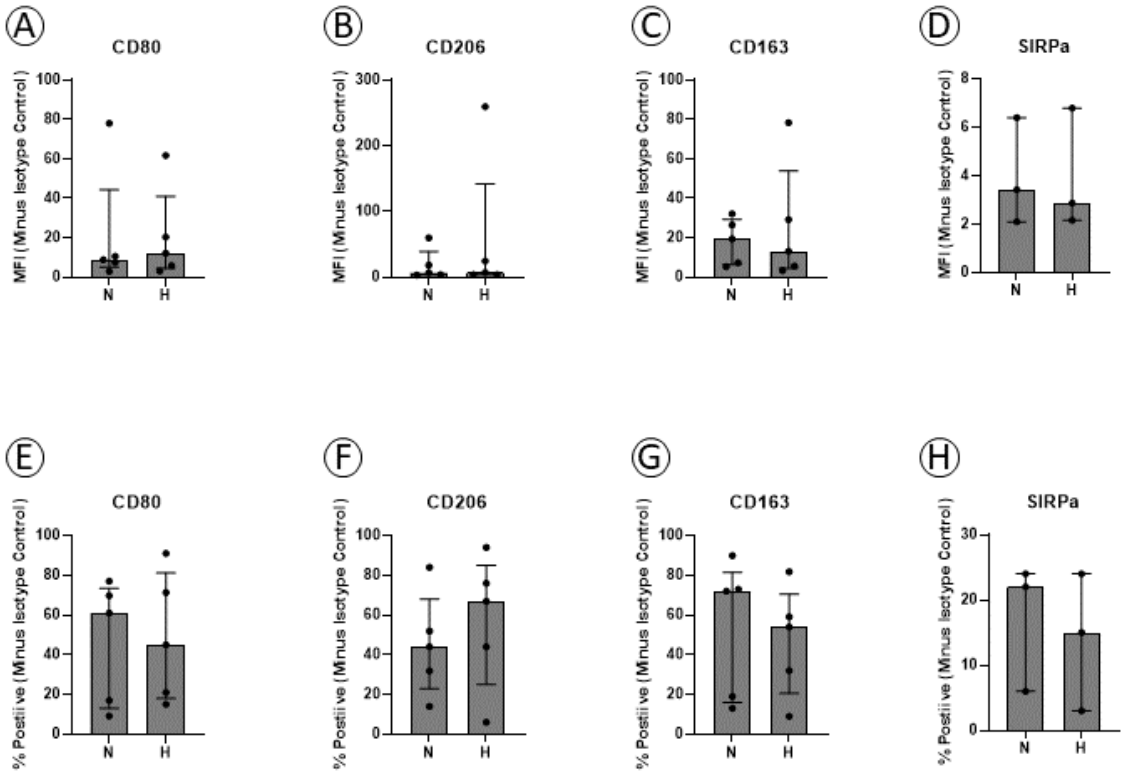

Figure 3.23 AM Surface Marker Expression. AMs were incubated in normoxia (21% O_2, 5% CO_2, 37°C) or hypoxia (1% O_2, 5% CO_2, 37°C) for 48 hours. Surface marker expression was subsequently measured by flow cytometry. The MFI of (A) CD80, (B) CD206 and (C) CD163 (D) SIRPα on the whole AM population were normalised by subtraction of the MFI of isotype control-stained cells. MFI CD80 p>0.9999, CD206 p=0.1875, CD163 p>0.9999, SIRPα p>0.9999. The percentage of AMs expressing (E) CD80, (F) CD206 (G) CD163 and (H) SIRPα were also normalised by subtracting the percentage of cells that stained positive with isotype control panel. MFI CD80 p=0.625, CD206 p=0.1250, CD163 p=0.625, SIRPα p=0.5. N=5, except for SIRPα where N=3. Comparisons were made using Wilcoxon's test. Data is presented as median (±IQR).

3.3.4 AM Secretion and Gene Expression

To further characterise the behaviour of AMs following hypoxic challenge, RNA expression of key genes implicated in the role of macrophages in fibrosis were assessed after 48 hours by qPCR analysis. Additionally, cumulative protein secretion was assessed after 48-hours by ELISA analysis of supernatants.

There no change in m*mp-7* expression after 48 hours hypoxia (Figure 3.24A), however, there was a statistically significant increase in MMP-7 secretion by AMs in hypoxia, relative to those

cultured in normoxia (Figure 3.24B)(p=0.0151). After normalisation to total protein content, the statistically significant increase in MMP-7 secretion remained (p= 0.0302) (Figure 3.24C).

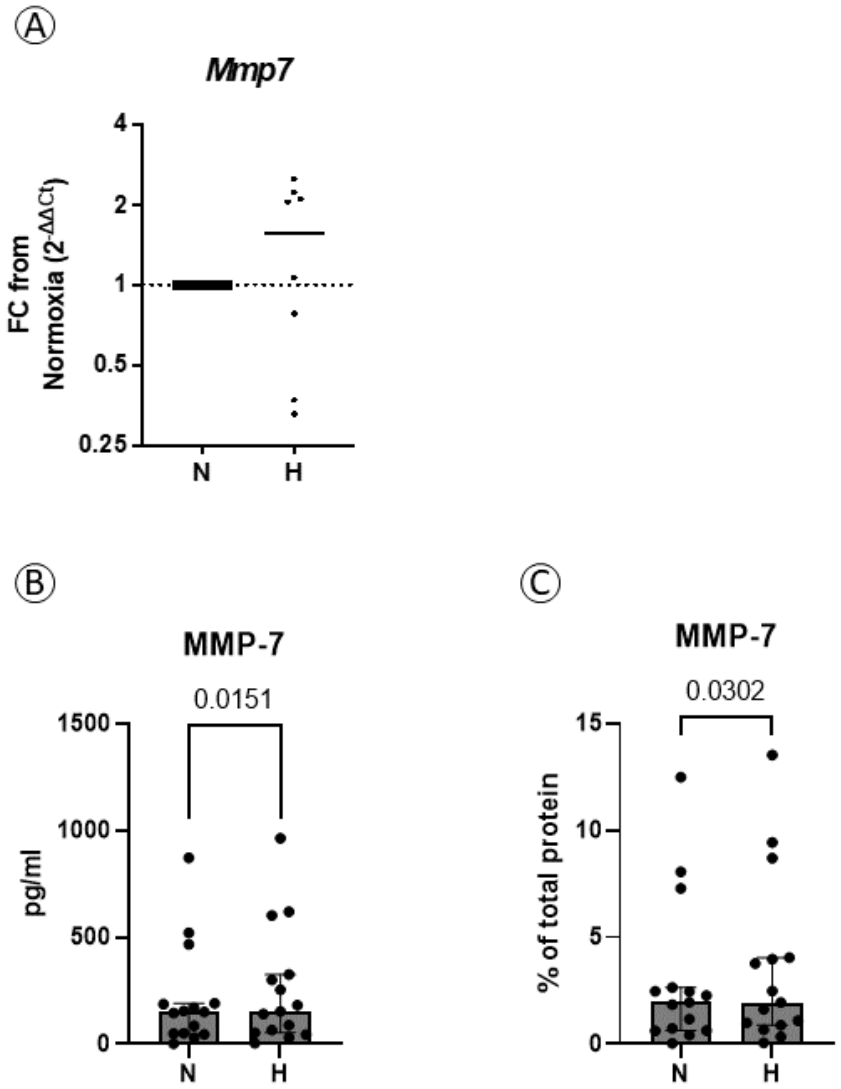

Figure 3.24 MMP-7 Gene and Protein Expression in AMs in Hypoxia. AMs were incubated in normoxia (21% O_2, 5% CO_2, 37°C) or hypoxia (1% O_2, 5% CO_2, 37°C) for 48 hours. (A) Mmp7 RNA transcript levels were subsequently assessed by qPCR, alongside 18S rRNA expression as a loading control. Data was presented as $2^{-\Delta\Delta Ct}$ relative to normoxic AM expression. N=8. N vs H p=0.25. (B) MMP7 protein secretion into supernatant after 48 hours was assessed by ELISA. N vs H p=0.0151 (C) MMP-7 protein secretion following normalisation to total protein concentrations, as assessed by BCA analysis. N vs H p=0.0302. N=15. Comparisons were made using Wilcoxon's tests. Data is presented as median (±IQR).

There was no change in *mmp-1* expression in hypoxia after 48 hours (Figure 3.25A). There was a significant increase in MMP-1 in supernatants (Figure 3.25B) ($p=0.0003$). Following normalisation against total protein content, MMP-1 secretion did not reach statistical significance, although a trend towards increased secretion remained ($p=0.0785$) (Figure 3.25C).

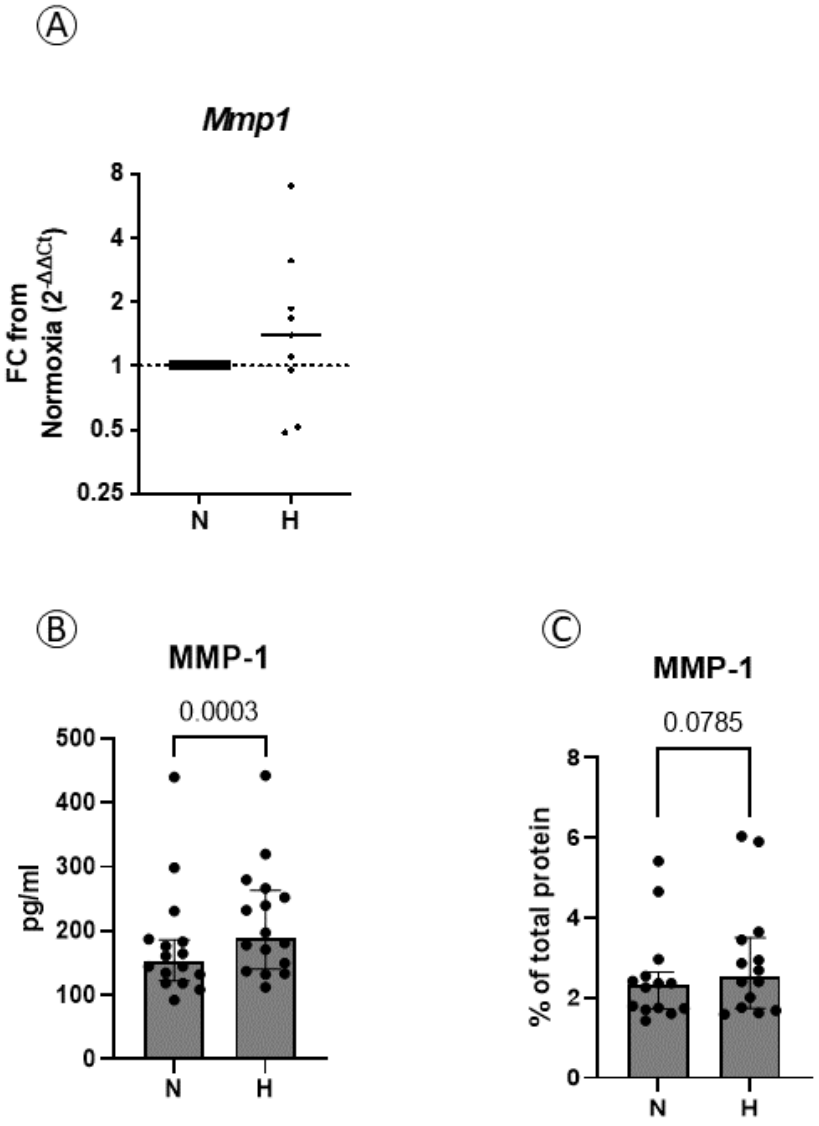

Figure 3.25 MMP-1 Gene and Protein Expression in AMs in Hypoxia. AMs were incubated in normoxia (21% O_2, 5% CO_2, 37°C) or hypoxia (1% O_2, 5% CO_2, 37°C) for 48 hours. (A) Mmp1 RNA transcript levels were subsequently assessed by qPCR, alongside 18S rRNA expression as a loading control. Data was presented as $2^{-\Delta\Delta Ct}$ relative to normoxic AM expression. N vs H p=0.1641. N=8. (B) MMP-1 protein secretion into supernatant after 48 hours was assessed by ELISA. N vs H p=0.0003. N=16. (C) MMP-1 protein secretion following normalisation to total protein concentrations, as assessed by BCA analysis. N vs H p=0.0785. N=14. Comparisons were made using Wilcoxon's test. Data is presented as median (±IQR).

TGFB gene expression was detected in AMs at baseline, however there were no significant changes in expression after hypoxia exposure (Figure 3.26A). In contrast, soluble TGFβ could

not be detected in AM supernatants, at baseline, or following LPS stimulation, once corrected for background TGF-β content in supplemented RPMI alone (Figure 3.26B).

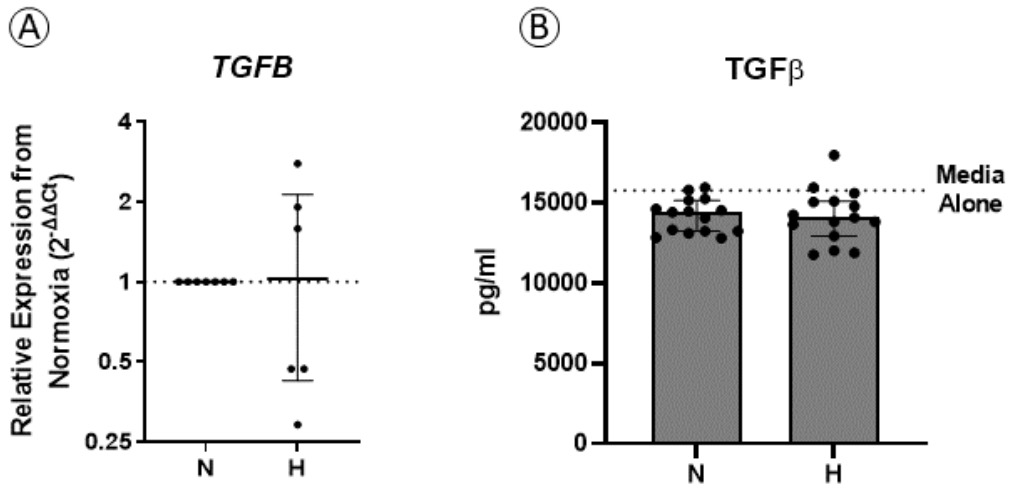

Figure 3.26 TGFβ Gene and Protein Expression in AMs in Hypoxia. AMs were incubated in normoxia (21% O_2, 5% CO_2, 37°C) or hypoxia (1% O_2, 5% CO_2, 37°C) for 48 hours. (A) TGFB RNA transcript levels were subsequently assessed by qPCR, alongside 18S rRNA expression as a loading control. Data was presented as $2^{-\Delta\Delta Ct}$ relative to normoxic AM expression. N vs H p=0.5313. N=6. (B) TGF-β protein secretion into supernatant after 48 hours was assessed by ELISA. TGF-β content was also measured in the media of AMs treated for with TGF-β for 48 hours in normoxia (NT) and hypoxia (HT). TGF-β concentration in media alone was also measured and is shown by a dashed line. N=15. Comparisons were made using Wilcoxon's test. Graphs show median (±IQR).

There were no changes in gene expression in additional fibrosis associated genes *mmp-9* (Figure 3.27A) and *Col1a1* (Figure 3.27B) after 48-hour hypoxia challenge.

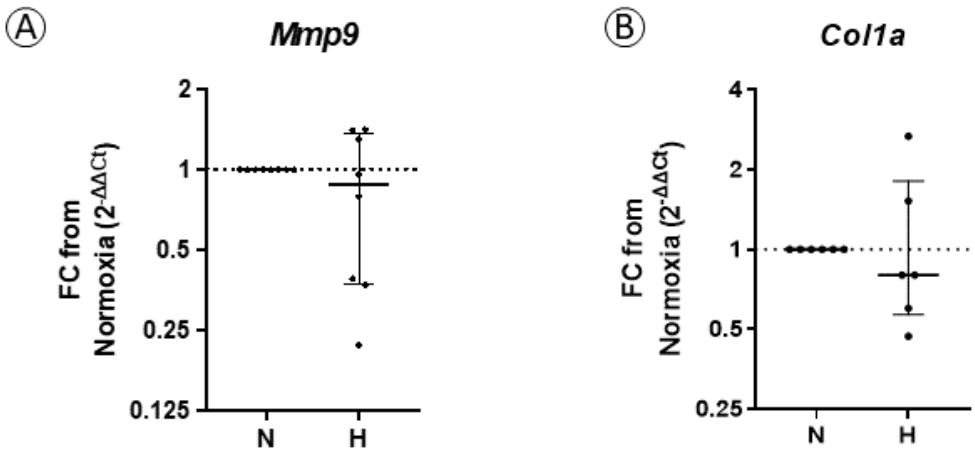

Figure 3.27 Mmp9 and Col1a1 Gene Expression in AMs After Hypoxia. AMs were incubated in normoxia (21% O_2, 5% CO_2, 37°C) or hypoxia (1% O_2, 5% CO_2, 37°C) for 48 hours. (A) Mmp9 and (B) Col1a1 RNA transcript levels were subsequently assessed by qPCR, alongside 18S rRNA expression as a loading control. Data was presented as $2^{-\Delta\Delta Ct}$ relative to normoxic AM expression. MMP9 N=8. N vs H p=0.4609. Col1A1 N=6. N vs H p=9375. Comparisons were made using Wilcoxon's test. Graphs show median (±IQR).

3.3.5 AM Function

3.3.5.1 Phagocytosis and Efferocytosis

AM phagocytosis was measured by 4-hour incubation with heat killed *Streptococcus pneumoniae*, followed by quantification by flow cytometry. The percentage of phagocytic cells and the median fluorescence intensity (MFI) of total AMs were both quantified. AM phagocytosis was unaffected by hypoxia using either measure (Figure 3.28A,B).

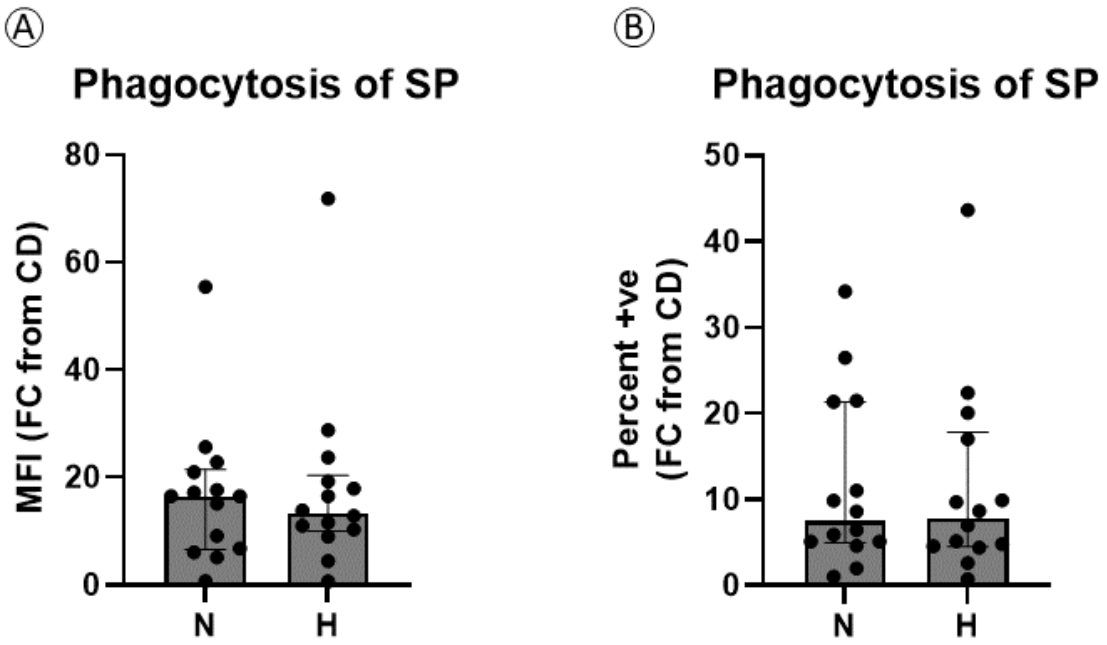

Figure 3.28 AM Phagocytosis in Hypoxia. AMs were incubated in normoxia (21% O_2, 5% CO_2, 37°C) or hypoxia (1% O_2, 5% CO_2, 37°C) for 48 hours. Subsequently, AMs were incubated with heat killed, fluorescently labelled Streptococcus pneumoniae for 4 hours, and phagocytosis was assessed by flow cytometry. (A) Mean fluorescence intensity (MFI) and (B) percentage positive events were presented comparing phagocytosis in normoxia and hypoxia. MFI N vs H p= 0.9515. % positive N vs H p= 5016. Data is presented as a fold change (FC) from cytochalasin D (CD) control. N=14. Comparisons were made using Wilcoxon's test. Graphs show median (±IQR).

To assess the effects of hypoxia on AM efferocytosis, AMs were incubated with apoptotic human neutrophils for 2 hours. The percentage of efferocytic cells and the MFI of total AMs was quantified by flow cytometry. AM efferocytosis of apoptotic neutrophils was significantly reduced by hypoxia. The percentage of AMs to efferocytose dropped from 11.7% (IQR: 16.4) to 2.8% (IQR: 9.4) in hypoxia ($p<0.0001$). Meanwhile, AM MFI dropped from 7.5 (IQR: 12.7) to 1.6 (IQR: 1.4) in hypoxia ($p=0.0003$) (Figure 3.29).

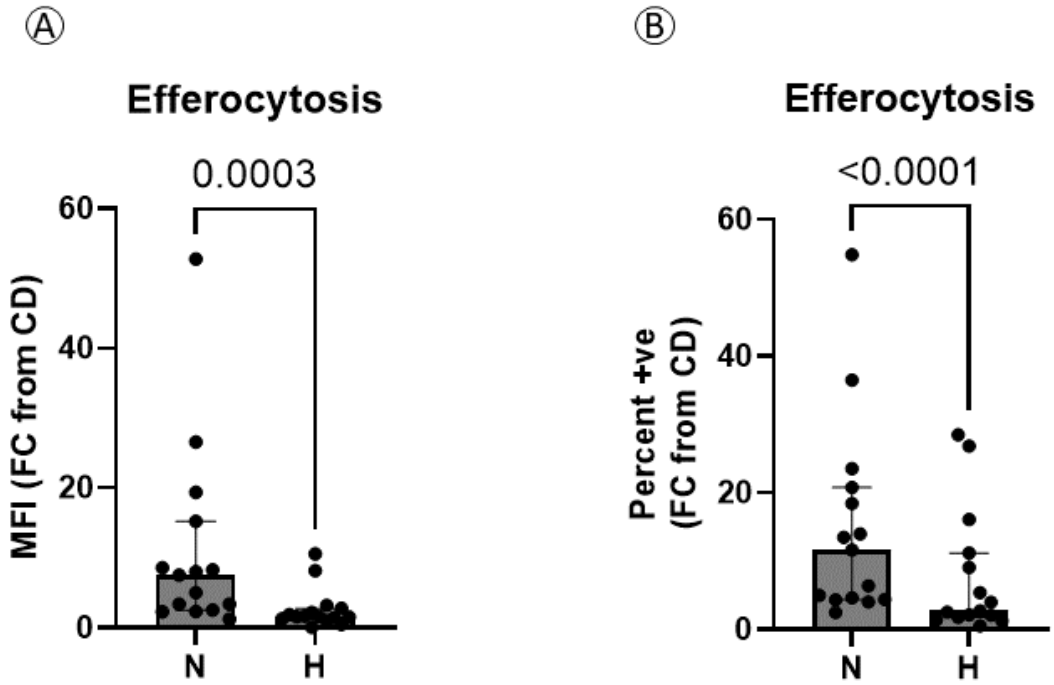

Figure 3.29 AM Efferocytosis in Hypoxia. AMs were incubated in normoxia (21% O_2, 5% CO_2, 37°C) or hypoxia (1% O_2, 5% CO_2, 37°C) for 48 hours. Subsequently, AMs were incubated with fluorescently labelled apoptotic neutrophils for 4 hours, and efferocytosis was assessed by flow cytometry. (A) MFI and (B) percentage positive events were presented comparing efferocytosis in normoxia and hypoxia. Data is presented as a fold change from cytochalasin D control. N=15. Comparisons were made using Wilcoxon's test. MFI N vs H p=0.0003. % positive N vs H p<0.0001. Graphs show median (±IQR).

3.3.5.2 Phagocytosis and Efferocytosis with TGF-β

TGF-β increased AM phagocytosis normoxia, as demonstrated in Figure 3.16. However, in samples for which TGF- β pre-treatment was included only, this increase could not be detected. In hypoxia, TGF-β also had no effect on AM phagocytosis, as assessed by percentage of positive AMs and MFI (Figure 3.30A).

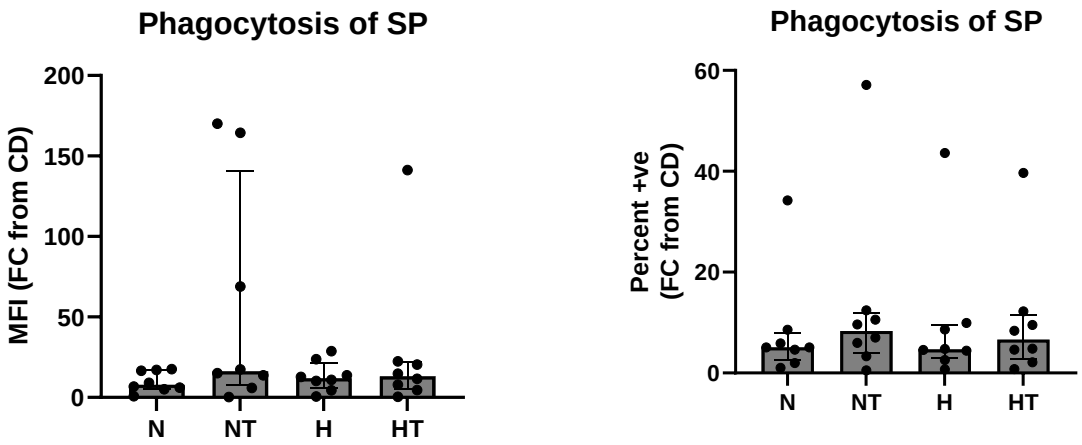

Figure 3.30 AM Phagocytosis with TGF-β in Hypoxia. AMs were incubated in normoxia (21% O_2, 5% CO_2, 37°C) or hypoxia (1% O_2, 5% CO_2, 37°C) with and without 10 ng/ml TGF-β for 48 hours. Subsequently, AMs were incubated with heat killed, fluorescently labelled Streptococcus pneumoniae for 4 hours, and phagocytosis was assessed by flow cytometry. (A) Mean fluorescence intensity (MFI) and (B) percentage positive events were presented comparing phagocytosis in normoxia and hypoxia with and without TGF-β. MFI N vs NT p=0.1990, N vs H p>0.9999, NT vs HT p=0.4882, H vs HT p>0.9999. % positive N vs NT p=0.1208. N vs H p>0.9999, NT vs HT p>0.9999, H vs HT p>0.9999. Normoxia (N), Hypoxia (H), Normoxia with TGF-β (NT), Hypoxia with TGF-β (HT). Data is presented as a fold change (FC) from cytochalasin D (CD) control. N=8. Comparisons were made using a Friedman's test with a Dunn's multiple comparison test. Graphs show median (±IQR).

As demonstrated in Figure 3.16, levels of efferocytosis were not significantly changed in AMs treated with TGF-β in normoxia. Efferocytosis was reduced to a similar extent with TGF-β in hypoxia, when compared to normoxia, in terms of the percentage of AMs to efferocytose and AM MFI. However, when examining only samples including TGF-β conditions, the difference in MFI did not reach statistical significance (p=1280), although reduction in the percent of AMs to efferocytose remained significant (p=0.0221). Statistical testing detected a reduction in efferocytosis in TGF-β stimulated AMs in hypoxia, when compared to TGF-β stimulated AMs in normoxia (Figure 3.31), when assessed as MFI.

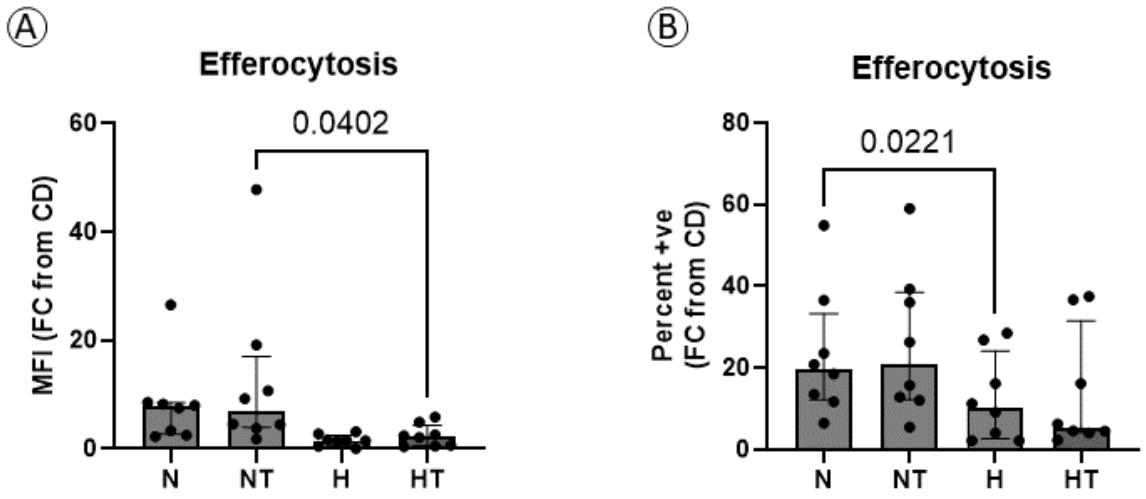

Figure 3.31 AM Efferocytosis with TGF-β in Hypoxia. AMs were incubated in normoxia (21% O_2, 5% CO_2, 37°C) or hypoxia (1% O_2, 5% CO_2, 37°C) with and without 10 ng/ml TGF-β for 48 hours. Subsequently, AMs were incubated with heat killed, fluorescently labelled Streptococcus pneumoniae for 4 hours, and phagocytosis was assessed by flow cytometry. (A) MFI and (B) percentage positive events were presented comparing phagocytosis in normoxia and hypoxia with and without TGF-β. Normoxia (N), Hypoxia (H), Normoxia with TGF-β (NT), Hypoxia with TGF-β (HT). Data is presented as a fold change (FC) from cytochalasin D (CD) control. N=8. MFI N vs NT p>0.9999, N vs H p=0.1280, NT vs HT p=0.0402. H vs HT p>0.9999. % positive N vs NT p>0.9999, N vs H p=0.0221, NT vs HT p=0.0709. H vs HT p>0.9999. Comparisons were made using a Friedman's test with a Dunn's multiple comparison test. Graphs show median (±IQR).

3.4 Discussion

This chapter aimed to assess the effects of hypoxia exposure on AM phenotype and function. AM hypoxia exposure was established and HIF1α responses were characterised. Subsequently, AM surface marker expression, growth factor and proteinase secretion, and gene expression were explored following hypoxia exposure. Finally, after validating tests for AM phagocytic and efferocytic function, AM phagocytosis and efferocytosis were assessed in hypoxia, with and without stimulation with TGF-β.

3.4.1 Smoking status versus AM number and yield.

Studies have previously shown that smokers have increased AM numbers (Skold, Hed and Eklund, 1992; Karimi et al., 2012), with impaired phagocytic capacity, bactericidal properties and efferocytic capacity (Hodge et al., 2003; Lugg, 2020; Lugg et al., 2022). AMs were therefore only obtained from never smokers or long-term ex-smokers (quit >4 years before surgery). Although using exclusively never smoker tissue may have minimised patient variability and removed smoking as a potential confounding factor, the decision to recruit long-term ex-smokers in addition to never smokers was made to maximise recruitment. Studies have shown AMs in BAL return to never smoker numbers within 6 months of quitting (Karimi et al. 2012). Additionally, previous studies by our group have indicated that AM efferocytotic function returns to near normal levels when patients quit smoking for at least 1 year (Lugg, 2020), justifying the comparison of long-term ex-smoker AMs to never smoker AMs. Accordingly, in this study AM yield (Figure 3.7), phagocytosis (Figure 3.7) and efferocytosis (Figure 3.13) were not significantly different between groups. This supports the decision to use both groups in combination for future analysis. Internal controls, comparing normoxia and hypoxia in the same patient sample, also allows for wider inclusion of patients.

3.4.2 Validation of Phagocytosis Assay

The assessment of phagocytosis was validated in section 3.3.1.2. Experimental variables were assessed to ensure existing protocols were effective with new reagents. Firstly, the efficacy of cytochalasin D in inhibiting phagocytosis was confirmed. Cytochalasin D consistently significantly reduced phagocytosis, when assessed as percentage of positive cells and MFI (Figure 3.4). This control is crucial for normalisation of patient samples, particularly as human AMs are known to show varying degrees of autofluorescence (Edelson et al. 1985). The effects

of cytochalasin D were confirmed visually using immunofluorescent staining and microscopy. As expected, cytochalasin D treated AMs did not internalise bacteria like untreated AMs, instead showing membrane binding of bacteria (Figure 3.5). For normalisation, all phagocytic sample data were expressed as a fold change from cytochalasin D control.

Next, the optimal timepoint for assessment of phagocytic capacity was assessed by time course. Previous work using a 4-hour timepoint (Belchamber et al. 2019) was used to guide time points of 2, 4 and 6 hours (Figure 3.6). Despite limited biological replication, a marked phagocytic response was consistently visible in human AMs after 4 hours, with more variability after 2 hours. As there was no discernible difference between the 4- and 6-hour timepoints, the 4-hour timepoint was continued in this work. The decision to proceed from validation after limited replication was made to preserve valuable patient samples, given that previous studies have also used this time point with success.

3.4.3 Validation of Efferocytosis Assay

The assessment of efferocytosis by flow cytometry was also validated. Firstly, consistent induction of neutrophil apoptosis was confirmed. As previously demonstrated (Mahida, Scott, Parekh, Lugg, Belchamber, et al., 2021), overnight serum starvation resulted in consistent neutrophil apoptosis (Figure 3.8). This was vital, as the assay requires the generation of new apoptotic neutrophils for each biological repeat, introducing possible variability between samples.

The efficacy of cytochalasin D was also demonstrated after efferocytic challenge. Cytochalasin D significantly reduced efferocytosis across all donors (Figure 3.10). This allowed for normalisation of all data, by calculating fold change. This was particularly important to control

for variability in neutrophil stimuli between biologic repeats. Additionally, internal normoxic controls were included for each patient sample serving as paired data for normoxic and hypoxic AMs.

A time course was used to confirm that a 2-hour incubation with apoptotic neutrophils was sufficient for detecting efferocytosis (Figure 3.12). As 2 hours provided a consistent signal, and aligned with previous published data (Mahida, Scott, Parekh, Lugg, Belchamber, et al., 2021), this timepoint was used for future analysis after a low number of biological repeats, to limit use of valuable patient samples.

Given that neutrophils would be incubated with AMs for 2 hours in normoxia or hypoxia for assessment of efferocytosis, neutrophil apoptosis was also assessed after these acute treatments. This was important because of the established antiapoptotic effects of hypoxia in neutrophils (Walmsley et al., 2005; Talla et al., 2019). There was no significant difference in the extent of apoptosis in neutrophils after 2 hours of hypoxia versus normoxia (Figure 3.9), likely because substantial apoptosis was induced by overnight serum starvation prior to exposure. This work validated that any changes to efferocytosis in hypoxia are not due to changes in neutrophil apoptosis.

3.4.4 Validation of Macrophage Stimulations

TGF-β was added to AM cultures for the duration of hypoxia, to mimic the profibrotic environment in the lung tissue more closely. To test the hypothesis that hypoxia may potentiate progression in IPF, it is crucial to test the effects of hypoxia in addition to established fibrotic stimuli, as well as in isolation. TGF-β was added at 10 ng/ml ± hypoxia, based on physiological concentrations of TGFB previously measured in BAL fluid of IPF patients (Stijn et al., 2013;

Hiwatari et al., 1997). This dose did not negatively impact viability in normoxia, confirming that any effects were not due to reduced cell viability.

In functional assays TGF-β significantly increased phagocytosis when assessed by MFI. The percentage of cells undergoing phagocytosis also significantly increased. TGF-β stimulation did not alter AM efferocytosis. Although TGF-β typically polarises monocytes and macrophages to a pro-resolution phenotype (F. Zhang et al. 2016), the effect of TGF-β stimulation on mature AMs that are likely naïve to high levels of TGFβ, due to their source from patients without confounding lung disease, could not have been predicted.

LPS has previously been shown to induce macrophage activation, resulting in a subsequent increase in phagocytosis (Fujihara et al., 2003; Wu, Chen and Chen, 2009). This effect has been demonstrated in porcine AMs *in vitro* (Islam et al. 2013). LPS was therefore added to AM cultures, to determine how the priming effects of LPS on macrophages are affected by hypoxia. Although a 10 μg/ml dose of LPS was not toxic, phagocytosis was not increased by a 48 exposure to LPS. It is possible that the known tolerogenic effect of LPS contributed in these conditions, resulting in no detectable increase in phagocytosis. Possibly a lower LPS dose, such as the 1 and 10 ng/ml doses used by Islam et al (2013), or a more acute LPS stimulation would have recapitulated the activation of AMs by LPS. As priming of function by LPS pre-treatment could not be recapitulated in AMs in normoxia, this condition was not assessed in alongside hypoxia challenge.

3.4.5 AM hypoxic challenge validation

AMs were exposed to hypoxia (1% O_2, 5% CO_2, 37^{o}C) for 48 hours, a challenge aimed to replicate the conditions found in hypoxic areas of the IPF lung. This oxygen concentration was

selected based on evidence in a repetitive bleomycin murine model of lung fibrosis. Following injection of pimonidazole in repeat bleomycin challenged mice, pimonidazole adducts demonstrated cellular hypoxia that overlapped with areas of lung fibrosis, particularly in AECIIs (Burman 2018). These adducts are formed in areas of extreme hypoxia, where oxygen levels less than 1% cause reductive activation of the drug, allowing pimonidazole to covalently bind protein thiol groups (Raleigh and Koch 1990). The decision to use this treatment for across this thesis is discussed further in section 6.5.1.

To validate this hypoxic challenge and confirm that 48 hours in hypoxia does not affect the viability of AMs, apoptotic and necrotic cells were differentiated by propidium iodide and annexin V staining. Hypoxia caused no reduction in AM viability (Figure 3.14). This validation ensures that future work is not biased by differential cell numbers because of cell death.

3.4.6 Hypoxia induced HIF1α activation

HIF1α stabilisation and signalling is a classic hypoxia response pathway, which is employed to different extents by different cell types. To confirm that AMs respond to hypoxic challenge via HIF1α signalling, the signalling pathways were assessed for changes at several points. Firstly, HIF1α protein stabilisation was demonstrated. Published literature demonstrates that HIF1α stabilisation peaks acutely in response to hypoxia and decreases over time (Jaśkiewicz et al. 2022). This trend was demonstrated here, as stabilisation at 4 hours was significantly increased over stabilisation at 48 hours (Figure 3.19).

There is less evidence on *hif1a* gene transcript levels as hypoxia persists. Evidence in epithelial cells indicates that *hif1a* mRNA instability (Jaśkiewicz et al. 2022), and negative regulation by hypoxia responsive miRNA (Bartoszewska et al. 2015) and HIF1α anti-sense transcripts (Uchida

et al. 2004) cause decreased transcript levels as hypoxia persists. However, there is limited evidence of this effect in macrophages or in lung tissue. Figure 3.20 demonstrates that after 48h hypoxic challenge, there was a trend towards reduced *hif1a* expression. This correlates with literature in epithelial cells and explains the relative reduction in HIF1α protein after 48 hours. *Hif1a* expression before 48 hours was not assessed. Therefore, this study may have missed an earlier peak in *hif1a* transcription before a plateau or decrease after 48h.

Beyond this, the response of two key HIF1α response genes were assessed to demonstrate activation of HIF1α response programs. *VEGFA* is an established HIF1α response gene, activated to increase angiogenesis in hypoxia. It has been widely used in the literature to demonstrate HIF1α activation (Balamurugan 2016). After 48 hours in hypoxia, *VEGFA* expression was significantly increased (Figure 3.21). Cumulative VEGFA secretion, as assessed by ELISA, was also significantly increased in hypoxia treated AMs. However, marginal differences in supernatant volumes observed after hypoxia exposure indicated differential levels of evaporation in the hypoxia chamber, when compared to the normal incubator. Therefore, total protein contents of the supernatants were assessed by BCA, to determine whether these differences were due to an artificial increase in total protein concentrations. ELISA results were normalised to total protein concentrations. The significant increase in VEGFA was real and remained significantly increased after this normalisation. This data confirms VEGFA transcriptional and translational response in AMs in response to hypoxia.

Beyond its relevance as a HIF1α response gene, VEGFA has been implicated in the disease mechanism of IPF, although results are conflicting (Barratt, Flower, et al., 2018). Some studies have identified an increase of VEGFA in IPF BAL, proposing a pathological role in the disease

(Simler et al. 2004; Ando et al. 2010), whilst others detect a decrease and suggest a protective function of VEGFA (Meyer, Cardoni and Xiang, 2000; Murray et al., 2017). One study has implicated differential VEGFA isoforms in the contradictory results seen in IPF patient samples, with the VEGF-A_{165}b isoform identified as highly enriched in IPF lung tissue (Barratt et al. 2017). Production of this isoform was demonstrated in epithelial cells, AMs and fibroblasts, although increased production in IPF tissue could only be detected in epithelial cells. Further studies of IPF AMs would be required to determine whether AMs contribute to this difference in VEGFA isoforms. It has previously been demonstrated that hypoxia induces expression of the $VEGFA_{165a}$ isoform in pulmonary fibroblasts, but not $VEGFA_{165b}$ (Barratt, Blythe, et al., 2018). Unfortunately, the VEGFA ELISA used here measures global VEGFA protein and the *VEGFA* primer binds multiple splice variants of the gene, meaning these results cannot differentiate between VEGFA isoforms. Therefore, further work would be required to predict the effects of hypoxia driven VEGFA release directly in IPF disease progression or protection.

GLUT1 is another frequently cited marker of HIF1α responses. The glucose transporter is typically upregulated to facilitate anaerobic glucose metabolism in response to hypoxia (Balamurugan 2016). Expression of the gene encoding GLUT1, *SLC2A1*, was significantly increased in AMs after 48 hours hypoxia (Figure 3.22). This change could not be determined at the protein level, as western blotting for GLUT1 required unreduced protein, which was incompatible with other proteins assessed by western blotting. GLUT1 is evident in areas of fibrosis in human lung tissue (Xie et al., 2015; Li et al., 2022a; Hamanaka et al., 2021; Cho et al., 2017), and although often associated with glycolytic and synthetic fibroblasts, it may also play a role in glycolytic reprogramming of AMs. This makes *SLC2A1* expression a potentially relevant change in AM function, as well as a marker of HIF1α signalling.

Together, these results confirm the activation of HIF1α dependent signalling in AMs after 48 hours of hypoxic challenge. This highlights HIF1α as one of the potential routes by which hypoxia may mediate its effects on AMs in future work, particularly given the evidence that HIF1α plays a role in macrophage polarisation. Although initial studies by Takeda et al (2015) indicated that HI1α was responsible for inflammatory macrophage polarisation and HIF2α was responsible for pro-resolution macrophage polarisation, evidence in bleomycin treated mice highlighted the glycolytic dependence of profibrotic AM polarisation (Xie et al. 2017). This emphasises the need to understand the role of HIF1α in this model.

3.4.7 AM Phenotype in Hypoxia

Surface markers are frequently used to differentiate polarisation states in macrophages. Some pro-resolution markers expressed by AMs, which are upregulated on IPF AMs, include CD206 and CD163 (Byrne, Maher and Lloyd, 2016). CD206 is a mannose receptor, capable of binding a range of pathogenic molecules (Martinez-Pomares et al. 2001). CD206 is also anti-inflammatory (S. J. Lee et al. 2002) and is closely associated with macrophage TGF-β release and fibroblast activation (Bellón et al. 2011). Meanwhile, CD163 functions as a cell free haemoglobin scavenger receptor, it also has key anti-inflammatory functions and plays a role in tolerance induction and efferocytosis (Savill et al., 1992; Schaer, Alayash and Buehler, 2007). Additionally, it can act as an immune sensor for gram negative and positive bacteria (Fabriek et al. 2009). Macrophages co-expressing CD206 and CD163 are demonstrated to have high efferocytic capacity (Zizzo et al. 2012).

Unfortunately, AM phenotype in hypoxia could only be assessed in a low number of biological replicates. Human AM phenotype is also markedly variable here, emphasising the need for

further biological replication. Hypoxia did not consistently alter the percentage of AMs expressing CD206 or the level of expression on total AMs (MFI) (Figure 3.23). This contrasts with a study of tumour associated macrophages in a murine model of OSA, where intermittent hypoxia induced an increase in CD206 expression, as well as other markers of pro-resolution polarisation, such as increased *il10* gene expression (Campillo et al. 2017). It also contrasts with studies of THP-1 macrophages and monocyte derived macrophages, in which LPS/IFN-γ induced 'M1 macrophages' cultured in hypoxia upregulated CD206 expression to a similar extent as IL-4 induced 'M2 macrophages' in normoxia (Raggi et al., 2017; Ke et al., 2019).

Similarly, CD163 expression did not change consistently on AMs in hypoxia, when assessed as percent positive or MFI (Figure 3.23). This is in line with a study showing that M-CSF polarised monocyte derived macrophages showed no change in CD163 expression after 24 hours hypoxia (1.5% O_2) (Jeny et al. 2021).

SIRPα is a surface receptor that binds CD47 on live cells, resulting in suppression of efferocytic response. This receptor was also not consistently modulated in hypoxia (Figure 3.23). While there is extensive evidence of hypoxia in tumours modulating CD47 expression on cancer cells for immune evasion, there is very little evidence of the effects on SIRPα expression on macrophages.

CD80 is a costimulatory molecule, typically indicative of inflammatory polarisation in macrophages (Bertani et al. 2017) including AMs (Balbo et al. 2001). CD-80 also showed no changes after hypoxia exposure (Figure 3.23). This contrasts with the published effects of hypoxia, which decreased CD-80 expression on MCSF (Jeny et al. 2021), IL-4 and LPS/IFNγ (Raggi et al. 2017) differentiated monocyte derived macrophages.

AM surface marker levels in response to hypoxic challenge were markedly variable. This could be due to patient variability in the level of these markers at baseline in the tissue. Therefore, it is possible that a larger number of biological replicates may have detected a statistical difference in the expression level of these markers or identified groups of patients whose AMs respond differently to hypoxia. Of relevance, smoking status results in increased co-expression of typically M1 and M2 markers, including increased expression of CD206 in AMs (Bazzan et al. 2017; S. T. Lugg et al. 2022) and CD163 (S. Lugg 2020). Additionally, in COPD, AMs from smokers expressed less CD163, compared to ex-smokers (Dewhurst et al. 2017). Therefore, the inclusion of long-term ex-smokers in this analysis may affect the sensitivity of results, by introducing more baseline variability in surface marker expression. Unfortunately, there are insufficient replicates in this data to compare baseline expression across smoking status in this study.

3.4.8 AMs Secretion in Hypoxia

In addition to surface markers, a range of key genes implicated in fibrosis were assessed in AMs at the gene transcription and protein level, with and without hypoxic challenge. There was no change detected in *mmp7* (Figure 3.24), *mmp1* (Figure 3.25) or *mmp9* (Figure 3.27) expression in hypoxic AMs at 48 hours. Cumulative MMP-7 and MMP-1 secretion over 48 hours were assessed by ELISA (Figure 3.24 and Figure 3.25). Following normalisation to total protein content, as described for VEGFA ELISAs above, MMP-7 concentrations were significantly increased in hypoxia, whilst MMP-1 concentrations were not significantly different, although the trend towards increased secretion remained.

In line with the increased MMP-7 secretion, but contrasting with expression data, *mmp-7* expression was increased after 16h hypoxia in human monocyte derived macrophages,

differentiated with human serum to an 'M0' phenotype. Although this study proposed a putative HIF1α response element in the *mmp-7* promoter, luciferase studies were unable to confirm this control mechanism (Burke et al. 2003). Although studies in several other cell types have found a similar increase in MMP-7 secretion in hypoxia exposed cells, a mechanism for this increase is yet to be identified (Sabha et al. 2006; Deguchi et al. 2009). There is more frequent evidence of MMP-1 induction by hypoxia in a range of cell types (Proulx-Bonneau, Guezguez and Annabi, 2011; Lee et al., 2012; Shin et al., 2015; Bolatkan et al., 2021), including macrophages (Tandel et al. 2022), supporting the trend shown here. The mechanisms of these changes vary between cell types, emphasising the cell specific nature of hypoxia responses and the importance of investigation in the cell type of interest.

Evidence from IPF cohorts has demonstrated significant increases in MMP-7 and MMP-1 in BAL from IPF patients (McKeown et al., 2009; Chuliá-Peris et al., 2022). AMs have been strongly implicated in MMP-7 release in the lung, however, there is no specific literature showing increased secretion by AMs in IPF (Zuo et al. 2002), meanwhile AMs have been directly implicated in MMP1 increases (Selman et al. 2000; Zuo et al. 2002). It has been proposed that dysregulated MMP expression results in tissue damage during IPF escalation, potentiating the aberrant wound healing response. The data presented here suggests that hypoxia potentiates lung fibrosis by increasing secretion of select proteinases. Interestingly, serum MMP-7 levels in IPF patients were increased in patients with severe OSA, when compared to those with no OSA and mild or moderate OSA (Gille et al., 2017a). Given the link between OSA and tissue hypoxemia, this trend supports the link between MMP-7 release and hypoxia proposed here. There is also evidence that in hypoxia MMP-7 is more active (Sabha et al. 2006). Although

beyond the scope of this study, this change would compound the damage caused by increased secretion.

TGF-β was also assessed at the gene and protein expression level, as AMs are key producers of the growth factor (Byrne, Maher and Lloyd, 2016), and TGF-β is highly implicated in IPF disease progression (Khalil et al. 1989; Jagirdar et al. 1996). Gene expression was unchanged in AMs after 48 hours hypoxia (Figure 3.26). Protein secretion in the media was assessed by ELISA of total TGF-β, after activation of TGF-β by acidification. There was a large amount of TGF-β in supplemented RPMI, likely due to FBS content, which contains 10000 to 20000 pg/ml TGF-β (Danielpour et al. 1989). No additional TGF-β secreted by AMs could be detected in this assay after normalisation using blank media. The sensitivity of this assay was severely hampered by the high TGF-β content of the media. For specific assessment of TGF-β content, FBS could have been depleted for TGF-β (Oida and Weiner 2010) or been replaced with BSA for culture. However, this would have required extensive validation in AM culture, which was beyond the scope of this thesis.

Expression of additional genes associated with AMs in IPF were assessed by qPCR. *Mmp-9* expression was assessed due to its increased presence in IPF BAL and evidence tying this increase to IPF AMs (Henry et al. 2002). However, no changes were found in *mmp-9* gene expression. This contrasts with a study showing that THP1 derived macrophages exposed to hypoxia expressed more *mmp-9* after 24 hours hypoxia (D'Alessandro et al. 2019). Additionally, *Col1a1* expression was assessed, to address the ability of AMs to produce ECM components. *Col1a1* has been shown to be increased in IPF AMs (Tsitoura et al. 2021) and is increased in fibroblasts in response to hypoxia (Robinson et al. 2012). No changes in *Col1a1* gene expression

were detected in hypoxia treated AMs. Although no evidence was found here for expression changes in these genes, protein concentration and enzyme activity assessment would be required to completely rule out changes missed due to timepoint assessed, or post-transciptional or post-translational control of these genes/proteins. For example, Rahat et al (2006) found that hypoxia reduced MMP-9 output from human monocytes by impairing secretion of the proteinase.

3.4.9 AM Phagocytosis in Hypoxia

AMs consistently phagocytose heat-killed *Streptococcus pneumoniae* in normoxia. Hypoxia caused no significant difference in phagocytosis by AMs. However, whereas TGF-β increased phagocytosis in normoxia, the effects of hypoxia on this trend were hard to determine. There was no increase in phagocytosis in hypoxia with TGFβ, however statistical testing also indicated no difference between phagocytosis in untreated and TGFβ treated AMs in normoxia following comparison of all four groups. Further replication may allow for reliable interpretation of these results, however the small effect size of TGFβ alone increases the power required to detect changes.

The lack of effect of hypoxia on phagocytosis contrasts with previously published data (Anand et al. 2007), which demonstrated that murine peritoneal macrophages increased phagocytosis of IgG opsonised latex beads in hypoxia in a HIF1α dependent manner. However, this was in response to an acute hypoxic challenge of just 2 hours, in macrophages adapted to low physiological concentrations found in the peritoneum. Additionally, this model used latex beads that provide a different level of immune challenge to macrophages. For these reasons, direct comparisons are difficult to draw here.

3.4.10 AM Efferocytosis in Hypoxia

Efferocytosis was consistently decreased in AMs cultured in hypoxia. This change persisted in the presence of TGFβ. The differential effects of hypoxia on phagocytosis and efferocytosis indicate that hypoxia may uniquely affect an element of efferocytic signalling or response. The most marked differences between efferocytosis and phagocytosis are in the receptors mediating the response. However, no differences were detected in key efferocytic receptors CD206 and CD163, or anti-efferocytic SIRPα after hypoxia. Although this data relies on limited biological repeats, and may change with replication, it raises the possibility that other unique factors of efferocytosis are impaired by hypoxia.

Efferocytosis induces a sequence of responses in phagocytes, which prepare the cell for continual efferocytosis (A-Gonzalez et al., 2009). Given that hypoxia invokes its own profound transcriptional responses, some of which have been linked to inflammatory polarisation in macrophages (Takeda et al. 2010), the modulatory effect of efferocytosis may be altered in hypoxic cells. Section 3.3.2 demonstrated a HIF1α response to hypoxia in AMs. The plethora of HIF1α response genes induced by hypoxia may have the capacity to differentially modulate efferocytosis and phagocytosis. The contribution of HIF1α signalling can be dissected using a range of inhibitors, which induce HIF1α stabilisation or downregulation. These inhibitors will be validated and their effect on AM function assessed in Chapter 4 of this thesis.

The impairment in efferocytosis detected here contrasts with recently published data, showing a hypoxia driven increase in efferocytosis by murine macrophages derived from immortalised bone marrow progenitors (Y.T. Wang et al. 2022). Bone marrow derived macrophages, both differentiated in hypoxia (1% O_2, 5% CO_2) and in normoxia (21% O_2, 5% CO_2) showed a

significant increase in efferocytosis of apoptotic thymocytes after 7 days of hypoxic exposure. This hypoxia driven increase was also seen in bone marrow and spleen resident macrophages, when investigated *ex vivo*.

This result was also reported in human monocyte derived macrophages differentiated with GMCSF and subsequently polarised using IL-4 to an 'M2' phenotype (Norris, Libreros and Serhan, 2019). Following 24-hour incubation in hypoxia (1% O_2, 5% CO_2), efferocytosis of human senescent red blood cells and human apoptotic neutrophils were increased.

There are some differences between the studies described above and the work presented here, which may explain the contrasting results. Namely, the different types of apoptotic cells delivered, and the different hypoxia exposure time points used. However, one study did use apoptotic neutrophils to assess efferocytosis, and the studies reporting increased efferocytosis in hypoxia, included one with a shorter hypoxia exposure and one with a longer hypoxia exposure than that used here. It is therefore possible that a factor beyond experimental design causes these contrasting results.

It is possible that a unique feature of AMs causes their impairment in hypoxia. Normal oxygen availability and metabolism of human AMs distinguishes them from the macrophages used in these studies. Wang et al (2022) focussed on macrophages differentiated in low oxygen environments, such as the spleen and bone marrow. A novel pentose phosphate pathway loop was identified in these macrophages, which allowed for generation of NADPH via a pathway similar to gluconeogenesis. Authors suggest that this metabolic adaptation permitted increased efferocytosis in hypoxia. In these macrophages, hypoxia is physiological, expected, and constant. Contrastingly, AMs are adapted to a tissue specific niche with low glucose and

relatively high oxygen availability (Gill et al. 2016). Therefore, AMs rely heavily on oxidative phosphorylation and fatty acid oxidation, with very little glycolysis (Svedberg et al., 2019a), even in response to stimulation with LPS (Woods et al., 2020a; Pereverzeva et al., 2022). This is markedly different to the behaviour of MDMs or BMDMs *in vitro*. Further differences in AM metabolic capacity may limit their capacity to employ a similar shunt towards the pentose phosphate pathway to adapt to hypoxia.

Interestingly, although some studies indicated that AMs did not respond to LPS stimulation by increasing glycolysis (Pereverzeva et al., 2022), Woods et al. (2020) also showed that in murine AMs, hypoxia did increase glycolysis and glycolytic reserve, in a HIF1α dependent way. This indicates that although AMs rely less on glycolysis in response to stimuli, they can mount a HIF1α mediated glycolytic response in response to hypoxia. This work is largely limited to murine AMs. Although Pereverzeva et al (2022) demonstrated a lack of glycolytic response to LPS in human AMs by measuring lactate release, real time analysis of AM metabolism in hypoxia has been shown in murine AMs only. Therefore, assumptions about human AMs must made with caution, given the nuances in human versus murine AMs.

Efferocytosis is a unique metabolic process for professional phagocytes requiring extraordinary metabolic flexibility in macrophages. Failure to maintain flexibility prevents continual efferocytosis, due to build-up of cholesterol and lipids, causing significant cellular stress and even death (Lara-Guzmán et al. 2018). Therefore, the metabolic flexibility of AMs in hypoxia may be of key importance to their function, and key in explaining why AMs, but not other tissue resident macrophages, fail to efferocytose in hypoxia. Lack of oxygen may impair one or more of the metabolic shifts required to keep AMs fit for continual efferocytosis.

3.5 LIMITATIONS

This work uses a unique source of human tissue to provide insight into human AM responses to hypoxia. There are limitations to this supply. As discussed, some patients are long term ex-smokers, introducing patient variability. However, smoking is a major risk factor for IPF, meaning that this previous exposure is not unexpected in IPF AMs. Additionally, limited and variable tissue volumes and AM yields mean not all experiments can be performed in all patient samples. Therefore, some experiments included low levels of biological replication, especially the validation and phenotypic characterisation. For this reason, results may change with increased biological replication. Furthermore, viability and function could not be directly compared in all assays, although viability can be inferred from consistent results seen in AMs assessed.

Tissue was obtained from patients with lung cancer. Although tissue accepted was histologically normal, its proximity to cancerous tissue may have had undetectable effects on AMs. Of relevance to this project is the potential of limited blood supply and hypoxia in the tissue surrounding a tumour. Some patient samples may have been pre-exposed to hypoxia due to this effect, possibly altering hypoxia responses in these experiments.

Tissue was obtained from otherwise healthy patients, without fibrotic lung disease. Although AMs from this tissue can be used to test whether hypoxia can initiate dysfunction in AMs, it cannot be used to directly test the effects of the development of hypoxia in IPF patients as the disease progresses. TGFβ stimulation was introduced to address this limitation, testing how hypoxia and profibrotic stimulus together effected AM function, however the combination was not used for phenotypic or expression assays. The introduction of TGFβ in functional assays was not introduced prior to hypoxia, to induce any polarising effect on AMs before hypoxia. This

limits the relevance of this challenge in modelling IPF AMs, however pre-treatment with TGFβ would have extended assays, prolonging *ex vivo* culture of AMs.

Furthermore, the fibrotic environment in human lung tissue is much more complex than TGFβ alone. To truly understand the effects of hypoxia on AMs as IPF progresses, a separate study would be required to examine the effects of hypoxia on IPF patient AMs, preferably from early disease BAL samples. This would be particularly important, as it is likely that monocytes are recruited to the lung during early IPF and replenish the AM pool by differentiating in a highly fibrotic environment (Misharin et al. 2017). This means that although the use of human AMs is useful for modelling the unique tissue resident cell population, the AM population in IPF may have a markedly different phenotype.

Surface marker expression analysis would have benefitted from inclusion of additional markers. For example, MERTK is an integral apoptosis receptor (Zizzo et al. 2012). MERTK levels were not detected consistently in preliminary staining and therefore could not be assessed for change in hypoxia. As HIF1α has been shown to modulate MERTK expression in cardiac tissue, this marker could be of relevance in the impaired efferocytosis seen (DeBerge et al. 2021).

RNA expression assessment of several fibrotic mediators performed in AMs provides insight into gene expression, however as RNA was only assessed at a 48-hour time point, information about RNA expression peaks earlier in exposure were lost. Secreted protein levels would have detected cumulative changes over the whole 48-hours and accounted for posttranscriptional and posttranslational control. Further still, the function of secreted proteins, particularly proteinases MMP-7 and MMP-1 were not assessed. This is particularly pertinent, as the activity

of some MMPs in hypoxia has been linked to activation by mediators such as ROS (Shin et al. 2015).

The phagocytosis and efferocytosis assays used for this work included a single timepoint to assess changes, as cell numbers were limited. Although the information on function is valuable, these assays do not capture information about the speed and duration of phagocytosis and efferocytosis, nor the long-term consequences of efferocytosis or phagocytosis. Multiple timepoints can be used to determine the progression of function over time. Further to this, timelapse microscopy would be valuable to track uptake of bacteria or apoptotic cells over time at a higher resolution. Finally, assessment of AM phenotype and function after phagocytosis or efferocytosis would be required to fully characterise the fitness of AMs for continual uptake. This would be particularly interesting to track the capacity of AMs for continual efferocytosis, as this process requires metabolic adaptation throughout, due to the complex cargo introduced by efferocytosis. This information would be crucial to determine at which point efferocytosis is impaired and how. For example, do AMs fail to initiate efferocytosis completely, or initially efferocytose normally, but fail to adapt for continual efferocytosis?

The phagocytosis assay used here used *Streptococcus pneumoniae*. This is a relevant pathogen for the study of respiratory infections in IPF patients, given that it is the most common bacteria in IPF patient BAL according to meta-analysis (Mostafaei et al. 2021). However, other organisms such as *Haemophilus influenzae* are also increased in IPF patient BAL. Distinct results may be found in this case, due to the significant differences in the PAMPs associated with each species, particularly as *Streptococcus pneumoniae* is gram positive and *Haemophilus influenzae* is gram negative. Additionally, bacteria in this assay were heat killed, to facilitate running these assays

within level 1 containment. However, live bacteria provide unique challenges to macrophages that cannot be recapitulated by heat killed strains. In particular, the phagocytosis assay described here cannot test the ability of AMs to kill bacteria, a necessary function that has been shown to be reduced in neutrophils in hypoxia, despite their sustained ability to phagocytose heat killed bacteria (McGovern et al. 2011).

The efferocytosis assay used for this work employs apoptotic neutrophils to model the process. Although neutrophils are increased in IPF BAL (Meyer et al. 2012), the widely accepted model of IPF progression implicate poorly controlled epithelial cell apoptosis in disease progression (Chambers and Mercer, 2015). Therefore, it would be valuable to confirm whether this impairment in efferocytosis extends to apoptotic epithelial cells. Such efferocytosis assays using apoptotic BEAS2B epithelial cell lines have been previously described (C. S. Lee et al. 2016).

3.6 Conclusion

This chapter establishes a model of hypoxic exposure of human AMs. Additionally, functional assessment of phagocytosis and efferocytosis by flow cytometry was comprehensively validated. A HIF1α response was confirmed in AMs across 48 hours, with HIF1α stabilisation and increased VEGFA and GLUT1 responses demonstrated. No changes in surface marker expression were detected accompanying these responses to hypoxia, although a significant increase in MMP-7 release was detected. Hypoxia significantly and markedly impaired efferocytosis, but not phagocytosis, in AMs. These results contrast with the effects of hypoxia on efferocytosis described in different macrophage types, possibly due to the distinct adaptations of AMs to the alveolar niche.

CHAPTER 4: MECHANISTIC INVESTIGATION INTO THE EFFECT OF HYPOXIA ON AMS

4.1 INTRODUCTION

Chapter 3 investigated the effects of hypoxia on AMs. The main effect of hypoxia demonstrated was an impairment of efferocytosis, while no effect was seen on phagocytic function. Efferocytic function in AMs is crucial to clear apoptotic cells resulting from microinjury and wound healing responses in the epithelium, which are key mechanistic drivers implicated in IPF development (Chambers and Mercer, 2015). Therefore, hypoxia driven impairment in AM efferocytosis could feasibly lead to establishment or potentiation of a fibrotic cascade in the lung.

It is important to understand why and how hypoxia impairs efferocytosis function in AMs. Importantly, phagocytosis is not impaired, indicating that the mechanism effects an element unique to the efferocytosis pathway. Initial investigation did not detect changes in the receptors involved in efferocytosis. Although this finding may change with additional biological replication, this highlights the possibility that a different distinction between efferocytosis and phagocytosis is affected by hypoxia.

In comparison to phagocytosis, efferocytosis involves the engulfment of much larger bodies, with high lipid content to be broken down in the phagolysosome and metabolised by the cell. This is compounded by continual efferocytosis, as lipid burden is continually increased (Yin and Heit 2021). Accordingly, Zhang et al. (2019) demonstrated that efferocytosis increases basal and maximal oxygen consumption rate in macrophages, alongside a smaller increase in extracellular acidification reflecting glycolytic rate. These changes were associated with a

marked increase in lipid metabolism, a process which is highly dependent on oxygen availability (Jain et al. 2020). Impairment of lipid processing limits continual efferocytosis. Although there are no studies directly comparing the metabolic demands of and adaptations required for efferocytosis and phagocytosis, the differences in cargo and the oxygen requirements associated with these differences suggests that metabolism differentiates the two processes in a way that could be affected by hypoxia.

Hypoxia activated HIF1α responses in AMs. HIF1α mediates a wide range of transcriptional responses and is a known modulator of metabolism in macrophages. These metabolic changes have previously been linked to macrophage polarisation. It is therefore possible that HIF1α mediated changes in AM metabolism alters their efferocytic capacity, whilst maintaining phagocytic capacity. To investigate the role of HIF1α in mediating efferocytic impairment, HIF1α can be artificially stabilised in normoxia or inhibited in hypoxia, using small molecule inhibitors.

HIF1α upregulates glycolysis in a wide range of cells (Corcoran and O'Neill 2016). Typically, under aerobic conditions most of the pyruvate generated by glycolysis enters the TCA cycle, whilst in hypoxic conditions pyruvate is converted to lactate as the end-product. Glycolysis is a key metabolic switch, which accompanies functional changes in macrophages upon activation (Semba et al. 2016). Glycolysis has also been identified as a process which is underutilised by AMs, when compared to other macrophage subtypes (Pereverzeva et al., 2022; Woods et al., 2020). Hypoxia reduces efferocytosis in AMs but increases efferocytosis in other tissue resident macrophage populations (Norris, Libreros and Serhan, 2019; Wang et al., 2022), making

differences in glycolytic capacity an interesting differentiating feature to explore in AMs in this thesis.

To investigate the mechanism behind changes in AM function, this chapter aimed to:

(1) Validate the use of IOX-2 for HIF1α stabilisation and PX-478 and KC7F2 for HIF1α inhibition in AMs,

(2) Assess the effects of these HIF1α manipulations on AM function,

(3) Assess how AM lactate release changes at baseline and following stimulation in hypoxia, as a surrogate of glycolytic activity.

4.2 METHODS

4.2.1 HIF1α Manipulations

AMs were treated with IOX-2 (chemical name: *N*-[[1,2-Dihydro-4-hydroxy-2-oxo-1-(phenylmethyl)-3-quinolinyl]carbonyl]glycine), a selective inhibitor of PHD-2 (J. K. Murray et al. 2010) (Figure 4.1). This is a compound used for stabilisation of HIF1α in the presence of oxygen and has an EC_{50} of between 49.5 and 114 μM established across multiple cell lines (Chan et al., 2015).

AMs were also treated with HIF1α inhibitor PX-478 (chemical name: 4-[*bis*(2-chloroethyl)oxidoamino]-L-phenylalanine, dihydrochloride). PX-478 is a small molecule inhibitor of HIF1α, which prevents HIF1α transcriptional program activation (Koh et al. 2008) (Figure 4.1). The IC_{50} of PX-478 is 20 μM (Palayoor et al., 2008).

Additionally, AMs were treated with HIF1α inhibitor KC7F2 (chemical name: N,N'-(dithiodi-2,1-ethanediyl)*bis*[2,5-dichloro-benzenesulfonamide). KC7F2 inhibits translation of the HIF1α

protein by supressing phosphorylation of eukaryotic translation initiation factor 4E binding protein 1 and p70 S6 kinase (Narita et al. 2009) (Figure 4.1). The IC_{50} of KC7F2 has previously been calculated at 20 µM (Narita et al., 2009).

HIF1α stabilising IOX-2 was added at 50 µM in DMSO for 48 hours to cells cultured in normoxia (21% O_2). Meanwhile, HIF1α inhibitors PX-478 and KC7F2 were added to cell culture at various concentrations in DMSO for 48 hours in hypoxia (1% O_2). DMSO concentrations were consistent across treatments and controls.

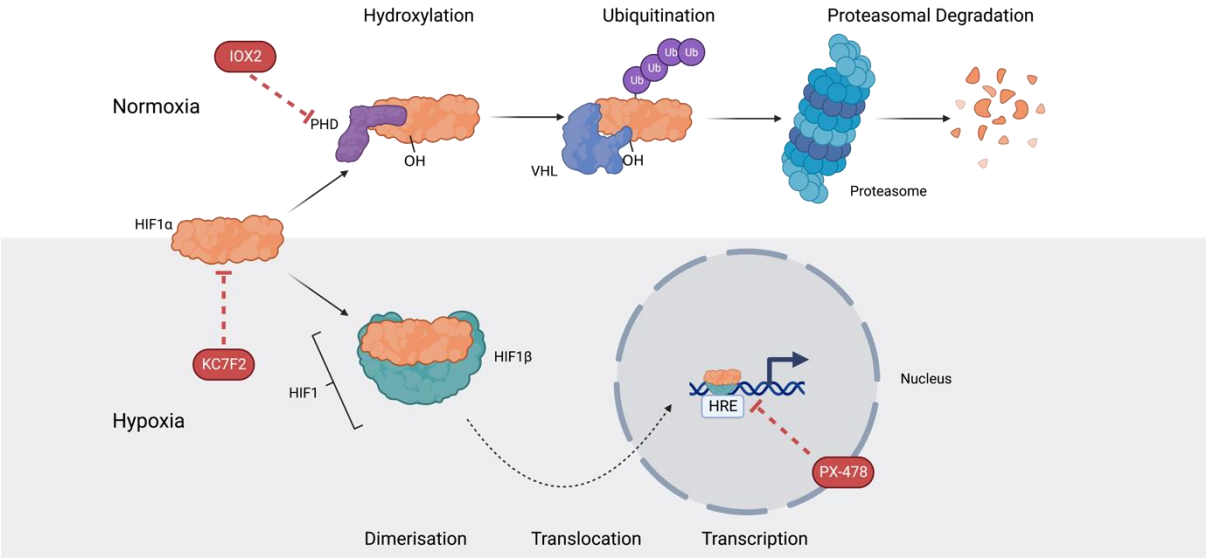

Figure 4.1 HIF1 Manipulations. *In normoxia (white) PHD enzymes bind to HIF1α and add hydroxyl groups in an oxygen dependent way. This tags HIF1α for ubiquitination by Von Hippel–Lindau (VHL) enzyme. Ubiquitination tags the protein for proteosomal digestion, causing the HIF1α to be digested in normoxia, preventing downstream signalling. Meanwhile, in hypoxia (grey) PHD enzymes are inactive due to lack of oxygen, preventing HIF1α digestion. Instead HIF1α dimerises with HIF1B and translocates to the nucleus, where it binds to HIF1 response elements within the DNA, to act as a transcription factor for gene expression. IOX-2 inhibits PHD enzyme PHD-2, preventing hydroxylation of HIF1α and allowing HIF1α accumulation in normoxia. KC7F2 blocks HIF1α gene translation, preventing the production of HIF1α. PX-478 prevents HIF1 binding to HIF1α response elements, blocking transcription factor activity.*

4.2.2 Lactate Quantification

The Lactate Assay Kit (Sigma-Aldrich. Catalogue number: MAK064) was run following manufacturer's advice. Supernatants were filtered through 0.5 ml Protein Concentrators PES (10 kDa molecular weight cut off) (Pierce. Catalogue number: 88513) into Eppendorf tubes, by centrifugation (15000 x g, 10 minutes), to remove protein, including LDH. Filtrate was diluted 1:10 in lactate assay buffer and plated at 50 µl per well. Standards were also diluted in lactate assay buffer and plated at 50 µl per well. Samples and standards were incubated with 50 µl master mix (containing: 92% Lactate Assay Buffer, 4% Lactate Enzyme Mix and 4% Lactate Probe) for 30 minutes at room temperature. Absorbance was then measured at a wavelength of 570 nm. A linear equation was derived from the standards and used to derive lactate concentrations.

4.3 RESULTS

4.3.1 Validation

4.3.1.1 HIF1α manipulations

Characterisation HIF1α stabilisation by IOX-2

AMs were treated with IOX-2, to investigate the contribution of HIF1α induced gene programs to AM function. IOX-2 inhibits PHD2, preventing the degradation of HIF1α in normoxia. Based on existing literature, a dose of 50 µM IOX-2 was investigated in this work (Otto et al. 2021; Brereton et al. 2022). To demonstrate the feasibility of using this IOX-2 dose, AM viability was determined after 48 hours treatment. Figure 4.2 demonstrates that 50 µM IOX-2 had no effect on the percentage of live, apoptotic, and necrotic AMs, when assessed by PI and annexin V staining.

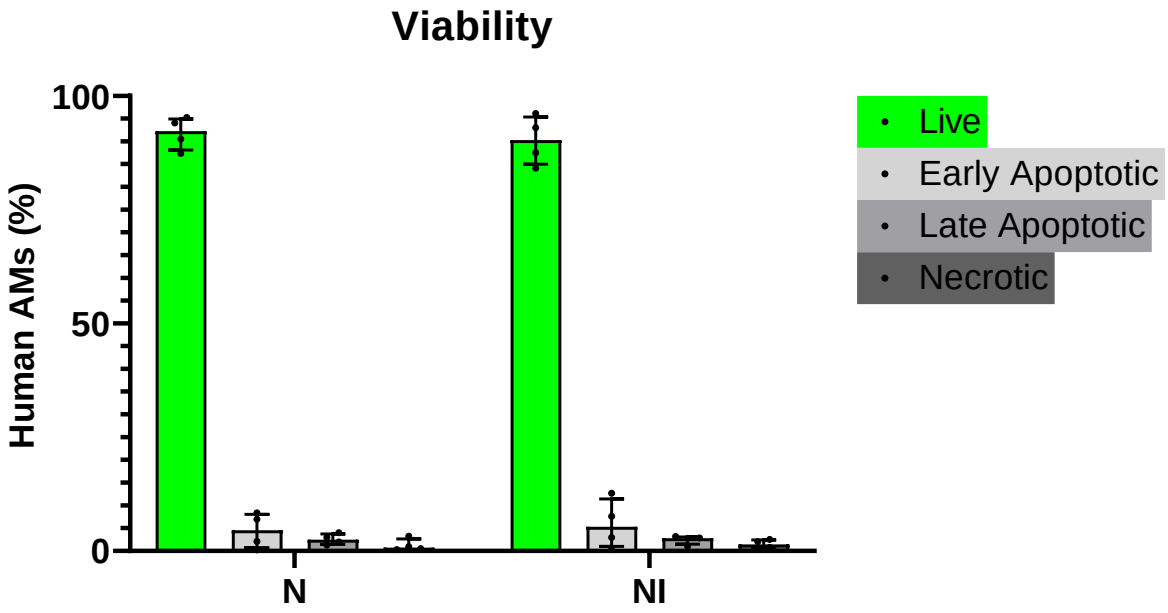

Figure 4.2 AM Viability with 48-hour IOX-2 Treatment. AM viability was assessed by propidium iodide and annexin V staining with and without 48-hour 50 µM IOX-2 treatment. Staining was used to differentiate live, necrotic, late apoptotic and early apoptotic cells. Comparison using a Mixed Effect Model with Tukey's Multiple Comparison. N vs NI live p=0.9453, early apoptotic p=0.9559, late apoptotic p>0.9999, necrotic p>0.9999, Data is presented as median (±IQR). N=4. N: normoxia. NI: normoxia with IOX-2. H: hypoxia.

The efficacy of 50 µM IOX-2 in causing HIF1α stabilisation in normoxia was illustrated by western blotting after 48-hour culture. HIF1α protein stabilisation in IOX treated AMs was increased significantly above untreated AMs in normoxia after 48 hours (p= 0.011) (Figure 4.3). The amount of HIF1α in cells treated with IOX-2 for 48 hours also exceeded levels in cells cultured in hypoxia (p=0.011).

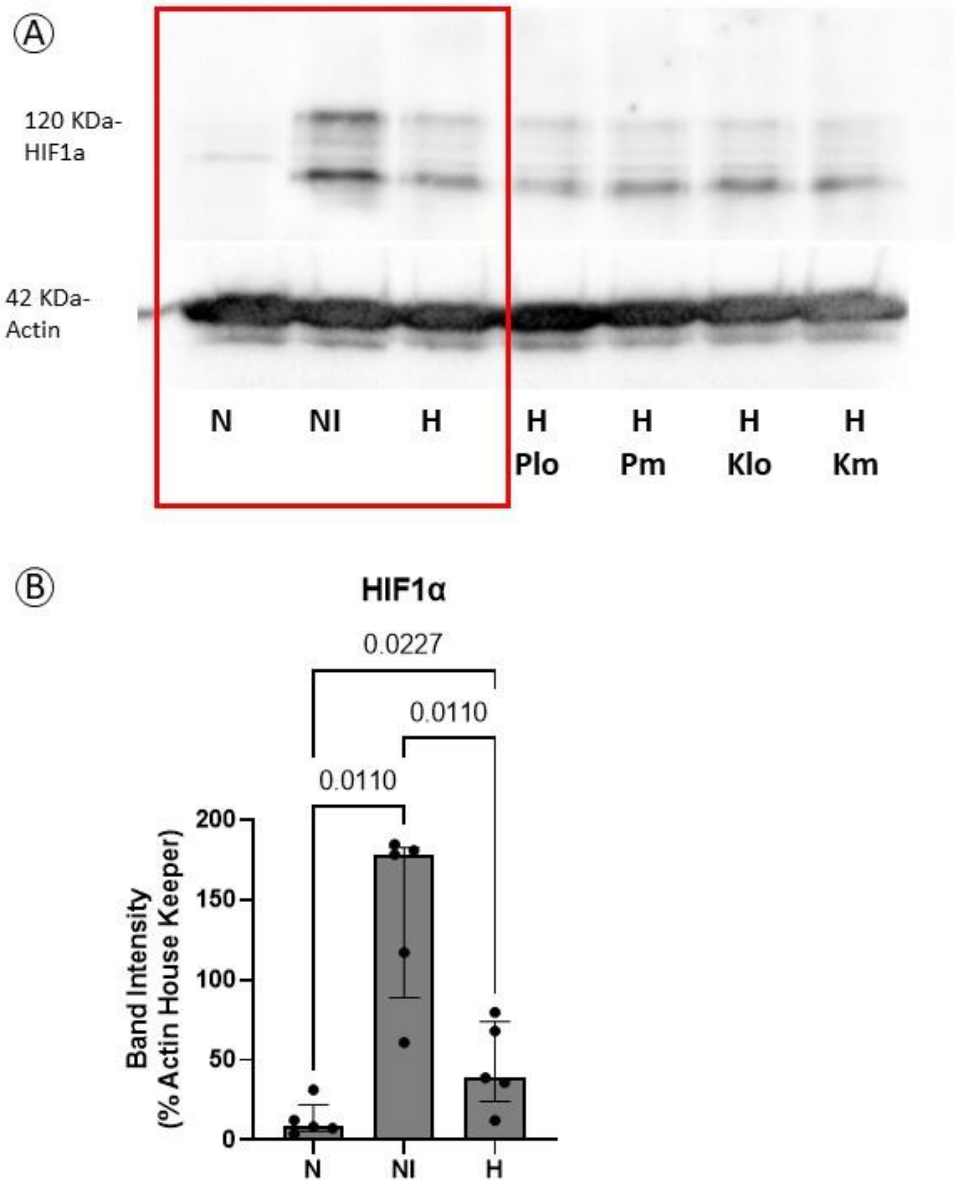

Figure 4.3 HIF1α Protein Stabilisation with IOX-2. AMs were incubated in normoxia (21% O_2, 5% CO_2, 37°C) with and without 50 µM IOX-2 or in hypoxia (1% O_2, 5% CO_2, 37°C) for 48 hours. HIF1α protein levels were subsequently assessed by western blotting, alongside actin B as a loading control. Representative western blot (A) showing HIF1α at 120 kDa and actin at 42 kDa. Band densities were assessed using Image J, and (B) HIF1α band intensity was presented as a percentage of actin band intensity. Comparisons were made using a One Way ANOVA with Tukey's multiple comparisons test. Graphs show median (±IQR). N=5. N: normoxia. NI: normoxia with IOX-2. H: hypoxia.

To demonstrate the functionality of HIF1α protein, HIF1α response gene expression levels in

IOX-2 treated cells were investigated. HIF1α response genes *VEGFA* (Figure 3.21A) and *SLC2A1*

(Figure 4.5) did not show a corresponding increase in expression. There was no difference in VEGFA protein secretion detected in AMs following hypoxia or IOX-2 treatment (Figure 3.21B).

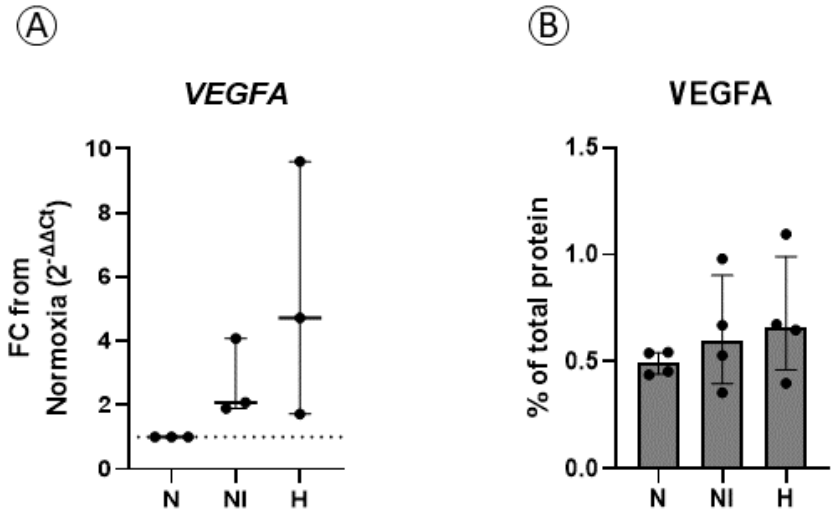

Figure 4.4 VEGFA Gene and Protein Expression with IOX-2. AMs were incubated in normoxia (21% O_2, 5% CO_2, 37°C), with and without IOX-2, or in hypoxia (1% O_2, 5% CO_2, 37°C) for 48 hours. (A) VEGFA RNA transcript levels were subsequently assessed by qPCR, alongside 18S rRNA expression as a loading control. Data was presented as $2^{-\Delta\Delta Ct}$ relative to normoxic AM expression. N=3. N vs NI p= 0.2049. N vs H p=0.0825. (B) VEGFA protein secretion into supernatant after 48 hours was assessed by ELISA, and concentrations were expressed as a percentage of total protein as assessed by BCA assay. N=4. N vs NI p>0.9999. N vs H p=0.5777. Comparisons were made using a Friedman's test with Dunn's multiple correction test. Graphs show median (±IQR) N: normoxia. NI: normoxia with IOX-2. H: hypoxia.

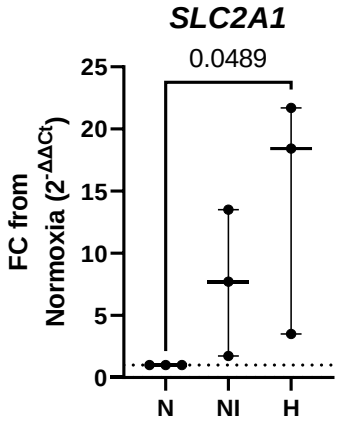

Figure 4.5 SLC2A1 Expression with IOX-2. AMs were incubated in normoxia (21% O_2, 5% CO_2, 37°C) with and without IOX-2, or in hypoxia (1% O_2, 5% CO_2, 37°C) for 48 hours. SLC2A1 RNA transcript levels were subsequently assessed by qPCR, alongside 18S rRNA expression as a loading control. Data was presented as $2^{-\Delta\Delta Ct}$ relative to normoxic AM expression. Comparisons were made using a Friedman's test with Dunn's multiple correction test. N=3. N vs NI p= 0.5338. N vs H p= 0.0489. Graphs show median (±IQR). N: normoxia. NI: normoxia with IOX-2. H: hypoxia.

Characterisation of HIF1α inhibition by PX-478

AMs cultured in hypoxia were treated with HIF1α inhibitor PX-478, to further assess the role of HIF1α activated gene expression programs on AMs in hypoxia. As a HIF1α inhibitor, PX-478 reduces HIF1α binding and transcriptional activity, without reducing protein levels. AMs were treated with PX-478 in normoxia and hypoxia for 48 hours, to assess effects on viability, given the known capacity of hypoxia to modulate cell death. PX-478 was assessed over three concentrations (5, 10 and 20 μM). For this analysis, Annexin V and propidium iodide staining were used to exclude early apoptotic, late apoptotic, and necrotic cells. The percentage of live cells were expressed in Figure 4.6. Cell viability was not affected by any PX-478 dose in normoxia and hypoxia. Due to limited cell yields, the highest PX-478 dose was not continued into functional assays.

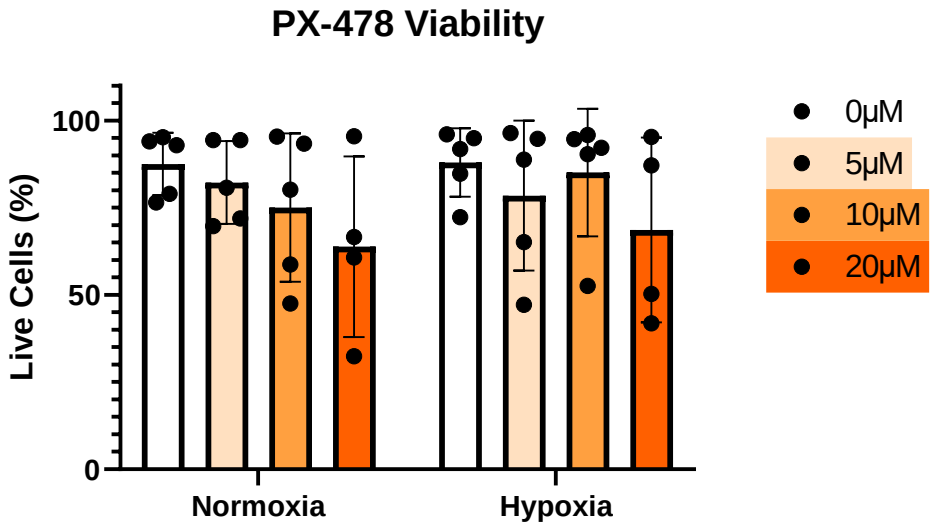

Figure 4.6 AM Viability with 48-hour PX-478 Treatment. AM viability was assessed by propidium iodide and annexin V staining to differentiate live, necrotic, late apoptotic, and early apoptotic cells. Viability was assessed after 48-hour treatment with 5 μM, 10 μM and 20 μM PX-478, both in normoxia (21% O_2, 5% CO_2, 37°C) and hypoxia (1% O_2, 5% CO_2, 37°C). Comparisons were made using a Two way ANOVA with Dunnet's multiple comparison test. Normoxia: 0 vs 5 μM p=0.9591, 0 vs 10 μM p= 0.6528 0 vs 20 μM p=0.1876. Hypoxia: 0 vs 5 μM p=0.8105, 0 vs 10 μM p= 0.9932 0 vs 20 μM p=0.3462. N=4-5.

To assess the effects of 5 μM and 10 μM PX-478 on HIF1α signalling, HIF1α protein levels after 48 hours culture in hypoxia with PX-478 were compared to levels in AMs in normoxia and hypoxia (Figure 4.7). PX-478 did not change HIF1α levels at the low and medium dose, when compared to hypoxia alone. This assessment was limited to 2 biological replicates.

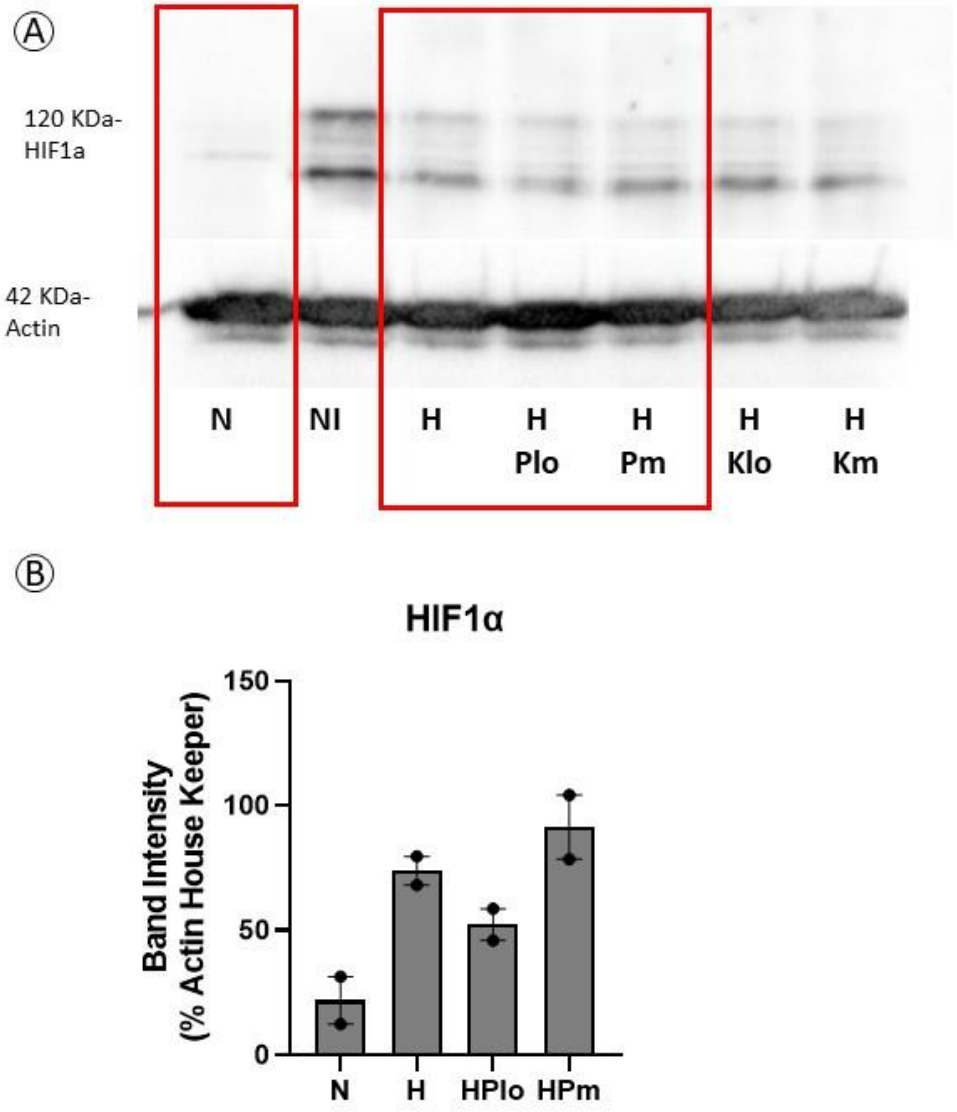

Figure 4.7 HIF1α Protein Stabilisation with PX-478. AMs were incubated in normoxia (21% O_2, 5% CO_2, 37°C) or in hypoxia (1% O_2, 5% CO_2, 37°C) with 10 µM or 20 µM PX-478 for 48 hours. HIF1α protein levels were subsequently assessed by western blotting, alongside actin as a loading control. Representative western blot (A) showing HIF1α at 120 kDa and actin at 42 kDa. Band densities were assessed using Image J, and (B) HIF1α band intensity was presented as a percentage of actin band intensity. N=2. Graphs show median (±IQR). N: normoxia. H: hypoxia. Plo: 5 µM P-X478. Pm: 10 µM PX-478.

HIF1α gene expression targets were subsequently assessed in AMs exposed to hypoxia with PX-478, using 5 µM and 10 µM PX-478. Changes in *VEGFA* and *SLC2A1* gene expression were not detected with either dose (Figure 4.8 and Figure 4.9). Although HIF1α modulation was not

detected in AMs treated with PX-478, 5 µM and 10 µM PX-478 were used in functional experiments, pending further replication of the validation above.

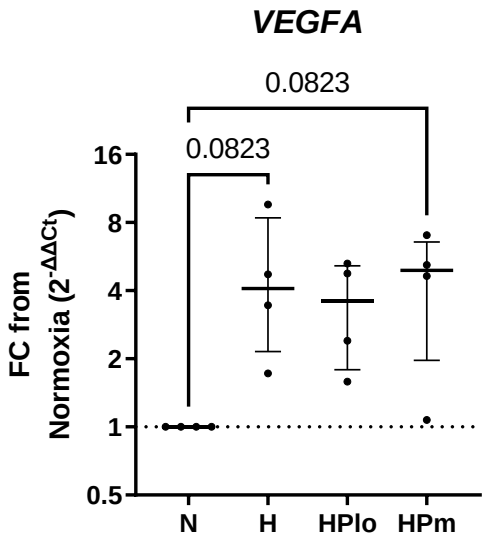

Figure 4.8 VEGFA Gene Expression with PX-478. AMs were incubated in normoxia (21% O_2, 5% CO_2, 37°C) or hypoxia (1% O_2, 5% CO_2, 37°C) with 5 µM and 10 µM PX-478 for 48 hours. VEGFA RNA transcript levels were subsequently assessed by qPCR, alongside 18S rRNA expression as a loading control. Data was presented as $2^{-\Delta\Delta Ct}$ relative to normoxic AM expression. Comparisons were made using a Friedan test with Dunn's multiple correction. N=4. N vs H p=0.0823. N vs Pilo p=0.6021. N vs Pim p=0.0823. Graphs show median (±IQR). N: normoxia. H: hypoxia. Plo: 5 µM PX-478. Pm: 10 µM PX-478.

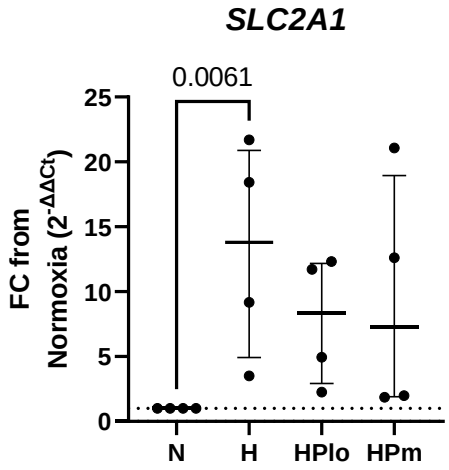

Figure 4.9 SLC2A1 Gene Expression with PX-478. AMs were incubated in normoxia (21% O_2, 5% CO_2, 37°C) or in hypoxia (1% O_2, 5% CO_2, 37°C) with 5 µM and 10 µM PX-478 for 48 hours. SLC2A1 RNA transcript levels were subsequently assessed by qPCR, alongside 18S rRNA expression as a loading control. Data was presented as $2^{-\Delta\Delta Ct}$ relative to normoxic AM expression. Comparisons were made using a Friedan test with Dunn's multiple correction. N vs H p=0.0061. N vs HPlo 0.6021. N vs HPm=0.6021. N=4. Graphs show median (±IQR). N: normoxia. H: hypoxia. Plo: 5 µM PX-478. Pm: 10 µM PX-478.

Characterisation of HIF1α inhibition by KC7F2

AMs cultured in hypoxia were treated with HIF1α inhibitor KC7F2, to assess the role of HIF1α activated gene expression programs on AMs in hypoxia. KC7F2 inhibits HIF1α translation (but not *Hif1a* gene transcription), resulting in reduced HIF1α protein and HIF1α gene program expression.

AMs were treated with 20, 40 and 80 µM KC7F2 in normoxia and hypoxia for 48 hours, to assess effects on viability. Cell viability was unaffected by the 20 and 40 µM KC7F2 in normoxia and hypoxia. However, 80 µM KC7F2 reduced viability in normoxia (p=0.003) and there was a trend towards reduced viability in hypoxia (p=0.0962)(Figure 4.10). For this reason, 80 µM KC7F2 was excluded from further investigation.

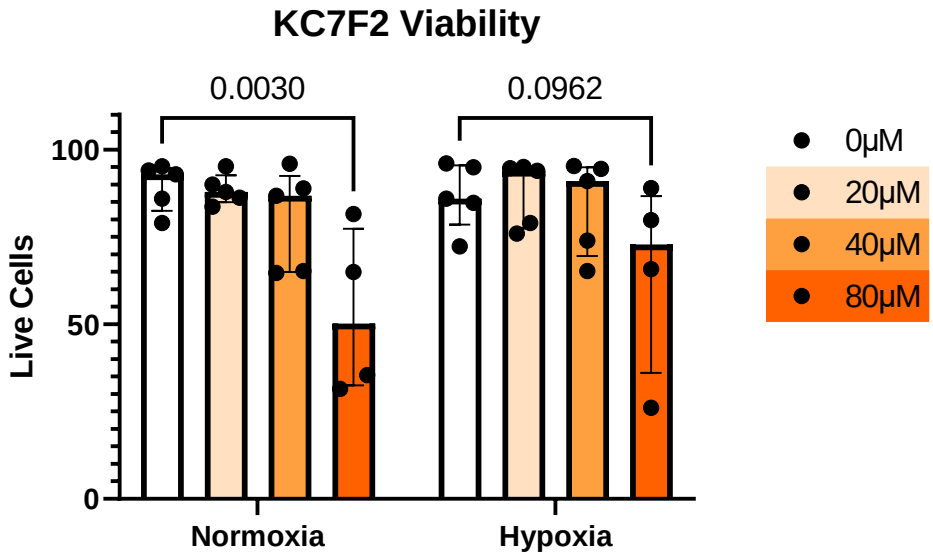

Figure 4.10 AM Viability with 48-hour KC7F2 Treatment. AM viability was assessed by propidium iodide and annexin V staining, 48-hour treatment with 10 µM, 20 µM and 40 µM KC7F2, both in normoxia (21% O_2, 5% CO_2, 37°C) and hypoxia (1% O_2, 5% CO_2, 37°C). Staining was used to differentiate live, necrotic, late apoptotic and early apoptotic cells. Comparisons were made using a Two way ANOVA with Dunnet's multiple comparisons test. Normoxia: 0 vs 20 µM p=0.9995, 0 vs 40 µM p= 0.6543 0 vs 80 µM p=0.003. Hypoxia: 0 vs 20 µM p=0.9993, 0 vs 40 µM p= 0.9825 0 vs 80 µM p=0.0962. N=4-5. Data is presented as media (±IQR).

HIF1α protein was measured after exposure to hypoxia with and without 20 and 40 µM KC7F2 (Figure 4.11). Neither dose altered HIF1α protein levels, although assessment was limited to 2 biological replicates. HIF1α response genes were assessed alongside treatment with KC7F2, to further investigate effects on HIF1α activity. Expression of HIF1α response genes *VEGFA* (Figure 4.12) and *SLC2A1* (Figure 4.13) were not reduced in hypoxia by the presence of KC7F2 at either dose. These results do not support the efficacy of KC7F2 in manipulating HIF1α gene responses in AMs, however the inhibitor was continued for use in on-going assays, pending increased biological replication in validation.

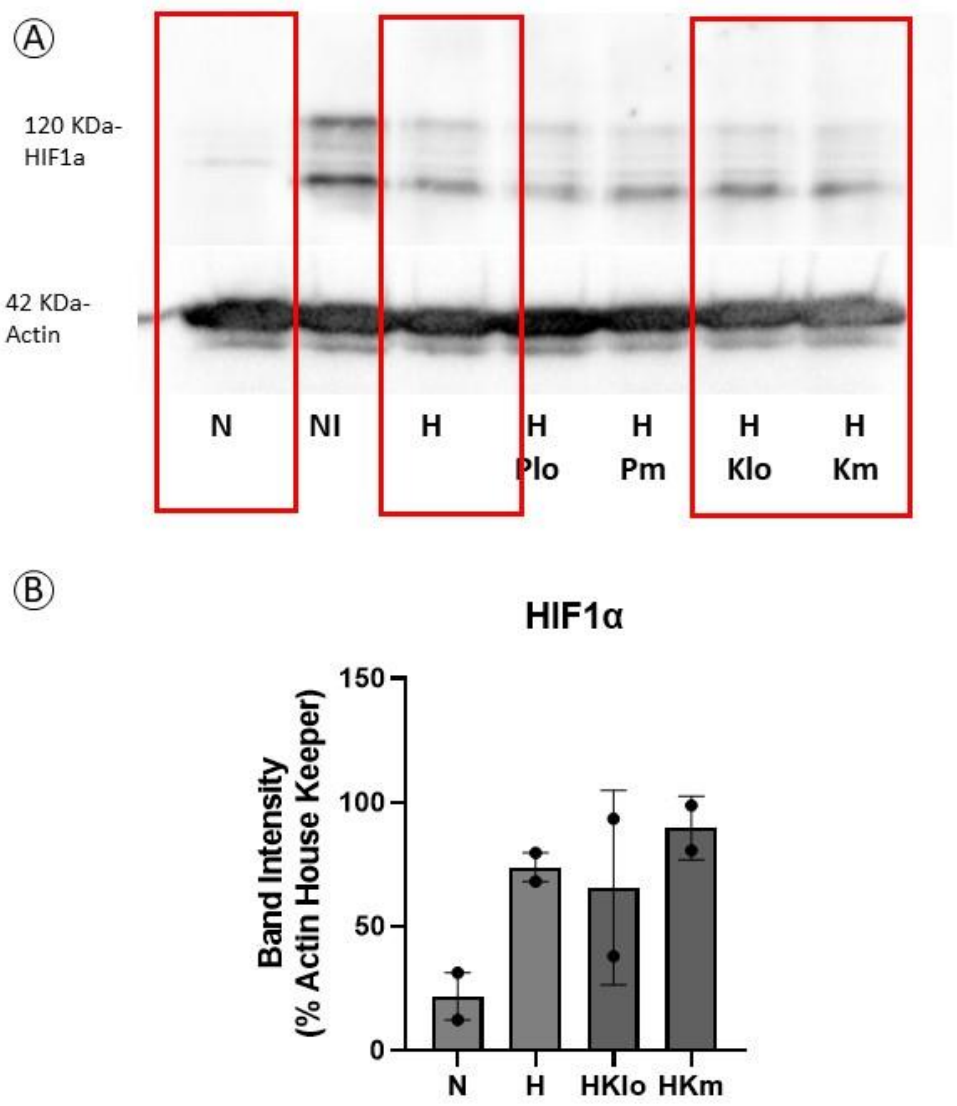

Figure 4.11 HIF1α Protein Stabilisation with KC7F2. AMs were incubated in normoxia (21% O_2, 5% CO_2, 37°C) or in hypoxia (1% O_2, 5% CO_2, 37°C) with 20 µM or 40 µM KC7F2 for 48 hours. HIF1α protein levels were subsequently assessed by western blotting, alongside actin as a loading control. Representative western blot (A) showing HIF1α at 120 kDa and actin at 42 kDa. Band densities were assessed using Image J, and (B) HIF1α band intensity was presented as a percentage of actin band intensity. N=2. Graphs show median (±IQR). H: hypoxia. Klo: 20 µM KC7F2. Km: 40 µM KC7F2.

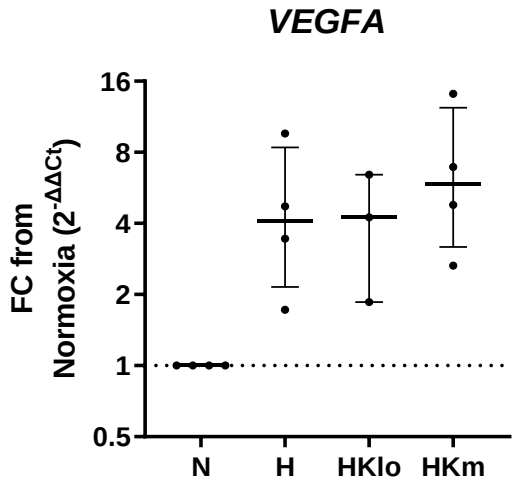

Figure 4.12 VEGFA *Gene and Protein Expression with KC7F2. AMs were incubated in normoxia (21% O_2, 5% CO_2, 37°C) or hypoxia (1% O_2, 5% CO_2, 37°C) with 20 µM and 40 µM KC7F2 for 48 hours. (A) VEGFA RNA transcript levels were subsequently assessed by qPCR, alongside 18S rRNA expression as a loading control. Data was presented as $2^{-\Delta\Delta Ct}$ relative to normoxic AM expression. (B) VEGFA protein secretion into supernatant after 48 hours was assessed by ELISA. Comparisons were made using a mixed effects model. N vs H = 0.2503. N vs HKlo p=0.2503. N Vs HKm p=0.2503. N=3-4. Graphs show median (±IQR). N: normoxia. H: hypoxia. Klo: 20 µM KC7F2. Km: 40 µM KC7F2.*

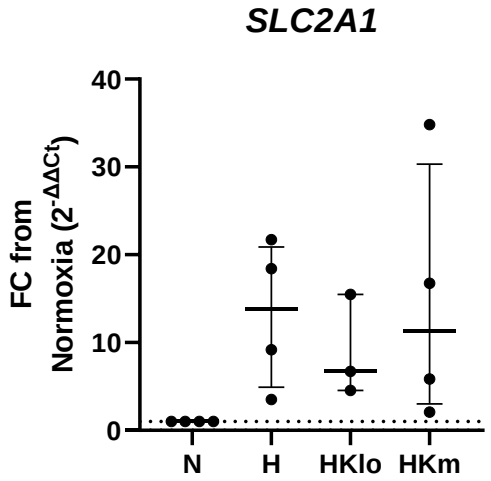

Figure 4.13 SLC2A1 Gene Expression with KC7F2. AMs were incubated in normoxia (21% O_2, 5% CO_2, 37°C) or in hypoxia (1% O_2, 5% CO_2, 37°C) with 20 µM and 40 µM KC7F2 for 48 hours. SLC2A1 RNA transcript levels were subsequently assessed by qPCR, alongside 18S rRNA expression as a loading control. Data was presented as $2^{-\Delta\Delta Ct}$ relative to normoxic AM expression. Comparisons were made using a mixed effects model. N vs H = 0.0.1830. N vs HKlo p=0.3136. N Vs HKm p=0.4170. N=3-4. Graphs show median (±IQR). N: normoxia. H: hypoxia. Klo: 20 µM KC7F2. Km: 40 µM KC7F2.

4.3.2 Role of HIF1α in Efferocytosis Impairment

Following its validation in earlier sections, functional experiments were carried out in cells treated with IOX-2 in normoxia, to assess the role of HIF1α driven transcriptional changes in the efferocytic impairment seen in AMs in hypoxia. After 2-hour incubation with fluorescently labelled apoptotic neutrophils, no change in efferocytosis could be detected in IOX-2 treated cells, when assessed as assessed by magnitude of fluorescent signal, MFI (Figure 3.29A), by percentage of efferocytic AMs (Figure 3.29B).

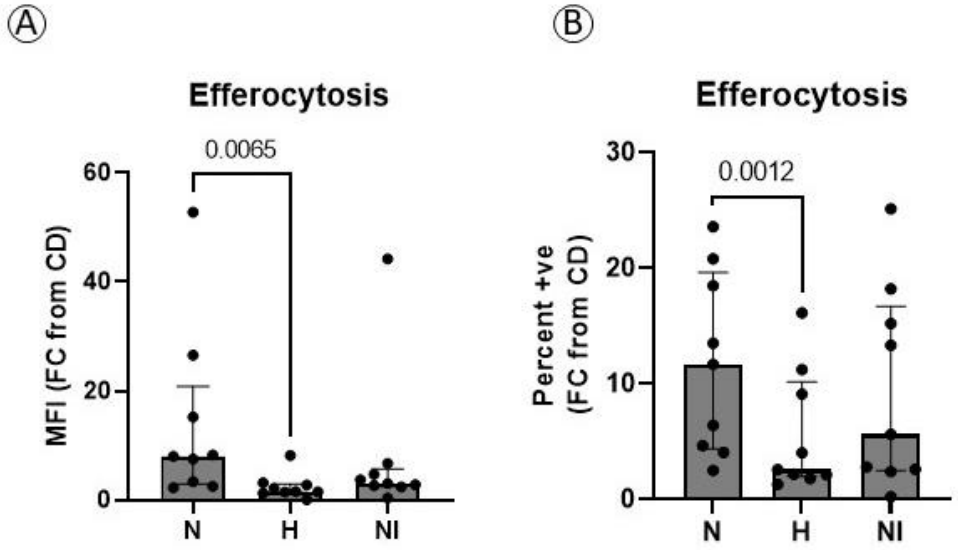

Figure 4.14 AM Efferocytosis with IOX-2. AMs were incubated in normoxia (21% O_2, 5% CO_2, 37°C) with or without IOX-2, or in hypoxia (1% O_2, 5% CO_2, 37°C) for 48 hours. Subsequently, AMs were incubated with fluorescently labelled apoptotic neutrophils for 2 hours, and efferocytosis was assessed by flow cytometry. (A) Median fluorescence intensity (MFI) and (B) percentage positive events were presented comparing efferocytosis in each condition. Comparisons were made using a Data is presented as a fold change (FC) from cytochalasin D (CD) control. Friedan test with Dunn's multiple correction. MFI comparisons: N vs H p=0.0065. N vs NI p=0.178. H vs NI p=0.7158 N= 9. Percentage comparisons: N vs H p=0.0012. N vs NI p=0.4719. H vs NI p=0.1017. N= 9. Graphs show median (±IQR). N: normoxia. NI: normoxia with IOX-2. H: hypoxia.

HIF1α inhibitor PX-478 was used to further distinguish the role of HIF1α in the efferocytosis impairment seen in AMs in hypoxia. After 48-hour incubation in hypoxia with PX-478,

efferocytic function was compared to untreated AMs in normoxia and hypoxia (Figure 4.15). HIF1α inhibitor PX-478 did not restore efferocytic function at the low (5 μM) or medium (10 μM) dose, when assessed as the MFI (Figure 4.15A) or percentage of efferocytic AMs (Figure 4.15B).

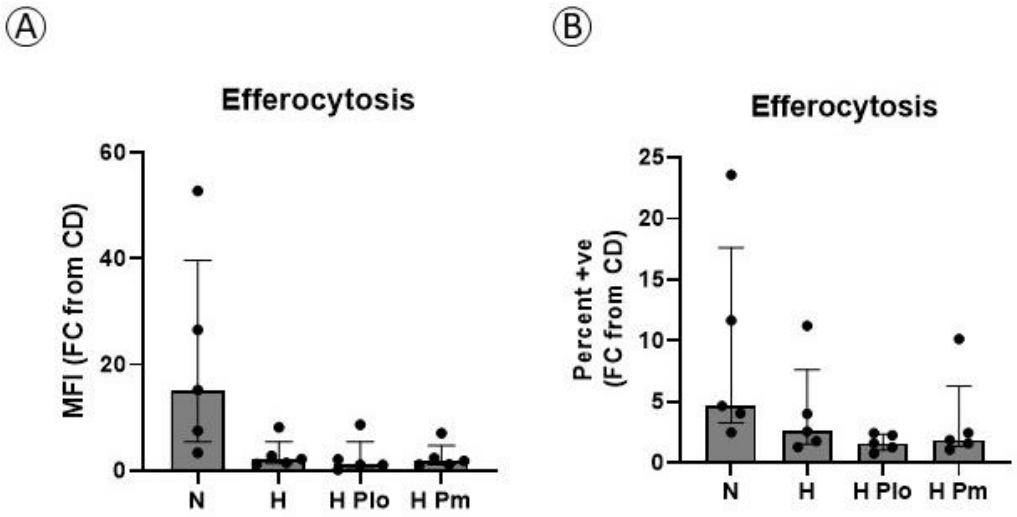

Figure 4.15 AM Efferocytosis in Hypoxia with PX-478. AMs were incubated in normoxia (21% O_2, 5% CO_2, 37°C) or in hypoxia (1% O_2, 5% CO_2, 37°C) with 5 μM and 10 μM PX-478 for 48 hours. Subsequently, AMs were incubated with fluorescently labelled apoptotic neutrophils for 2 hours, and efferocytosis was assessed by flow cytometry. (A) Mean fluorescence intensity (MFI) and (B) percentage positive events were presented comparing efferocytosis in each condition. Data is presented as a fold change (FC) from cytochalasin D (CD) control. Comparisons were made using a Friedan test with Dunn's multiple correction. Percentage comparisons: N= 5. N vs H p= 0.2694. H vs Plo p>0.9999. H vs Pm p>0.9999. MFI comparisons: N= 5. N vs H p>0.999. H vs Plo p=0.5185. H vs Pm p=0.6681. Graphs show median (±IQR). N: normoxia. H: hypoxia. Plo: 5 μM PX-478. Pm: 10 μM PX-478.

Alongside validation determining whether KC7F2 inhibited HIF1α, the inhibitor was introduced at the lower doses of 20 μM and 40 μM during the efferocytosis assay. After incubation in hypoxia with and without KC7F2, efferocytic function was determined in comparison to untreated AMs incubated in normoxia and hypoxia. Neither dose of KC7F2 restored efferocytosis determined by MFI or percentage of efferocytic AMs (Figure 4.16A,B).

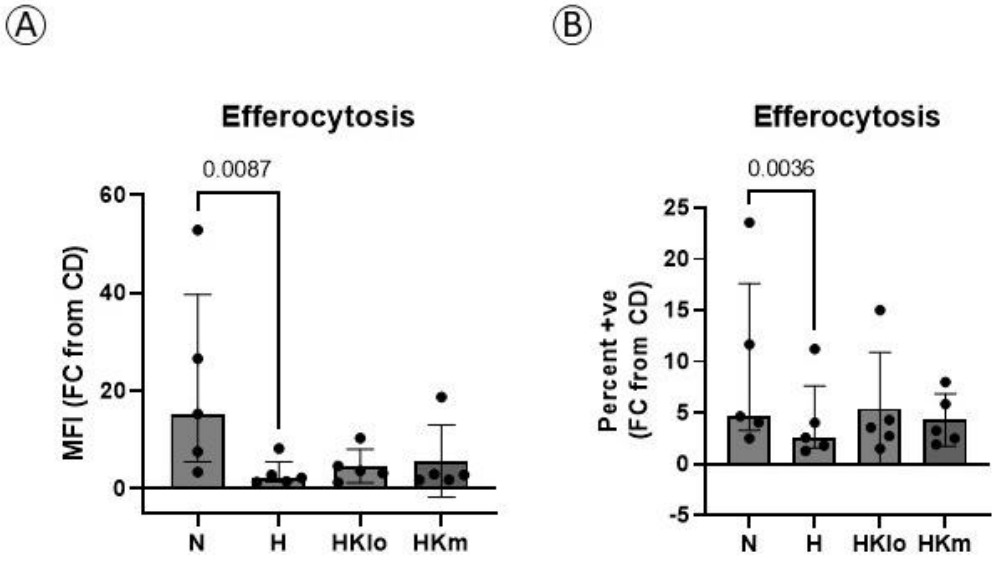

Figure 4.16 AM Efferocytosis in Hypoxia with KC7F2. AMs were incubated in normoxia (21% O_2, 5% CO_2, 37°C) or in hypoxia (1% O_2, 5% CO_2, 37°C) with 20 µM and 40 µM KC7F2 for 48 hours. Subsequently, AMs were incubated with fluorescently labelled apoptotic neutrophils for 2 hours, and efferocytosis was assessed by flow cytometry. (A) Mean fluorescence intensity (MFI) and (B) percentage positive events were presented comparing efferocytosis in each condition. Data is presented as a fold change (FC) from cytochalasin D (CD) control. Graphs show median (±IQR). N=5. MFI comparisons: N= 5. N vs H p=0.0087 H vs Klo p>0.9999. H vs Km p>0.9999. Percentage comparisons: N= 5. N vs H p= 0.2694. H vs Plo p>0.9999. H vs Pm p>0.9999. N: normoxia. H: hypoxia. Klo: 20 µM KC7F2. Km: 40 µM KC7F2.

4.3.3 Lactate Release from AMs

Lactate secretion into the media was assessed as a surrogate for glycolytic activity. Lactate was measured with and without LPS stimulation, to probe whether AMs respond to LPS stimulation by releasing lactate. AMs were stimulated with 10 µg/ml LPS for 48 hours, in normoxia or hypoxia. LPS stimulation significantly increased lactate release in AMs (p= 0.0285) above untreated AMs cultured in normoxia (Figure 4.17).

Lactate secretion was also measured in AMs cultured in hypoxia, with and without LPS stimulation for 48 hours. Lactate secretion in unstimulated AMs was significantly increased in hypoxia, when compared to normoxia (p= 0.017)(Figure 4.18A). The levels of lactate released by unstimulated hypoxic AMs were similar to the levels of lactate released by LPS stimulated

AMs in normoxia. When AMs were treated with LPS in hypoxia, there was no further increase in lactate secretion beyond levels released by untreated AMs in hypoxia (Figure 4.18B). For these assays, levels of lactate were within the range of detection, meaning that this plateau was not an artefact of the assay limit of detection.

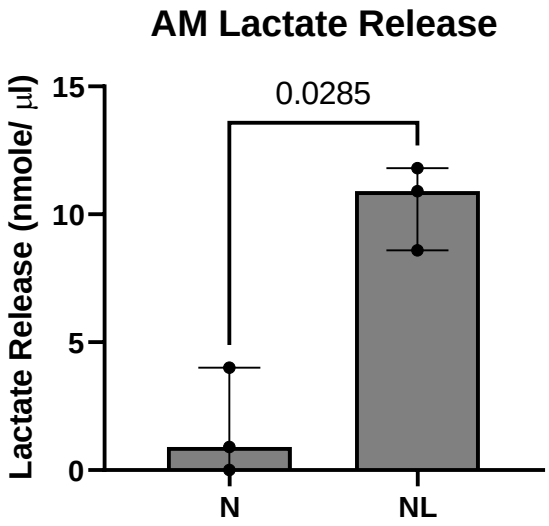

Figure 4.17 Lactate Release by AMs and MDMs in Response to LPS. (A) AMs were incubated in normoxia (21% O_2, 5% CO_2, 37°C) for 48 hours, with and without 10 µg/ml LPS. Lactate secretion into supernatant after these respective treatments was assessed using a lactate colorimetric assay, with background levels of lactate in culture media subtracted. N: normoxia. NL: normoxia with LPS. Comparisons performed using a paired T test. N=3. Graph shows median (±IQR).

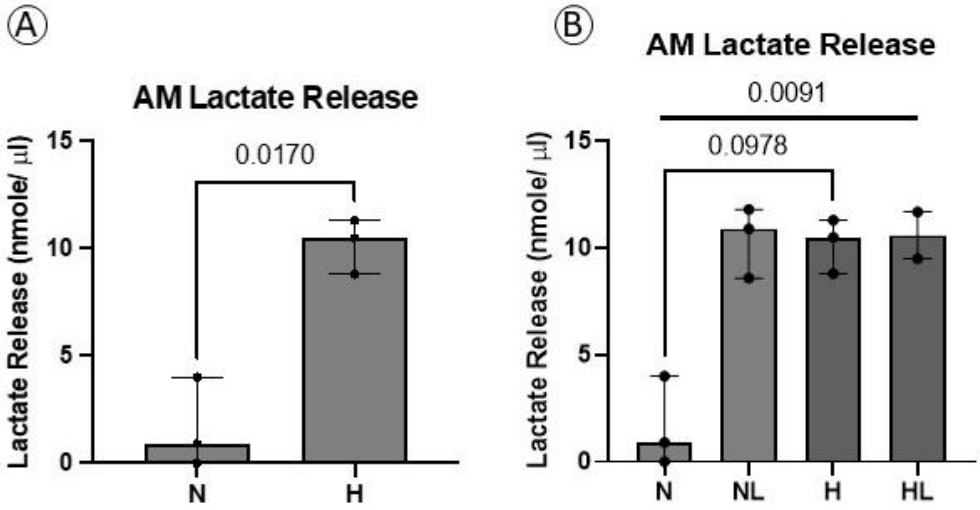

Figure 4.18 Lactate Release by AMs in Hypoxia. AMs were incubated in normoxia (21% O_2, 5% CO_2, 37°C) or hypoxia (1% O_2, 5% CO_2, 37°C) for 48 hours (A), with and without 10 µg/ml LPS (B). Lactate secretion into supernatant after these respective treatments was assessed using a lactate colorimetric assay, with background levels of lactate in culture media subtracted. (A) Comparison performed using a paired T test. (B) Comparison performed using mixed effects model. Treatment effect across all treatments p=0.0091. N vs NL p=0.1345. N vs H p=0.0978. NL vs HL p= 0.9901. H vs HL p= 0.9813. N: normoxia. NL: normoxia with LPS. H: hypoxia. HL: hypoxia with LPS. Graphs show median (±IQR).

4.3.4 Role of HIF1α in Phagocytosis

To characterise the role of HIF1α in the capacity of AMs to phagocytose, phagocytosis in normoxia with after 48-hour treatment with 50 µM IOX-2 was assessed. There was a trend towards increased phagocytosis in AMs with IOX-2 induced HIF1α stabilisation in normoxia when assessed as percentage of phagocytic cells (p=0.0781) (Figure 4.19A).

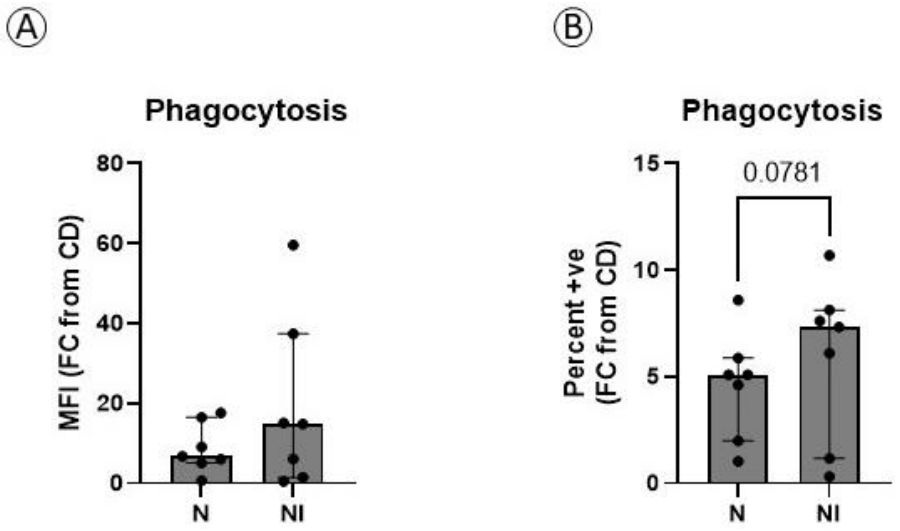

Figure 4.19 AM Phagocytosis with IOX-2. AMs were incubated in normoxia (21% O_2, 5% CO_2, 37°C) with or without IOX-2, or in hypoxia (1% O_2, 5% CO_2, 37°C) for 48 hours. Subsequently, AMs were incubated with fluorescently labelled heat killed Streptococcus pneumoniae for 4 hours, and phagocytosis was assessed by flow cytometry. (A) Median fluorescence intensity (MFI) and (B) percentage positive events were presented comparing phagocytosis in each condition. Data is presented as a fold change (FC) from cytochalasin D (CD) control. N=7. Comparisons were made using a Wilcoxon's test. MFI N vs NI p=0.1094. Percentage N vs NI p= 0.0781. Graphs show median (±IQR). N: normoxia. NI: normoxia with IOX-2. H: hypoxia.

4.4 Discussion

This chapter aimed to delineate how hypoxia prevented efferocytosis, independent of phagocytosis. Firstly, inhibitors were validated for the manipulation of HIF1α, as HIF1α is a key hypoxic signalling node that may play a role in dysregulating AM function. Subsequently, the effects of these inhibitors on AM function were dissected, to assess the role of HIF1α in efferocytosis and phagocytosis. Finally, lactate release from AMs in hypoxia was measured as a surrogate to infer AM glycolytic capacity.

4.4.1 HIF1α inhibitor validation

Inhibitors for manipulation of the HIF1α signalling pathways were validated alongside their use, to maximise output from precious patient samples. IOX-2 inhibits PHD-2, resulting in HIF1α stabilisation in normoxia. The effect of 50 μM IOX-2 on AM viability was assessed, and no

toxicity was identified after 48 hours exposure in normoxia. Therefore, the ability of IOX-2 to activate HIF1α signalling was subsequently investigated. Chapter 3 demonstrated activation of HIF1α signalling in hypoxia by showing HIF1α protein stabilisation and increased *VEGFA* and *SLC2A1* expression. These markers of HIF1α signalling were assessed in AMs treated with IOX-2 to demonstrate its efficacy in activating this pathway. As expected, 48-hour IOX-2 treatment resulted in potent HIF1α stabilisation. The amount of HIF1α protein in IOX-2 treated AMs was higher than the level seen in cells cultured in normoxia without IOX-2 and higher than the level seen in cells exposed to hypoxia for 48 hours. This illustrates that IOX-2 is a useful tool for the stabilisation of HIF1α, however levels of HIF1α stabilised by constant PHD2 inhibition are likely not representative of the acute peak and subsequent plateau in HIF1α described following real hypoxic challenge (Jaśkiewicz et al. 2022). This work began to confirm the HIF1α activating function of IOX-2 in AMs by assessing *VEGFA* and *SLC2A1* transcription. Although neither gene was statistically significantly upregulated in hypoxia, both were consistently upregulated in all samples. Alongside increased HIF1α protein levels, this data increases confidence in the assertion that IOX-2 results in HIF1α signalling, despite limited biological replication in this validation.

Two HIF1α inhibitors, PX-478 and KC7F2, were also validated for use in AMs. PX-478 inhibits HIF1α binding, reducing HRE transcription, whilst KC7F2 inhibits HIF1α transcription, reducing protein stabilisation and HRE transcription. The toxicity of these two inhibitors were assessed using PI uptake and Annexin V binding to exclude apoptotic and necrotic cells. All doses of PX-478 and the lower two doses KC7F2 (20 μM and 40 μM) had no effects on viability in hypoxia or normoxia. Therefore, these concentrations were investigated at the protein and RNA level.

Established markers of HIF1α signalling were assessed with both inhibitors. HIF1α stabilisation was examined in a small number of samples (n=2) with the low and medium doses of KC7F2 and PX-478. Although these results will contribute to future validation of the HIF1α inhibitors, their utility at this point is limited by low biological replication. HIF1α response genes were also assessed with HIF1α inhibition. PX-478 did not alter *VEGFA* or *SLC2A1* expression. KC7F2 also did not reduce *VEGFA* or *SLC2A1* expression at either concentration. Cumulatively, these results represent the beginning of validation of inhibitors for HIF1α manipulation, however validation is underpowered to detect changes in HIF1α responses in hypoxia, meaning that it is not clear the exact effects that these inhibitors have in HIF1α signalling in hypoxic AMs.

4.4.2 HIF1α inhibitor effects on AM function

Alongside validation experiments, IOX-2, PX-478 and KC7F2 were used as pre-treatments alongside hypoxia, to determine whether HIF1α responses reduce AM efferocytosis. Despite limited validation in some cases, this work ran alongside validation studies, as less cells were required for functional assays. This study did not detect a change in efferocytic function in AMs cultured in normoxia with IOX-2 for 48 hours. Power calculations indicate that 41 patient samples would be required to distinguish the difference in efferocytosis MFI currently seen between the medians of the two groups with sufficient power to detect a significant difference (SD = 13.74, α=0.05, power=0.8). In contrast, there was a trend indicating that pseudohypoxic HIF1α stabilisation increased the percent AMs to phagocytose of *Streptococcus pneumoniae*. This effect is not seen in hypoxia itself, however it does indicate that HIF1α signalling has differential effects on the capacity of a cell to efferocytose and phagocytose.

Overall, this data provides no evidence that HIF1α stabilisation induces changes in AMs that limit their efferocytic capacity. There is some evidence that HIF1α stabilisation has differential effects on phagocytic and efferocytic capacity, based on the effects of IOX-2 on the two functions. Further dissection of AM function is required to identify the basis of this differential effect. In particular, the metabolic flexibility of AMs and their reliance on glycolysis at baseline, in hypoxia and during phagocytosis and efferocytosis remains of relevance.

4.4.3 AM metabolic flexibility in normoxia and hypoxia

Previous data has indicated that AMs underutilise glycolysis in comparison to monocyte derived macrophages, instead relying on oxidative phosphorylation for most of their energy at baseline and in response to stimulation with LPS (Pereverzeva et al., 2022; Woods et al., 2020). However, AMs can increase glycolysis via HIF1α in response to hypoxia (Woods et al., 2022). AMs have also been shown to activate glycolysis in response to intracellular TB infection (Gleeson et al. 2016), although this induction is less efficient than the glycolytic response of IMs to TB infection (Huang et al. 2018).

Evidence from Chapter 3 showing upregulation of the gene encoding GLUT1 in hypoxia supports the potential activation of glycolysis in these conditions, as GLUT1 is integral to glucose uptake during glycolysis. Therefore, this chapter began exploration of the glycolytic activity of AMs at baseline and in response to LPS stimulation. Lactate release was measured as a surrogate marker for the rate of glycolysis in AMs. Although released during aerobic glycolysis, lactate is released in excess during anaerobic glycolysis, due to the inhibition of aerobic glycolysis enzymes that usually push most pyruvate towards the TCA cycle. This results

in lactate dehydrogenase converting pyruvate to lactate, to regenerate NAD for the early stages of glycolysis (Torres-Soria et al. 2022).

Lactate was measured after 48 hours at baseline and following LPS stimulation, in hypoxia and normoxia. Based on previous literature (Pereverzeva et al. 2022), it was expected that human AMs would not release lactate in response to LPS in normoxia. However, AMs responded to LPS with an increase in lactate secretion indicative of a glycolytic response. There are several differences between this study and the study by Pereverzeva et al. (2022) that may account for the contrasting results described here. This study used a higher dose of 10 μg/ml LPS, rather than the 100 ng/ml dose used in the previous study. It is likely that the higher dose of LPS pushed AMs further towards maximal metabolic capacity, resulting in the activation of glycolytic metabolism. Although Pereverzeva et al. (2022) demonstrated cytokine release from AMs in response to 100 ng/ml LPS, as this study did not measure the same cytokines, the magnitude of AM responses to stimulation cannot be compared. Pending an LPS dose titration, to determine whether increasing LPS doses have differential effects on glycolytic rate in AMs, this difference may indicate that although AMs are less dependent on glycolysis to respond to LPS, they do induce glycolysis in response to the increased metabolic demand of a high, but non-toxic, LPS dose.

Figure 4.18A demonstrates that baseline lactate production in untreated AMs is significantly increased in hypoxia. This is in line with murine studies, showing the hypoxic or pseudohypoxic HIF1α signalling in AMs results in increased glycolysis and glycolytic reserve. Interestingly, AMs cultured in hypoxia with LPS for 48 hours do not further increase their glycolytic output beyond those at baseline. This could indicate that these cells have reached their maximal glycolytic

capacity and cannot increase glycolysis further in response to stimuli. Alternatively, it has previously been demonstrated that lactate can inhibit glycolysis in macrophages, by blocking key enzymes including phosphofructokinase (Ó Maoldomhnaigh et al. 2021). Therefore, it is possible that the build-up of lactate in hypoxia prevents further glycolysis from being employed. As the success of LPS stimulation in inducing inflammatory cytokine secretion was not assessed here, differences in lactate secretion cannot be directly linked to differences in function across conditions.

These lactate assays were designed to begin to interrogate the metabolic capacity of AMs in hypoxia, as a potential mechanism by which efferocytosis is impaired. Metabolic pathways may prove integral in this defect, because recent studies into the metabolic regulation of efferocytosis have emphasised several key shifts as the process continues, likely due to the large and metabolically demanding cargo taken up during the process (Trzeciak et al. 2021).

Exploration has demonstrated that professional phagocytes generally respond to initial apoptotic cell binding by upregulating glycolysis and glucose uptake, and then respond to apoptotic cell internalisation by increasing lactate exporter SLC16A1 and thereby lactate excretion (Morioka et al. 2018). Although an increase in fatty acid oxidation accompanies increased glycolysis as efferocytosis progresses, initial studies have indicated that internalisation requires ATP generated by glycolysis, whilst pro-resolving mediator generation is mediated by fatty acid oxidation (Zhang et al., 2019). Further unique metabolic shifts have been mapped out that facilitate continuous efferocytosis (Park et al., 2011; Yurdagul et al., 2020; Schilperoort et al., 2023). For example, in a murine thymus model, lactate produced during the glycolytic response to apoptotic cell contact initiates increased expression of MerTK

for continual efferocytosis (Schilperoort et al. 2023). In murine bone marrow derived macrophages, arginine from cell cargo of the initial efferocytic event was converted to putrescine, resulting in the activation of Rac1 for further efferocytosis (Yurdagul et al. 2020). Additionally, lipid metabolism and fatty acid oxidation is increased during continual efferocytosis, likely reflecting the breakdown of cargo to maintain cell fitness (Zhang et al., 2019). Unfortunately, the sequential metabolic responses of AMs undergoing efferocytosis have not been completely investigated. Therefore, direct inferences cannot be made from this literature, as AM metabolism is divergent from metabolism in other tissues, likely due to the unique environmental niche they are adapted to (Svedberg et al., 2019).

Overall, efferocytosis likely requires a combination of glycolysis and oxidative phosphorylation in AMs. A combination of limited glycolytic capacity and insufficient oxygen for oxidative phosphorylation may therefore impair initial and/or continuous glycolysis. Further study into the resting metabolism of AMs in hypoxia is warranted to continue this work, as well as investigation of the sequential metabolic responses of AMs during initial and continual efferocytosis, both in normoxia and hypoxia. These pathways provide interesting possible routes by which efferocytosis, but not phagocytosis, is perturbed in hypoxia in AMs in a way that contrasts other tissue resident macrophage subtypes, which have unique metabolic adaptations and resources. In combination with further work described in Chapter 3, dissecting the capacity of AMs to efferocytose initially versus continually, evidence on metabolic flexibility of AMs may highlight how hypoxia uniquely effects efferocytosis.

4.4.4 Limitations

This chapter explores the role of HIF1α in the efferocytic impairment seen in AMs after exposure to hypoxia. However, there are some limitations to this exploration. Namely, experiments included low levels of biological replication. Validation was most limited as RNA and protein extraction required higher cell numbers than functional assays. Although the results from IOX-2 activated HIF1α responses can be viewed in combination to increase confidence in the effect of IOX-2, HIF inhibitors efficacy cannot be assessed beyond effects on viability due to low power.

IOX-2 constantly and highly increases HIF1α protein stabilisation. This is not reflective of the natural changes in HIF1α protein over time when a cell is exposed to constant hypoxia, where HIF1α levels peak acutely and drop over time (Torres-Soria et al. 2022), as demonstrated in Figure 3.19. Furthermore, PHD enzymes degrade other proteins in normoxia, such as IκB kinase-β (IKKβ). This means that in hypoxia or in the absence of PHD enzymes, IKKβ phosphorylation of IκBα increases, releasing more NF-κB and increasing sensitivity of NF-κB responses (D'ignazio and Rocha, 2016; Frost, Ciulli and Rocha, 2019). Therefore, IOX-2 alone is insufficient to completely isolate the role of HIF1α gene transcription.

Investigating whether HIF1α inhibitors correct efferocytic capacity in hypoxia is a useful way of confirming the role of HIF1α. However, these inhibitors also had limitations in this study. As described above, further replication is required to completely characterise the inhibitors and the extent of their effects. Additionally, when inhibitors, including IOX-2, were used in functional assays in this study, they were removed during the media change immediately

before the addition of apoptotic cells. It is possible that some of the effects of the inhibitors were reversed during the 2-hour period, reducing their effects.

Due to limited yield in some samples, inhibitor responses could not be confirmed at the protein or RNA level in all samples assessed for efferocytosis. Therefore, variable responses to inhibitors, seen at the protein and RNA levels, likely increase the variability of their effects on efferocytosis, increasing the need for repetition.

In a similar way to chapter 3, the efferocytosis assay used here is limited as it investigates only a single time point. This prevents in depth investigation into the dynamics of efferocytosis as it progresses. Temporal changes have proved crucial in understanding how HIF1α responses progress and could therefore be instrumental in understanding how efferocytosis is regulated by these changes.

Using lactate output as a surrogate for the assessment of glycolysis also has limitations. Firstly, as cumulative lactate is measured, no information on the dynamics of glycolysis is provided, and lactate produced by aerobic or anaerobic glycolysis cannot be distinguished. Furthermore, as lactate can be reversibly converted back into pyruvate or metabolised by mitochondrial metabolism, lactate levels may not completely reflect the extent of glycolysis that has occurred.

Although the high dose of LPS used here likely pushes AMs towards their maximal metabolic output, the types of metabolism triggered by apoptotic cell contact and engulfment are very different. Therefore, it would be valuable to study lactate output in response to apoptotic cell stimuli, as efferocytosis progresses, and in comparison to phagocytosis. To provide high-resolution, real-time information on AM metabolism before and during efferocytosis, this study would benefit from extracellular flux analysis to interrogate how glycolysis and oxidative

phosphorylation are employed by AMs during efferocytosis over time in normoxia. Additionally, extracellular flux technology would provide insight into how hypoxia effects the metabolic flexibility of AMs. This work, in combination with measuring metabolic enzymes at the protein and RNA level, would explain how the real time changes come about. This data would provide a rich source of information for understanding AM metabolism due to its real-time nature.

Investigation of AM metabolism in this model has some caveats. Importantly, the supplemented RPMI used in this study contains 11.1 mM glucose. As AMs reside in a low glucose environment, with approximately 0.4 mM glucose (Baker and Baines 2018), it is possible that AMs adapt *in vitro* in response to higher that physiological glucose concentrations, increasing their glycolytic capacity. Indeed, recent studies have demonstrated substantial changes in the expression of genes associated with glucose metabolism in AMs in response to culture in high glucose RPMI (Svedberg et al., 2019a). This is in line with the well documented highly plastic nature of macrophages. It would be valuable to optimise low glucose culture for future analysis of AM function, as prolonged exposure to high glucose is not physiologically relevant.

4.5 Conclusion

This chapter explored key pathways known to be activated in hypoxia, to understand their potential role in impairing efferocytosis. The main signalling node investigated was the HIF1α pathway. IOX-2 validation showed that 50 μM stabilised HIF1α without reducing viability. IOX-2 did not change levels of efferocytosis, however there was a trend towards increased phagocytosis with HIF1α stabilisation in normoxia. This indicates that HIF1α signalling has differential effects on the two processes and may contribute to this distinction in hypoxia.

HIF1α inhibitors underwent preliminary validation, however their efficacy could not be demonstrated. Additionally, no effect of the inhibitors could be seen efferocytic function. Finally, measurement of lactate secretion demonstrated a glycolytic response to LPS and hypoxic challenge in AMs, although the two treatments did not have additive effects on glycolysis, indicating AMs may be operating at maximal glycolytic capacity in hypoxia. Future work using high sensitivity, real time analysis of metabolism at baseline and during efferocytosis would be required to understand how AM efferocytosis occurs in normoxia and hypoxia.

CHAPTER 5: THE EFFECTS OF HYPOXIA ON HUMAN PRECISION CUT LUNG SLICES

5.1 INTRODUCTION

Precision cut lung slices (PCLS) are a novel tool used to model lung cells in their native architecture. Lung tissue is inflated with low melting point agarose and cut into thin slices for relatively short-term culture (G. Liu et al. 2019). This model offers powerful enrichment to standard single cell cultures and animal models. Murine PCLS reduce the number of animals required, giving an opportunity for high-throughput screening in line with the 3Rs (Tannenbaum and Bennett 2015). Human PCLS provide an arguably more complete representation of the human lung than any other *in vitro* model currently in widespread use, as most of the relevant resident cell types, including stromal and immune cells, remain intact, embedded in the associated extracellular matrix (G. Liu et al. 2019).

The use of human PCLS in IPF research is emerging. Several groups have generated PCLS from IPF transplant tissue, providing a near-complete *ex vivo* model of end stage disease for assessment of druggable targets and disease mechanism (Mercer et al. 2016; Tatler et al. 2016; Wei et al. 2021). Alsafadi et al (2017) also described a pro-fibrotic cocktail containing TGF-β, LPA, TNFα and PDGF to induce fibrosis in PCLS representative of early disease. Single-cell RNA sequencing characterisation using this cocktail has demonstrated a gene expression signature in these PCLS reminiscent of that seen in the IPF cell atlas (N. Lang et al. 2022). This PCLS fibrotic cocktail model has now been used in various contexts (Alsafadi Hani et al. 2020). The mechanisms of the two approved IPF drugs, Nintedanib and Pirfenidone, have been explored using fibrotic cocktail treated PCLS. The compounds both reduced fibrotic markers in PCLS treated with the fibrotic cocktail (Lehmann et al. 2018). Two compounds in preclinical and

clinical testing also reduced fibrotic gene expression in PCLS treated with the fibrotic cocktail (Stegmayr et al. 2021). Meanwhile, PCLS treated with this cocktail have been used to for preclinical testing of Saracatinib, EP300 inhibitors and a miR-29 mimic, alongside single cell and animal models (Rubio et al., 2019; Ahangari et al., 2022; Chioccioli et al., 2022). Saracatinib has now been granted orphan drug status by the FDA and is proceeding into clinical trials (NCT04598919).

There is growing evidence of the pro-fibrotic capacity of hypoxia in various single cell models of human pulmonary stromal cells. For example, hypoxia drives profibrotic behaviours, such as increased proliferation (Mizuno et al., 2009; Bodempudi et al., 2014; Senavirathna et al., 2018), collagen production (Robinson et al., 2012), and myofibroblast differentiation (Robinson et al., 2012; Aquino-Gálvez et al., 2019) in lung fibroblasts derived from none IPF and IPF tissue. Epithelial mesenchymal transition was also demonstrated in lung epithelial cells in response to hypoxia (S. H. Jeong et al. 2022). The main mechanistic drivers implicated in these effects are HIF1α (Goodwin et al. 2018) and HIF2α (Senavirathna et al., 2018, Bodempudi et al., 2014) mediated transcriptional changes, resulting in changes that drive proliferation and synthetic activity.

While the effects of intermittent hypoxia have been investigated in *in vivo* models of lung fibrosis (Table 1.3), there is currently no information on how human pulmonary cells react to hypoxia in a multicellular model. This is an important development beyond murine models, given the expansive differences between humans and mice, and the lack of a truly representative animal model of lung fibrosis (Jenkins et al., 2017; Kolb et al., 2020). PCLS are particularly valuable, as they model the crosstalk between stromal cells and AMs in response

to a challenge in a human system. Although AMs have been modelled *in vitro*, the cumulative effects of AM secretion can be modelled in the PCLS model. In addition, cell contact effects can be modelled. Given that AMs have been shown to control fibroblast activation in part via direct contact, this is of key importance (Novak et al. 2023).

Further still, PCLS have the potential to model features of IPF such as the existence of reparative intermediate cell subtypes like immature basaloid cells, which are incompletely understood and not recapitulated in single cell cultures. It is important to include these cells in models of the lung, as the effects of relevant stimuli, including Nintedanib and the previously described fibrotic cocktail, are highly cell specific and relevant in these populations (N. J. Lang et al. 2023). This model offers the opportunity to build on the evidence from single cell stromal cell cultures and the results of Chapter 3 and 4, by modelling the additional effects of hypoxia mediated by cell-cell interactions.

This chapter hypothesised that hypoxia increases fibrotic markers in PCLS in a HIF1α dependent way. The aims for this chapter were to:

(1) Establish and validate a PCLS hypoxic challenge model,
(2) Assess profibrotic markers in PCLS exposed to hypoxia for 48 hours, with and without simultaneous fibrotic cocktail treatment,
(3) Dissect the role of HIF1α in any profibrotic changes, using a range of inhibitors.

5.2 METHODS

5.2.1 Tissue Slicing

Lung tissue sections, obtained as described in Section 2.2.1, were stored at 4°C until use, for maximum 18 hours. Using a syringe and 25-gauge needle, human lung tissue was gently inflated with 3% Ultrapure low melting point agarose (Invitrogen. Catalogue number: 16520-050) via visible airways. Agarose was held at 37°C in a water bath. Tissue was cooled to set agarose and cores were cut using the Tissue Coring Press (Alabama R&D. Catalogue number: MD5000). Tissue cores were kept on ice to maintain integrity.

The Alabama R&D Tissue Slicer (Alabama R&D. Catalogue number: MD6000) was fitted with a razor blade, cooled to ice cold temperature, and filled with ice cold PBS. Tissue cores were transferred into the slicing chamber, and the Tissue Slicer was used to cut 300 µM slices. PCLS were emptied from the machine and kept on ice to ensure agarose maintained solid state. Individual PCLS were then gently transferred to 24 well plates in 500 µl Dulbecco's Modified Eagle Media (DMEM)/ F12 Nutrient Mix (1:1) containing 0.5% FBS (Gibco. Catalogue number: 11330032), and incubated at 37°C, 5% CO_2, allowing agarose to melt. This process is summarised in Figure 5.1.

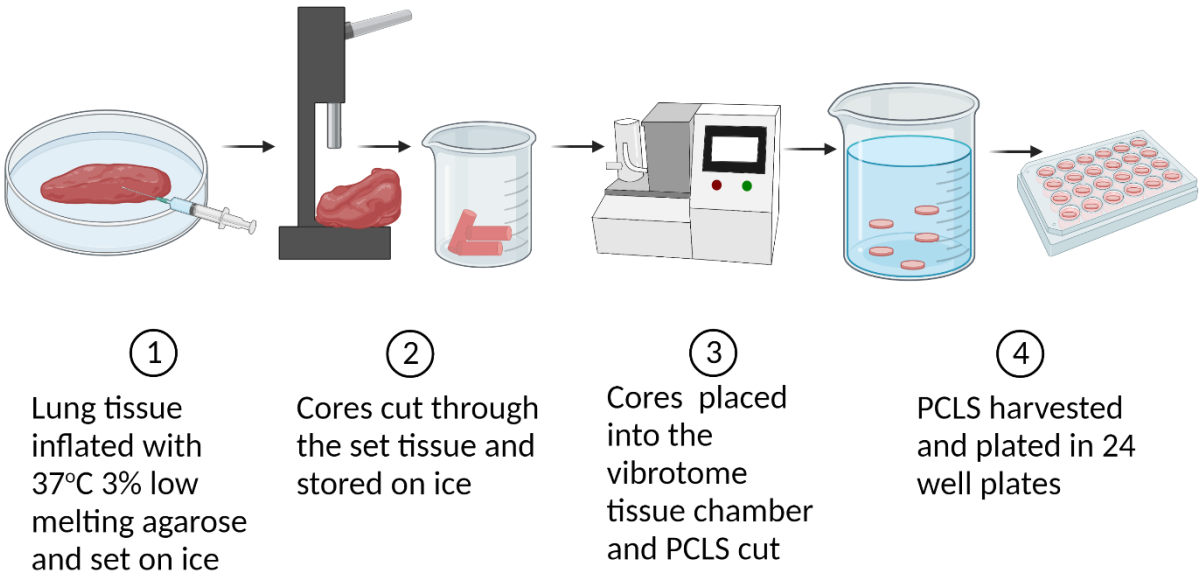

Figure 5.1 Generation of Precision Cut Lung Slices (PCLS) from human lung tissue. *(1) Lung tissue was inflated with 3% low melting point agarose warmed to 37°C using a syringe and 25-gauge needle, via visible airways. Agarose was allowed to set on ice. (2) A tissue coring press was used to cut tissue cores from the inflated tissue, which were transferred to a beaker and stored on ice. (3) The vibratome was filled with ice cold PBS. Tissue cores were placed into the tissue chamber. The vibratome was set to cut 300 µM slices, which were released into the attached tank. (4) PCLS and slices were drained from the vibratome into a beaker, which was immediately transferred into the biological safety cabinet. Slices were transferred gently into individual wells of a 24 well plate, containing 500 µl culture media. Slices were incubated in at 37°C, 5% CO_2 overnight, to allow agarose to melt.*

5.2.2 PCLS treatments

PCLS were treated with the previously described profibrotic cocktail (Alsafadi et al. 2017), containing 5 ng/ml recombinant TGF-β, 5 µM PDGF-AB (Gibco. Catalogue number: PHG0134), 10 ng/ml TNFα (R&D Systems. Catalogue number: P06804), and 5 µM LPA (Biotechne. Catalogue: number 3854), for 48 hours.

HIF1α inhibitors described in Chapter 4 were also used to treat PCLS. PCLS cultured in normoxia were treated with 50 µM IOX-2 for 48-hours. PCLS cultured in hypoxia were treated with 5 and 10 µM PX-478, and 20 and 40 µM KC7F2 for the 48-hour hypoxic period. All HIF1α inhibitor

doses were added in equal volumes of DMSO and matching DMSO concentrations were added to untreated controls.

5.2.3 Protein and RNA extraction for PCLS

5.2.3.1 Direct Laemmli Protein Extraction

PCLS were lysed directly in 500 µl Laemmli buffer using a Tissue Tearor (BioSpec. Catalogue Number: 985370EUR-04), fitted with a 45 mm blade, to disrupt the sample for 30 seconds. 6 slices were lysed per condition. PCLS exposed to hypoxia were lysed immediately upon removal from the hypoxystation, to minimise the breakdown of hypoxia dependent proteins. Lysates were stored at -80°C until use.

5.2.3.2 Trizol Extraction of RNA and Protein

PCLS (6 per condition) were lysed in 1 ml trizol (Life Technologies. Catalogue number: 15596026) using a Tissue Tearor with 45 mm blade, for 30 seconds to disrupt all visible pieces of tissue. Lysate was stored at -80°C until processing for the extraction of RNA and protein, following the manufacturer's instructions.

100 µl chloroform was added per 1 ml trizol and samples were shaken vigorously. After standing for 10 minutes at room temperature and samples were centrifuged at 12,000 x g, 15 minutes, at 4°C. The resultant 3 phases visible within the samples can be collected for RNA, DNA and protein extraction. The upper clear phase was isolated into a RNase free Eppendorf for RNA collection. The white interphase containing genomic DNA was removed and discarded. The lower pink organic phase was collected for downstream protein isolation.

RNA extraction from clear trizol phase

The collected clear aqueous phase was mixed with 500 µl isopropanol and incubated for 10 minutes at room temperature, then centrifuged at 12,000 x g, 10 minutes, 4°C. The supernatant was removed and discarded leaving a white RNA pellet. The pellet was washed in 1 ml 75% ethanol (7,500 x g, 5 minutes, 4°C). Remaining ethanol was removed, leaving the RNA pellet to almost completely dry. RNA was then dissolved in RNase free water, before immediate storage at -80°C.

Protein extraction from pink trizol phase

The lower organic phase was mixed with 300 µl 100% ethanol and incubated for 3 minutes at room temperature and centrifuged at 2000 x g for 5 minutes, 4°C. The resultant protein pellet was mixed with 1 ml isopropanol, left to stand for 10 minutes at room temperature and centrifuged again at 12,000 x g for 10 minutes, 4°C. Supernatant was removed and discarded. The protein pellet was washed 3 times in 1 ml 100% ethanol, with gentle shaking between washes (7,500 x g, 5 minutes, 4°C). After washing, all ethanol was removed, and pellet was left to airdry. Protein was resuspended in 1% SDS and stored at -80°C.

5.2.3.3 Protein Quantification by BCA

Protein isolated using Trizol was quantified using a bicinchoninic acid (BCA) assay, according to the manufacturer's instructions. Briefly, bovine serum albumin (BSA) standards were made up in 1% SDS ranging from 2000 µg/ml to 25 µg/ml. Samples were also diluted in 1% SDS. 25 µl standards and samples were added to a flat bottom 96 well plates in duplicate. 200 µl working reagent (BCA reagents A and B mixed 1:1) (ThermoFisher Scientific. Catalogue number: 23227) was added per well. The plate was briefly mixed on a plate shaker before incubation at 37°C for

30 minutes. Absorbance at 562 nm was determined on a plate reader (Synergy HT, Bio-Tek). Standards of known concentration were used to derive the linear equation for calculation of protein concentrations in experimental samples.

5.2.3.4 SDS-PAGE using Protein from Trizol Extraction

Protein isolated using the trizol method was diluted in ddH_2O according to BCA analysis, to achieve loading of consistent amounts of protein in every lane. 6X Laemmli buffer was also added to samples for a final dilution of 1:6, to visualise protein loading and increase sample density. Samples were boiled at 100^oC for 5 minutes immediately before loading. Onward SDS-PAGE and western blot analysis were performed as described in section 2.8.2.

5.2.4 LDH Quantification

The CytoTox 96® Non-Radioactive Cytotoxicity Assay (Promega. Catalogue number: G1780) was used as per manufacturer's instructions to quantify lactate dehydrogenase (LDH) in supernatant. To measure PCLS LDH content, 1 PCLS was weighed and disrupted in 1X lysis buffer from the CytoTox 96® Non-Radioactive Cytotoxicity Assay kit. To measure LDH release from PCLS, supernatants were collected. For assessment, 50 µl lysate or supernatants were mixed with CytoTox 96 Reagent in triplicate, with culture media plated alone to control for supernatant background. Plates were incubated at room temperature for 30 minutes. Stop solution was added and absorbance was measured at 490 nm on the Synergy HT plate reader. LDH content in PCLS was expressed as arbitrary units (AU) per mg tissue. Background LDH levels in media alone were subtracted from supernatant LDH values, for expression as AU.

5.3 RESULTS

5.3.1 Tissue Donor Demographics

PCLS were generated from 15 lung tissue samples Table 5.1. 13 samples (86.7%) were from long-term ex-smokers, who quit smoking at least 4 years ago. 2 samples (13.3%) were from never smokers.

		Never Smoker	Long Term Ex-Smoker	
	Summary	2 (13.3%)	13 (86.7%)	P Value
Age	73 (IQR 11)	61 (IQR 30)	73 (IQR 10.5)	*0.4381*
Sex	7 (47%) M 8 (53%) F	1 (50%) M 1 (50%) F	6 (46%) M 7 (54%) F	*>0.9999*

Table 5.1 Donor Details for Lung Tissue Used for PCLS Generation. Age of smoking groups were compared using a Mann-Whitney statistical test. Sex distributions between smoking groups were compared using a Fisher's exact test.

5.3.2 PCLS viability over time

PCLS LDH release was assessed as a surrogate for viability. LDH content within a PCLS slice was assessed following lysis every day for 7 days. Total LDH was expressed as AU/mg for normalisation (Figure 5.2B). On day 6 and day 7, LDH content was reduced below LDH content on day 1 (p= 0.008 and p=0.0004 respectively). Media LDH content was also assessed on days 2, 4 and 6. Background LDH in media was subtracted, and LDH was expressed cumulatively due to media changes every 2 days (Figure 5.2A). In line with the drop in LDH content seen in PCLS, LDH was consistently released into media by PCLS over 6 days.

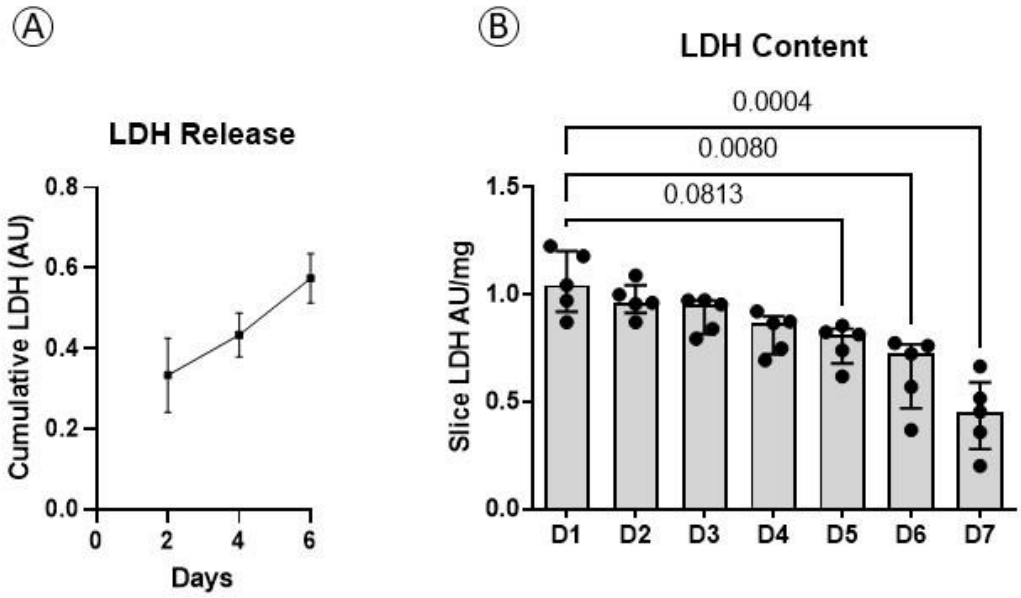

Figure 5.2 LDH release by PCLS over time. PCLS were cultured in DMEM/F12 (1:1) supplemented with 0.5% FCS. (A) Media was collected and replaced every 2 days for LDH measurement. LDH release was averaged across 3 PCLS and was expressed cumulatively due to these media exchanges. N=3. (B) On each day, 1 PCLS was weighed and then disrupted in lysis buffer, to release total LDH. LDH content was normalised to PCLS weight, resulting in expression as AU/mg. N=5. D1 vs D2 p>0.9999, D1 vs D3 p>0.9999, D1 vs D4 p=0.3342, D1 vs D5 p=0.0813, D1 vs D6 p=0.008, D1 vs D7 p=0.0004. Comparisons were drawn using a Kruskal-Wallis test with Dunn's multiple correction test. Data is expressed as median (±IQR). LDH: Lactate dehydrogenase.

5.3.3 Fibrotic Cocktail Validation

5.3.3.1 PCLS viability with FC

The fibrotic cocktail published by Alsafadi et al (2017), for the generation of PCLS which reflect early IPF disease changes, was validated in our hands. Firstly, LDH release was compared in treated and untreated PCLS, to confirm that the cocktail had no toxic effects (Figure 5.3). There was no difference in LDH release between treated and untreated PCLS.

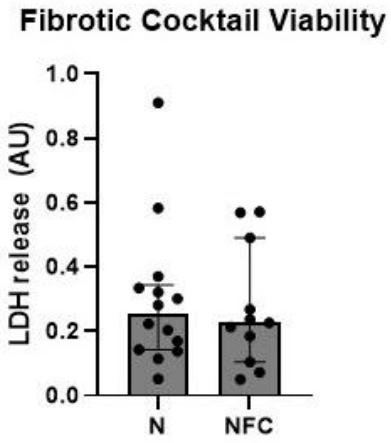

Figure 5.3 LDH release by PCLS with fibrotic cocktail. PCLS were cultured for 48 hours DMEM/F12 (1:1) supplemented with 0.5% FCS, with and without a profibrotic cocktail (5 ng/ml TGF-β, 5 μM PDGF-AB, 10 ng/ml TNFα, and 5 μM LPA). (A) Media was collected after 48 hours for LDH measurement, for assessment of the effects of the profibrotic cocktail. LDH release was averaged across 3 PCLS per condition. N=14. N vs NFC p=0.8984. Comparison made using a Wilcoxon's test. Data is expressed as median (±IQR). N: normoxia. NFC: normoxia with fibrotic cocktail.

5.3.3.2 Characterisation of PCLS treated with fibrotic cocktail

The efficacy of the fibrotic cocktail in inducing early IPF like changes was assessed by gene and protein expression after 48 hours. Key fibrotic markers collagen I and αSMA were assessed at the protein and RNA level. Protein was quantified by SDS PAGE and western blotting. Actin B was used as a housekeeper, to control for protein loaded. Additionally, a composite housekeeper, combining levels of actin B and GAPDH, was derived to reduce variability in more accurately represent protein loading.

Col1a1 expression was not changed by fibrotic cocktail (Figure 5.4A). Using normalisation to Actin B or the composite housekeeper value, no change in collagen I protein was detected with the fibrotic cocktail (Figure 5.4B-D). Expression of the gene encoding αSMA, *Acta2,* was also not significantly increased by fibrotic cocktail treatment (Figure 5.5A). When levels of αSMA were normalised to Actin B or the housekeeping composite, there was no change with

profibrotic cocktail treatment (Figure 5.5B-D). This data fails to demonstrate the profibrotic effects of this cocktail with the markers measured.

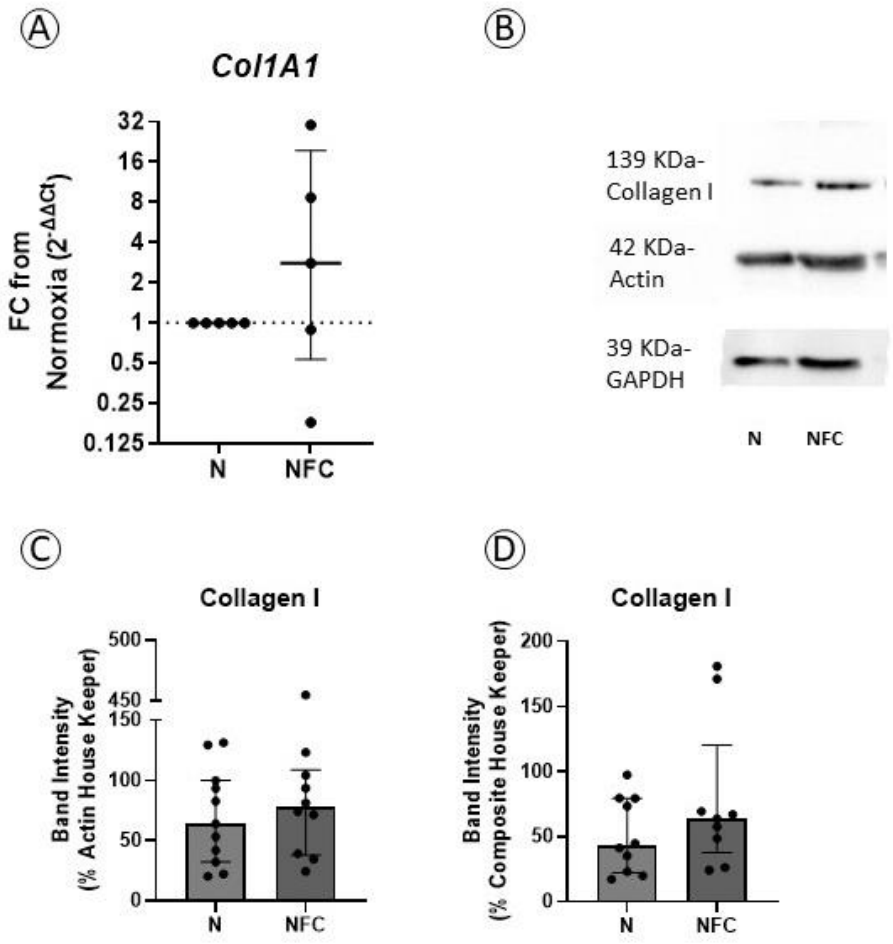

Figure 5.4 Collagen expression in PCLS with fibrotic cocktail. PCLS were cultured for 48 hours DMEM/F12 (1:1) supplemented with 0.5% FCS, with and without a profibrotic cocktail (5 ng/ml TGF-β, 5 µM PDGF-AB, 10 ng/ml TNFα, and 5 µM LPA). (A) RNA was extracted from 6 pooled PCLS and expression of Col1A1 was assessed by qPCR. Expression is displayed as $2^{-\Delta\Delta Ct}$ values, in comparison to expression in untreated PCLS. N=5. N vs NFC p=0.3125. Protein was extracted from 6 pooled PCLS and expression of Collagen 1A1 was assessed by western blotting. Representative blot shown from one sample (B). The same representative blot is used across several figures in this chapter. Expression was normalised as a percentage of Actin B (N=14) (C) and housekeeping composite (N=10) (D) loading controls. Actin loading control N vs NFC p=0.4922. Housekeeping Composite loading control N vs NFC p= 0.3594. Comparisons were made using a Wilcoxon's test. Data is presented as median (±IQR) N: normoxia. NFC: normoxia with fibrotic cocktail.

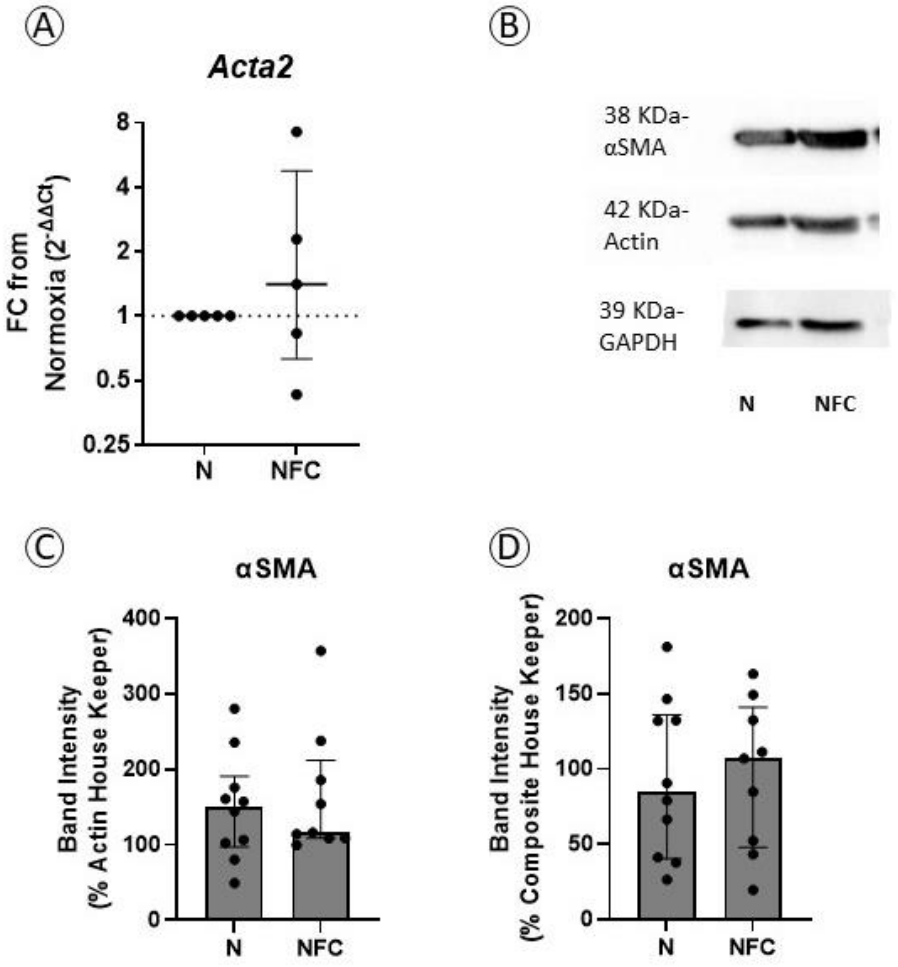

Figure 5.5 αSMA expression in PCLS with fibrotic cocktail. PCLS were cultured for 48 hours DMEM/F12 (1:1) supplemented with 0.5% FCS, with and without a profibrotic cocktail (5 ng/ml TGF-β, 5 µM PDGF-AB, 10 ng/ml TNFα, and 5 µM LPA). (A) RNA was extracted from 6 pooled PCLS and expression of Acta2 was assessed by qPCR. Expression is displayed as $2^{-\Delta\Delta Ct}$ values, in comparison to expression in untreated PCLS. N=5. N vs NFC p=0.4375. Protein was extracted from 6 pooled PCLS and expression of αSMA was assessed by western blotting. Representative blot shown from one sample (B). The same representative blot is used across several figures in this chapter. Expression was normalised as a percentage of Actin B (C) and housekeeping composite (D) loading controls. N=9. Actin loading control N vs NFC p=0.4258. Housekeeping Composite loading control N vs NFC p= 0.6523. Comparisons were made using a Wilcoxon's test. Data is presented as median (±IQR) N: normoxia. NFC: normoxia with fibrotic cocktail.

5.3.4 Hypoxic Challenge Validation

5.3.4.1 Viability

The feasibility of exposing PCLS to hypoxia (1% O_2, 5% CO_2) for 48 hours was assessed by measuring LDH release, to determine whether viability was affected by the challenge. LDH release was not significantly different in PCLS exposed to hypoxia, in comparison to those cultured in normoxia (Figure 5.6).

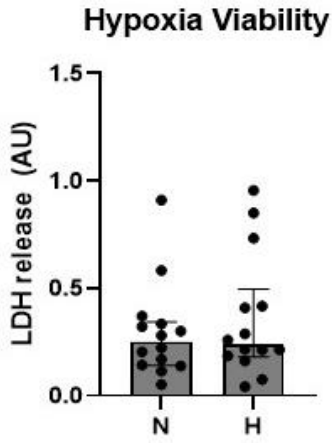

Figure 5.6 LDH release by PCLS in hypoxia. *PCLS were cultured in normoxia (21% O_2, 5% CO_2) or hypoxia (1% O_2, 5% CO_2) for 48 hours. Media was collected after 48 hours for LDH measurement. LDH release was averaged across 3 PCLS. N=14. N vs H p= 0.8077. Comparisons were made using a Wilcoxon's test. Data is expressed as median (±IQR). N: normoxia. H: hypoxia.*

5.3.4.2 HIF1α blot attempt

PCLS were homogenised in Laemmli buffer immediately after removal from the hypoxia chamber, in an attempt to maintain HIF1α protein in a reduced state for detection by western blotting. However, assessment by western blotting was unable to detect HIF1α protein after hypoxic exposure (Figure 5.7), despite the presence of protein loading demonstrated by housekeeping control bands.

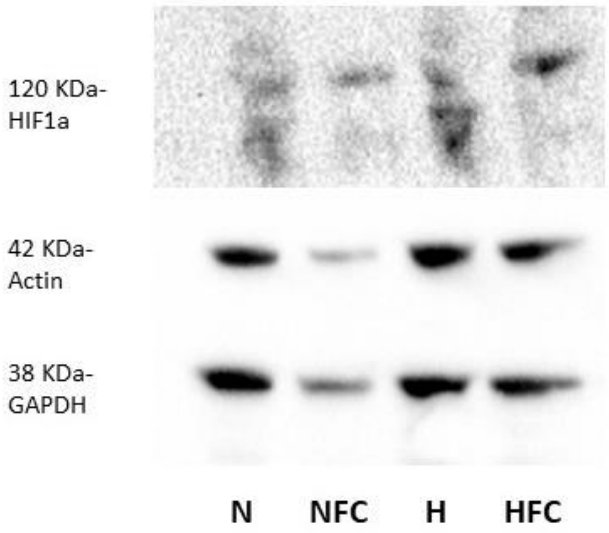

Figure 5.7 HIF1α in PCLS in hypoxia. PCLS were cultured in normoxia (21% O_2, 5% CO_2) or hypoxia (1% O_2, 5% CO_2) for 48 hours. 6 PCLS were pooled and homogenised directly in Laemmli buffer, for analysis by western blotting. Equal amounts of lysate were loaded in each lane. Membranes were probed sequentially for HIF1α, Actin B and GAPDH. This is a representative blot of n=3. N: normoxia. NFC: normoxia with fibrotic cocktail. H: hypoxia. HFC: hypoxia with fibrotic cocktail. HIF1α: hypoxia inducible factor 1α. GAPDH: Glyceraldehyde 3-phosphate dehydrogenase.

5.3.4.3 HIF1α response gene activation

Expression of HIF1α response genes was measured as a surrogate for HIF1α protein to confirm activation of HIF1α signalling in PCLS incubated in hypoxia. VEGFA expression was assessed at the gene and protein level. No difference was detected in *VEGFA* gene expression PCLS exposed to hypoxia for 48 hours (Figure 5.8A). However, cumulative VEGFA release into the media was increased in hypoxia after normalisation to total protein content of supernatants (p= 0.043) (Figure 5.8B). HIF1α response gene *SLC2A1* expression was consistently increased after 48 hours of hypoxia, although this trend did not reach the threshold for statistical significance (p=0.0625) (Figure 5.9). Together, this data suggests activation of HIF1α signalling in PCLS incubated in hypoxia.

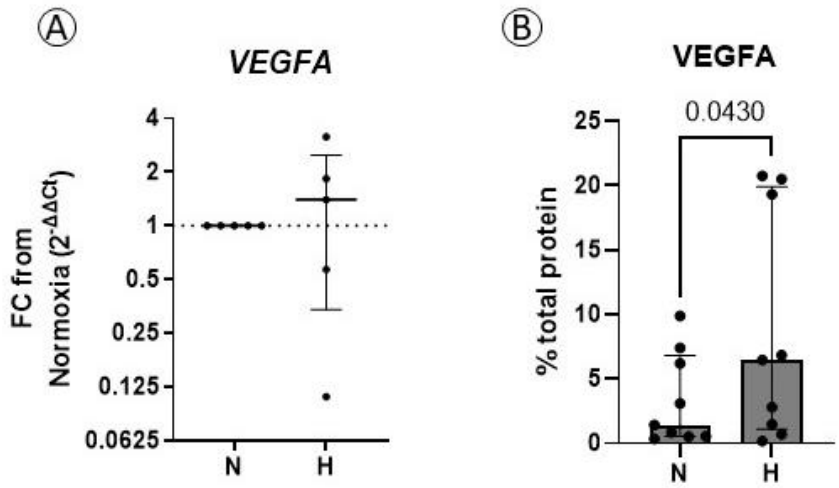

Figure 5.8 VEGFA expression in PCLS in hypoxia. PCLS were cultured normoxia (21% O_2, 5% CO_2, 37°C) or hypoxia (1% O_2, 5% CO_2, 37°C) for 48 hours. (A) RNA was extracted from 6 pooled PCLS and expression of VEGFA was assessed by qPCR. Expression is displayed as $2^{-\Delta\Delta Ct}$ values, in comparison to expression in PCLS cultured in normoxia. N=5. N vs H p= 0.8125. (B) Supernatants were also collected after 48 hours and VEGFA release was assessed by ELISA. VEGFA content is normalised to total protein content as measured by BCA assay. N=9. N vs H p=0.0430. Comparisons were made using a Wilcoxon's test. Data is expressed as median (±IQR). N: normoxia. H: hypoxia.

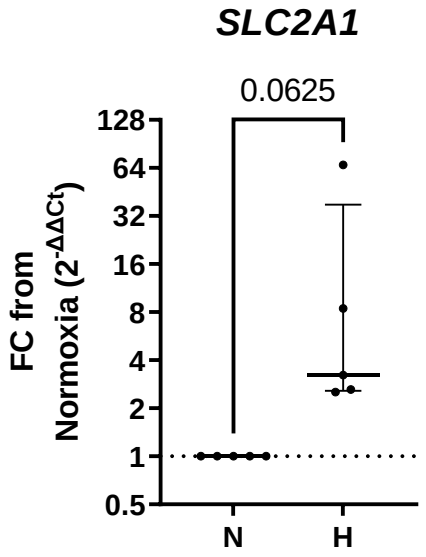

Figure 5.9 SLC2A1 expression in PCLS in hypoxia. PCLS were cultured normoxia (21% O_2, 5% CO_2, 37°C) or hypoxia (1% O_2, 5% CO_2, 37°C) for 48 hours. RNA was extracted from 6 pooled PCLS and expression of SLC2A1 was assessed by qPCR. Expression is displayed as $2^{-\Delta\Delta Ct}$ values, in comparison to expression in PCLS cultured in normoxia. N=5. N vs H p=0.0625. Comparisons were made using a Wilcoxon's test. Data is expressed as median (±IQR). N: normoxia. H: hypoxia.

5.3.5 PCLS fibrosis markers in hypoxia

Key fibrotic markers, αSMA and collagen I were assessed at the protein and RNA level, to determine whether hypoxia induced profibrotic changes in PCLS. Expression of *Col1A1* was not consistently changed by hypoxic challenge, when compared to PCLS cultured in normoxia (Figure 5.10A). No change in the amount of collagen I level was detected following normalisation to actin B alone, however an increase was detected following normalisation to the composite housekeeper ($p= 0.0273$) (Figure 5.10B-D).

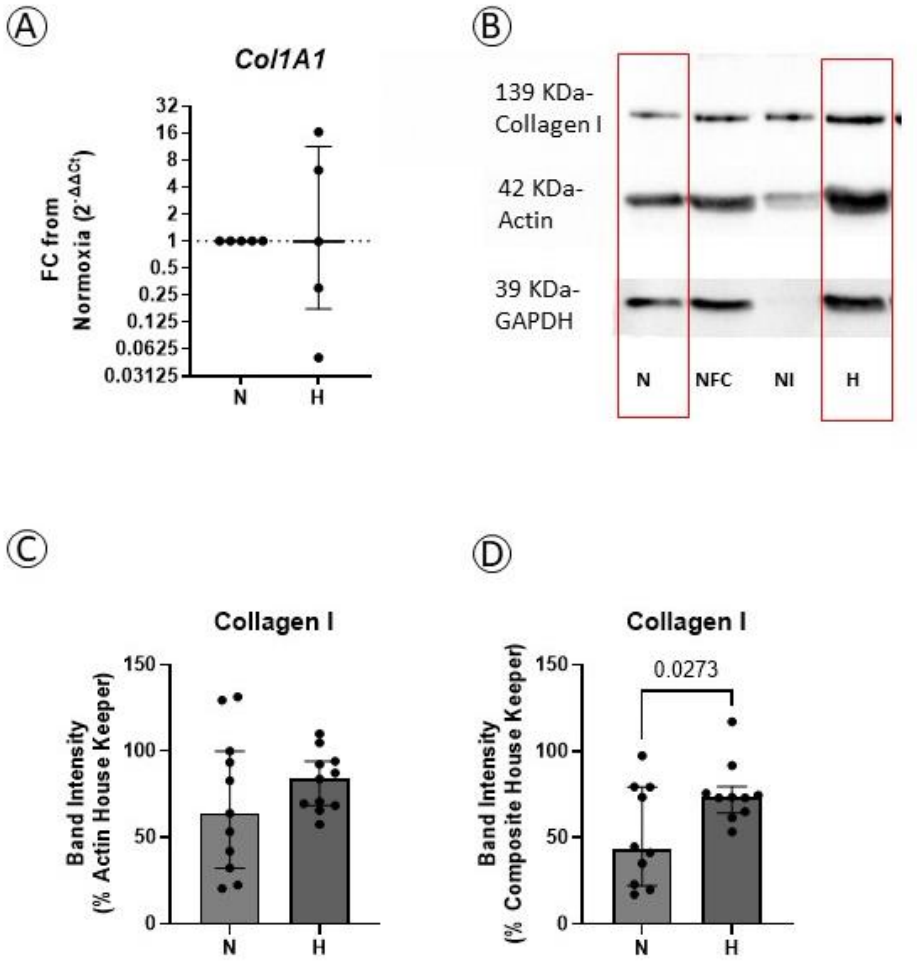

Figure 5.10 Collagen I in PCLS in hypoxia. PCLS were cultured for 48 hours in normoxia (21% O_2, 5% CO_2) or hypoxia (1% O_2, 5% CO_2). (A) RNA was extracted from 6 pooled PCLS and expression of Col1A1 was assessed by qPCR. Expression is displayed as $2^{-\Delta\Delta Ct}$ values, in comparison to expression in PCLS cultured in normoxia. N=5. Protein was extracted from 6 pooled PCLS and expression of Collagen 1A1 was assessed by western blotting. Representative blot shown from one sample (B). The same representative blot is used across several figures in this chapter. Expression was normalised as a percentage of (C) actin B (N=11) and (D) composite housekeeper (N=10) loading controls. Actin loading control N vs H p=0.3023. Housekeeping Composite loading control N vs H p= 0.0273. Comparisons were made using a Wilcoxon's test. Data is presented as median (±IQR). N: normoxia. H: hypoxia.

Expression of *ACTA2* was assessed in PCLS with and without hypoxic challenge. *ACTA2* expression was not consistently changed following 48 hours of hypoxia challenge (Figure 5.11A). αSMA protein levels in hypoxia were unchanged following normalisation to housekeeping composite and Actin B (Figure 5.11B-D).

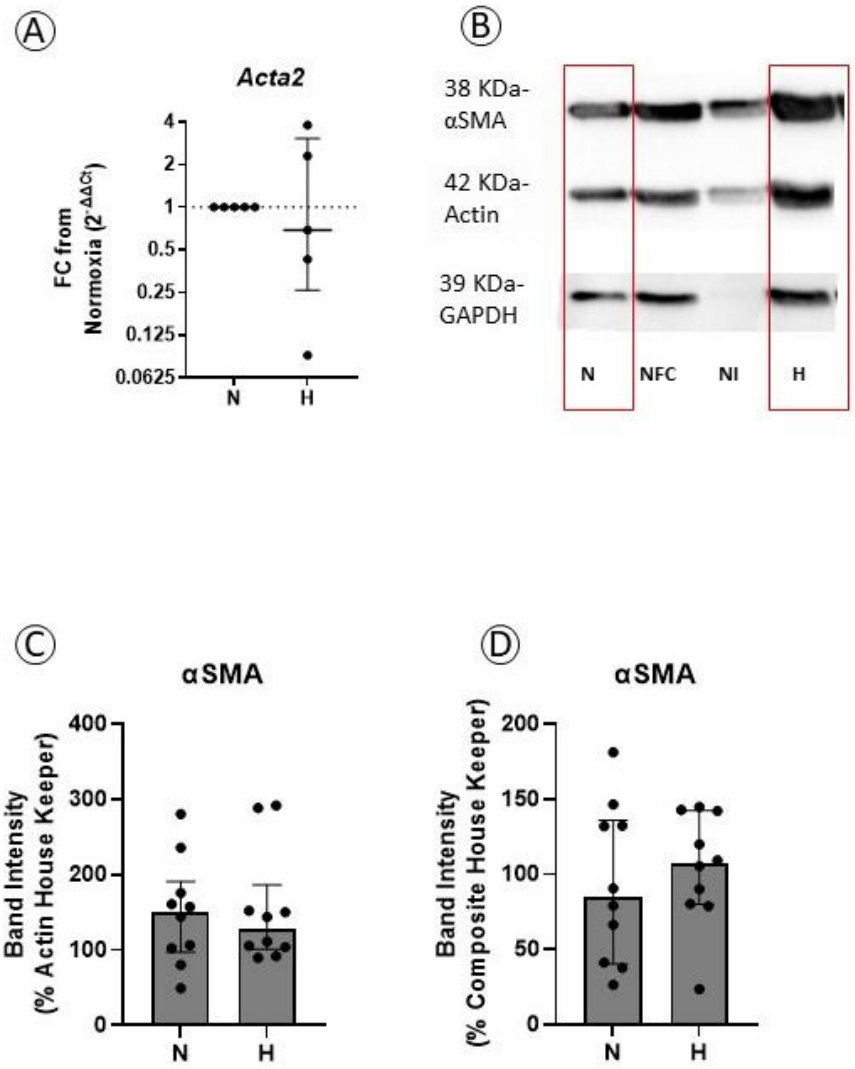

Figure 5.11 αSMA in PCLS in hypoxia. PCLS were cultured for 48 hours in normoxia (21% O_2, 5% CO_2) or hypoxia (1% O_2, 5% CO_2). (A) RNA was extracted from 6 pooled PCLS and expression of ACTA2 (αSMA) was assessed by qPCR. Expression is displayed as $2^{-\Delta\Delta Ct}$ values, in comparison to expression in PCLS cultured in normoxia. N=5. N vs H p=0.8125. Protein was extracted from 6 pooled PCLS and expression of αSMA was assessed by western blotting. Representative blot shown from one sample (B). The same representative blot is used across several figures in this chapter. Expression was normalised as a percentage of (C) actin B and (D) housekeeper composite loading controls. N=10. Actin loading control N vs H p=0.6250. Housekeeping Composite loading control N vs H p= 0.1602. Comparisons were made using a Wilcoxon's test. N: normoxia. H: hypoxia. Data is presented as median (±IQR)

5.3.6 Fibrotic cocktail and hypoxic challenge

The same fibrotic markers were assessed in PCLS with concurrent hypoxia and fibrotic cocktail treatment, to determine whether the combined treatments have an additive effect on fibrosis.

Col1A1 expression remained inconsistent following combined treatment (Figure 5.12A) and there was no additive effect detected in collagen I protein expression following normalisation to Actin B or the housekeeper composite (Figure 5.12B-D). *Acta2* expression was also unchanged by hypoxia and fibrotic cocktail treatment (Figure 5.13A), with no changes detected in αSMA protein following exposure to hypoxia and fibrotic cocktail (Figure 5.13C,D).

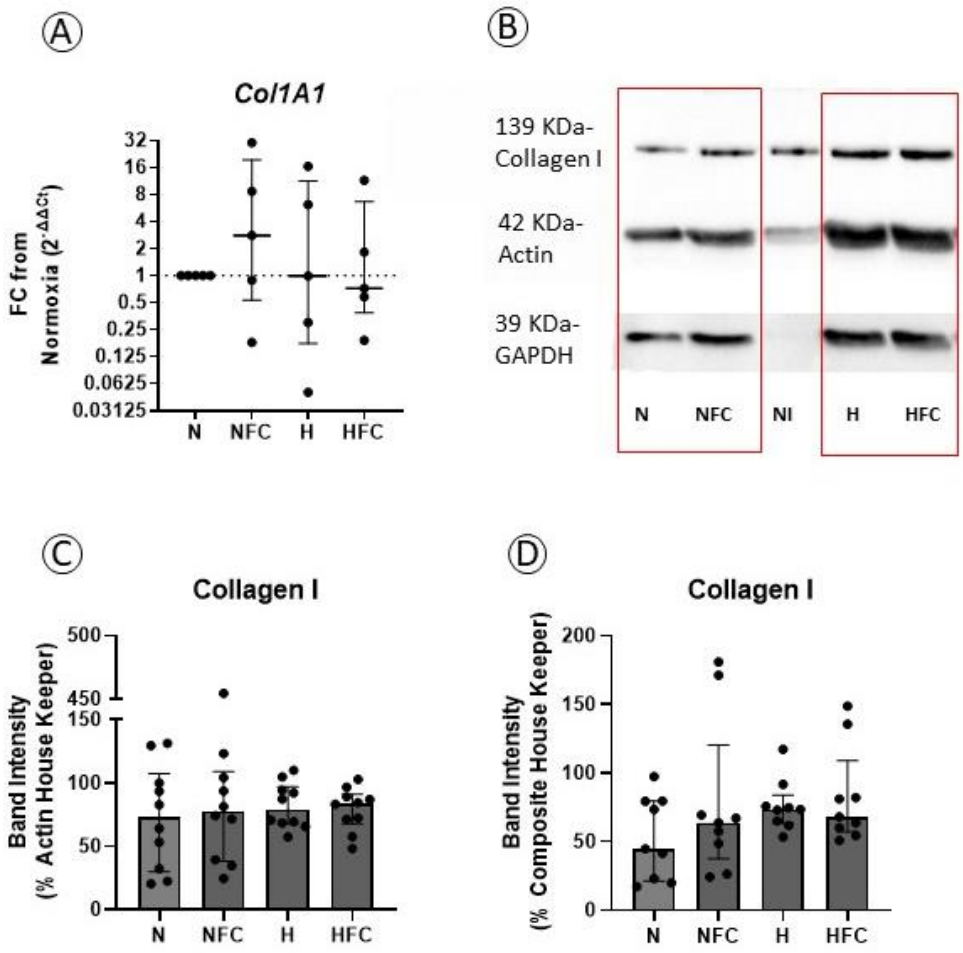

Figure 5.12 Collagen I in PCLS in hypoxia with fibrotic cocktail. PCLS were cultured for 48 hours in normoxia (21% O_2, 5% CO_2) or hypoxia (1% O_2, 5% CO_2), with or without profibrotic cocktail. (A) RNA was extracted from 6 pooled PCLS and expression of Col1A1 was assessed by qPCR. Expression is displayed as $2^{-\Delta\Delta Ct}$ values, in comparison to expression in PCLS cultured in normoxia. N=5. N vs NFC p>0.9999, N vs H p>0.9999, N vs HFC p>0.9999. Protein was extracted from 6 pooled PCLS and expression of Collagen 1A1 was assessed by western blotting. Representative blot shown from one sample (B). The same representative blot is used across several figures in this chapter. Expression was normalised as a percentage of (C) actin B (N=10) and (D) composite housekeeper (N=9) loading controls. Actin B loading control: N vs NFC p>0.9999, N vs H p>0.9999, N vs HFC p>0.9999. H vs HFC p>0.9999. Housekeeper composite loading control: N vs NFC p>0.9999, N vs H p=0.2677, N vs HFC p=0.4073. H vs HFC p>0.9999. Comparisons were made using a Friedman's test and Dunn's multiple comparison test. Data is presented as median (±IQR). N: normoxia. H: hypoxia. NFC: normoxia with fibrotic cocktail. HFC: hypoxia with fibrotic cocktail.

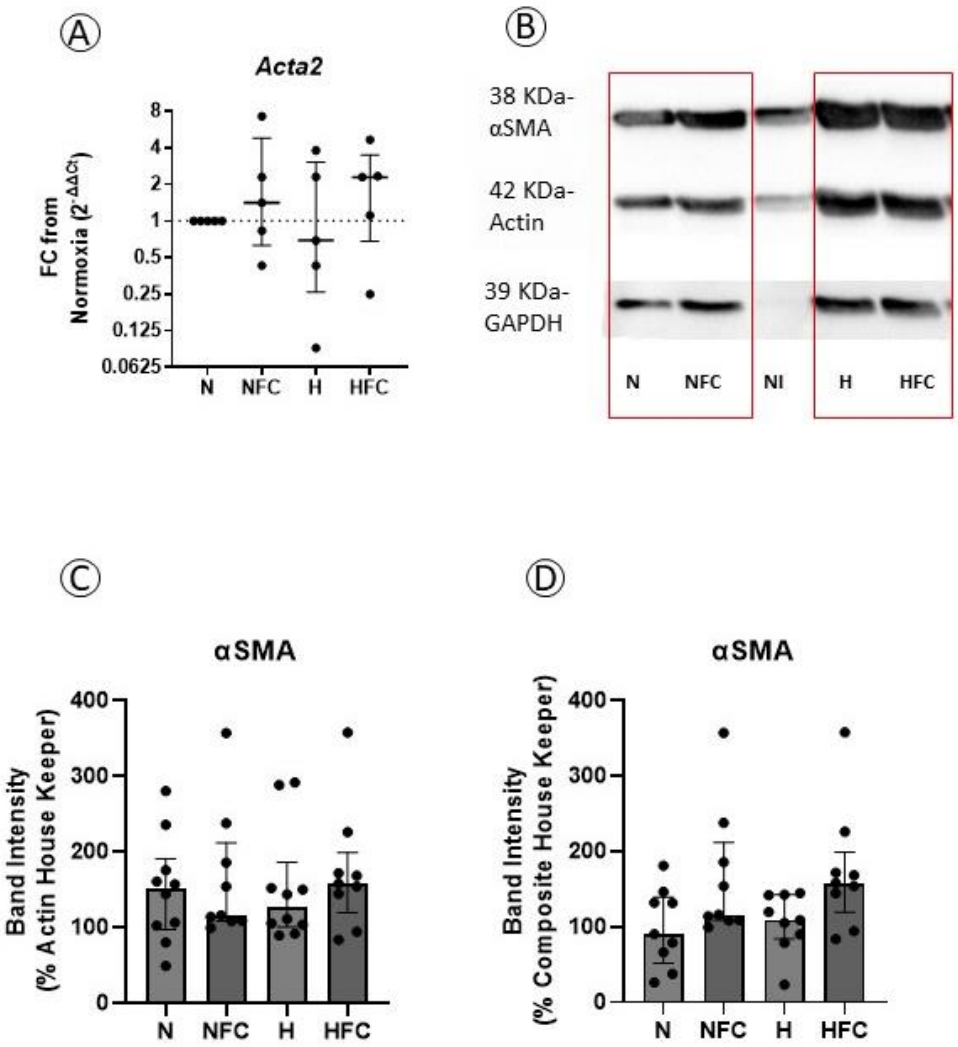

Figure 5.13 αSMA in PCLS in hypoxia with fibrotic cocktail. PCLS were cultured for 48 hours in normoxia (21% O_2, 5% CO_2) or hypoxia (1% O_2, 5% CO_2) with or without profibrotic cocktail. (A) RNA was extracted from 6 pooled PCLS and expression of ACTA2 (αSMA) was assessed by qPCR. Expression is displayed as $2^{-\Delta\Delta Ct}$ values, in comparison to expression in PCLS cultured in normoxia. N vs NFC p>0.9999, N vs H p>0.9999, N vs HFC p=0.4249. Protein was extracted from 6 pooled PCLS and expression of αSMA was assessed by western blotting. Representative blot shown from one sample (B). The same representative blot is used across several figures in this chapter. Expression was normalised as a percentage of (C) actin B (N=10) and (D) housekeeper composite (N=9) loading controls. Actin B loading control: N vs NFC p>0.9999, N vs H p>0.9999, N vs HFC p>0.9999. H vs HFC p>0.9999. Housekeeper composite loading control: N vs NFC p>0.9999, N vs H p=0.6021, N vs HFC p=0.8648, H vs HFC p>0.9999. Comparisons were made using a Friedman's test and Dunn's multiple comparison test. Data is presented as median (±IQR). N: normoxia. H: hypoxia. NFC: normoxia with fibrotic cocktail. HFC: hypoxia with fibrotic cocktail.

5.3.7 Validation of IOX-2

IOX-2 was introduced for normoxic stabilisation of HIF1α in PCLS. The feasibility of a 50 µM dose for 48 hours was determined measuring LDH release following treatment. This dose selected based on studies exposing human fibroblasts (Brereton et al. 2022) and bronchial epithelial cells (Ramirez-Moral et al. 2022) to IOX-2, because no studies were found to use the inhibitor in a 3D model. There was no change in LDH release following IOX-2 treatment (Figure 5.14).

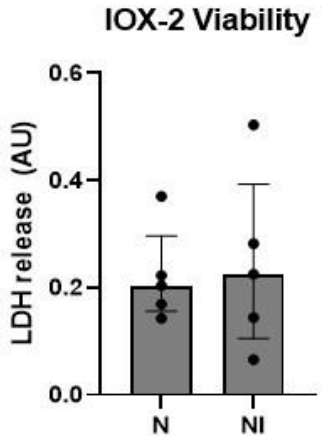

Figure 5.14 LDH release by PCLS treated with IOX-2. *PCLS were cultured in normoxia (21% O_2, 5% CO_2) with 50 µM IOX-2 for 48 hours. Media was collected after 48 hours for LDH measurement. LDH release was averaged across 3 PCLS. N=5. N vs NI p= 0.8125. Comparisons were made using a Wilcoxon's test. Data is expressed as median (±IQR). N: normoxia. NI: normoxia with 50 µM IOX-2. LDH: lactate dehydrogenase.*

The efficacy of IOX-2 in inducing HIF1α driven transcriptional programs was determined by measuring HIF1α response genes. Changes in *VEGFA* expression could not be detected in response to IOX-2 (Figure 5.15A). Similarly, no changes were detected in cumulative VEGFA secretion over 48 hours (Figure 5.15B).

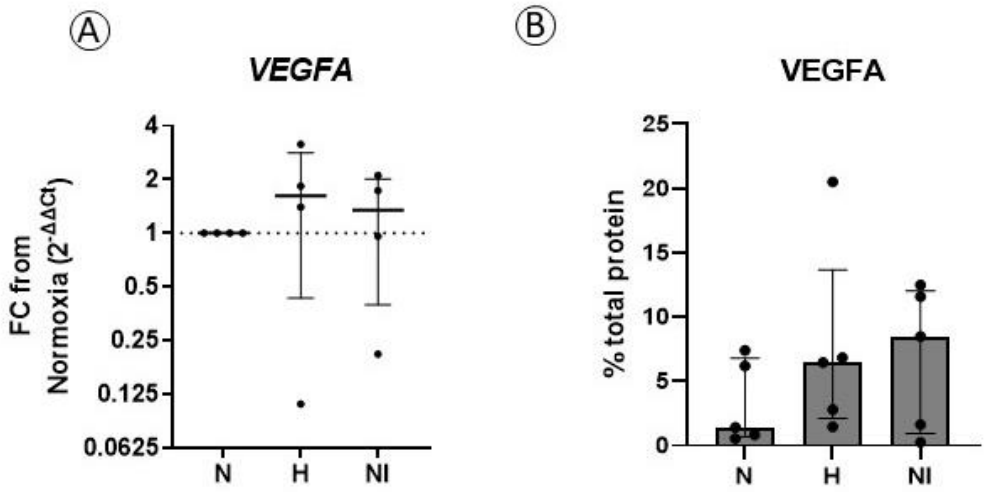

Figure 5.15 VEGFA expression in PCLS with IOX-2. PCLS were cultured normoxia (21% O_2, 5% CO_2) for 48 hours with 50 µM IOX-2. (A) RNA was extracted from 6 pooled PCLS and expression of vegfa was assessed by qPCR. Expression is displayed as $2^{-\Delta\Delta Ct}$ values, in comparison to expression in PCLS cultured without IOX-2. N=4. N vs NI p>0.9999. N vs H p=0.959. (B) Supernatants were also collected after 48 hours and VEGFA release was assessed by ELISA. VEGFA content is normalised to total protein content as measured by BCA assay. N=5. N vs NI p=0.4118. N vs H p=0.2277. Comparisons were made using a Friedman's test and Dunn's multiple comparison test. Data is expressed as median (±IQR). N: normoxia. NI: normoxia with 50 µM IOX-2. H: hypoxia.

Induction of *SLC2A1* expression was also assessed in IOX-2 treated AMs. Gene expression was consistently increased by IOX-2, although the increase did not reach statistical significance (Figure 5.16A). These preliminary results cannot confirm the activity of IOX-2 in stabilising HIF1α in this model.

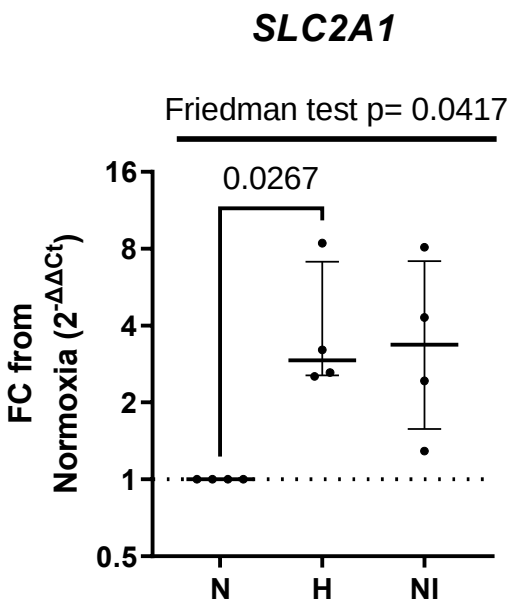

Figure 5.16 SLC2A1 expression in PCLS with IOX-2. PCLS were cultured normoxia (21% O_2, 5% CO_2, 37°C) for 48 hours with 50 µM IOX-2. RNA was extracted from 6 pooled PCLS and expression of SLC2A1 was assessed by qPCR. Expression is displayed as $2^{-\Delta\Delta Ct}$ values, in comparison to expression in PCLS cultured without IOX-2. N=5. N vs H p=0.0267, N vs NI p=0.1542. N vs H vs NI p=0.0417. Comparisons were made using a Friedman's test and Dunn's multiple comparison test. Data is expressed as median (±IQR). N: normoxia. NI: normoxia with 50 µM IOX-2. H: hypoxia.

5.3.8 PCLS response to IOX

Profibrotic markers collagen I and αSMA were assessed in PCLS exposed to IOX-2, to assess the potential of HIF1α to drive fibrosis in the model. No changes in *Col1a1* expression were detected in response to IOX-2 (Figure 5.17A). Although there was no difference in collagen I protein following normalisation to Actin B, collagen I was increased following normalisation to the housekeeper composite (p=0.04) (Figure 5.17B-D). *Acta2* expression was not changed by IOX-2 treatment (Figure 5.18A). The corresponding αSMA protein was not changed relative to actin B protein levels or the housekeeper composite (Figure 5.18B-D).

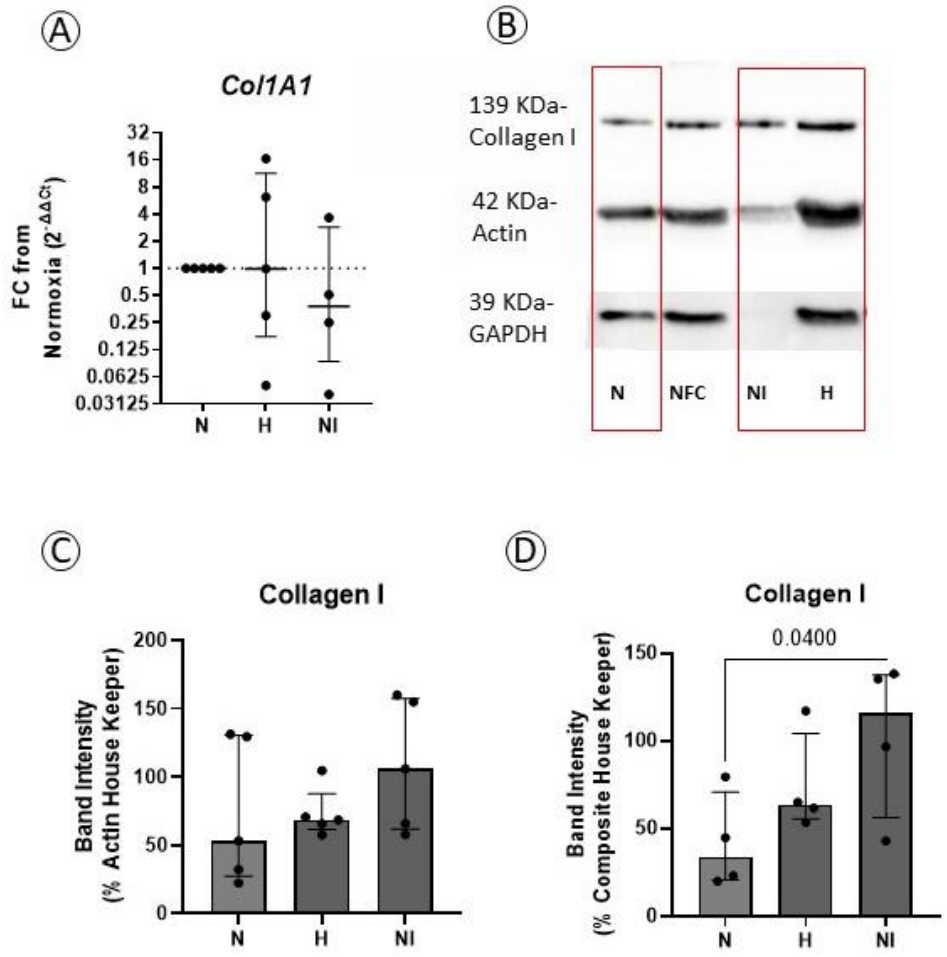

Figure 5.17 Collagen 1 in PCLS with IOX-2. PCLS were cultured for 48 hours in normoxia (21% O_2, 5% CO_2), with or without IOX-2, or in hypoxia (1% O_2, 5% CO_2). (A) RNA was extracted from 6 pooled PCLS and expression of Col1A1 was assessed by qPCR. Expression is displayed as $2^{-\Delta\Delta Ct}$ values, in comparison to expression in untreated PCLS cultured in normoxia. N=4. N vs NI p= 0.3146. N vs H p=0.959. Protein was extracted from 6 pooled PCLS and expression of Collagen I was assessed by western blotting. Representative blot shown from one sample (B). The same representative blot is used across several figures in this chapter. Expression was normalised as a percentage of (C) actin B (N=5) and (D) housekeeper composite (N=4) loading controls. Actin loading control: N vs NI p=0.3415, N vs H p>0.9999, NI vs H p=0.6177. Housekeeping composite loading control: N vs NI p=0.04, N vs H p=0.2313, NI vs H p>0.9999. Comparisons were made using a Friedman's test and Dunn's multiple comparison test. Data is presented as median (±IQR). N: normoxia. NI: normoxia with 50 µM IOX-2. H: hypoxia.

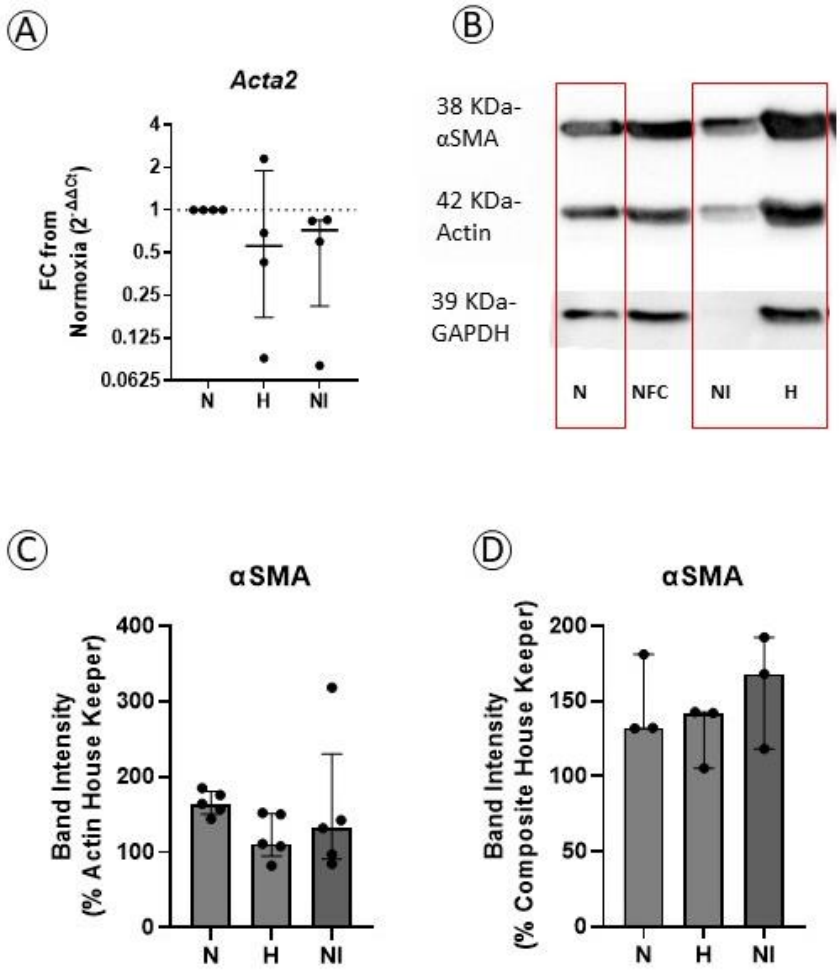

Figure 5.18 αSMA in PCLS with IOX-2. PCLS were cultured for 48 hours in normoxia (21% O_2, 5% CO_2), with or without IOX-2, or in hypoxia (1% O_2, 5% CO_2). (A) RNA was extracted from 6 pooled PCLS and expression of Acta2 was assessed by qPCR. Expression is displayed as $2^{-\Delta\Delta Ct}$ values, in comparison to expression in untreated PCLS cultured in normoxia. N=4. N vs NI p=0.1543, N vs H p= 0.3146. Protein was extracted from 6 pooled PCLS and expression of αSMA was assessed by western blotting. Representative blot shown from one sample (B). The same representative blot is used across several figures in this chapter. Expression was normalised as a percentage of (C) actin B (N=5) and (D) housekeeper composite (N=3) loading controls. Actin loading control: N vs NI p=0.0.6177, N vs H p=0.3415, NI vs H p>0.9999. Housekeeping composite loading control: N vs NI p>0.9999, N vs H p>0.9999, NI vs H p>0.9999. Comparisons were made using a Friedman's test and Dunn's multiple comparison test. Data is presented as median (±IQR). N: normoxia. NI: normoxia with 50 µM IOX-2. H: hypoxia.

5.3.9 Validation of PX-478 and KC7F2

HIF1α inhibitors PX-478 and KC7F2 were subsequently introduced for HIF1α inhibition in hypoxia. The feasibility of a 5 or 10 µM dose of PX-478 for 48 hours in hypoxia was determined

by measuring LDH release following treatment (Figure 5.19). There was no change in LDH release in response to either dose. Similarly, the feasibility of a 20 or 40 µM dose of KC7F2 was assessed by measuring LDH secretion over 48 hours (Figure 5.20). There was no difference detected with either dose, although LDH responses were more variable following treatment with the inhibitor at both concentrations.

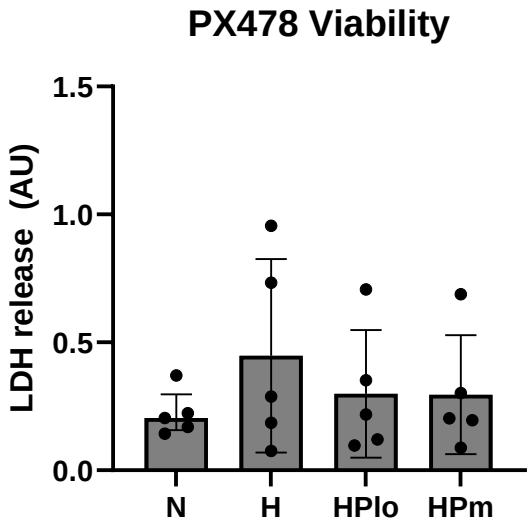

Figure 5.19 LDH release by PCLS treated with PX-478. *PCLS were cultured in normoxia (21% O_2, 5% CO_2) or hypoxia (1% O_2, 5% CO_2) with or without 5 or 10 µM PX-478 (Plo and Pm respectively) for 48 hours. Media was collected after 48 hours for LDH measurement. LDH release was averaged across 3 PCLS. N=5. N vs H p>0.9999. N vs HPlo p>0.9999. N vs HPm p>0.9999. Comparisons were made using a Friedman's test and Dunn's multiple comparison test Data is expressed as median (±IQR). N: normoxia. H: hypoxia. HPlo: hypoxia with 5 µM PX-478. HPm: hypoxia with 10 µM PX-478.*

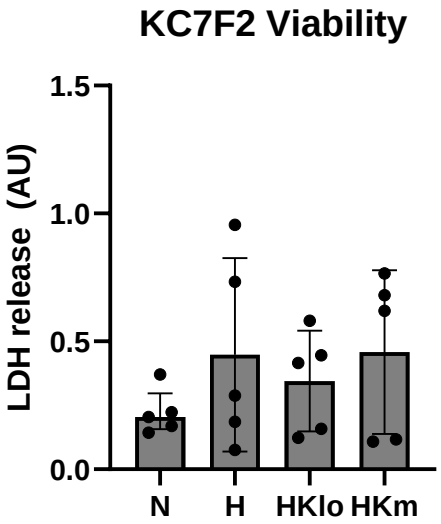

Figure 5.20 LDH release by PCLS treated with KC7F2. *PCLS were cultured in normoxia (21% O_2, 5% CO_2) or hypoxia (1% O_2, 5% CO_2) with or without 20 or 40 µM KC7F2 (Klo and Km respectively) for 48 hours. Media was collected after 48 hours for LDH measurement. LDH release was averaged across 3 PCLS. N=5. N vs H p=0.8499. N vs HKlo p>0.9999. N vs HKm p>0.9999. Comparisons were made using a Friedman's test and Dunn's multiple comparison test Data is expressed as median (±IQR). . N: normoxia. H: hypoxia. HKlo: hypoxia with 20 µM KC7F2. HKm: hypoxia with 40 µM KC7F2.*

The efficacy of HIF1α inhibitors in inhibiting HIF1α mediated changes in gene expression was assessed using expression of key target genes. *VEGFA* expression was not reduced by either dose of PX-478 (Figure 5.21A) and cumulative VEGFA secretion showed no change in the presence of PX-478 at both doses (Figure 5.21B). *SLC2A1* expression was also assessed with PX-478 treatment (Figure 5.22), although no decrease in expression was detected.

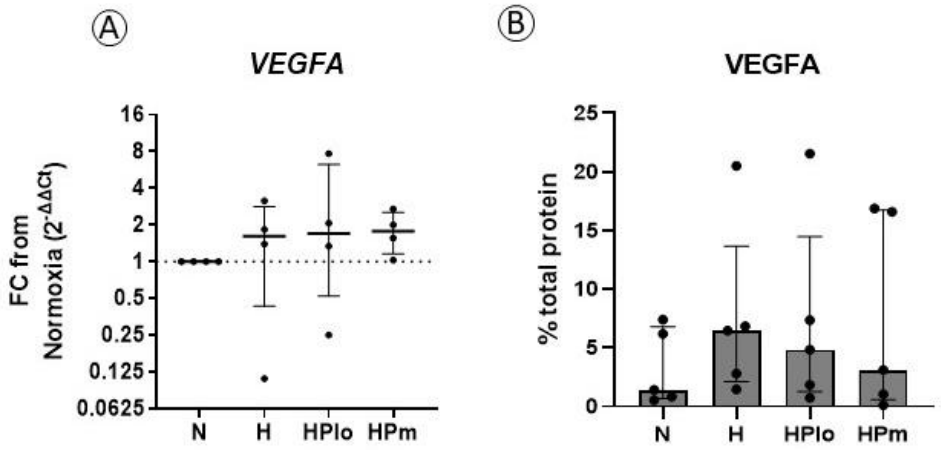

Figure 5.21 VEGFA expression in PCLS with PX-478. PCLS were cultured normoxia (21% O_2, 5% CO_2) or hypoxia (1% O_2, 5% CO_2) for 48 hours with 5 or 10 µM PX-478 (Plo and Pm respectively). (A) RNA was extracted from 6 pooled PCLS and expression of VEGFA was assessed by qPCR. Expression is displayed as $2^{-\Delta\Delta Ct}$ values, in comparison to expression in PCLS cultured in normoxia. N=4. N vs H p=0.82, N vs HPlo p=0.1657, N vs HPm p=0.5127. (B) Supernatants were also collected after 48 hours and VEGFA release was assessed by ELISA. VEGFA content is normalised to total protein content as measured by BCA assay. N=5. N vs H p=0.5185. H vs HPlo p>0.9999. H vs HPm p>0.9999. Comparisons were made using a Friedman's test and Dunn's multiple comparison test. Data is expressed as median (±IQR). N: normoxia. H: hypoxia. HPlo: hypoxia with 5 µM PX-478. HPm: hypoxia with 10 µM PX-478.

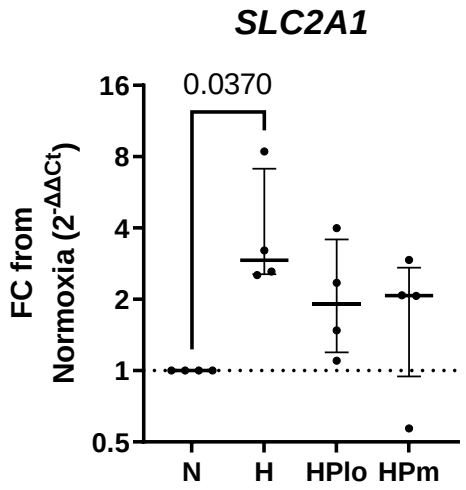

Figure 5.22 SLC2A1 expression in PCLS with PX-478. PCLS were cultured in normoxia (21% O_2, 5% CO_2) or hypoxia (1% O_2, 5% CO_2) for 48 hours with 5 or 10 µM PX-478 (Plo and Pm respectively). RNA was extracted from 6 pooled PCLS and expression of SLC2A1 was assessed by qPCR. Expression is displayed as $2^{-\Delta\Delta Ct}$ values, in comparison to expression in PCLS cultured in normoxia. N=4. N vs H p=0.0370, N vs HPlo p=0.3314, N vs Pm p>0.9999. Comparisons were made using a Friedman's test and Dunn's multiple comparison test. Data is expressed as median (±IQR). N: normoxia. H: hypoxia. HPlo: hypoxia with 5 µM PX-478. HPm: hypoxia with 10 µM PX-478.

Meanwhile, *VEGFA* expression was not changed by either dose of HIF1α inhibitor KC7F2 (Figure 5.23A). Nor was VEGFA protein secretion altered in the presence of the inhibitor (Figure 5.23B).

Similarly, *SLC2A1* expression was not reduced by either dose of KC7F2 (Figure 5.24).

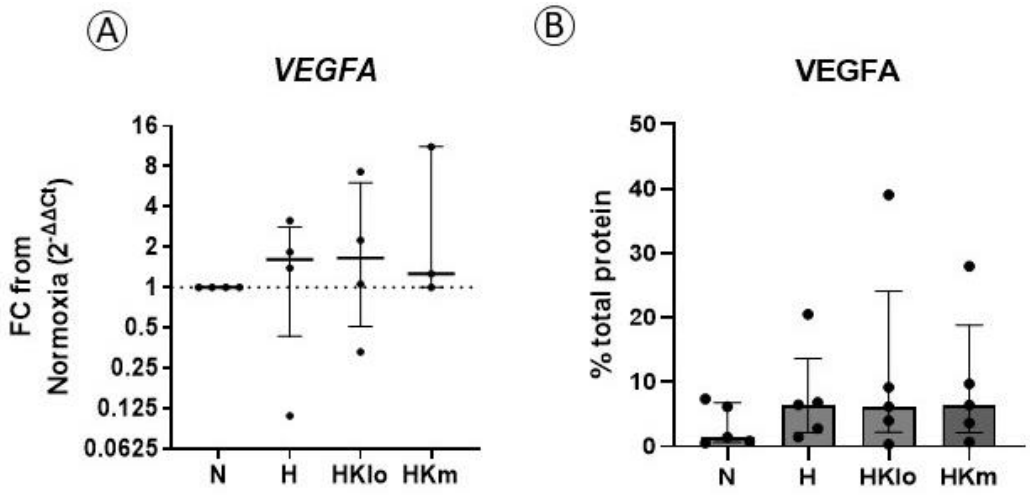

Figure 5.23 VEGFA expression in PCLS with KC7F2. PCLS were cultured for 48 hours in normoxia (21% O_2, 5% CO_2) or hypoxia (1% O_2, 5% CO_2) with 20 or 40 µM KC7F2 (Klo and Km respectively). (A) RNA was extracted from 6 pooled PCLS and expression of VEGFA was assessed by qPCR. Expression is displayed as $2^{-\Delta\Delta Ct}$ values, in comparison to expression in PCLS cultured in normoxia. N=4. N vs H p>0.9999, N vs HKlo p>0.9999, N vs HKm p>0.9999. (B) Supernatants were also collected after 48 hours and VEGFA release was assessed by ELISA. VEGFA content is normalised to total protein content as measured by BCA assay. N=5. . N vs H p>0.9999. H vs HKlo p>0.9999. H vs HKm p>0.9999. Comparisons were made using a Friedman's test and Dunn's multiple comparison test. N: normoxia. H: hypoxia. HKlo: hypoxia with 20 µM KC7F2. HKm: hypoxia with 40 µM KC7F2. Data is expressed as median (±IQR).

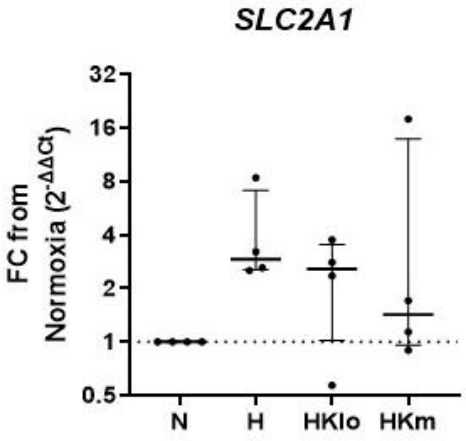

Figure 5.24 SLC2A1 expression in PCLS with KC7F2. PCLS were cultured normoxia (21% O_2, 5% CO_2) or hypoxia (1% O_2, 5% CO_2) for 48 hours with 20 or 40 µM KC7F2 (Klo and Km respectively). RNA was extracted from 6 pooled PCLS and expression of SLC2A1 was assessed by qPCR. Expression is displayed as $2^{-\Delta\Delta Ct}$ values, in comparison to expression in PCLS cultured in normoxia. N=4. N vs H p=0.1675, N vs HKlo p= 0.5127, N vs HKm p=0.82. Comparisons were made using a Friedman's test and Dunn's multiple comparison test. Data is expressed as median (±IQR). N: normoxia. H: hypoxia. HKlo: hypoxia with 20 µM KC7F2. HKm: hypoxia with 40 µM KC7F2.

5.3.10 PCLS response to HIF1α inhibitors

Profibrotic markers collagen I and αSMA were assessed in PCLS exposed to hypoxia with HIF1α inhibitors, to further explore the contribution of HIF1α signalling in hypoxia driven changes in PCLS. *Col1a1* expression was not changed by 5 or 10 µM PX-478 or 20 or 40 µM KC7F2 (Figure 5.25A). Meanwhile, collagen I protein levels did not change with inhibitor treatment following normalisation to actin B and the housekeeping composite (Figure 5.25C,D). *Acta2* expression was also not altered by either HIF1α inhibitor (Figure 5.26A). The corresponding αSMA protein was not changed relative to actin B protein levels or the housekeeper composite (Figure 5.26B-D).

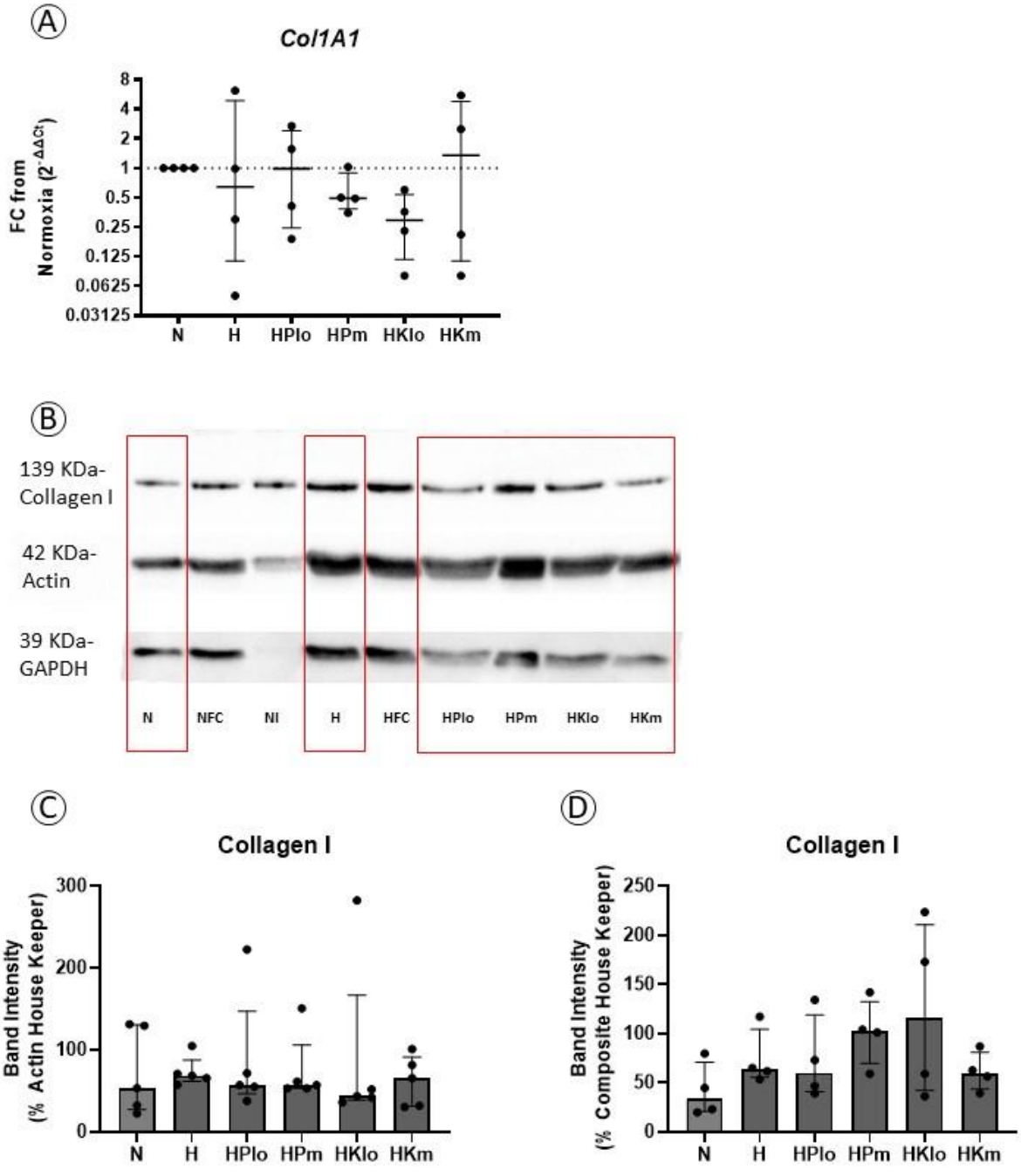

Figure 5.25 Collagen I in PCLS with HIF1α inhibitors. PCLS were cultured for 48 hours in normoxia (21% O_2, 5% CO_2) or hypoxia (1% O_2, 5% CO_2) with 5 or 10 µM PX-478 (Plo and Pm respectively) or 20 or 40 µM KC7F2 (Klo and Km respectively). (A) RNA was extracted from 6 pooled PCLS and expression of Col1A1 was assessed by qPCR. Expression is displayed as $2^{-\Delta\Delta Ct}$ values, in comparison to expression in untreated PCLS cultured in normoxia. N=4. N vs H p>0.9999, N vs HPlo p>0.9999, N vs HPm p>0.9999, N vs HKlo p= 0.2361, N vs HKm p>0.9999. Protein was extracted from 6 pooled PCLS and expression of Collagen I was assessed by western blotting. Representative blot shown from one sample (B). The same representative blot is used across several figures in this chapter. Expression was normalised as a percentage of (C) actin B (N=5)

and (D) housekeeper composite (N=4) loading controls. Actin loading controls: N vs H p>0.9999, H vs HPlo p>0.9999, H vs HPm p>0.9999, H vs HKlo p>0.9999, H vs HKm p>0.9999. Housekeeping composite loading controls: N vs H p=0.5645, H vs HPlo p>0.9999, H vs HPm p>0.9999, H vs HKlo p>0.9999, H vs HKm p>0.9999. Comparisons were made using a Friedman's test and Dunn's multiple comparison test. Data is presented as median (±IQR). N: normoxia. H: hypoxia. HPlo: hypoxia with 5 µM PX-478. HPm: hypoxia with 10 µM PX-478. HKlo: hypoxia with 20 µM KC7F2. HKm: hypoxia with 40 µM KC7F2.

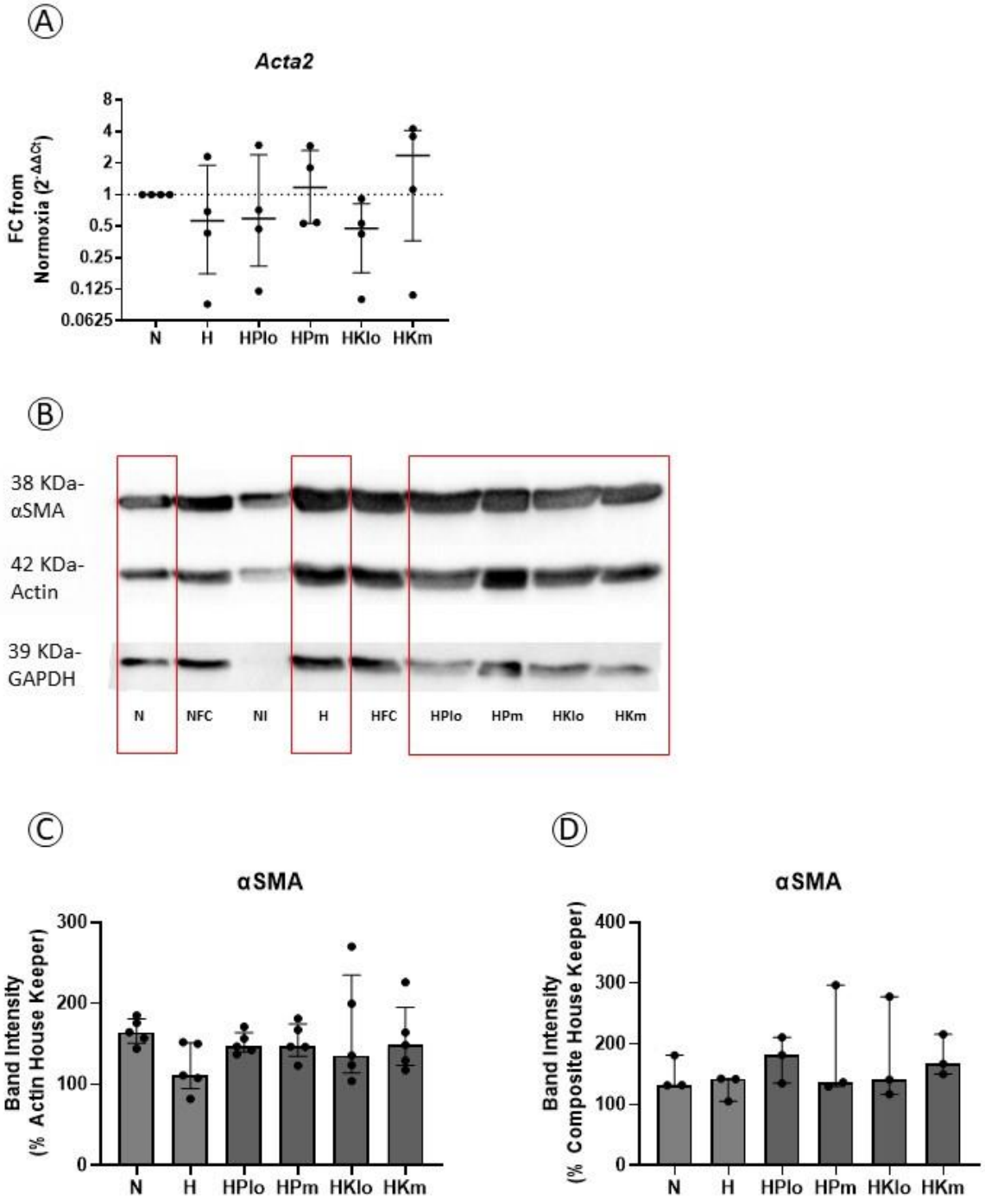

Figure 5.26 αSMA in PCLS with HIF1α inhibitors. PCLS were cultured for 48 hours in normoxia (21% O_2, 5% CO_2) or hypoxia (1% O_2, 5% CO_2) with 20 or 40 µM PX-478 (Plo and Pm respectively) or 20 or 40 µM KC7F2 (Klo and Km respectively). (A) RNA was extracted from 6 pooled PCLS and expression of ACTA2 was assessed by qPCR. Expression is displayed as $2^{-\Delta\Delta Ct}$ values, in comparison to expression in untreated PCLS cultured in normoxia. N=4. N vs H p>0.9999, N vs HPlo p>0.9999, N vs HPm p>0.9999, N vs HKlo p= 0.2939, N vs HKm p>0.9999. Protein was extracted from 6 pooled PCLS and expression of αSMA was assessed by western blotting. Representative blot shown from one sample (B). The same representative blot is used across

several figures in this chapter. Expression was normalised as a percentage of (C) actin B (N=5) and (D) housekeeper composite (N=3) loading controls. . Actin loading controls: N vs H p>0.9999, H vs HPlo p>0.9999, H vs HPm p>0.9999, H vs HKlo p>0.9999, H vs HKm p>0.9999. Housekeeping composite loading controls: N vs H p>0.9999, H vs HPlo p>0.9999, H vs HPm p>0.9999, H vs HKlo p>0.9999, H vs HKm p>0.9999. Comparisons were made using a Friedman's test and Dunn's multiple comparison test. Data is presented as median (±IQR). N: normoxia. H: hypoxia. HPlo: hypoxia with 5 µM PX-478. HPm: hypoxia with 10 µM PX-478. HKlo: hypoxia with 20 µM KC7F2. HKm: hypoxia with 40 µM KC7F2.

5.4 Discussion

This chapter aimed to validate a hypoxia exposure model for use with PCLS and characterise the associated HIF1α responses in the model. Further, this work explored whether the published profibrotic effects seen in single cell cultures were reflected in a PCLS model. To describe the mechanisms behind these changes, the chapter finally attempted to validate small molecule manipulations of HIF1α signalling and characterise their effects on fibrotic markers in PCLS.

5.4.1 Validation of PCLS model

To demonstrate that PCLS maintain integrity and viability over 5 days of culture, LDH content was used as a surrogate marker. LDH is released during cell death. As such, cellular LDH content can be compared to extracellular LDH, to track loss of viability in the PCLS model. LDH content was therefore measured in one slice every day for 7 days and expressed relative to the weight of the PCLS. As expected, LDH content gradually decreased over the 7-day period, reaching a significant decrease at day 6 and dropping most significantly at day 7. To demonstrate the reverse, supernatant LDH was measured every 2 days, and expressed cumulatively, as media was changed every 2 days. In this case, LDH release was averaged over 3 PCLS. In line with intracellular changes, extracellular LDH was released consistently over the 6-day period. Based

on this validation, PCLS were left to rest for 24 hours prior to use, to allow for cellular stress to decrease, and were used as soon as possible within that time, and not beyond 5 days.

5.4.2 Validation of Methods for qPCR and Western Blot Analysis

Continued analysis of PCLS responses to various stimuli were assessed in bulk, using western blotting to quantify gross protein changes and qPCR to quantify RNA changes. Replicates for qPCR analysis are limited due to the extensive time taken to optimise RNA extraction, which was hampered by agarose contamination during earlier repeats. Ultimately, trizol extraction of RNA was optimised by removing a standard heating step, to prevent agarose dissolving into isolated RNA during the final stages of processing.

Protein levels were also compared in bulk. Two normalisation methods were employed to account for variable protein loading, particularly necessary for protein isolated directly into laemmli buffer, as BCA protein normalisation could not be performed on these samples. Given the cellular diversity of the PCLS model, selecting an individual housekeeper unaffected by multiple stimuli was challenging. Furthermore, identifying a housekeeper totally unaffected by hypoxia, even in single cellular models, has been previously shown to be challenging (Caradec et al. 2010).

Firstly, actin B was used as a loading control protein. This protein is widely used across various fields for protein normalisations and was used in the initial characterisation of the profibrotic cocktail published by Alsafadi et al (2017), indicating that actin B levels change minimally during the establishment of early fibrosis in PCLS models. Although some studies have demonstrated that hypoxia modulates the actin B in the cytoskeleton, most indicate an effect on actin structure, rather than expression (Zieseniss 2014). However, some studies demonstrate

increased levels of actin B in response to hypoxia in specific cell types (Wang, Cheng and Zhu, 2021).

To increase confidence and reduce variability caused by using a single housekeeping gene, a housekeeping composite was derived based on Actin B and GAPDH levels. GAPDH is another widely used housekeeping gene, however in some tissues, including synovial fibroblasts, GAPDH expression is increased by activation of HIF1α (Del Rey et al. 2017). Further model specific optimisation of loading control proteins, or reliable measurement of total protein loading, using a technique such as Stain-Free technology (Gürtler et al. 2013), may form future work to increase the reliability and sensitivity of these western blots. However, given that the literature predicts a possible increase in both housekeeping genes in hypoxia, upregulation of proteins of interest relative to these genes can be assumed to be real, as these limitations would result in underestimation, rather than overestimation, of hypoxia driven increases in proteins of interest.

After initial validation of PCLS viability, the fibrotic cocktail previously published by Alfasadi et al (2017) was validated in our model. Consistent with previous findings over 5-day treatment, 48-hour treatment did not reduce viability in this study. Unfortunately, results did not detect changes in collagen I or αSMA at the RNA or protein level. Limited biological replication and a high level of variability, particularly in RNA expression changes, prevented detection of effects previously described using this treatment.

In comparison to previous use of this cocktail, these results are unsurprising. In the initial characterisation study (Alsafadi et al., 2017), *Col1A1* and *ACTA2* were increased by ~2-fold relative to untreated PCLS in 7 biological replicates. These established effects show a relatively

small increase in expression and would require further replication to be detected in this study. In line with the results of this study, αSMA protein levels were not changed during original characterisation. Although collagen I secretion was significantly increased with the cocktail during initial characterisation, collagen I levels within the PCLS was not measured, which may explain the disparate results shown here.

Overall, this data does not show that the effects of the fibrotic cocktail here were the same as in previous studies. Further replication particularly at the RNA level would be required to detect the early changes caused by the exposure, and measurement of additional markers including fibronectin and MMP-7 expression would be valuable, as these showed a higher magnitude response to the fibrotic cocktail. Imaging has been widely used to detect early changes induced by the cocktail in previous studies. This likely provides higher resolution than bulk protein and RNA assessment.

5.4.3 Establishment and Validation of Hypoxia Exposure Model in PCLS

Following initial validation of the PCLS model, a hypoxia challenge model in PCLS was established and validated. 48 hours hypoxia did not affect viability of PCLS when assessed by LDH release. HIF1α stabilisation could not be directly established in the PCLS following exposure, likely due to degradation of the protein in the brief normoxic period prior to PCLS dissociation. However, HIF1α response genes were assessed to confirm HIF1α signalling. Although an increase in *VEGFA* expression could not be detected, possibly due to high levels of variability and limited biological replication, or due to the 48-hour time point selected, there was a significant increase in VEGFA secretion over the 48-hour period ($p= 0.0430$). There was a trend towards increased expression of *SLC2A1*, encoding GLUT1, after 48 hours hypoxia

(p=0.0625). Despite a lack of significance, in combination with the significant increase in VEGFA secretion, this data supports the activation of HIF1α signalling in PCLS cultured in hypoxia.

Beyond their implications as HIF1α response genes, these genes likely play a role in the progression of IPF and are therefore pertinent when investigating the role of hypoxia in driving fibrosis in PCLS. As previously described, there are contrasting reports indicating that VEGFA levels are increased or decreased in IPF BAL (Barratt, Flower, et al., 2018). There is developing understanding of how differential VEGFA isoforms may have protective and pathological effects in lung fibrosis, with $VEGFA_{165b}$ increased in IPF tissue and therefore likely the pathological isoform (Barratt et al. 2017). Pulmonary fibroblasts have previously been shown to preferentially increase $VEGFA_{165a}$ (Barratt, Blythe, et al., 2018) in response to hypoxia, however the assays used here cannot distinguish between isoforms, which limits in depth interpretation of whether VEGFA released by PCLS in response to hypoxia has pathological potential.

Meanwhile, GLUT1 permits glucose uptake for glycolysis. GLUT1 levels are increased in IPF patient fibroblasts, compared to healthy controls (Z. Li et al., 2022), and increased in fibrotic areas of human IPF lung and bleomycin treated murine lungs (Andrianifahanana et al. 2016a). GLUT1 has been identified as integral in myofibroblast transition in fibroblasts in response to TGFβ (Andrianifahanana et al. 2016a) in the lung and in other fibrotic conditions (Henderson et al. 2020). Indeed, targeting the GLUT1 channel reduced bleomycin induced fibrosis in mice (Andrianifahanana et al., 2016a; Cho et al., 2017). This strongly implicates GLUT1 in facilitating glycolysis that drives pulmonary fibrosis, and therefore makes GLUT1 activation in PCLS in hypoxia an interesting potential mechanism in any profibrotic effects driven by the exposure.

5.4.4 Fibrotic Markers in Hypoxia

After establishing and characterising a hypoxia exposure model in PCLS, this chapter sought to probe whether the exposure induced profibrotic changes in PCLS. Therefore, the key markers of fibrosis collagen I and αSMA were assessed at the protein and RNA level. No consistent changes in αSMA were detected at the RNA or protein level. In contrast, although no change was detected in *Col1A1* gene expression in the small sample size examined, collagen I protein levels were increased relative to housekeeping composite controls. This result was not seen following normalisation to actin B alone. The improved power achieved using a housekeeping composite was likely due to reduced inter-sample variability following this method. Power calculations indicate that when using Actin B alone as a housekeeper gene, 18 replicates would be required to detect the effect size described here with sufficient power (SD = 17.09, α=0.05, power=0.8).

This data provides the first evidence that suggests that hypoxia has profibrotic effects in a PCLS model. This is particularly interesting as the profibrotic effects of the previously described fibrotic cocktail could not be detected with sufficient power in the same samples. This suggests that the magnitude of collagen I deposition induced by hypoxia may exceed that seen in the well-established model of early IPF in PCLS. The increased collagen I deposition seen here is in line with studies in human lung fibroblast monocultures, where collagen secretion was increased by hypoxia (Robinson et al. 2012).

5.4.5 Additive effects of hypoxia in early fibrosis

The hypothesis of this thesis proposed that hypoxia may act as an initiating factor in a subgroup of IPF patients, and as potentiating factor in other IPF patients as fibrosis develops. To

determine whether additive effects of hypoxia could be detected in a widely used model of early IPF in PCLS, PCLS were cultured with simultaneous fibrotic cocktail and hypoxia challenge. No additive effects could be seen in collagen I expression at the RNA or protein levels, further to the effects of hypoxia alone. Additionally, hypoxia and fibrotic cocktail treatment together had no additive effects on expression of *ACTA2* or αSMA protein expression. This preliminary evidence does not support the hypothesis that hypoxia exaggerates the effects of early fibrosis induced by the profibrotic cocktail, although further replication and investigation is required, particularly to demonstrate the efficacy of the fibrotic cocktail alone.

5.4.6 Pseudohypoxic Stabilisation of HIF1α by IOX-2

IOX-2 was previously used in this thesis, for the pseudohypoxic stabilisation of HIF1α in normoxic AMs. This allows the effects of HIF1α gene transcription programs to be studied in isolation from other hypoxia signalling pathways. Given that GLUT1 mediated glucose uptake and metabolism has shown to be of key relevance in fibrotic lung tissue and myofibroblast differentiation (Andrianifahanana et al., 2016; Cho et al., 2017), and this chapter has demonstrated the increased expression of this HIF1α response gene following hypoxia exposure in the PCLS model, the role of HIF1α in driving PCLS fibrosis was further characterised here.

PCLS LDH release was unchanged by IOX-2 treatment, indicating a lack of toxicity of the inhibitor. IOX-2 efficacy could not be determined by assessing HIF1α expression, and there was insufficient data to demonstrate changes in HIF1α response genes *SLC2A1* and VEGFA, although SLC2A1 expression was consistently increased in the presence of the inhibitor. This data does not demonstrate the efficacy of IOX-2 in inducing HIF1α responses in PCLS.

5.4.7 Effects of IOX-2 on PCLS fibrosis markers

To isolate the effects of HIF1α signalling alone in PCLS fibrotic cascades, the same markers of fibrosis were assessed following 48-hour treatment in normoxia. Neither *ACTA2* or *Col1A1* were significantly changed by IOX-2 treatment. Additionally, no changes were seen in αSMA protein levels. However, an increase in collagen I protein was demonstrated when normalised using housekeeper composite values. This difference was not evident following normalisation to actin B alone, which may be due to the reduced inter-sample variability achieved by using a composite value. This change is difficult to interpret in the absence of complete validation of IOX-2, however pending further replication of IOX-2 validation, demonstrating its efficacy, this may highlight a role for HIF1α in hypoxia associated collagen deposition in PCLS.

5.4.8 Preliminary HIF1α Inhibitor Validation

IOX-2 is a global PHD2 inhibitor, meaning it inhibits other PHD2 functions in normoxia. For example, PHD2 prevents activation of NFκB signalling in normoxia by degrading IKKβ and thereby preventing IκBα degradation and NFκB activation (D'ignazio and Rocha, 2016; Frost, Ciulli and Rocha, 2019). Additionally, PHD2 prevents eukaryotic elongation factor 2 kinase induced cell stress responses by degrading the elongation factor in normoxia (C. E. J. Moore et al. 2015). Therefore, further investigation would be required before concluding that hypoxia induced HIF1α activation is responsible for collagen deposition in PCLS in hypoxia. HIF1α inhibitors KC7F2 and PX-478 provide an opportunity for further analysis of the role of HIF1α in hypoxia induced fibrosis in PCLS. Validation of both inhibitors was performed. No adverse effects on viability were identified using PX-478 at 5 and 10 μM and KC7F2 20 and 40 μM, when assessed by LDH release.

The efficacy of the inhibitors in preventing HIF1α transcriptional responses was investigated alongside the assessment of effects on viability. The validation of these inhibitors is largely negative and relies upon low numbers to detect changes due to sample restraints. PX-478 did not alter *VEGFA* expression or VEGF protein secretion, and no effect was detected on *SLC2A1* expression. Similarly, KC7F2 had no impact on VEGFA RNA or protein, and changes in *SLC2A1* expression were not detected. This early validation begins to characterise the use of these inhibitors in a human PCLS model and indicates that they may not be efficacious. However, further work is required to confirm this, particularly as the expected effect size may be small.

5.4.9 Preliminary Effects of HIF1α inhibitors on Fibrotic Markers in PCLS

Alongside on-going validation of HIF1α inhibitors, their effects on PCLS fibrosis was assessed. Again, the inhibitors showed largely negative results. Expression of *Col1a1* and *ACTA2* was unchanged by either inhibitor. Collagen and αSMA protein levels were also unchanged by PX-478 and KC7F2. These results require extensive replication alongside further validation described above. Overall, these results provide no additional support for the role of HIF1α in increased collagen deposition caused by hypoxia.

5.4.10 HIF1α Dependent Mechanisms

Although this data highlights a possible role for HIF1α in the increased collagen deposition seen in PCLS in hypoxia, the specific HIF1α response genes responsible for activating increased collagen synthesis remain unknown. As previously described, increased GLUT1 has been linked to the fibrotic cascade in lung tissue (Andrianifahanana et al. 2016a; S. J. Cho et al. 2017). Associated changes to glucose metabolism and increased glycolysis have also been highlighted in IPF fibroblasts and IPF tissue, particularly within the fibrotic foci (Xie et al., 2015; Hamanaka

et al., 2021; J. Li et al., 2022). Increased lactate in IPF BAL (Kottmann et al. 2012) and BAL from bleomycin treated mice (Cui et al., 2021a) also indicates that this glycolysis is often anaerobic. This is a metabolic switch largely controlled by HIF1α activation. Previous studies have indicated that increased glycolysis seen in IPF fibroblasts facilitates their highly synthetic nature, not only by providing ATP, but also as a source of biosynthetic intermediates for ECM output and proliferation (Xie et al. 2015). Indeed, inhibition of key glycolytic enzymes can prevent escalation of fibrotic markers in IPF fibroblasts and bleomycin treated mice (Xie et al., 2015; Chen et al., 2021), whilst blocking natural inhibitors of glycolysis has the capacity to drive lung fibrosis (Lai et al. 2023). For example, HIF1α response gene PDK1 is upregulated in hypoxia to increase glycolysis and decrease mitochondrial respiration. Inhibition of this gene in murine bleomycin induced fibrosis reversed fibrotic progression (Goodwin et al. 2018).

Beyond the synthetic capacity permitted by excessive glycolysis, lactate, the by-product of glycolysis produced most abundantly by anaerobic glycolysis, is thought to form part of a positive feedback loop in in lung fibrosis. Lactate produced by glycolytic and synthetic fibroblasts can activate ECM bound TGF-ß (Tuder, Lara and Thannickal, 2012), further driving the fibrotic environment, and thereby increasing lactate secretion. Lactate transporter inhibitors have been employed to modulate murine models of IPF, due to their role in facilitating continued glycolysis (Ziehr et al. 2022), increasing the evidence of a role for lactate in the disease. On top of its roles in TGF-β activation and glycolytic reprogramming in stromal cells, crosstalk between lactate releasing fibroblasts and AMs has been implicated in driving profibrotic phenotype in lung macrophages, via histone lactylation at profibrotic genes (Cui et al., 2021a).

The mechanisms proposed above have been demonstrated in murine models and human single cell cultures. To prove that hypoxia triggers anaerobic glycolysis in PCLS and to probe whether this shift drives increased collagen output, further work is required. Firstly, metabolic studies would be required to demonstrate lactate release via anaerobic glycolysis. Beyond this, inhibition of glycolytic enzymes and lactate transport channels would be valuable to identify whether these changes facilitate increased collagen output. Spatial tissue analysis would enrich this data, providing higher resolution information to determine which cellular populations employ anaerobic glycolysis, and identify whether these glycolytic cells are directly responsible for collagen output, or whether release of mediators such as lactate trigger further fibrosis in a paracrine way.

5.4.11 HIF1α independent mechanisms

Given the overlapping nature of hypoxia responses and their cell specific nature, it is likely that HIF1α independent responses also contribute to any profibrotic effects of hypoxia in the PCLS model. For example, Robinson et al (2012) explored the mechanism behind increased collagen deposition in hypoxia exposed fibroblasts and showed that global DNA hypermethylation, including hypermethylation of the promoter of the Thy1 gene resulting in reduced Thy1 expression, which has previously been implicated in myofibroblast differentiation. DNA hypermethylation is widely reported in hypoxia, particularly in tumour associated hypoxia (Batie and Rocha 2020). It is widely believed to be mediated by ten-eleven translocation (TET) enzymes, which act in a HIF1α independent way (Thienpont et al. 2016).

Additional HIF1α independent mechanisms with the potential to contribute to profibrotic changes include HIF2α induced changes. HIF2α is likely to play a role following this exposure,

as HIF2α has been shown to predominate over HIF1α when hypoxia lasts beyond 24 hours (Torres-Soria et al. 2022). HIF2α has previously been shown to increase IPF fibroblast proliferation in hypoxia by increasing expression of hypoxamir miR210, which is increased in IPF patient tissue (Bodempudi et al. 2014). The hypoxamir represses MNT function, allowing cMyc activation, which drives cellular proliferation. HIF2α also increases nuclear factor of activated T-cells (NFAT) levels to drive fibroblast proliferation in hypoxia. HIF2α mediated responses warrant further analysis and may be probed using HIF2α inhibitor TCS7009 (Scheuermann et al. 2013), alongside analysis of miR210 expression, which is modulated by both HIF1α and HIF2α stabilisation.

5.4.12 Limitations

5.4.12.1 Limitation of the PCLS model

The PCLS model provides insight into human cell-cell interactions, which are unparalleled by single cells cultures. However, there are some limitations of the model that must still be considered. PCLS cut here are derived from lung tissue taken from various anatomical locations, depending on surgical requirements. The orientation of the tissue during coring and slicing also varies, as it is not possible to assess internal structures prior to processing. Therefore, PCLS have variable cellular composition and orientation within and between patients. This variation is accounted for within samples by pooling PCLS for protein and RNA, and pooling supernatants for assessment. However, some inevitable variation likely remains between patient samples.

Variability between patient samples is compounded by the inclusion of patients who quit smoking at least 4 years ago, alongside never smokers. The consequences of smoking history on PCLS function are incompletely characterised, however, it can be assumed that PCLS derived

from these patients retain changes induced by this smoking history, similar to the changes previously demonstrated in epithelial cells, fibroblasts and macrophages depending on smoking history (Spira et al., 2004; D'Anna et al., 2015; Lugg et al., 2022). To achieve sufficient recruitment, this work could not be limited to never smokers.

An integral environmental factor in lung tissue is the presence of oxygen across a gradient from alveoli to tissue. This gradient cannot be replicated when PCLS are submerged in culture media, meaning that alveolar epithelial cells are not oriented towards air, as they would be in physiology, or in models like air liquid interface cultures. Therefore, it is important to use this model in combination with ALI models and even animal models to account for this difference, particularly when in testing interventions that differentially target cells via uptake through circulation or inhalation.

Beyond this, PCLS retain some agarose contaminant, which is evident during protein and RNA extraction. The effect of this is unclear, however agarose may inhibit diffusion of soluble mediators or cell migration, preventing physiologically relevant cellular interactions. Agarose also interfered with extraction of high-quality RNA in this study. Some studies have proposed culturing PCLS in a shaking incubator with regular media changes for the first 3 hours, to encourage the agarose to dissolve and dissipate (Tigges et al. 2021). A lower agarose concentration is typically used for murine PCLS (Tigges et al. 2021). Although harder to work with when slicing, the lower percentage may facilitate better agarose dissipation during culture.

PCLS retain much of the cellular integrity of the lung tissue, however the model lacks circulation of immune cells. Therefore, the role of invading immune cells in hypoxic tissue cannot be assessed here. More complex co-culture systems could probe these relationships in further

studies (Hofmann et al. 2015). Similarly, the effects of stretch, which has been demonstrated to play a role in fibroblast phenotype and TGF-ß activation (Froese et al., 2016; D'Urso and Kurniawan, 2020), cannot be assessed by this model. Various groups developed models to recreate stretch in PCLS to model this factor (Dassow et al., 2010; Davidovich, Huang and Margulies, 2013). An interesting technique that may be used alongside PCLS to explore the hypotheses in this thesis in future is a recently published chip-based model of the lung, that models cyclic stretch and intermittent hypoxia (Campillo et al. 2016). Although initial publication demonstrated the effect of hypoxia and stretch on murine mesenchymal stem cells only, this technology could be developed for the exposure of complex co cultures, or even PCLS in future, providing a cutting edge and modifiable model of human lung tissue.

5.4.12.2 Limitations of Work Presented Here

The work presented in this chapter is hampered by low sample numbers. Lung tissue sections yield between 20-80 PCLS, and protein and RNA extraction require 6 PCLS per condition. Particularly when protein and RNA were extracted separately, using Laemmli buffer protein extraction in an attempt to stabilise HIF1α, the conditions that could be compared per sample were limited. This was compounded by the difficulties in isolating RNA from these PCLS, resulting in limited numbers particularly in RNA samples and work with HIF1α manipulations.

Some of the limitations outlined here, including the indiscriminate anatomical sources of PCLS and the inclusion of patients who quit smoking at least 4 years prior to surgery, contribute to high levels of variability in this model. Although this study reduced intra-sample variability by pooling multiple PCLS or supernatants for each condition, inter-sample variability remains, and is evident in some of the results described here. For example, RNA expression changes are

variable, even in response to the well characterised fibrotic cocktail that has been published elsewhere. The value of the PCLS model outweighs these limitations, however, to overcome variability, higher power is required to detect changes.

Whilst individual tests do not reach statistical significance in most areas of this chapter, testing multiple markers in the same pathway, at the RNA and protein level, helps to improve confidence in the results detected. For example, although the characterisation of HIF1α response to hypoxia and IOX-2 requires biological replication to reach statistical significance, trends across 2 HIF1α response genes improve confidence that HIF1α responses are proceeding as expected.

This work would benefit from measurement of fibrosis markers beyond collagen I and αSMA. Although these are key markers of ECM deposition and myofibroblast differentiation, these proteins cannot summarise fibrosis in its entirety. This is particularly evident in the initial characterisation of the profibrotic cocktail published by Alsafadi et al (2017). Although expression of the genes for collagen I and αSMA were significantly increased after 48-hours in the original study, only changes in collagen I expression translated into increased secretion. Contrastingly, αSMA protein was not increased by the fibrotic cocktail, with the authors hypothesising that it would take further time for the development of sufficiently stiff ECM for induction of αSMA at the protein level (Alsafadi et al., 2017). Other markers associated with IPF, including fibronectin and MMP-7, did show increases after 48 hours fibrotic cocktail treatment, while markers associated with epithelial health, including E-cadherin and surfactant protein C, were reduced after the treatment (Alsafadi et al., 2017). Given the similar time frames employed in this study for hypoxic challenge, these markers would be good candidate

targets for more complete characterisation of the fibrotic response of PCLS to hypoxia. MMP-7 would be of particular interest, given the identification of increased AM MMP-7 following hypoxic challenge in Chapter 3, as well as the predictive nature of BAL MMP-7 in IPF disease progression (Bauer et al. 2017) and the association demonstrated between OSA severity in IPF patients and serum MMP-7 levels (Gille et al., 2017a).

The assessment of PCLS described here relies on bulk assessment of protein and RNA, as well as secretion profiles. Although this provides preliminary information on the hypothesis, higher resolution data is needed to place these changes into context. Spatial analysis would be a valuable addition to this work, providing insight into the cellular make up of PCLS at baseline and the cell types or relationships implicated in fibrotic changes. This can be achieved using paraffin embedding of PCLS for imaging and could be developed for high resolution analysis using multiplexing techniques for RNA and protein analysis (Alsafadi et al. 2017). Alternatively, two-photon imaging has been used for live PCLS imaging. This technique has been used widely for assessment of PCLS viability at a cellular level, to extend assessment of viability by LDH secretion (Neuhaus et al., 2017; Akram et al., 2019). The benefit of this technique lies in its ability to differentiate the viability of different cell types over time, which LDH release alone does not detect. Beyond use in confirming PCLS viability, this technique can be used to track migrating cells within the PCLS model (Hoang et al., 2012; Lyons-Cohen et al., 2018).

Current data in the PCLS model is impossible to link back to AM responses to hypoxia identified in previous chapters, as results identify global changes in expression. The spatial analysis described above would firstly confirm the presence and location of AMs within the PCLS model. Furthermore, changes in AM characteristics when seeded within the PCLS may be compared to

changes seen in AM monocultures. In particular, as described above, MMP-7 is increased by the fibrotic cocktail in PCLS (Alsafadi et al. 2017). The role of AMs in this change, and the ability of hypoxia to recapitulate this change in PCLS, would connect the results of this thesis.

5.5 Conclusion

This chapter established and validated a hypoxia exposure model for human PCLS. HIF1α responses were confirmed in this model after 48-hour treatment. The profibrotic effects of hypoxia were measured at the RNA and protein level, demonstrating increased collagen I content in hypoxia treated PCLS at the protein level, but no change in αSMA levels. There were no additive effects of a previously published profibrotic cocktail on these markers of fibrosis in hypoxia.

HIF1α stabilisation by IOX-2 could not be proven here, however IOX-2 resulted in increased collagen I output in these PCLS. This raises the possibility that collagen deposition is HIF1α driven, although further validation of IOX-2 effects in PCLS are required to confirm this mechanism. Although this chapter also began validation of HIF1α inhibitors, data was insufficient to further corroborate the role of HIF1α in hypoxic responses.

The value of this work lies in modelling complex cell-cell interactions, which gives PCLS the potential to predict mechanisms driving fibrosis more accurately in the human lung, by more closely modelling the complexity of the fibrotic environment. Further work should extend characterisation of PCLS in hypoxia and develop analysis of the effects of HIF1α activity. Additionally, characterisation HIF1α dependent glycolytic responses in PCLS would be valuable, as this is a possible driver of the fibrotic changes.

CHAPTER 6: GENERAL DISCUSSION

6.1 OVERVIEW

This thesis aimed to characterise the contribution of tissue hypoxia to initiation or potentiation of fibrosis in IPF. Results found in AMs and PCLS are summarised in Table 6.1 and Table 6.2 respectively. The potential effects of the results summarised here are annotated on Figure 6.1.

Marker	RNA	Protein	N		
HIF1α	↓?	↑	10, 6		
VEGFA	↑	↑	10, 15		
GLUT1	↑		9		
CD80		-	5		
CD206		-	5		
CD163		-	5		
SIRPα		-	3		
MMP-7	-	↑	8, 15		
MMP-1	-	↑?	8, 14		
MMP-9	-		6		
TGFβ	-		6		
Collagen I	-		6		
Function	Hypoxia	N	IOX-2	N	
Phagocytosis	-	14	↑?	7	
Efferocytosis	↓	15	-	9	

Table 6.1 Table summarising the effects of 48-hour hypoxia on AMs. ↑ *indicates an increase in expression or function,* ↓ *indicates a decrease in expression or function, ? indicates a trend (p<0.1) that did not reach statistical significance, - indicates no change in expression or function. N indicates the number of biological replicates. HIF1α: hypoxia inducible factor 1a, VEGFA: vascular endothelial growth factor A, GLUT1: glucose transporter protein type 1, CD: cluster of differentiation, SIRPα: signal regulatory protein a, MMP: matrix metalloproteinase, TGFβ: transforming growth factor B.*

	Hypoxia			IOX-2		
	RNA	Protein	N	RNA	Protein	N
VEGFA	-	↑	5, 9	-	-	4, 5
GLUT1	↑?		5	-		4
Collagen I	-	↑?	5, 10	-	↑?	4, 4
αSMA	-	-	5, 10	-	-	4, 5

Table 6.2 Table summarising the effects of 48-hour hypoxia on PCLS. ↑ *indicates an increase in expression or function,* ↓ *indicates a decrease in expression or function, ? indicates a trend (p<0.1) that did not reach statistical significance, or a result that reached statistical significance in some, but not all, analysis, - indicates no change in expression or function. N indicates the number of biological replicates. VEGFA: vascular endothelial growth factor A, GLUT1: glucose transporter protein type 1. αSMA: α smooth muscle actin.*

Firstly, Chapter 3 aimed to identify the effects of hypoxia on AM phenotype and function, using human lung tissue to maximise the relevance of this exploration to human disease. This analysis found that exposure to 1% O_2 for 48 hours did not alter AM surface marker expression, or the expression of key factors implicated in the role of AMs in lung fibrosis, including TGF-ß, MMP-9 and collagen 1. However, hypoxia did increase release of MMP-7 and there was a trend towards increased release of MMP-1, although no changes in RNA of either proteinase were detected. Both MMP-1 and MMP-7 are key proteinases implicated in tissue damage during the escalation of IPF (Henry et al., 2002; McKeown et al., 2009; Bauer et al., 2017). Beyond this hypoxia impaired efferocytosis of apoptotic neutrophils but had no effect on phagocytosis of heat killed *Streptococcus pneumoniae*. Efferocytosis is a key function involved in efficient wound healing. An increase in apoptotic cells in BAL of IPF patients provides evidence for a possible reduction of efferocytosis in IPF (Morimoto, Janssen and Terada, 2012). The specific impairment of efferocytosis but not phagocytosis could not be explained by changes in surface marker expression in hypoxia, as no change in expression of efferocytic receptors CD163 and

CD206, and anti-efferocytic receptor SIRPα in hypoxia were detected. The mechanism differentiating the two functions therefore remained undetermined.

Chapter 4 progressed this work, aiming to dissect the role of HIF1α in reducing efferocytosis in hypoxia. To this end, efferocytosis was measured in the presence of inhibitors for HIF1α stabilisation in normoxia and HIF1α inhibition in hypoxia. Whilst inhibitors were validated using HIF1α response gene expression, the use of these inhibitors was hampered by low biological repetition. Despite these limitations, preliminary results show no role for IOX-2-mediated HIF1α stabilisation in impairing efferocytosis. Contrastingly, IOX-2 stabilisation of HIF1α resulted in a trend towards increased phagocytosis, suggesting that HIF1α activation has a differential role in the two processes. Chapter 4 also began to dissect how AMs utilise glycolysis in normoxia and hypoxia, using lactate as a surrogate marker. AMs markedly increased lactate release in hypoxia compared to normoxia, indicating that unstimulated AMs utilise glycolysis in hypoxia. In normoxia AMs increased glycolysis in response to a high dose of LPS, however, in hypoxia and LPS did not have additive effects on lactate release. Although this suggests that AMs are close to their glycolytic capacity in hypoxia, further real time analysis would be required to confirm this and to assess how glycolysis is employed in AM efferocytosis in normoxia and hypoxia.

Chapter 5 utilised human lung tissue to derive PCLS for further characterisation of the role of hypoxia in lung fibrosis. A previously published profibrotic cocktail for the modelling of early IPF disease was tested, however changes in collagen I and αSMA expression after 48-hour treatment could not be detected in our model. Hypoxic exposure in PCLS was also established and validated, with associated HIF1α responses demonstrated. Preliminary work validated IOX-

2 treatment of PCLS, although HIF1α responses could not be confirmed. Finally, fibrosis markers collagen 1 and αSMA were assessed in PCLS following hypoxia or IOX-2 treatment. While genes of interest showed no difference in expression, this work was limited by low numbers and high variability. By contrast, western blotting demonstrated that the amount of collagen I protein within the PCLS was increased by hypoxic challenge, following normalisation to a housekeeping compositive value. Collagen I protein was also increased relative to the housekeeping composite value by IOX-2, indicating that HIF1α may play a role in this change. However, further validation of the inhibitor effects would be required to confirm this. These results indicate potential profibrotic effects of hypoxia for the first time in a human PCLS model of the lung.

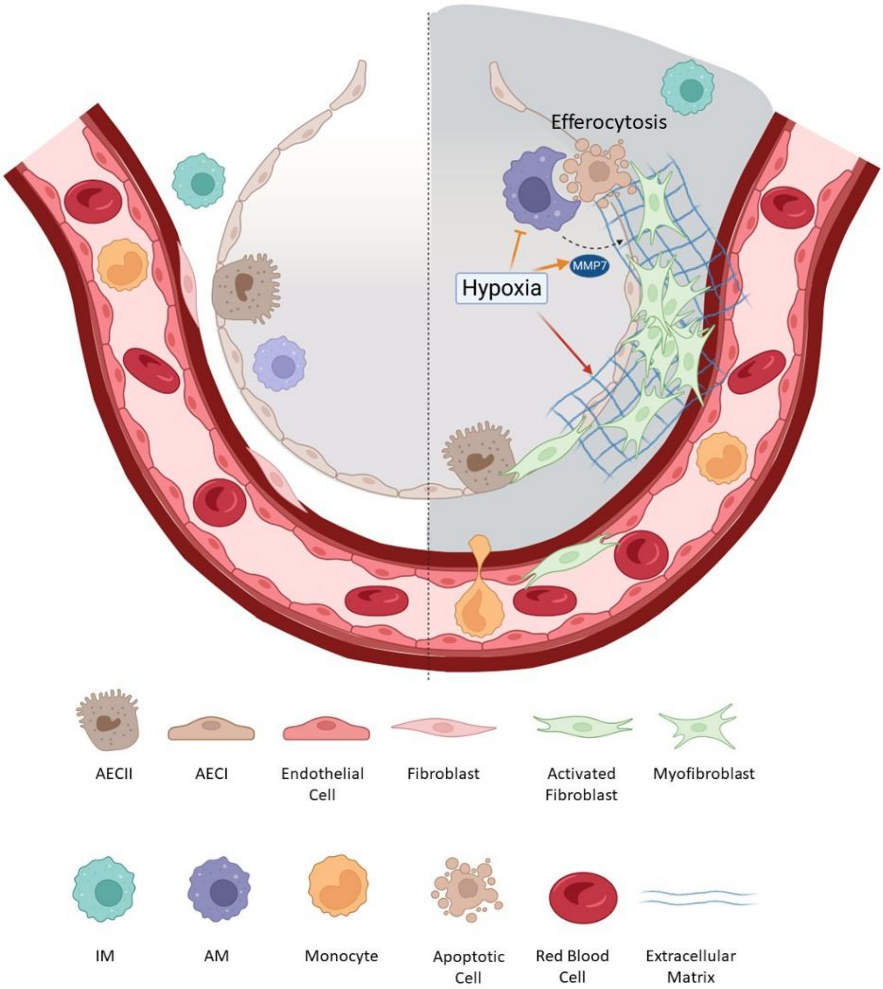

Figure 6.1 The effects of hypoxia in relation to the proposed model of aberrant wound healing response in IPF. *A cross sectional diagram of an alveoli, with adjacent capillary. LEFT side shows the alveoli during homeostasis. AECIs line the alveoli, with occasional AECIIs for surfactant secretion. Alveolar macrophages patrol the airspaces, while interstitial macrophages are resident in the parenchyma beneath the epithelial barrier. The parenchyma is made up of stromal cells, including fibroblasts. RIGHT side shows the proposed mechanism by which IPF escalates. Epithelial cells undergo frequent apoptosis, due to repeated microinjuries. Inefficient reepithelialisation, insufficient apoptotic cell clearance and inappropriate cellular signalling causes continued tissue damage and membrane denudation. Fibroblasts become activated and some differentiate into contractile myofibroblasts. Epithelial cells and endothelial cells undergo transdifferentiation into fibroblasts. This response generates excessive extracellular matrix, particularly at fibrotic foci, resulting in impaired gas exchange and loss of lung function. The effects of hypoxia on AMs are annotated using orange arrows. Hypoxia impairs AM efferocytosis, which would contribute to the build-up of apoptotic cells in the alveolar space within the lung tissue. Furthermore, hypoxia increases MMP-7 output, which would likely increase tissue damage in the lung during hypoxia. The effects of hypoxia on PCLS are annotated using red arrows. Hypoxia causes increased collagen I protein deposition in PCLS. EMT: epithelial mesenchymal transition. EndMT: endothelial mesenchymal transition. AEC: alveolar epithelial cell. IM: interstitial macrophage. AM: alveolar macrophage. MMP-7: matrix metalloproteinase 7.*

6.2 IMPLICATIONS FOR THE FIELD

Overall, this work builds on evidence in the field that explores how hypoxia contributes to lung fibrosis. The value and novelty of the work lies in the use of human lung tissue to derive models of human AMs and the complex cellular interactions represented by PCLS.

6.2.1 AMs

The value of using human AMs lies in the unique and incompletely understood characteristics of AMs, which cannot be recapitulated using cells differentiated *in vitro*. AMs express a combination of markers typical of proinflammatory and pro-resolution macrophages, which are not expressed by monocytes differentiated *in vitro* (Hussell and Bell 2014; Mitsi et al. 2018). Additionally, AM metabolism is differentiated from monocyte derived macrophages. For example, AMs demonstrate a higher reliance on oxidative phosphorylation (Svedberg et al., 2019a). For these reasons, results generated from macrophages derived *ex vivo* cannot be reliably used to extrapolate effects on tissue resident macrophages.

The value of using this model to understand the role of AMs in IPF in this study is emphasised by the fact that hypoxia impaired efferocytosis in human AMs. This contrasts with a previous study using human MDMs, a model frequently used for tissue resident macrophages, which described a hypoxia driven increase in efferocytosis (Norris, Libreros and Serhan, 2019). These results may be opposing due to the marked differences between AMs and MDMs derived *in vitro.* In combination, this indicates that AMs are best used to determine the highly cell specific response to hypoxia in the lung.

The reduction in efferocytosis caused by hypoxia highlights one potential way in which hypoxia contributes to aberrant wound healing as IPF develops. This thesis began further investigation

to understand the mechanism behind this change. Overall, this work could not identify why AMs lose capacity to efferocytose but not phagocytose in hypoxia. No changes in efferocytic receptors were detected in association with hypoxia, although this may be due to the limited power of these experiments, or the range of receptors assessed. Further replication with receptors including MerTK and CD36 would be required to rule out this potential differentiating mechanism.

Beyond receptors, the major distinguishing feature of phagocytosis and efferocytosis is their metabolic demands. Efferocytosis introduces complex, high lipid cargo, which likely requires glycolysis and oxidative phosphorylation for uptake and processing in normoxic conditions (Yin and Heit, 2021; Boada-Romero et al., 2020). While macrophages derived *in vitro* and tissue resident macrophages from low oxygen tissues have been shown to co-opt the pentose phosphate pathway to facilitate increased efferocytosis in hypoxia (Wang et al., 2022), AMs may have reduced glycolytic capacity and/or metabolic flexibility, limiting uptake, processing or continual efferocytosis.

It is possible that some element of the efferocytic signalling pathway itself, which is unique to the internalisation and processing of apoptotic cells, may operate in an oxygen dependent manner. Hypoxia response genes, including those responding to HIFs, have not been universally identified and the efferocytic machinery specifically employed by AMs are incompletely characterised. Therefore, it is possible that future work exploring these two unknown factors may explain the distinction seen here.

6.2.2 PCLS

Developing our understanding of the profibrotic effects of hypoxia in PCLS builds on evidence in the field. PCLS provide unique opportunities to model cell-cell interactions. Of particular relevance to this thesis are the AM-fibroblast interactions modelled within a PCLS, including paracrine and contact-based communication, which have proven necessary for IPF fibroblast activation (Novak et al., 2023). Additionally, PCLS have been shown to contain cell types that are incompletely understood and therefore not represented in single cell cultures, such as the progenitor cell populations suspected of developing into intermediate basaloid cell subsets (Lang et al., 2023). The ability to model these cell types in crucial to gaining a full picture of the effects of hypoxia in the human lung. The PCLS model offers powerful enrichment to studies using murine models, by adding human relevance to use of models of murine lung fibrosis to investigate complex multicellular systems. This is crucial given the lack of representative animal models of IPF (Jenkins et al., 2017; Kolb et al., 2020).

This work indicates for the first time that collagen I production may be increased by hypoxia in a PCLS model of the lung. In addition, this data highlights HIF1α signalling as a possible driver of increased collagen I in PCLS, using pseudohypoxic IOX-2 treatment, although further validation is required to confirm this result. This assessment investigates hypoxia-driven changes in bulk, however data provides a valuable starting point to investigate how cells respond to hypoxia in a multicellular system. With further protocol development, the model may be used to delineate the contribution of AMs, IMs, fibroblasts and epithelial cells to the effects seen. For example, increased AM MMP-7 secretion seen in single cell cultures could be assessed in the PCLS system, providing information on the relative contribution of AMs compared to other cell types and the consequences of this change to stromal cells and ECM.

The benefits of this model would be maximised by spatial interrogation and/or dissociation of slices for further analysis.

There have historically been comparisons drawn between cancer and lung fibrosis (Vancheri, 2013; Spek and Duitman, 2019). Highly synthetic and glycolytic solid cancers contain tumour associated macrophages, which are programmed by the tumour environment for impaired function. Some of the metabolic crosstalk implicated in these interactions may be evident in IPF tissue as fibroblasts expand, as the metabolic products and hypoxic microenvironment are shared between the two diseases. PCLS provide an ideal system to model these interactions in a complex system relevant to human disease.

6.3 Implications for other lung diseases

Although this thesis focusses on the effect of hypoxia in the context of IPF, the use of non-disease tissue means that results may translate into various lung diseases with demonstrable tissue hypoxia, with consideration of the unique tissue environment that would be present in different diseases.

Unsurprisingly, evidence of hypoxia has been identified in lung tissue from patients with other fibrotic ILDs, including NSIP and HP (Khawaja et al. 2020). Due to the shared pathological mechanisms of fibrotic ILDs, it is likely that the role of hypoxia is similar in this broader disease group. Therefore, results described here may be translated for interpretation in the context of other fibrotic ILDs.

Additional lung diseases feature tissue hypoxia, widening the possible implications of these findings. Acute lung injury (ALI) and the more severe acute respiratory distress syndrome (ARDS) are associated with severe inflammation of the lungs, preceded by events such as sepsis

or trauma. While some ALI and ARDS triggers have been shown to directly cause hypoxia, such as shock (Greer 2010) and altitude (Luks, Swenson and Bärtsch, 2017), as the syndromes progress to pulmonary oedema in the alveolar spaces, severe inflammatory hypoxia develops regardless of the initial trigger (Vohwinkel, Hoegl and Eltzschig, 2015). The contribution of hypoxia to ALI and ARDS has been explored in a variety of models. Some evidence indicates that HIF signalling plays a protective role in ALI and ARDS, for example HIF1α inhibition *in vivo* resulted in worse outcomes in a ventilator induced murine model of ALI (Eckle et al. 2013). Contrastingly, acute hypoxia exacerbated ARDS in an LPS induced murine model of sepsis (G. Wu et al. 2018).

Evidence in this thesis, showing that hypoxia impairs efferocytosis in human AMs, adds an important element to understanding the role of hypoxia in ALI and ARDS progression, because dysregulated control of apoptosis has long been implicated in the mechanism of these syndromes (Bardales et al. 1996; Mantell et al. 1997). Indeed, results from Mahida et al., (2021) demonstrated impaired efferocytosis in AMs from ARDS patient BAL, whilst phagocytic function was unaffected. This distinction between efferocytosis and phagocytosis is replicated by hypoxic challenge, indicating possible shared mechanisms. Overactivation of Rac1 inhibitor ROCK was implicated in reduced efferocytosis by ALI AMs downstream of MERTK. The results of this thesis cannot determine whether similar signalling changes occur in response to hypoxia, however further investigation could delineate whether there are shared mechanisms.

6.4 Clinical and Therapeutic Implications

6.4.1 Oxygen Therapy

Given the growing evidence that hypoxia has a pathological role in lung fibrosis, application of oxygen therapy would appear a plausible treatment option. Currently, patients are referred for evaluation for long term oxygen therapy (LTOT) when their oxygen saturations drop below 92% at rest (Hardinge et al. 2015). Additionally, ambulatory oxygen (AOT) is recommended during activity if patients desaturate to below 88% during these periods (Raghu et al., 2011a). Due to these recommendations, oxygen is used in a clinical setting to manage symptoms and improve quality of life, although AOT has not been demonstrated to improve quality of life in patients who desaturate during activity (Visca et al. 2018).

Guidelines for the use of oxygen in IPF patients make minimal reference to its effect on mortality, due to a paucity of evidence and the relative rarity of the disease. A small number of studies have examined the outcome of oxygen therapy on mortality in patients who met the clinical requirements outlined above. In these patients, no effect on mortality was detected, although the small sample sizes in these studies may impact the accuracy of this assertion (Douglas, Ryu and Schroeder, 2000; Crockett, Cranston and Antic, 2001). Indeed, expert opinions extrapolate from studies in COPD to suggest that there may be a beneficial effect of oxygen therapy in these patients (O'Driscoll et al. 2017).

There are no studies investigating the effect of oxygen therapy on mortality and disease progression in patients who do not meet clinical thresholds for LTOT or AOT. This is probably due to the lack of established benefit to mortality in hypoxemic patients, and the published negative side effects of oxygen therapy with and without mechanical ventilation in other clinical

scenarios. Oxygen therapy associated hyperoxia induces cellular stress in the lung due to oxygen toxicity, resulting in increased ROS, which overwhelms cellular antioxidant mechanisms (Amarelle et al., 2021; Hochberg, Semler and Brower, 2021). This cascade is associated with the development of bronchopulmonary dysplasia in preterm infants and with hyperoxic acute lung injury (HALI) in critically ill adults receiving oxygen supplementation (Amarelle et al., 2021; Hochberg, Semler and Brower, 2021). Ventilator associated mechanical ventilation injury compounds this effect in patients receiving oxygen under positive pressure, as excessive stretch causes additional cellular stress. These cascades cause repetitive damage to the alveolar epithelium, resulting in damage and loss of function. Furthermore, oxygen therapy increases the risk of hypercapnic respiratory failure in patients, where ventilation effort decreases in response to high oxygen, preventing sufficient CO_2 excretion (Lius and Syafaah 2022).

Whilst these general limitations point against the universal use of conventional oxygen therapy to correct the hypoxic component of IPF, there are alternative emerging oxygen therapy programs under investigation. Hyperbaric oxygen therapy programs, in which patients are exposed to high oxygen concentrations at above atmospheric pressure for repeated daily sessions, have proved to be well tolerated and safe in patients without lung disease (Hadanny et al. 2019). These regimes are under clinical testing for a range of diseases, particularly neurological complications such as post stroke brain injury (Boussi-Gross et al., 2013; Efrati et al., 2013). Recently, hyperbaric oxygen therapy has been employed in bleomycin treated mice after the establishment of fibrosis, between days 7-20. Daily sessions of 90 minutes hyperbaric oxygen (2.5 ATA (absolute atmospheric pressure)) resulted in a reduction of fibrotic markers in bleomycin treated mice, including Masson's trichrome staining and hydroxyproline content (Y. Yuan et al. 2021). The mechanism of this benefit was not fully characterised in the murine

model. There is currently no evidence of the use of hyperbaric therapy in IPF patients. Treatment in this manner presents a possible therapeutic method of modulating the aberrant hypoxia described in this thesis, pending future preclinical and clinical investigation. However, the therapy is limited by its time intensive and continuous nature, with studies showing a rapid return to hypoxia after exposures are stopped (Kinoshita et al. 1999).

6.4.2 AM targeting in the lung

Due to the limitations and complications associated with oxygen therapy, more targeted approaches are likely required to target hypoxia associated changes in the lung. Firstly, AMs provide an interesting target, as they can be targeted specifically via inhalation and are highly phagocytic, making them the ideal target for inhaled therapies, including nanoparticles and liposomes (Costa, Sarmento and Seabra, 2015; Lee et al., 2015). CD206 expressing AMs have successfully been targeted *in vivo* with mannosylated nanoparticles containing siRNA against the TGF-β gene (Singh et al. 2022). Following uptake by AMs, these nanoparticles partially rescued bleomycin induced fibrosis in mice. Nanoparticles have also been developed and tested *in vivo* for antibiotic targeting of intracellular *Mycobacterium tuberculosis* infection in AMs (Makled, Boraie and Nafee, 2021; Maurya et al., 2022) and for AM targeting during ARDS, with steroids and mucolytic agents (Arber Raviv et al. 2022). Although the safety and efficacy of these AM targeted nanoparticles are yet to be tested in clinical trials, inhaled nanoparticles are under investigation in clinical trials for a range of chronic lung diseases (Gulati et al. 2021).

Pending further understanding of how the fibrotic environment, including hypoxia, alters AM function, the technologies described above may be employed to target these mechanisms in IPF. Interestingly, efferocytic impairment has been targeted in macrophages elsewhere using

nanoparticles. Nanoparticles loaded with inhibitors of the CD47-SIRPα axis were specifically targeted to macrophages within atherosclerotic plaques *in vivo*, resulting in rescue of efferocytic function without systemic side effects of excessive efferocytosis, such as anaemia (Flores et al. 2020; Sha et al. 2022). Although preliminary evidence in this thesis does not identify alterations in the CD47-SIRPα pathway, this is an interesting proof of concept study for the use of targeted delivery by nanoparticles to rescue efferocytosis and reverse disease.

6.4.3 Hypoxia targeting in the lung

Beyond macrophage specific targeting, hypoxia lends itself to specific drug targeting, due to the reductive nature of extremely hypoxic environments. This technique has been adopted in novel cancer therapies, which rely on the hypoxic environment of tumours for localised activation of highly toxic anti-cancer drugs (Li, Zhao and Li, 2021). Although these hypoxia-activated prodrugs (HAPs), have so far been focussed on solid cancers, a recent study described the use of a HAP for targeting a hypoxic inflammatory environment. The HAP targeted COX-2 and CA-9 inhibitors to areas of hypoxia in a murine model of myocarditis (W. Zhou et al. 2022). These delivery systems are in their infancy, however they could be used in future to harness the hypoxic nature of the IPF lung for drug targeting.

6.5 Limitations and Challenges of Hypoxia Exposure Models

6.5.1 Defining Relevant Hypoxia

Whilst there is evidence in mice showing pimonidazole adducts in the lung tissue of bleomycin treated mice, which reflects areas of <1% oxygen, equivalent information in IPF patients is lacking. Research has defined the oxygen concentrations spanning the human respiratory tract in health. Several studies have suggested that the air in the healthy human lung ranges from

19% O_2 in the large airways to 14.5% O_2 in the alveolar spaces (Jagannathan, Cuddapah and Costa, 2016). Limited studies investigating the lung tissue itself indicate average concentrations of 5.6% O_2 (Wild et al., 2005; Le et al., 2006; Miller et al., 2010). Some studies have extended these studies into IPF patients. An initial study using systemically delivered ^{18}F-MISO, which covalently binds proteins in hypoxic areas, for detection by positron emission tomography (PET)-CT scanning, was designed to detect areas of hypoxia in the human lung (Porter et al. 2021). However, no areas of hypoxia were detected in 10 IPF patients. This contrasts with studies using the same technique in bleomycin treated mice (Tanguy et al. 2021) and extensive evidence of hypoxia in human IPF tissue.

There were some limitations of the study by Tanguy et al. (2021), which may explain this disparity. Firstly, ^{18}F-MISO levels were internally controlled, by comparing none-fibrotic regions to fibrotic regions within the same patient scan. Since Porter et al. (2021) demonstrated that ^{18}F-MISO binding was established in nonfibrotic areas in the bleomycin mouse model, this method of control may have reduced the sensitivity of the technique. Additionally, patients in this study were at rest during the day, reducing the influence of exercise or sleep induced desaturation. Despite the limitations of current applications, these types of PET/CT studies may in future determine the range of oxygen concentrations in the human IPF lung.

In the absence of direct human evidence, and as the physiological concentration of oxygen in the human alveoli is on a gradient from 14.9-5.6%, challenge at 1% O_2 tests the effect of an oxygen concentration markedly lower than that seen in physiological conditions, guided by murine studies. Additionally, this concentration has the benefit of aligning with most other *in vitro* studies of pulmonary cells, allowing for more appropriate comparison.

6.5.2 Constant Versus Intermittent Hypoxia

Beyond the oxygen concentration, the temporal changes in oxygen concentration must be considered. It is likely that oxygen levels fluctuate *in situ*, dropping during periods of desaturation, for example during sleep and exercise. However, there is insufficient evidence of the fluctuation and timings of this exposure to guide *in vitro* implementation of these programs. Therefore, this work maintained constant hypoxia to understand the potential of hypoxia to cause changes in AMs and PCLS. As there is evidence demonstrating the differential effects of constant versus intermittent hypoxia on hypoxia responses, including in HIF1α and HIF2α dependent responses (G. Yuan et al. 2008; Nanduri et al. 2009), further experimentation with appropriate intermittent hypoxia regime when characterised would be beneficial. The 48-hour time point was selected because RNA and protein changes could be detected after this period in PCLS following fibrotic stimulus (Alsafadi et al., 2017) and changes in macrophage phenotype and function in hypoxia could be detected after 24 and 48 hours (Norris, Libreros and Serhan, 2019; Jeny et al., 2021). Although a more extended exposure may have detected further changes, extended *ex vivo* culture could not be achieved in PCLS due to viability loss and was avoided in AMs as prolonged culture results in loss of tissue specific cell features (Aktories et al., 2022; Subramanian et al., 2022a).

6.5.3 Defining Physioxia

This study uses a conventional cell culture incubator, with 5% CO_2 and maximum humidity at 37^{o}C, for normoxic control conditions. Although widely described as 21% O_2 conditions, based on Dalton's law of partial pressures and Amagat's law of partial volumes, the oxygen concentration in these conditions is ~18.6% (Place, Domann and Case, 2017). As with most *in vitro* cell culture assays, this oxygen concentration is not reflective of healthy tissue. As oxygen

exists on a gradient from 14.9-5.6% in the alveolar space, 18.6% oxygen may cause non-physiological changes in AMs and PCLS, due to the relative hyperoxic exposure. To fully dissect the contribution of hyperoxia in control samples versus hypoxia in treated samples, an oxygen concentration reflecting tissue physioxia would be required. Unfortunately, this was prohibited in the current study, as we are limited to using one hypoxystation for comparison with conventional cell culture incubators.

6.5.4 Pericellular Oxygen

When using hypoxia models, it is also important to consider the concentration of oxygen dissolved in cell culture media, which is inevitably lower than the oxygen concentration of the air and fluctuates with media changes (Metzen et al. 1995). Further still, pericellular oxygen level can vary depending on cell culture conditions, such as the depth of covering media, and the metabolic rate of the cells (Metzen et al. 1995). As such, pericellular oxygen concentrations may drop or even fluctuate as oxygen dissolves and is consumed. The combination of these considerations is that pericellular oxygen availability is markedly lower than the oxygen concentration of the air. Although various methods have been proposed to control pericellular oxygen levels (Place, Domann and Case, 2017; Pavlacky and Polak, 2020), from shaking to gas permeable culture dishes, and to measure pericellular oxygen concentrations levels, such as oxygen sensing electrodes and O_2 quenched fluorescent films, these techniques could not be employed in this study. Therefore, while the differences described are due to relative differences in oxygen availability, the actual differences in pericellular oxygen availability are unclear.

Pericellular oxygen in 3D models like PCLS is further complicated by variable thickness and the lack of oxygen circulation (Gomes et al., 2016; Mcmurtrey, 2016). This conceivably results in oxygen gradients from the outside to the inside of PCLS, which would be exacerbated during periods of high cellular activity. Agarose contamination likely also disrupts oxygen diffusion within the PCLS model. Emerging methods have been developed to assess 3D model oxygenation, including seeding oxygen quenched probes into hydrogel structures, for high resolution assessment of oxygen concentrations (Dmitriev et al., 2014; Lesher-Pérez et al., 2017). However, as these techniques could not be employed here, it is important to consider that although PCLS are subjected to relative hypoxia, actual oxygen availability is unknown and likely variable across the slice. This would become more relevant upon spatial assessment of PCLS hypoxic response.

6.6 Additional Limitations

Tissue utilised in this work was derived from patients undergoing resections to remove solid tumours. Although only distal tissue sections with no histological abnormalities were accepted, there is the possibility that the effects of abnormal cancer growth had effects on tissue. Of importance to this study is the possibility that tumours occlude blood supply (Mitzner and Wagner 2004), preconditioning the tissue to hypoxia, or introduce inflammatory changes, such as immune cell infiltration into the tissue (Z. Tan et al. 2021). These limitations are outweighed by the value of access to human tissue, and likely contribute to inter-sample variability, which can be overcome by increased biological replication.

Ex vivo culture inevitably induces some changes cells and models derived from human tissues (Subramanian et al., 2022a; Aktories et al., 2022). Factors such as exposure to high oxygen

levels during processing, culture in high glucose media and culture on tissue culture plastic contribute to these differences. Steps were taken to minimise these changes by using tissue and tissue derived models within a limited time frame. Future work may further combat some of these changes, for example by validating the use of a low glucose media to replicate tissue biology.

Due to the nature of tissue supply, all assays could not be repeated in all samples. This means that some experiments have limited biological replication, which is compounded by variability between samples. Therefore, sections of this thesis require further replication, as conclusions have been drawn based on small numbers and results may change in either direction following repetition.

6.7 Future Work

6.7.1 AMs

This thesis begins to delineate the effects of hypoxia on human AMs. The findings discussed here raise additional questions, which could be answered with further work.

1. Repetition of this work with additional biological replicates is required to achieve sufficient power to reach a conclusion on some of the aims of this work. For example, cell surface marker expression in response to hypoxia and efferocytic capacity in the presence of IOX-2 should be measured in additional samples.
2. Further surface markers would also be valuable in understanding why hypoxia reduces efferocytosis in AMs without also limiting phagocytosis. For example, MerTK is a key efferocytic receptor identified in AMs, with some studies showing downregulation in hypoxia (Mahida et al., 2021b; DeBerge et al., 2021).

3. As the widely supported model of IPF disease mechanism is associated with accumulation of apoptotic epithelial cells, it should be determined whether efferocytosis of apoptotic epithelial cells is impaired in AMs in hypoxia, as well as efferocytosis of apoptotic neutrophils.
4. Given that hypoxia responses beyond HIF1α likely contribute to changes in AMs, additional hypoxia signalling pathways should be characterised in AMs. In particular HIF2α, which is detected in macrophages in IPF tissue and is stabilised during chronic hypoxia (Bodempudi et al., 2014), should be measured in hypoxic AMs, and may be manipulated using inhibitor TCS7009 to determine its role in AM responses.
5. AM metabolism should be explored in detail using real time extracellular flux analysis alongside the assessment of metabolic enzyme expression, to further our understanding of the metabolic flexibility of AMs.
6. Our understanding of the metabolic shifts required for initial and continual efferocytosis in AMs specifically should be characterised using real time extracellular flux analysis and time lapse microscopy, alongside appropriate metabolic inhibitors.
7. Efferocytosis in normoxia and hypoxia should be explored using similar real time techniques, to determine at which stage efferocytosis is impaired by hypoxia.
8. AMs derived from patients with early (BAL) or late (transplant tissue) IPF should be exposed to hypoxia, to determine whether hypoxia differentially effects their phenotype and function.

6.7.2 PCLS

Chapter 5 utilised PCLS to further our understanding of the profibrotic effects of hypoxia in the lung tissue. There is some future work that would build on the impact of the work performed

so far, with cutting edge techniques increasing the resolution of information that can be derived from this model.

1. Further biological replication is required to increase the power of this work, to allow thorough characterisation of the effects of hypoxia in PCLS. In particular, RNA from additional samples is needed to overcome inherent inter-sample variability and detect hypoxia induced changes in gene expression in PCLS.
2. Although Chapter 5 focused on two key profibrotic markers in PCLS, this work would benefit from the assessment of additional markers associated with fibrosis (fibronectin, MMP-7) and loss of epithelial health (E-cadherin, surfactant protein C). This would increase confidence in the conclusion that hypoxia causes fibrosis in a PCLS model.
3. To improve mechanistic understanding of the effects of hypoxia in PCLS at a single cell level, imaging of protein and/or RNA levels would provide more insight. For example, imaging could determine whether AMs increased MMP-7 expression in a PCLS in the same way they did in a single cell culture. As the spatial imaging field develops, with techniques for spatial transcriptomics and metabolomics constantly improving, this could provide a wealth of information about the responses of specific cell types within a PCLS to hypoxia at high resolution.

6.7.2.1 Co-culture Models

In addition to the work described above using AM and PCLS models in isolation, PCLS may be employed to assess the effects of hypoxia exposed AMs on lung tissue. Conditioned media transfer from hypoxic AMs to PCLS may be employed to detect the combined effect of the AM

secretome on PCLS fibrosis. Additionally, co-culture of hypoxia exposed AMs with PCLS has the potential to identify the effects of direct cell contact between AMs and stromal cells.

6.8 Conclusion

In conclusion, this thesis validated hypoxic exposures in human AMs and PCLS, confirming induction of HIF1α responses in both models. Beyond this, pseudohypoxic IOX-2 stabilisation of HIF1α was validated in AMs. Hypoxia reduced the efferocytic capacity of human AMs, without affecting phagocytosis. Meanwhile, isolated HIF1α stabilisation had no effect on efferocytosis, but increased phagocytosis, indicating a differential role for HIF1α in the two functions. Additionally, this thesis demonstrates for the first time that hypoxia may induce collagen deposition in a human PCLS model, in line with previous effects seen in single cell fibroblast cultures. The effects explored in this thesis indicate the potential of therapeutically targeting hypoxia signalling or its downstream metabolic effects, to correct aberrant wound healing and limit extracellular matrix deposition.

CHAPTER 7: REFERENCES

Aderem, A. and Underhill, D.M. (1999) Mechanisms of phagocytosis in macrophages. *Annual Review of Immunology*, 17: 593–623. doi:10.1146/ANNUREV.IMMUNOL.17.1.593.

Aegerter, H., Kulikauskaite, J., Crotta, S., et al. (2020) Influenza-induced monocyte-derived alveolar macrophages confer prolonged antibacterial protection. *Nature Immunology 2020 21:2*, 21 (2): 145–157. doi:10.1038/s41590-019-0568-x.

A-Gonzalez, N., Bensinger, S.J., Hong, C., et al. (2009) Apoptotic Cells Promote Their Own Clearance and Immune Tolerance through Activation of the Nuclear Receptor LXR. *Immunity*, 31 (2): 245–258. doi:10.1016/J.IMMUNI.2009.06.018.

Ahangari, F., Becker, C., Foster, D.G., et al. (2022) Saracatinib, a Selective Src Kinase Inhibitor, Blocks Fibrotic Responses in Preclinical Models of Pulmonary Fibrosis. *American journal of respiratory and critical care medicine*, 206 (12). doi:10.1164/RCCM.202010-3832OC.

Ahluwalia, N., Shea, B.S. and Tager, A.M. (2014) New therapeutic targets in idiopathic pulmonary fibrosis. Aiming to rein in runaway wound-healing responses. *American Journal of Respiratory and Critical Care Medicine*, 190 (8): 867–878. doi:10.1164/RCCM.201403-0509PP/SUPPL_FILE/DISCLOSURES.PDF.

Akahori, D., Inui, N., Inoue, Y., et al. (2022) Effect of Hypoxia on Pulmonary Endothelial Cells from Bleomycin-Induced Pulmonary Fibrosis Model Mice. *International Journal of Molecular Sciences*, 23 (16). doi:10.3390/IJMS23168996/S1.

Akram, K.M., Yates, L.L., Mongey, R., et al. (2019) Live imaging of alveologenesis in precision-cut lung slices reveals dynamic epithelial cell behaviour. *Nature Communications 2019 10:1*, 10 (1): 1–16. doi:10.1038/s41467-019-09067-3.

Aktories, P., Petry, P., Glatz, P., et al. (2022) An improved organotypic cell culture system to study tissue-resident macrophages ex vivo. *Cell Reports Methods*, 2 (8): 100260. doi:10.1016/J.CRMETH.2022.100260.

Alder, J.K., Chen, J.J.L., Lancaster, L., et al. (2008) Short telomeres are a risk factor for idiopathic pulmonary fibrosis. *Proceedings of the National Academy of Sciences of the United States of America*, 105 (35): 13051–13056. doi:10.1073/PNAS.0804280105/SUPPL_FILE/0804280105SI.PDF.

Allden, S.J., Ogger, P.P., Ghai, P., et al. (2019) The Transferrin Receptor CD71 Delineates Functionally Distinct Airway Macrophage Subsets during Idiopathic Pulmonary Fibrosis. *American journal of respiratory and critical care medicine*, 200 (2): 209–219. doi:10.1164/RCCM.201809-1775OC.

Allen, L.A.H. and Aderem, A. (1996) Molecular definition of distinct cytoskeletal structures involved in complement- and Fc receptor-mediated phagocytosis in macrophages. *Journal of Experimental Medicine*, 184 (2): 627–637. doi:10.1084/JEM.184.2.627.

Alsafadi Hani, Uhl Franziska, Pineda Ricardo, et al. (2020) Applications and Approaches for Three-Dimensional Precision-Cut Lung Slices. Disease Modeling and Drug Discovery. *American journal of respiratory cell and molecular biology*, 62 (6): 681–691. doi:10.1165/RCMB.2019-0276TR.

Alsafadi, H.N., Staab-Weijnitz, C.A., Lehmann, M., et al. (2017) An ex vivo model to induce early fibrosis-like changes in human precision-cut lung slices. *American journal of physiology. Lung cellular and molecular physiology*, 312 (6): L896–L902. doi:10.1152/AJPLUNG.00084.2017.

Amaral, E.P., Costa, D.L., Namasivayam, S., et al. (2019) A major role for ferroptosis in Mycobacterium tuberculosis–induced cell death and tissue necrosis. *Journal of Experimental Medicine*, 216 (3): 556–570. doi:10.1084/JEM.20181776.

Amarelle, L., Quintela, L., Hurtado, J., et al. (2021) Hyperoxia and Lungs: What We Have Learned From Animal Models. *Frontiers in Medicine*, 8: 235. doi:10.3389/FMED.2021.606678/BIBTEX.

Anand, R.J., Gribar, S.C., Li, J., et al. (2007) Hypoxia causes an increase in phagocytosis by macrophages in a HIF-1alpha-dependent manner. *Journal of leukocyte biology*, 82 (5): 1257–1265. doi:10.1189/JLB.0307195.

Ando, M., Miyazaki, E., Ito, T., et al. (2010) Significance of serum vascular endothelial growth factor level in patients with idiopathic pulmonary fibrosis. *Lung*, 188 (3): 247–252. doi:10.1007/S00408-009-9223-X/FIGURES/3.

Andrianifahanana, M., Hernandez, D.M., Yin, X., et al. (2016) Profibrotic up-regulation of glucose transporter 1 by TGF-β involves activation of MEK and mammalian target of rapamycin complex 2 pathways. *FASEB Journal*, 30 (11): 3733–3744. doi:10.1096/FJ.201600428R/-/DC1.

Anthony, D., McQualter, J.L., Bishara, M., et al. (2014) SAA drives proinflammatory heterotypic macrophage differentiation in the lung via CSF-1R-dependent signaling. *FASEB journal : official publication of the Federation of American Societies for Experimental Biology*, 28 (9): 3867–3877. doi:10.1096/FJ.14-250332.

Aquino-Gálvez, A., González-Ávila, G., Jiménez-Sánchez, L.L., et al. (2019) Dysregulated expression of hypoxia-inducible factors augments myofibroblasts differentiation in idiopathic pulmonary fibrosis. *Respiratory research*, 20 (1): 130. doi:10.1186/S12931-019-1100-4/FIGURES/5.

Araki, N., Hatae, T., Furukawa, A., et al. (2003) Phosphoinositide-3-kinase-independent contractile activities associated with Fcγ-receptor-mediated phagocytosis and macropinocytosis in macrophages. *Journal of Cell Science*, 116 (2): 247–257. doi:10.1242/JCS.00235.

Arandjelovic, S. and Ravichandran, K.S. (2015) Phagocytosis of apoptotic cells in homeostasis. *Nature Immunology 2015 16:9*, 16 (9): 907–917. doi:10.1038/ni.3253.

Arango Duque, G. and Descoteaux, A. (2016) Macrophages Tell the Non-Professionals What to Do. *Developmental Cell*, 39 (6): 633–635. doi:10.1016/j.devcel.2016.12.009.

Arber Raviv, S., Alyan, M., Egorov, E., et al. (2022) Lung targeted liposomes for treating ARDS. *Journal of Controlled Release*, 346: 421–433. doi:10.1016/J.JCONREL.2022.03.028.

Ariel, A. and Serhan, C.N. (2012) New lives given by cell death: Macrophage differentiation following their encounter with apoptotic leukocytes during the resolution of inflammation. *Frontiers in Immunology*, 3 (JAN). doi:10.3389/FIMMU.2012.00004.

Arosio, P., Ingrassia, R. and Cavadini, P. (2009) Ferritins: a family of molecules for iron storage, antioxidation and more. *Biochimica et biophysica acta*, 1790 (7): 589–599. doi:10.1016/J.BBAGEN.2008.09.004.

Asano, S., Ito, S., Takahashi, K., et al. (2017) Matrix stiffness regulates migration of human lung fibroblasts. *Physiological Reports*, 5 (9): e13281. doi:10.14814/PHY2.13281.

Azad, A.K., Torrelles, J.B. and Schlesinger, L.S. (2008) Mutation in the DC-SIGN cytoplasmic triacidic cluster motif markedly attenuates receptor activity for phagocytosis and endocytosis of mannose-containing ligands by human myeloid cells. *Journal of Leukocyte Biology*, 84 (6): 1594–1603. doi:10.1189/JLB.0308192.

Azuma, A., Li, Y.J., Abe, S., et al. (2005) Interferon-{beta} inhibits bleomycin-induced lung fibrosis by decreasing transforming growth factor-{beta} and thrombospondin. *American journal of respiratory cell and molecular biology*, 32 (2): 93–98. doi:10.1165/RCMB.2003-0374OC.

Bai, R., Li, Y., Jian, L., et al. (2022) The hypoxia-driven crosstalk between tumor and tumor-associated macrophages: mechanisms and clinical treatment strategies. *Molecular cancer*, 21 (1). doi:10.1186/S12943-022-01645-2.

Baker, E.H. and Baines, D.L. (2018) Airway Glucose Homeostasis: A New Target in the Prevention and Treatment of Pulmonary Infection. *Chest*, 153 (2): 507–514. doi:10.1016/J.CHEST.2017.05.031.

Balamurugan, K. (2016) HIF-1 at the crossroads of hypoxia, inflammation, and cancer. *International Journal of Cancer*, 138 (5): 1058–1066. doi:10.1002/IJC.29519.

Balbo, P., Silvestri, M., Rossi, G.A., et al. (2001) Differential role of CD80 and CD86 on alveolar macrophages in the presentation of allergen to T lymphocytes in asthma. *Clinical and experimental allergy : journal of the British Society for Allergy and Clinical Immunology*, 31 (4): 625–636. doi:10.1046/J.1365-2222.2001.01068.X.

Balestro, E., Calabrese, F., Turato, G., et al. (2016) Immune Inflammation and Disease Progression in Idiopathic Pulmonary Fibrosis. *PLOS ONE*, 11 (5): e0154516. doi:10.1371/JOURNAL.PONE.0154516.

Barbarin, V., Arras, M., Misson, P., et al. (2004) Characterization of the effect of interleukin-10 on silica-induced lung fibrosis in mice. *American journal of respiratory cell and molecular biology*, 31 (1): 78–85. doi:10.1165/RCMB.2003-0299OC.

Bardales, R.H., Xie, S.S., Schaefer, R.F., et al. (1996) Apoptosis is a major pathway responsible for the resolution of type II pneumocytes in acute lung injury. *The American Journal of Pathology*, 149 (3): 845. Available at: /pmc/articles/PMC1865166/?report=abstract (Accessed: 5 March 2023).

Barratt, S.L., Blythe, T., Jarrett, C., et al. (2017) Differential expression of VEGF-Axxx isoforms is critical for development of pulmonary fibrosis. *American Journal of Respiratory and Critical Care Medicine*, 196 (4): 479–493. doi:10.1164/RCCM.201603-0568OC/SUPPL_FILE/DISCLOSURES.PDF.

Barratt, S.L., Blythe, T., Ourradi, K., et al. (2018a) Effects of hypoxia and hyperoxia on the differential expression of VEGF-A isoforms and receptors in Idiopathic Pulmonary Fibrosis (IPF). *Respiratory Research*, 19 (1): 1–5. doi:10.1186/S12931-017-0711-X/FIGURES/1.

Barratt, S.L., Flower, V.A., Pauling, J.D., et al. (2018b) VEGF (Vascular Endothelial Growth Factor) and Fibrotic Lung Disease. *International Journal of Molecular Sciences*, 19 (5). doi:10.3390/IJMS19051269.

Bartoszewska, S., Kochan, K., Piotrowski, A., et al. (2015) The hypoxia-inducible miR-429 regulates hypoxia-inducible factor-1α expression in human endothelial cells through a negative feedback loop.

FASEB journal : official publication of the Federation of American Societies for Experimental Biology, 29 (4): 1467–1479. doi:10.1096/FJ.14-267054.

Batie, M. and Rocha, S. (2020) Gene transcription and chromatin regulation in hypoxia. *Biochemical Society Transactions*, 48 (3): 1121–1128. doi:10.1042/BST20191106.

Bauer, Y., White, E.S., de Bernard, S., et al. (2017) MMP-7 is a predictive biomarker of disease progression in patients with idiopathic pulmonary fibrosis. *ERJ Open Research*, 3 (1). doi:10.1183/23120541.00074-2016.

Baumgartner, K.B., Samet, J.M., Coultas, D.B., et al. (2000) Occupational and Environmental Risk Factors for Idiopathic Pulmonary Fibrosis: A Multicenter Case-Control Study. *American Journal of Epidemiology*, 152 (4): 307–315. doi:10.1093/AJE/152.4.307.

Bazewicz, C.G., Dinavahi, S.S., Schell, T.D., et al. (2019) Aldehyde dehydrogenase in regulatory T-cell development, immunity and cancer. *Immunology*, 156 (1): 47–55. doi:10.1111/IMM.13016.

Bazzan, E., Turato, G., Tinè, M., et al. (2017) Dual polarization of human alveolar macrophages progressively increases with smoking and COPD severity. *Respiratory Research*, 18 (1): 1–8. doi:10.1186/S12931-017-0522-0/FIGURES/6.

Bedoret, D., Wallemacq, H., Marichal, T., et al. (2009) Lung interstitial macrophages alter dendritic cell functions to prevent airway allergy in mice. *Journal of Clinical Investigation*, 119 (12): 3723–3738. doi:10.1172/JCI39717.

Beemiller, P., Zhang, Y., Mohan, S., et al. (2010) A Cdc42 activation cycle coordinated by PI 3-kinase during Fc receptor-mediated phagocytosis. *Molecular Biology of the Cell*, 21 (3): 470–480. doi:10.1091/MBC.E08-05-0494/ASSET/IMAGES/LARGE/ZMK0031093350007.JPEG.

Begg, K. and Tavassoli, M. (2020) Inside the hypoxic tumour: reprogramming of the DDR and radioresistance. *Cell death discovery*, 6 (1). doi:10.1038/S41420-020-00311-0.

Belchamber, K.B.R., Singh, R., Batista, C.M., et al. (2019) Defective bacterial phagocytosis is associated with dysfunctional mitochondria in COPD macrophages. *European Respiratory Journal*, 54 (4). doi:10.1183/13993003.02244-2018.

Bellón, T., Martínez, V., Lucendo, B., et al. (2011) Alternative activation of macrophages in human peritoneum: implications for peritoneal fibrosis. *Nephrology, dialysis, transplantation : official publication of the European Dialysis and Transplant Association - European Renal Association*, 26 (9): 2995–3005. doi:10.1093/NDT/GFQ771.

Bertani, F.R., Mozetic, P., Fioramonti, M., et al. (2017) Classification of M1/M2-polarized human macrophages by label-free hyperspectral reflectance confocal microscopy and multivariate analysis. *Scientific Reports*, 7 (1). doi:10.1038/S41598-017-08121-8.

Betensley, A., Sharif, R. and Karamichos, D. (2016) A Systematic Review of the Role of Dysfunctional Wound Healing in the Pathogenesis and Treatment of Idiopathic Pulmonary Fibrosis. *Journal of clinical medicine*, 6 (1). doi:10.3390/JCM6010002.

Betsuyaku, T., Fukuda, Y., Parks, W.C., et al. (2000) Gelatinase B is required for alveolar bronchiolization after intratracheal bleomycin. *The American journal of pathology*, 157 (2): 525–535. doi:10.1016/S0002-9440(10)64563-4.

Birgersdotter, A., Sandberg, R. and Ernberg, I. (2005) Gene expression perturbation in vitro--a growing case for three-dimensional (3D) culture systems. *Seminars in cancer biology*, 15 (5): 405–412. doi:10.1016/J.SEMCANCER.2005.06.009.

Bissonnette, E.Y., Lauzon-Joset, J.F., Debley, J.S., et al. (2020) Cross-Talk Between Alveolar Macrophages and Lung Epithelial Cells is Essential to Maintain Lung Homeostasis. *Frontiers in Immunology*, 11: 2734. doi:10.3389/FIMMU.2020.583042/BIBTEX.

Blackwell, T.S., Tager, A.M., Borok, Z., et al. (2014) Future directions in idiopathic pulmonary fibrosis research. An NHLBI workshop report. *American journal of respiratory and critical care medicine*, 189 (2): 214–222. doi:10.1164/RCCM.201306-1141WS.

Blokland, K.E.C., Nizamoglu, M., Habibie, H., et al. (2022) Substrate stiffness engineered to replicate disease conditions influence senescence and fibrotic responses in primary lung fibroblasts. *Frontiers in Pharmacology*, 13: 4742. doi:10.3389/FPHAR.2022.989169/BIBTEX.

Boada-Romero, E., Martinez, J., Heckmann, B.L., et al. (2020a) The clearance of dead cells by efferocytosis. *Nature Reviews Molecular Cell Biology 2020 21:7*, 21 (7): 398–414. doi:10.1038/s41580-020-0232-1.

Boada-Romero, E., Martinez, J., Heckmann, B.L., et al. (2020b) The clearance of dead cells by efferocytosis. *Nature Reviews Molecular Cell Biology 2020 21:7*, 21 (7): 398–414. doi:10.1038/s41580-020-0232-1.

Bodempudi, V., Hergert, P., Smith, K., et al. (2014) miR-210 promotes IPF fibroblast proliferation in response to hypoxia. *American Journal of Physiology - Lung Cellular and Molecular Physiology*, 307 (4): 283–294. doi:10.1152/AJPLUNG.00069.2014/ASSET/IMAGES/LARGE/ZH50161465770005.JPEG.

Bolatkan, A., Asada, K., Kaneko, S., et al. (2021) Downregulation of METTL6 mitigates cell progression, migration, invasion and adhesion in hepatocellular carcinoma by inhibiting cell adhesion molecules. *International Journal of Oncology*, 59 (6): 1–15. doi:10.3892/IJO.2021.5282/HTML.

Booth, A.J., Hadley, R., Cornett, A.M., et al. (2012) Acellular normal and fibrotic human lung matrices as a culture system for in vitro investigation. *American Journal of Respiratory and Critical Care Medicine*, 186 (9): 866–876. doi:10.1164/RCCM.201204-0754OC.

Bosi, M., Milioli, G., Fanfulla, F., et al. (2017) OSA and Prolonged Oxygen Desaturation During Sleep are Strong Predictors of Poor Outcome in IPF. *Lung*, 195 (5): 643–651. doi:10.1007/S00408-017-0031-4.

Bosurgi, L., Cao, Y.G., Cabeza-Cabrerizo, M., et al. (2017) Macrophage function in tissue repair and remodeling requires IL-4 or IL-13 with apoptotic cells. *Science*, 356 (6342): 1072–1076. doi:10.1126/SCIENCE.AAI8132/SUPPL_FILE/AAI8132_BOSURGI_SM.PDF.

Boussi-Gross, R., Golan, H., Fishlev, G., et al. (2013) Hyperbaric Oxygen Therapy Can Improve Post Concussion Syndrome Years after Mild Traumatic Brain Injury - Randomized Prospective Trial. *PLOS ONE*, 8 (11): e79995. doi:10.1371/JOURNAL.PONE.0079995.

Braun, R.K., Broytman, O., Braun, F.M., et al. (2018) Chronic intermittent hypoxia worsens bleomycin-induced lung fibrosis in rats. *Respiratory physiology & neurobiology*, 256: 97–108. doi:10.1016/J.RESP.2017.04.010.

Brereton, C.J., Yao, L., Davies, E.R., et al. (2022) Pseudohypoxic HIF pathway activation dysregulates collagen structure-function in human lung fibrosis. *eLife*, 11. doi:10.7554/ELIFE.69348.

Brinker, K.G., Garner, H. and Wright, J.R. (2003) Surfactant protein A modulates the differentiation of murine bone marrow-derived dendritic cells. *American journal of physiology. Lung cellular and molecular physiology*, 284 (1). doi:10.1152/AJPLUNG.00187.2002.

Brown, E.J. (1992) Complement receptors, adhesion, and phagocytosis. *Infectious agents and disease*, 1 (2): 63–70. doi:10.1007/978-0-387-28669-3_4/COVER.

Brown, G.D. and Gordon, S. (2001) A new receptor for β-glucans. *Nature 2001 413:6851*, 413 (6851): 36–37. doi:10.1038/35092620.

Brown, S., Heinisch, I., Ross, E., et al. (2002) Apoptosis disables CD31-mediated cell detachment from phagocytes promoting binding and engulfment. *Nature 2002 418:6894*, 418 (6894): 200–203. doi:10.1038/nature00811.

Burgstaller, G., Gerckens, M., Eickelberg, O., et al. (2021) Decellularized human lung scaffolds as complex three-dimensional tissue culture models to study functional behavior of fibroblasts. *Methods in Molecular Biology*, 2299: 447–456. doi:10.1007/978-1-0716-1382-5_30.

Burke, B., Giannoudis, A., Corke, K.P., et al. (2003) Hypoxia-Induced Gene Expression in Human Macrophages: Implications for Ischemic Tissues and Hypoxia-Regulated Gene Therapy. *The American Journal of Pathology*, 163 (4): 1233. doi:10.1016/S0002-9440(10)63483-9.

Burman, A., Kropski, J.A., Calvi, C.L., et al. (2018) Localized hypoxia links ER stress to lung fibrosis through induction of C/EBP homologous protein. *JCI Insight*, 3 (16). doi:10.1172/JCI.INSIGHT.99543.

Byrne, A.J., Maher, T.M. and Lloyd, C.M. (2016) Pulmonary Macrophages: A New Therapeutic Pathway in Fibrosing Lung Disease? *Trends in molecular medicine*, 22 (4): 303–316. doi:10.1016/J.MOLMED.2016.02.004.

Byrne, A.J., Powell, J.E., O'Sullivan, B.J., et al. (2020) Dynamics of human monocytes and airway macrophages during healthy aging and after transplant. *Journal of Experimental Medicine*, 217 (3). doi:10.1084/JEM.20191236/133575.

Cabrera, S., Gaxiola, M., Arreola, J.L., et al. (2007) Overexpression of MMP9 in macrophages attenuates pulmonary fibrosis induced by bleomycin. *The international journal of biochemistry & cell biology*, 39 (12): 2324–2338. doi:10.1016/J.BIOCEL.2007.06.022.

Caldwell, C.C., Kojima, H., Lukashev, D., et al. (2001) Differential Effects of Physiologically Relevant Hypoxic Conditions on T Lymphocyte Development and Effector Functions. *The Journal of Immunology*, 167 (11): 6140–6149. doi:10.4049/JIMMUNOL.167.11.6140.

Campillo, N., Jorba, I., Schaedel, L., et al. (2016) A novel chip for cyclic stretch and intermittent hypoxia cell exposures mimicking obstructive sleep apnea. *Frontiers in Physiology*, 7 (JUL): 319. doi:10.3389/FPHYS.2016.00319/BIBTEX.

Campillo, N., Torres, M., Vilaseca, A., et al. (2017) Role of Cyclooxygenase-2 on Intermittent Hypoxia-Induced Lung Tumor Malignancy in a Mouse Model of Sleep Apnea. *Scientific Reports*, 7. doi:10.1038/SREP44693.

Canton, J., Khezri, R., Glogauer, M., et al. (2014) Contrasting phagosome pH regulation and maturation in human M1 and M2 macrophages. *Molecular Biology of the Cell*, 25 (21): 3330–3341. doi:10.1091/MBC.E14-05-0967/ASSET/IMAGES/LARGE/3330FIG6.JPEG.

Caradec, J., Sirab, N., Keumeugni, C., et al. (2010) 'Desperate house genes': the dramatic example of hypoxia. *British Journal of Cancer*, 102 (6): 1037. doi:10.1038/SJ.BJC.6605573.

Carreau, A., Hafny-Rahbi, B. el, Matejuk, A., et al. (2011) Why is the partial oxygen pressure of human tissues a crucial parameter? Small molecules and hypoxia. *Journal of Cellular and Molecular Medicine*, 15 (6): 1239–1253. doi:10.1111/J.1582-4934.2011.01258.X.

Carreto-Binaghi, L.E., Aliouat, E.M. and Taylor, M.L. (2016) Surfactant proteins, SP-A and SP-D, in respiratory fungal infections: their role in the inflammatory response. *Respiratory research*, 17 (1). doi:10.1186/S12931-016-0385-9.

Cash, T.P., Pan, Y. and Simon, M.C. (2007) Reactive oxygen species and cellular oxygen sensing. *Free radical biology & medicine*, 43 (9): 1219–1225. doi:10.1016/J.FREERADBIOMED.2007.07.001.

Chakarov, S., Lim, H.Y., Tan, L., et al. (2019) Two distinct interstitial macrophage populations coexist across tissues in specific subtissular niches. *Science*, 363 (6432). doi:10.1126/SCIENCE.AAU0964/SUPPL_FILE/AAU0964_TABLE_S5.XLSX.

Chambers, R.C. and Mercer, P.F. (2015) Mechanisms of Alveolar Epithelial Injury, Repair, and Fibrosis. *https://doi.org/10.1513/AnnalsATS.201410-448MG*, 12: S16–S20. doi:10.1513/ANNALSATS.201410-448MG.

Chao, J., Donham, P., van Rooijen, N., et al. (2011) Monocyte chemoattractant protein-1 released from alveolar macrophages mediates the systemic inflammation of acute alveolar hypoxia. *American journal of respiratory cell and molecular biology*, 45 (1): 53–61. doi:10.1165/RCMB.2010-0264OC.

Chao, J., Wood, J.G. and Gonzalez, N.C. (2009) Alveolar hypoxia, alveolar macrophages, and systemic inflammation. *Respiratory Research*, 10 (1): 1–8. doi:10.1186/1465-9921-10-54/FIGURES/1_768.

Chen, W., Zhang, J., Zhong, W., et al. (2021) Anlotinib Inhibits PFKFB3-Driven Glycolysis in Myofibroblasts to Reverse Pulmonary Fibrosis. *Frontiers in Pharmacology*, 12: 2496. doi:10.3389/FPHAR.2021.744826/BIBTEX.

Cheng, P., Li, S. and Chen, H. (2021) Macrophages in Lung Injury, Repair, and Fibrosis. *Cells*, 10 (2): 1–17. doi:10.3390/CELLS10020436.

Chioccioli, M., Roy, S., Newell, R., et al. (2022) A lung targeted miR-29 mimic as a therapy for pulmonary fibrosis. *eBioMedicine*, 85: 104304. doi:10.1016/j.ebiom.2022.104304.

Cho, S.H., Raybuck, A.L., Stengel, K., et al. (2016) Germinal centre hypoxia and regulation of antibody qualities by a hypoxia response system. *Nature*, 537 (7619): 234–238. doi:10.1038/NATURE19334.

Cho, S.J., Moon, J.S., Lee, C.M., et al. (2017) Glucose transporter 1-dependent glycolysis is increased during aging-related lung fibrosis, and phloretin inhibits lung fibrosis. *American Journal of Respiratory Cell and Molecular Biology*, 56 (4): 521–531. doi:10.1165/RCMB.2016-0225OC/SUPPL_FILE/DISCLOSURES.PDF.

Chopra, A., Adhikary, H., Willmore, W.G., et al. (2020) Insights into The Function and Regulation of Jumonji C Lysine Demethylases as Hypoxic Responsive Enzymes. *Current protein & peptide science*, 21 (7): 642–654. doi:10.2174/1389203721666191231104225.

Christoforidis, S., McBride, H.M., Burgoyne, R.D., et al. (1999) The Rab5 effector EEA1 is a core component of endosome docking. *Nature 1999 397:6720*, 397 (6720): 621–625. doi:10.1038/17618.

Chuliá-Peris, L., Carreres-Rey, C., Gabasa, M., et al. (2022) Matrix Metalloproteinases and Their Inhibitors in Pulmonary Fibrosis: EMMPRIN/CD147 Comes into Play. *International journal of molecular sciences*, 23 (13). doi:10.3390/IJMS23136894.

Chung, E.Y., Liu, J., Homma, Y., et al. (2007) Interleukin-10 Expression in Macrophages during Phagocytosis of Apoptotic Cells Is Mediated by Homeodomain Proteins Pbx1 and Prep-1. *Immunity*, 27 (6): 952–964. doi:10.1016/J.IMMUNI.2007.11.014.

Colegio, O.R., Chu, N.Q., Szabo, A.L., et al. (2014) Functional polarization of tumour-associated macrophages by tumour-derived lactic acid. *Nature*, 513 (7519): 559–563. doi:10.1038/NATURE13490.

Collard, H.R. (2012) The Age of Idiopathic Pulmonary Fibrosis. *https://doi.org/10.1164/rccm.201001-0049ED*, 181 (8): 771–772. doi:10.1164/RCCM.201001-0049ED.

Corcoran, S.E. and O'Neill, L.A.J. (2016) HIF1α and metabolic reprogramming in inflammation. *The Journal of clinical investigation*, 126 (10): 3699–3707. doi:10.1172/JCI84431.

Costa, A., Sarmento, B. and Seabra, V. (2015) Targeted Drug Delivery Systems for Lung Macrophages. *Current drug targets*, 16 (14): 1565–1581. doi:10.2174/1389450115666141114152713.

Cottin, V., Wollin, L., Fischer, A., et al. (2019) Fibrosing interstitial lung diseases: knowns and unknowns. *European Respiratory Review*, 28 (151). doi:10.1183/16000617.0100-2018.

Craig, V.J., Polverino, F., Laucho-Contreras, M.E., et al. (2014a) Mononuclear phagocytes and airway epithelial cells: novel sources of matrix metalloproteinase-8 (MMP-8) in patients with idiopathic pulmonary fibrosis. *PloS one*, 9 (5). doi:10.1371/JOURNAL.PONE.0097485.

Craig, V.J., Polverino, F., Laucho-Contreras, M.E., et al. (2014b) Mononuclear Phagocytes and Airway Epithelial Cells: Novel Sources of Matrix Metalloproteinase-8 (MMP-8) in Patients with Idiopathic Pulmonary Fibrosis. *PLOS ONE*, 9 (5): e97485. doi:10.1371/JOURNAL.PONE.0097485.

Craig, V.J., Zhang, L., Hagood, J.S., et al. (2015) Matrix metalloproteinases as therapeutic targets for idiopathic pulmonary fibrosis. *American Journal of Respiratory Cell and Molecular Biology*, 53 (5): 585–600. doi:10.1165/RCMB.2015-0020TR/SUPPL_FILE/DISCLOSURES.PDF.

Cramer, T., Yamanishi, Y., Clausen, B.E., et al. (2003) HIF-1α is essential for myeloid cell-mediated inflammation. *Cell*, 112 (5): 645–657. doi:10.1016/S0092-8674(03)00154-5.

Crockett, A., Cranston, J.M. and Antic, N. (2001) Domiciliary oxygen for interstitial lung disease. *Cochrane Database of Systematic Reviews*, 2010 (12). doi:10.1002/14651858.CD002883/MEDIA/CDSR/CD002883/IMAGE_N/NCD002883-CMP-001-01.PNG.

Crosby, L.M. and Waters, C.M. (2010) Epithelial repair mechanisms in the lung. *American Journal of Physiology - Lung Cellular and Molecular Physiology*, 298 (6): 715–731. doi:10.1152/AJPLUNG.00361.2009/ASSET/IMAGES/LARGE/ZH50061056760002.JPEG.

Cui, H., Xie, N., Banerjee, S., et al. (2021a) Lung myofibroblasts promote macrophage profibrotic activity through lactate-induced histone lactylation. *American Journal of Respiratory Cell and Molecular Biology*, 64 (1): 115–125. doi:10.1165/RCMB.2020-0360OC/SUPPL_FILE/DISCLOSURES.PDF.

Cui, Y., Zhang, Z., Zhou, X., et al. (2021b) Microglia and macrophage exhibit attenuated inflammatory response and ferroptosis resistance after RSL3 stimulation via increasing Nrf2 expression. *Journal of Neuroinflammation*, 18 (1): 1–15. doi:10.1186/S12974-021-02231-X/FIGURES/7.

Dahl, M., Bauer, A.K., Arredouani, M., et al. (2007) Protection against inhaled oxidants through scavenging of oxidized lipids by macrophage receptors MARCO and SR-AI/II. *The Journal of Clinical Investigation*, 117 (3): 757–764. doi:10.1172/JCI29968.

D'Alessandro, S., Magnavacca, A., Perego, F., et al. (2019) Effect of hypoxia on gene expression in cell populations involved in wound healing. *BioMed Research International*, 2019. doi:10.1155/2019/2626374.

Daniel, C., Wiede, J., Krutzsch, H.C., et al. (2004) Thrombospondin-1 is a major activator of TGF-beta in fibrotic renal disease in the rat in vivo. *Kidney international*, 65 (2): 459–468. doi:10.1111/J.1523-1755.2004.00395.X.

Danielpour, D., Kim, K.Y., Dart, L.L., et al. (1989) Sandwich enzyme-linked immunosorbent assays (SELISAs) quantitate and distinguish two forms of transforming growth factor-beta (TGF-beta 1 and TGF-beta 2) in complex biological fluids. *Growth factors (Chur, Switzerland)*, 2 (1): 61–71. doi:10.3109/08977198909069082.

D'Anna, C., Cigna, D., Costanzo, G., et al. (2015) Cigarette smoke alters cell cycle and induces inflammation in lung fibroblasts. *Life Sciences*, 126: 10–18. doi:10.1016/J.LFS.2015.01.017.

Dassow, C., Wiechert, L., Martin, C., et al. (2010) Biaxial distension of precision-cut lung slices. *Journal of Applied Physiology*, 108 (3): 713–721. doi:10.1152/JAPPLPHYSIOL.00229.2009/ASSET/IMAGES/LARGE/ZDG0031089580009.JPEG.

Davidovich, N., Huang, J. and Margulies, S.S. (2013) Reproducible uniform equibiaxial stretch of precision-cut lung slices. *American journal of physiology. Lung cellular and molecular physiology*, 304 (4). doi:10.1152/AJPLUNG.00224.2012.

DeBerge, M., Lantz, C., Dehn, S., et al. (2021) Hypoxia-inducible factors individually facilitate inflammatory myeloid metabolism and inefficient cardiac repair. *Journal of Experimental Medicine*, 218 (9). doi:10.1084/JEM.20200667/212520.

Deguchi, J.O., Yamazaki, H., Aikawa, E., et al. (2009) Chronic hypoxia activates the akt and β-catenin pathways in human macrophages. *Arteriosclerosis, Thrombosis, and Vascular Biology*, 29 (10): 1664–1670. doi:10.1161/ATVBAHA.109.194043.

Desai, O., Winkler, J., Minasyan, M., et al. (2018) The role of immune and inflammatory cells in idiopathic pulmonary fibrosis. *Frontiers in Medicine*, 5 (MAR): 43. doi:10.3389/FMED.2018.00043/BIBTEX.

Devaraj, A. (2014) Imaging: how to recognise idiopathic pulmonary fibrosis. *European Respiratory Review*, 23 (132): 215–219. doi:10.1183/09059180.00001514.

Dewhurst, J.A., Lea, S., Hardaker, E., et al. (2017) Characterisation of lung macrophage subpopulations in COPD patients and controls. *Scientific Reports 2017 7:1*, 7 (1): 1–12. doi:10.1038/s41598-017-07101-2.

Diakonova, M., Bokoch, G. and Swanson, J.A. (2002) Dynamics of cytoskeletal proteins during Fcγ receptor-mediated phagocytosis in macrophages. *Molecular Biology of the Cell*, 13 (2): 402–411. doi:10.1091/MBC.01-05-0273/ASSET/IMAGES/LARGE/MK0221756006.JPEG.

D'ignazio, L. and Rocha, S. (2016) Hypoxia Induced NF-κB. *Cells 2016, Vol. 5, Page 10*, 5 (1): 10. doi:10.3390/CELLS5010010.

Dmitriev, R.I., Kondrashina, A. V., Koren, K., et al. (2014) Small molecule phosphorescent probes for O2 imaging in 3D tissue models. *Biomaterials Science*, 2 (6): 853–866. doi:10.1039/C3BM60272A.

Doran, A.C., Yurdagul, A. and Tabas, I. (2019) Efferocytosis in health and disease. *Nature Reviews Immunology 2019 20:4*, 20 (4): 254–267. doi:10.1038/s41577-019-0240-6.

Dorrington, M.G. and Fraser, I.D.C. (2019) NF-κB signaling in macrophages: Dynamics, crosstalk, and signal integration. *Frontiers in Immunology*, 10 (APR): 705. doi:10.3389/FIMMU.2019.00705/BIBTEX.

Douglas, W.W., Ryu, J.H. and Schroeder, D.R. (2000) Idiopathic pulmonary fibrosis: Impact of oxygen and colchicine, prednisone, or no therapy on survival. *American journal of respiratory and critical care medicine*, 161 (4 Pt 1): 1172–1178. doi:10.1164/AJRCCM.161.4.9907002.

Doyle, S.E., O'Connell, R.M., Miranda, G.A., et al. (2004) Toll-like Receptors Induce a Phagocytic Gene Program through p38. *Journal of Experimental Medicine*, 199 (1): 81–90. doi:10.1084/JEM.20031237.

D'Urso, M. and Kurniawan, N.A. (2020) Mechanical and Physical Regulation of Fibroblast–Myofibroblast Transition: From Cellular Mechanoresponse to Tissue Pathology. *Frontiers in Bioengineering and Biotechnology*, 8: 1459. doi:10.3389/FBIOE.2020.609653/BIBTEX.

Dustin, M.L. (2017) Complement Receptors in Myeloid Cell Adhesion and Phagocytosis. *Myeloid Cells in Health and Disease: A Synthesis*, pp. 429–445. doi:10.1128/9781555819194.CH23.

Ebina-Shibuya, R., Watanabe-Matsui, M., Matsumoto, M., et al. (2016) The double knockout of Bach1 and Bach2 in mice reveals shared compensatory mechanisms in regulating alveolar macrophage function and lung surfactant homeostasis. *Journal of biochemistry*, 160 (6): 333–344. doi:10.1093/JB/MVW041.

Eckle, T., Brodsky, K., Bonney, M., et al. (2013) HIF1A Reduces Acute Lung Injury by Optimizing Carbohydrate Metabolism in the Alveolar Epithelium. *PLOS Biology*, 11 (9): e1001665. doi:10.1371/JOURNAL.PBIO.1001665.

Edelson, J.D., MacFadden, D.K., Klein, M., et al. (1985) Autofluorescence of alveolar macrophages: Problems and potential solutions. *Medical Hypotheses*, 17 (4): 403–407. doi:10.1016/0306-9877(85)90099-4.

Efrati, S., Fishlev, G., Bechor, Y., et al. (2013) Hyperbaric Oxygen Induces Late Neuroplasticity in Post Stroke Patients - Randomized, Prospective Trial. *PLOS ONE*, 8 (1): e53716. doi:10.1371/JOURNAL.PONE.0053716.

Elmore, S. (2007) Apoptosis: A Review of Programmed Cell Death. *Toxicologic pathology*, 35 (4): 495. doi:10.1080/01926230701320337.

Eltzschig, H.K. and Carmeliet, P. (2011) Hypoxia and Inflammation. *The New England journal of medicine*, 364 (7): 656. doi:10.1056/NEJMRA0910283.

Endo, M., Oyadomari, S., Terasaki, Y., et al. (2003) Induction of arginase I and II in bleomycin-induced fibrosis of mouse lung. *American journal of physiology. Lung cellular and molecular physiology*, 285 (2). doi:10.1152/AJPLUNG.00434.2002.

Enomoto, T., Usuki, J., Azuma, A., et al. (2003) Diabetes mellitus may increase risk for idiopathic pulmonary fibrosis. *Chest*, 123 (6): 2007–2011. doi:10.1378/CHEST.123.6.2007.

Fabriek, B.O., Bruggen, R. van, Deng, D.M., et al. (2009) The macrophage scavenger receptor CD163 functions as an innate immune sensor for bacteria. *Blood*, 113 (4): 887–892. doi:10.1182/BLOOD-2008-07-167064.

Fadok, V.A., Bratton, D.L., Konowal, A., et al. (1998) Macrophages that have ingested apoptotic cells in vitro inhibit proinflammatory cytokine production through autocrine/paracrine mechanisms involving TGF-beta, PGE2, and PAF. *The Journal of Clinical Investigation*, 101 (4): 890–898. doi:10.1172/JCI1112.

Fairn, G.D. and Grinstein, S. (2012) How nascent phagosomes mature to become phagolysosomes. *Trends in Immunology*, 33 (8): 397–405. doi:10.1016/J.IT.2012.03.003.

Fernandez, S., Jose, P., Avdiushko, M.G., et al. (2004) Inhibition of IL-10 Receptor Function in Alveolar Macrophages by Toll-Like Receptor Agonists. *The Journal of Immunology*, 172 (4): 2613–2620. doi:10.4049/JIMMUNOL.172.4.2613.

Fichtner-Feigl, S., Strober, W., Kawakami, K., et al. (2005) IL-13 signaling through the IL-13α2 receptor is involved in induction of TGF-β1 production and fibrosis. *Nature Medicine 2005 12:1*, 12 (1): 99–106. doi:10.1038/nm1332.

Fingerlin, T.E., Murphy, E., Zhang, W., et al. (2013) Genome-wide association study identifies multiple susceptibility loci for pulmonary fibrosis. *Nature genetics*, 45 (6): 613. doi:10.1038/NG.2609.

Fink, S.L. and Cookson, B.T. (2005) Apoptosis, pyroptosis, and necrosis: Mechanistic description of dead and dying eukaryotic cells. *Infection and Immunity*, 73 (4): 1907–1916. doi:10.1128/IAI.73.4.1907-1916.2005/ASSET/282919DA-59F2-4E73-9A5D-C8BF2A6C76CF/ASSETS/GRAPHIC/ZII0040547300003.JPEG.

Flores, A.M., Hosseini-Nassab, N., Jarr, K.U., et al. (2020) Pro-efferocytic nanoparticles are specifically taken up by lesional macrophages and prevent atherosclerosis. *Nature Nanotechnology 2020 15:2*, 15 (2): 154–161. doi:10.1038/s41565-019-0619-3.

Folcik, V.A., Garofalo, M., Coleman, J., et al. (2013) Idiopathic pulmonary fibrosis is strongly associated with productive infection by herpesvirus saimiri. *Modern Pathology 2014 27:6*, 27 (6): 851–862. doi:10.1038/modpathol.2013.198.

Fond, A.M., Lee, C.S., Schulman, I.G., et al. (2015) Apoptotic cells trigger a membrane-initiated pathway to increase ABCA1. *The Journal of clinical investigation*, 125 (7): 2748–2758. doi:10.1172/JCI80300.

Frangogiannis, N.G. (2020) Transforming growth factor–ß in tissue fibrosis. *Journal of Experimental Medicine*, 217 (3). doi:10.1084/JEM.20190103/133821.

Franke-Ullmann, G., Pförtner, C., Walter, P., et al. (1996) Characterization of murine lung interstitial macrophages in comparison with alveolar macrophages in vitro. *Journal of immunology*.

Freeburn, R.W., Armstrong, L. and Millar, A.B. (2005) Cultured alveolar macrophages from patients with idiopathic pulmonary fibrosis (IPF) show dysregulation of lipopolysaccharide-induced tumor necrosis factor-α (TNF-α) and interleukin-10 (IL-10) inductions. *European Cytokine Network*, 16 (1): 5–16. Available at: https://www.jle.com/fr/revues/ecn/e-docs/cultured_alveolar_macrophages_from_patients_with_idiopathic_pulmonary_fibrosis_ipf_show_dysregulation_of_lipopolysaccharide_i_266012/article.phtml?tab=texte (Accessed: 6 January 2023).

Freeman, S.A. and Grinstein, S. (2014) Phagocytosis: receptors, signal integration, and the cytoskeleton. *Immunological Reviews*, 262 (1): 193–215. doi:10.1111/IMR.12212.

Freemerman, A.J., Johnson, A.R., Sacks, G.N., et al. (2014) Metabolic reprogramming of macrophages: glucose transporter 1 (GLUT1)-mediated glucose metabolism drives a proinflammatory phenotype. *The Journal of biological chemistry*, 289 (11): 7884–7896. doi:10.1074/JBC.M113.522037.

Freire-de-Lima, C.G., Yi, Q.X., Gardai, S.J., et al. (2006) Apoptotic cells, through transforming growth factor-β, coordinately induce anti-inflammatory and suppress pro-inflammatory eicosanoid and NO synthesis in murine macrophages. *Journal of Biological Chemistry*, 281 (50): 38376–38384. doi:10.1074/jbc.M605146200.

Froese, A.R., Shimbori, C., Bellaye, P.S., et al. (2016) Stretch-induced activation of transforming growth factor-b1 in pulmonary fibrosis. *American Journal of Respiratory and Critical Care Medicine*, 194 (1): 84–96. doi:10.1164/RCCM.201508-1638OC/SUPPL_FILE/DISCLOSURES.PDF.

Frost, J., Ciulli, A. and Rocha, S. (2019) RNA-seq analysis of PHD and VHL inhibitors reveals differences and similarities to the hypoxia response. *Wellcome Open Research*, 4. doi:10.12688/WELLCOMEOPENRES.15044.1.

Fujihara, M., Muroi, M., Tanamoto, K.I., et al. (2003) Molecular mechanisms of macrophage activation and deactivation by lipopolysaccharide: roles of the receptor complex. *Pharmacology & Therapeutics*, 100 (2): 171–194. doi:10.1016/J.PHARMTHERA.2003.08.003.

Fukuda, Y., Basset, F., Ferrans, V.J., et al. (1995) Significance of early intra-alveolar fibrotic lesions and integrin expression in lung biopsy specimens from patients with idiopathic pulmonary fibrosis. *Human Pathology*, 26 (1): 53–61. doi:10.1016/0046-8177(95)90114-0.

G, R., KJ, A., TE, K., et al. (2012) Prednisone, azathioprine, and N-acetylcysteine for pulmonary fibrosis. *The New England journal of medicine*, 366 (21): 1968–1977. doi:10.1056/NEJMOA1113354.

García-Sancho, C., Buendía-Roldán, I., Fernández-Plata, M.R., et al. (2011) Familial pulmonary fibrosis is the strongest risk factor for idiopathic pulmonary fibrosis. *Respiratory Medicine*, 105 (12): 1902–1907. doi:10.1016/J.RMED.2011.08.022.

García-Sancho Figueroa, M.C., Carrillo, G., Pérez-Padilla, R., et al. (2010) Risk factors for idiopathic pulmonary fibrosis in a Mexican population. A case-control study. *Respiratory medicine*, 104 (2): 305–309. doi:10.1016/J.RMED.2009.08.013.

Gardai, S.J., Xiao, Y.Q., Dickinson, M., et al. (2003) By binding SIRPα or calreticulin/CD91, lung collectins act as dual function surveillance molecules to suppress or enhance inflammation. *Cell*, 115 (1): 13–23. doi:10.1016/S0092-8674(03)00758-X.

Gauldie, J. (2002) Pro: Inflammatory mechanisms are a minor component of the pathogenesis of idiopathic pulmonary fibrosis. *American journal of respiratory and critical care medicine*, 165 (9): 1205–1206. doi:10.1164/RCCM.2202054.

Gibbings, S.L., Goyal, R., Desch, A.N., et al. (2015) Transcriptome analysis highlights the conserved difference between embryonic and postnatal-derived alveolar macrophages. *Blood*, 126 (11): 1357–1366. doi:10.1182/BLOOD-2015-01-624809.

Gibbings, S.L., Thomas, S.M., Atif, S.M., et al. (2017) Three unique interstitial macrophages in the murine lung at steady state. *American Journal of Respiratory Cell and Molecular Biology*, 57 (1): 66–76. doi:10.1165/RCMB.2016-0361OC/SUPPL_FILE/DISCLOSURES.PDF.

Gibbons, M.A., MacKinnon, A.C., Ramachandran, P., et al. (2012) Ly6Chi Monocytes Direct Alternatively Activated Profibrotic Macrophage Regulation of Lung Fibrosis. *https://doi.org/10.1164/rccm.201010-1719OC*, 184 (5): 569–581. doi:10.1164/RCCM.201010-1719OC.

Gill, S.K., Hui, K., Farne, H., et al. (2016) Increased airway glucose increases airway bacterial load in hyperglycaemia. *Scientific Reports*, 6. doi:10.1038/SREP27636.

Gille, T., Didier, M., Boubaya, M., et al. (2017a) Obstructive sleep apnoea and related comorbidities in incident idiopathic pulmonary fibrosis. *European Respiratory Journal*, 49 (6). doi:10.1183/13993003.01934-2016.

Gille, T., Didier, M., Boubaya, M., et al. (2017b) Obstructive sleep apnoea and related comorbidities in incident idiopathic pulmonary fibrosis. *European Respiratory Journal*, 49 (6). doi:10.1183/13993003.01934-2016.

Gille, T., Didier, M., Rotenberg, C., et al. (2018) Intermittent hypoxia increases the severity of bleomycin-induced lung injury in mice. *Oxidative Medicine and Cellular Longevity*, 2018. doi:10.1155/2018/1240192.

Gleeson, L.E., Sheedy, F.J., Palsson-McDermott, E.M., et al. (2016) Cutting Edge: Mycobacterium tuberculosis Induces Aerobic Glycolysis in Human Alveolar Macrophages That Is Required for Control of Intracellular Bacillary Replication. *The Journal of Immunology*, 196 (6): 2444–2449. doi:10.4049/JIMMUNOL.1501612.

Gomes, A., Guillaume, L., Grimes, D.R., et al. (2016) Oxygen Partial Pressure Is a Rate-Limiting Parameter for Cell Proliferation in 3D Spheroids Grown in Physioxic Culture Condition. *PLOS ONE*, 11 (8): e0161239. doi:10.1371/JOURNAL.PONE.0161239.

Gomez Perdiguero, E., Klapproth, K., Schulz, C., et al. (2015) Tissue-resident macrophages originate from yolk-sac-derived erythro-myeloid progenitors. *Nature*, 518 (7540): 547–551. doi:10.1038/NATURE13989.

Goodwin, J., Choi, H., Hsieh, M.H., et al. (2018) Targeting hypoxia-inducible factor-1a/pyruvate dehydrogenase kinase 1 axis by dichloroacetate suppresses bleomycin-induced pulmonary fibrosis. *American Journal of Respiratory Cell and Molecular Biology*, 58 (2): 216–231. doi:10.1165/RCMB.2016-0186OC/SUPPL_FILE/DISCLOSURES.PDF.

Gordon, S. and Plüddemann, A. (2017) Tissue macrophages: heterogeneity and functions. *BMC Biology 2017 15:1*, 15 (1): 1–18. doi:10.1186/S12915-017-0392-4.

Grabiec, A.M. and Hussell, T. (2016) The role of airway macrophages in apoptotic cell clearance following acute and chronic lung inflammation. *Seminars in Immunopathology 2016 38:4*, 38 (4): 409–423. doi:10.1007/S00281-016-0555-3.

Greer, R. (2010) The temporal evolution of acute respiratory distress syndrome following shock. *European Journal of Anaesthesiology*, 27 (3): 226–232. doi:10.1097/EJA.0B013E3283308E7F.

Gribbin, J., Hubbard, R. and Smith, C. (2009) Role of diabetes mellitus and gastro-oesophageal reflux in the aetiology of idiopathic pulmonary fibrosis. *Respiratory medicine*, 103 (6): 927–931. doi:10.1016/J.RMED.2008.11.001.

Gu, Y., Lawrence, T., Mohamed, R., et al. (2022) The emerging roles of interstitial macrophages in pulmonary fibrosis: A perspective from scRNA-seq analyses. *Frontiers in Immunology*, 13: 5291. doi:10.3389/FIMMU.2022.923235/BIBTEX.

Guilliams, M., de Kleer, I., Henri, S., et al. (2013) Alveolar macrophages develop from fetal monocytes that differentiate into long-lived cells in the first week of life via GM-CSF. *Journal of Experimental Medicine*, 210 (10): 1977–1992. doi:10.1084/JEM.20131199.

Gulati, N., Chellappan, D.K., MacLoughlin, R., et al. (2021) Inhaled nano-based therapeutics for inflammatory lung diseases: Recent advances and future prospects. *Life sciences*, 285. doi:10.1016/J.LFS.2021.119969.

Gürtler, A., Kunz, N., Gomolka, M., et al. (2013) Stain-Free technology as a normalization tool in Western blot analysis. *Analytical biochemistry*, 433 (2): 105–111. doi:10.1016/J.AB.2012.10.010.

Hadanny, A., Zubari, T., Tamir-Adler, L., et al. (2019) Hyperbaric oxygen therapy effects on pulmonary functions: A prospective cohort study. *BMC Pulmonary Medicine*, 19 (1): 1–6. doi:10.1186/S12890-019-0893-8/TABLES/3.

Hamanaka, R.B., Okhan, G., Mutlu, M., et al. (2021) Metabolic requirements of pulmonary fibrosis: role of fibroblast metabolism. *The FEBS Journal*, 288 (22): 6331–6352. doi:10.1111/FEBS.15693.

Hancock, A., Armstrong, L., Gama, R., et al. (2012) Production of Interleukin 13 by Alveolar Macrophages from Normal and Fibrotic Lung. *https://doi.org/10.1165/ajrcmb.18.1.2627*, 18 (1): 60–65. doi:10.1165/AJRCMB.18.1.2627.

Hardinge, M., Annandale, J., Bourne, S., et al. (2015) British Thoracic Society guidelines for home oxygen use in adults: accredited by NICE. *Thorax*, 70 (Suppl 1): i1–i43. doi:10.1136/THORAXJNL-2015-206865.

Hartshorn, K.L., Crouch, E., White, M.R., et al. (1998) Pulmonary surfactant proteins A and D enhance neutrophil uptake of bacteria. *American Journal of Physiology - Lung Cellular and Molecular Physiology*, 274 (6 18-6): 958–969. doi:10.1152/AJPLUNG.1998.274.6.L958/ASSET/IMAGES/LARGE/ALUN60614008Y.JPEG.

Hashimoto, D., Chow, A., Noizat, C., et al. (2013) Tissue-resident macrophages self-maintain locally throughout adult life with minimal contribution from circulating monocytes. *Immunity*, 38 (4): 792–804. doi:10.1016/J.IMMUNI.2013.04.004.

Hayton, C. and Chaudhuri, N. (2016) Nintedanib for treating idiopathic pulmonary fibrosis. *British Journal of Health Care Management*, 22 (5): 250–251. doi:10.12968/bjhc.2016.22.5.250.

Hazlett, H.F., Hampton, T.H., Aridgides, D.S., et al. (2020) Altered iron metabolism in cystic fibrosis macrophages: the impact of CFTR modulators and implications for Pseudomonas aeruginosa survival. *Scientific Reports 2020 10:1*, 10 (1): 1–14. doi:10.1038/s41598-020-67729-5.

Henderson, J., Duffy, L., Stratton, R., et al. (2020) Metabolic reprogramming of glycolysis and glutamine metabolism are key events in myofibroblast transition in systemic sclerosis pathogenesis. *Journal of Cellular and Molecular Medicine*, 24 (23): 14026–14038. doi:10.1111/JCMM.16013.

Henry, M.T., McMahon, K., Mackarel, A.J., et al. (2002) Matrix metalloproteinases and tissue inhibitor of metalloproteinase-1 in sarcoidosis and IPF. *The European respiratory journal*, 20 (5): 1220–1227. doi:10.1183/09031936.02.00022302.

Henson, P.M. and Tuder, R.M. (2008) Apoptosis in the lung: Induction, clearance and detection. *American Journal of Physiology - Lung Cellular and Molecular Physiology*, 294 (4): 601–611. doi:10.1152/AJPLUNG.00320.2007/ASSET/IMAGES/LARGE/ZH50040851290004.JPEG.

Herold, S., Mayer, K. and Lohmeyer, J. (2011) Acute lung injury: how macrophages orchestrate resolution of inflammation and tissue repair. *Frontiers in immunology*, 2 (NOV). doi:10.3389/FIMMU.2011.00065.

Herre, J., Marshall, A.S.J., Caron, E., et al. (2004) Dectin-1 uses novel mechanisms for yeast phagocytosis in macrophages. *Blood*, 104 (13): 4038–4045. doi:10.1182/BLOOD-2004-03-1140.

Heukels, P., van Hulst, J.A.C., van Nimwegen, M., et al. (2018) Fibrocytes are increased in lung and peripheral blood of patients with idiopathic pulmonary fibrosis. *Respiratory Research*, 19 (1): 1–12. doi:10.1186/S12931-018-0798-8/FIGURES/6.

Hewitt, R.J. and Maher, T.M. (2019) Idiopathic Pulmonary Fibrosis: New and Emerging Treatment Options. *Drugs and Aging*, 36 (6): 485–492. doi:10.1007/S40266-019-00647-Y/FIGURES/1.

de Hilster, R.H.J., Sharma, P.K., Jonker, M.R., et al. (2020) Human lung extracellular matrix hydrogels resemble the stiffness and viscoelasticity of native lung tissue. *American Journal of Physiology - Lung Cellular and Molecular Physiology*, 318 (4): L698. doi:10.1152/AJPLUNG.00451.2019.

Hiwatari, N., Shimura, S., Yamauchi, K., et al. (1997) Significance of elevated procollagen-III-peptide and transforming growth factor-beta levels of bronchoalveolar lavage fluids from idiopathic

pulmonary fibrosis patients. *The Tohoku journal of experimental medicine*, 181 (2): 285–295. doi:10.1620/TJEM.181.285.

Hoang, A.T.N., Chen, P., Juarez, J., et al. (2012) Dendritic cell functional properties in a three-dimensional tissue model of human lung mucosa. *American Journal of Physiology - Lung Cellular and Molecular Physiology*, 302 (2): 226–237. doi:10.1152/AJPLUNG.00059.2011/ASSET/IMAGES/LARGE/ZH50031260320008.JPEG.

Hochberg, C.H., Semler, M.W. and Brower, R.G. (2021) Oxygen toxicity in critically ill adults. *American Journal of Respiratory and Critical Care Medicine*, 204 (6): 632–641. doi:10.1164/RCCM.202102-0417CI/SUPPL_FILE/DISCLOSURES.PDF.

Hodge, S., Hodge, G., Scicchitano, R., et al. (2003) Alveolar macrophages from subjects with chronic obstructive pulmonary disease are deficient in their ability to phagocytose apoptotic airway epithelial cells. *Immunology and Cell Biology*, 81 (4): 289–296. doi:10.1046/J.1440-1711.2003.T01-1-01170.X.

Hoeffel, G., Chen, J., Lavin, Y., et al. (2015) C-Myb(+) erythro-myeloid progenitor-derived fetal monocytes give rise to adult tissue-resident macrophages. *Immunity*, 42 (4): 665–678. doi:10.1016/J.IMMUNI.2015.03.011.

Hofmann, F., Bläsche, R., Kasper, M., et al. (2015) A Co-Culture System with an Organotypic Lung Slice and an Immortal Alveolar Macrophage Cell Line to Quantify Silica-Induced Inflammation. *PLoS ONE*, 10 (1). doi:10.1371/JOURNAL.PONE.0117056.

Hoppstädter, J., Diesel, B., Zarbock, R., et al. (2010) Differential cell reaction upon Toll-like receptor 4 and 9 activation in human alveolar and lung interstitial macrophages. *Respiratory Research*, 11 (1): 1–15. doi:10.1186/1465-9921-11-124/FIGURES/8_967.

Hortobágyi, L., Kierstein, S., Krytska, K., et al. (2008) Surfactant protein D inhibits TNF-alpha production by macrophages and dendritic cells in mice. *The Journal of allergy and clinical immunology*, 122 (3): 521–528. doi:10.1016/J.JACI.2008.05.002.

Huang, L., Nazarova, E. V., Tan, S., et al. (2018) Growth of Mycobacterium tuberculosis in vivo segregates with host macrophage metabolism and ontogeny. *Journal of Experimental Medicine*, 215 (4): 1135–1152. doi:10.1084/JEM.20172020.

Hughes, G., Toellner, H., Morris, H., et al. (2016) Real World Experiences: Pirfenidone and Nintedanib are Effective and Well Tolerated Treatments for Idiopathic Pulmonary Fibrosis. *Journal of Clinical Medicine 2016, Vol. 5, Page 78*, 5 (9): 78. doi:10.3390/JCM5090078.

Humbert, M.V., Spalluto, C.M., Bell, J., et al. (2022) Towards an artificial human lung: modelling organ-like complexity to aid mechanistic understanding. *European Respiratory Journal*, 60 (6): 2200455. doi:10.1183/13993003.00455-2022.

Hussell, T. and Bell, T.J. (2014) Alveolar macrophages: plasticity in a tissue-specific context. *Nature Reviews Immunology 2014 14:2*, 14 (2): 81–93. doi:10.1038/nri3600.

Imai, K., Hiramatsu, A., Fukushima, D., et al. (1997) Degradation of decorin by matrix metalloproteinases: identification of the cleavage sites, kinetic analyses and transforming growth factor-β1 release. *Biochemical Journal*, 322 (3): 809–814. doi:10.1042/BJ3220809.

Ishikawa, E., Ishikawa, T., Morita, Y.S., et al. (2009) Direct recognition of the mycobacterial glycolipid, trehalose dimycolate, by C-type lectin Mincle. *Journal of Experimental Medicine*, 206 (13): 2879–2888. doi:10.1084/JEM.20091750.

Islam, M.A., Pröll, M., Hölker, M., et al. (2013) Alveolar macrophage phagocytic activity is enhanced with LPS priming, and combined stimulation of LPS and lipoteichoic acid synergistically induce pro-inflammatory cytokines in pigs. *Innate Immunity*, 19 (6): 631–643. doi:10.1177/1753425913477166/ASSET/IMAGES/LARGE/10.1177_1753425913477166-FIG2.JPEG.

Iyonaga, K., Suga, M., Yamamoto, T., et al. (n.d.) *Elevated bronchoalveolar concentrations of MCP-1 in patients with pulmonary alveolar proteinosis*.

Izbicki, G., Segel, M.J., Christensen, T.G., et al. (2002) Time course of bleomycin-induced lung fibrosis. *International Journal of Experimental Pathology*, 83 (3): 111–119. doi:10.1046/J.1365-2613.2002.00220.X.

Jagannathan, L., Cuddapah, S. and Costa, M. (2016) Oxidative stress under ambient and physiological oxygen tension in tissue culture. *Current pharmacology reports*, 2 (2): 64. doi:10.1007/S40495-016-0050-5.

Jagirdar, J., Begín, R., Dufresne, A., et al. (1996) Transforming growth factor-beta (TGF-beta) in silicosis. *American journal of respiratory and critical care medicine*, 154 (4 Pt 1): 1076–1081. doi:10.1164/AJRCCM.154.4.8887610.

Jain, I.H., Calvo, S.E., Markhard, A.L., et al. (2020) Genetic Screen for Cell Fitness in High or Low Oxygen Highlights Mitochondrial and Lipid Metabolism. *Cell*, 181 (3): 716-727.e11. doi:10.1016/J.CELL.2020.03.029.

Janssen, W.J., Barthel, L., Muldrow, A., et al. (2011) Fas determines differential fates of resident and recruited macrophages during resolution of acute lung injury. *American journal of respiratory and critical care medicine*, 184 (5): 547–560. doi:10.1164/RCCM.201011-1891OC.

Jaśkiewicz, M., Moszyńska, A., Króliczewski, J., et al. (2022) The transition from HIF-1 to HIF-2 during prolonged hypoxia results from reactivation of PHDs and HIF1A mRNA instability. *Cellular & Molecular Biology Letters 2022 27:1*, 27 (1): 1–19. doi:10.1186/S11658-022-00408-7.

Jenkins, G. (2008) The role of proteases in transforming growth factor-β activation. *The International Journal of Biochemistry & Cell Biology*, 40 (6–7): 1068–1078. doi:10.1016/J.BIOCEL.2007.11.026.

Jenkins, R.G., Moore, B.B., Chambers, R.C., et al. (2017) An Official American Thoracic Society Workshop Report: Use of Animal Models for the Preclinical Assessment of Potential Therapies for Pulmonary Fibrosis. *American journal of respiratory cell and molecular biology*, 56 (5): 667–679. doi:10.1165/RCMB.2017-0096ST.

Jeny, F., Bernaudin, J.F., Valeyre, D., et al. (2021) Hypoxia Promotes a Mixed Inflammatory-Fibrotic Macrophages Phenotype in Active Sarcoidosis. *Frontiers in Immunology*, 12: 3202. doi:10.3389/FIMMU.2021.719009/BIBTEX.

Jeong, H., Kim, S., Hong, B.J., et al. (2019) Tumor-Associated Macrophages Enhance Tumor Hypoxia and Aerobic Glycolysis. *Cancer research*, 79 (4): 795–806. doi:10.1158/0008-5472.CAN-18-2545.

Jeong, S.H., Son, E.S., Lee, Y.E., et al. (2022) Histone deacetylase 3 promotes alveolar epithelial–mesenchymal transition and fibroblast migration under hypoxic conditions. *Experimental & Molecular Medicine 2022 54:7*, 54 (7): 922–931. doi:10.1038/s12276-022-00796-y.

Ji, W.J., Ma, Y.Q., Zhou, X., et al. (2014) Temporal and spatial characterization of mononuclear phagocytes in circulating, lung alveolar and interstitial compartments in a mouse model of bleomycin-induced pulmonary injury. *Journal of Immunological Methods*, 403 (1–2): 7–16. doi:10.1016/J.JIM.2013.11.012.

Kage, H. and Borok, Z. (2012) EMT and Interstitial Lung Disease: A Mysterious Relationship. *Current opinion in pulmonary medicine*, 18 (5): 517. doi:10.1097/MCP.0B013E3283566721.

Kang, H.H., Kim, I.K., Yeo, C.D., et al. (2020) The Effects of Chronic Intermittent Hypoxia in Bleomycin-Induced Lung Injury on Pulmonary Fibrosis via Regulating the NF-κB/Nrf2 Signaling Pathway. *Tuberculosis and respiratory diseases*, 83 (Supple 1): S63–S74. doi:10.4046/TRD.2020.0112.

Kanzaki, T., Olofsson, A., Morén, A., et al. (1990) TGF-β1 binding protein: A component of the large latent complex of TGF-β1 with multiple repeat sequences. *Cell*, 61 (6): 1051–1061. doi:10.1016/0092-8674(90)90069-Q.

Karimi, R., Tornling, G., Grunewald, J., et al. (2012) Cell Recovery in Bronchoalveolar Lavage Fluid in Smokers Is Dependent on Cumulative Smoking History. *PLOS ONE*, 7 (3): e34232. doi:10.1371/JOURNAL.PONE.0034232.

Karuga, F.F., Kaczmarski, P., Szmyd, B., et al. (2022) The Association between Idiopathic Pulmonary Fibrosis and Obstructive Sleep Apnea: A Systematic Review and Meta-Analysis. *Journal of Clinical Medicine*, 11 (17): 5008. doi:10.3390/JCM11175008/S1.

Ke, X., Chen, C., Song, Y., et al. (2019) Hypoxia modifies the polarization of macrophages and their inflammatory microenvironment, and inhibits malignant behavior in cancer cells. *Oncology Letters*, 18 (6): 5871. doi:10.3892/OL.2019.10956.

Khadem Ali, M., Kim, R.Y., Brown, A.C., et al. (2020) Crucial role for lung iron level and regulation in the pathogenesis and severity of asthma. *European Respiratory Journal*, 55 (4). doi:10.1183/13993003.01340-2019.

Khalil, N., Bereznay, O., Sporn, M., et al. (1989) Macrophage production of transforming growth factor beta and fibroblast collagen synthesis in chronic pulmonary inflammation. *The Journal of experimental medicine*, 170 (3): 737–737. doi:10.1084/JEM.170.3.727.

Khawaja, A.A., Chong, D.L.W., Sahota, J., et al. (2020) Identification of a Novel HIF-1α-αMβ2 Integrin-NET Axis in Fibrotic Interstitial Lung Disease. *Frontiers in immunology*, 11. doi:10.3389/FIMMU.2020.02190.

Kim, J.S., Podolanczuk, A.J., Borker, P., et al. (2017) Obstructive sleep apnea and subclinical interstitial lung disease in the multi-ethnic study of atherosclerosis (MESA). *Annals of the American Thoracic Society*, 14 (12): 1786–1795. doi:10.1513/ANNALSATS.201701-091OC/SUPPL_FILE/DISCLOSURES.PDF.

Kim, K.K., Dotson, M.R., Agarwal, M., et al. (2018) Efferocytosis of apoptotic alveolar epithelial cells is sufficient to initiate lung fibrosis. *Cell Death & Disease*, 9 (11). doi:10.1038/S41419-018-1074-Z.

King, E.M., Hume, P.S., Janssen, W.J., et al. (2022) Isolation and Analysis of Macrophage Subsets from the Mouse and Human Lung. *Methods in molecular biology (Clifton, N.J.)*, 2506: 257–267. doi:10.1007/978-1-0716-2364-0_18.

King, T.E., Albera, C., Bradford, W.Z., et al. (2009) Effect of interferon gamma-1b on survival in patients with idiopathic pulmonary fibrosis (INSPIRE): a multicentre, randomised, placebo-controlled trial. *Lancet (London, England)*, 374 (9685): 222–228. doi:10.1016/S0140-6736(09)60551-1.

King, T.E., Bradford, W.Z., Castro-Bernardini, S., et al. (2014) A Phase 3 Trial of Pirfenidone in Patients with Idiopathic Pulmonary Fibrosis. *New England Journal of Medicine*, 370 (22): 2083–2092. doi:10.1056/NEJMOA1402582/SUPPL_FILE/NEJMOA1402582_DISCLOSURES.PDF.

Kinoshita, Y., Kohshi, K., Kunugita, N., et al. (1999) Preservation of tumour oxygen after hyperbaric oxygenation monitored by magnetic resonance imaging. *British Journal of Cancer 2000 82:1*, 82 (1): 88–92. doi:10.1054/bjoc.1999.0882.

Kitano, M., Nakaya, M., Nakamura, T., et al. (2008) Imaging of Rab5 activity identifies essential regulators for phagosome maturation. *Nature 2008 453:7192*, 453 (7192): 241–245. doi:10.1038/nature06857.

Kitowska, K., Zakrzewicz, D., Königshoff, M., et al. (2008) Functional role and species-specific contribution of arginases in pulmonary fibrosis. *American Journal of Physiology - Lung Cellular and Molecular Physiology*, 294 (1): 34–45. doi:10.1152/AJPLUNG.00007.2007/ASSET/IMAGES/LARGE/ZH50120750680008.JPEG.

Kline, J.N., Schwartz, D.A., Monick, M.M., et al. (1993) Relative Release of lnterleukin-1β and lnterleukin-1 Receptor Antagonist by Alveolar Macrophages: A Study in Asbestos-Induced Lung Disease, Sarcoidosis, and Idiopathic Pulmonary Fibrosis. *Chest*, 104 (1): 47–53. doi:10.1378/CHEST.104.1.47.

Kobayashi, T., Kim, H.J., Liu, X., et al. (2014) Matrix metalloproteinase-9 activates TGF-β and stimulates fibroblast contraction of collagen gels. *American Journal of Physiology - Lung Cellular and Molecular Physiology*, 306 (11): L1006. doi:10.1152/AJPLUNG.00015.2014.

Koh, M.Y., Spivak-Kroizman, T., Venturini, S., et al. (2008) Molecular mechanisms for the activity of PX-478, an antitumor inhibitor of the hypoxia-inducible factor-1α. *Molecular Cancer Therapeutics*, 7 (1): 90–100. doi:10.1158/1535-7163.MCT-07-0463.

Kolb, P., Upagupta, C., Vierhout, M., et al. (2020) The importance of interventional timing in the bleomycin model of pulmonary fibrosis. *The European respiratory journal*, 55 (6). doi:10.1183/13993003.01105-2019.

Kottmann, R.M., Kulkarni, A.A., Smolnycki, K.A., et al. (2012) Lactic Acid Is Elevated in Idiopathic Pulmonary Fibrosis and Induces Myofibroblast Differentiation via pH-Dependent Activation of Transforming Growth Factor-β. *American Journal of Respiratory and Critical Care Medicine*, 186 (8): 740. doi:10.1164/RCCM.201201-0084OC.

Kuhn, C., Boldt, J., King, T.E., et al. (1989) An immunohistochemical study of architectural remodeling and connective tissue synthesis in pulmonary fibrosis. *The American review of respiratory disease*, 140 (6): 1693–1703. doi:10.1164/AJRCCM/140.6.1693.

Kuhn, C. and McDonald, J.A. (1991) The roles of the myofibroblast in idiopathic pulmonary fibrosis. Ultrastructural and immunohistochemical features of sites of active extracellular matrix synthesis. *The American Journal of Pathology*, 138 (5): 1257. Available at: /pmc/articles/PMC1886011/?report=abstract (Accessed: 30 December 2022).

Kulikauskaite, J. and Wack, A. (2020) Teaching Old Dogs New Tricks? The Plasticity of Lung Alveolar Macrophage Subsets. *Trends in immunology*, 41 (10): 864–877. doi:10.1016/J.IT.2020.08.008.

van der Laan, L.J.W., Döpp, E.A., Haworth, R., et al. (1999) Regulation and Functional Involvement of Macrophage Scavenger Receptor MARCO in Clearance of Bacteria In Vivo. *The Journal of Immunology*, 162 (2): 939–947. doi:10.4049/JIMMUNOL.162.2.939.

van de Laar, L., Saelens, W., de Prijck, S., et al. (2016) Yolk Sac Macrophages, Fetal Liver, and Adult Monocytes Can Colonize an Empty Niche and Develop into Functional Tissue-Resident Macrophages. *Immunity*, 44 (4): 755–768. doi:10.1016/J.IMMUNI.2016.02.017.

Lai, X., Huang, S., Lin, Y., et al. (2023) DACT2 protects against pulmonary fibrosis via suppressing glycolysis in lung myofibroblasts. *International Journal of Biological Macromolecules*, 226: 291–300. doi:10.1016/J.IJBIOMAC.2022.11.324.

Lang, N., Ansari, M., Porras-Gonzalez, D., et al. (2022) Ex vivo modelling of human lung fibrogenesis and drug mode of action screens using single-cell RNA-seq in precision-cut lung slices. *ERJ Open Research*, 8 (suppl 8): 72. doi:10.1183/23120541.LSC-2022.72.

Lang, N.J., Gote-Schniering, J., Porras-Gonzalez, D., et al. (2023) Ex vivo tissue perturbations coupled to single cell RNA-seq reveal multi-lineage cell circuit dynamics in human lung fibrogenesis. *bioRxiv*, p. 2023.01.16.524219. doi:10.1101/2023.01.16.524219.

Lappi-Blanco, E., Soini, Y. and Pääkkö, P. (1999) Apoptotic activity is increased in the newly formed fibromyxoid connective tissue in bronchiolitis obliterans organizing pneumonia. *Lung*, 177 (6): 367–376. doi:10.1007/PL00007654/METRICS.

Lara-Guzmán, O.J., Gil-Izquierdo, Á., Medina, S., et al. (2018) Oxidized LDL triggers changes in oxidative stress and inflammatory biomarkers in human macrophages. *Redox Biology*, 15: 1–11. doi:10.1016/J.REDOX.2017.11.017.

Larson-Casey, J.L., Deshane, J.S., Ryan, A.J., et al. (2016) Macrophage Akt1 Kinase-Mediated Mitophagy Modulates Apoptosis Resistance and Pulmonary Fibrosis. *Immunity*, 44 (3): 582–596. doi:10.1016/j.immuni.2016.01.001.

Lavin, Y., Mortha, A., Rahman, A., et al. (2015) Regulation of macrophage development and function in peripheral tissues. *Nature Publishing Group*, 15. doi:10.1038/nri3920.

Le, Q.T., Chen, E., Salim, A., et al. (2006) An evaluation of tumor oxygenation and gene expression in patients with early stage non-small cell lung cancers. *Clinical cancer research : an official journal of the American Association for Cancer Research*, 12 (5): 1507–1514. doi:10.1158/1078-0432.CCR-05-2049.

Lederer, D.J., Jelic, S., Basner, R.C., et al. (2012) Is Obstructive Sleep Apnea a Cause of Idiopathic Pulmonary Fibrosis? *Archives of pathology & laboratory medicine*, 136 (5): 470. doi:10.5858/ARPA.2011-0650-LE.

Lee, C.S., Penberthy, K.K., Wheeler, K.M., et al. (2016) Boosting apoptotic cell clearance by colonic epithelial cells attenuates inflammation in vivo. *Immunity*, 44 (4): 807. doi:10.1016/J.IMMUNI.2016.02.005.

Lee, S.J., Evers, S., Roeder, D., et al. (2002) Mannose receptor-mediated regulation of serum glycoprotein homeostasis. *Science (New York, N.Y.)*, 295 (5561): 1898–1901. doi:10.1126/SCIENCE.1069540.

Lee, W.H., Loo, C.Y., Traini, D., et al. (2015) Nano- and micro-based inhaled drug delivery systems for targeting alveolar macrophages. *Expert opinion on drug delivery*, 12 (6): 1009–1026. doi:10.1517/17425247.2015.1039509.

Lee, Y.A., Choi, H.M., Lee, S.H., et al. (2012) Hypoxia differentially affects IL-1β-stimulated MMP-1 and MMP-13 expression of fibroblast-like synoviocytes in an HIF-1α-dependent manner. *Rheumatology*, 51 (3): 443–450. doi:10.1093/RHEUMATOLOGY/KER327.

Lehmann, M., Buhl, L., Alsafadi, H.N., et al. (2018) Differential effects of Nintedanib and Pirfenidone on lung alveolar epithelial cell function in ex vivo murine and human lung tissue cultures of pulmonary fibrosis. *Respiratory research*, 19 (1). doi:10.1186/S12931-018-0876-Y.

Lesher-Pérez, S.C., Kim, G.A., Kuo, C.H., et al. (2017) Dispersible oxygen microsensors map oxygen gradients in three-dimensional cell cultures. *Biomaterials Science*, 5 (10): 2106–2113. doi:10.1039/C7BM00119C.

Leslie, K.O. (2012) Idiopathic pulmonary fibrosis may be a disease of recurrent, tractional injury to the periphery of the aging lung: a unifying hypothesis regarding etiology and pathogenesis. *Archives of pathology & laboratory medicine*, 136 (6): 591–600. doi:10.5858/ARPA.2011-0511-OA.

Levin, R., Grinstein, S. and Canton, J. (2016) The life cycle of phagosomes: formation, maturation, and resolution. *Immunological Reviews*, 273 (1): 156–179. doi:10.1111/IMR.12439.

LeVine, A.M., Whitsett, J.A., Gwozdz, J.A., et al. (2000) Distinct effects of surfactant protein A or D deficiency during bacterial infection on the lung. *Journal of immunology (Baltimore, Md. : 1950)*, 165 (7): 3934–3940. doi:10.4049/JIMMUNOL.165.7.3934.

Lewkowicz, E., Herit, F., Clainche, C. le, et al. (2008) The microtubule-binding protein CLIP-170 coordinates mDia1 and actin reorganization during CR3-mediated phagocytosis. *Journal of Cell Biology*, 183 (7): 1287–1298. doi:10.1083/JCB.200807023.

Ley, B., Collard, H.R. and King, T.E. (2012) Clinical Course and Prediction of Survival in Idiopathic Pulmonary Fibrosis. *https://doi.org/10.1164/rccm.201006-0894CI*, 183 (4): 431–440. doi:10.1164/RCCM.201006-0894CI.

Li, J., Zhai, X., Sun, X., et al. (2022a) Metabolic reprogramming of pulmonary fibrosis. *Frontiers in Pharmacology*, 13: 4868. doi:10.3389/FPHAR.2022.1031890/BIBTEX.

Li, K. and Underhill, D.M. (2020) C-Type Lectin Receptors in Phagocytosis. *Current Topics in Microbiology and Immunology*, 429: 1–18. doi:10.1007/82_2020_198/COVER.

Li, Y., Zhao, L. and Li, X.F. (2021) Targeting Hypoxia: Hypoxia-Activated Prodrugs in Cancer Therapy. *Frontiers in Oncology*, 11: 2920. doi:10.3389/FONC.2021.700407/BIBTEX.

Li, Z., Geng, J., Xie, B., et al. (2022b) Dihydromyricetin Alleviates Pulmonary Fibrosis by Regulating Abnormal Fibroblasts Through the STAT3/p-STAT3/GLUT1 Signaling Pathway. *Frontiers in Pharmacology*, 13: 515. doi:10.3389/FPHAR.2022.834604/BIBTEX.

van Liempt, E., Bank, C.M.C., Mehta, P., et al. (2006) Specificity of DC-SIGN for mannose- and fucose-containing glycans. *FEBS Letters*, 580 (26): 6123–6131. doi:10.1016/J.FEBSLET.2006.10.009.

Liu, F., Mih, J.D., Shea, B.S., et al. (2010) Feedback amplification of fibrosis through matrix stiffening and COX-2 suppression. *Journal of Cell Biology*, 190 (4): 693–706. doi:10.1083/JCB.201004082.

Liu, G., Betts, C., Cunoosamy, D.M., et al. (2019) Use of precision cut lung slices as a translational model for the study of lung biology. *Respiratory Research 2019 20:1*, 20 (1): 1–14. doi:10.1186/S12931-019-1131-X.

Lius, E.E. and Syafaah, I. (2022) Hyperoxia in the management of respiratory failure: A literature review. *Annals of Medicine and Surgery*, 81. doi:10.1016/J.AMSU.2022.104393.

Lloyd, C.M. and Snelgrove, R.J. (2018) Type 2 immunity: Expanding our view. *Science Immunology*, 3 (25). doi:10.1126/SCIIMMUNOL.AAT1604.

Lobato-Pascual, A., Saether, P.C., Fossum, S., et al. (2013) Mincle, the receptor for mycobacterial cord factor, forms a functional receptor complex with MCL and FcεRI-γ. *European Journal of Immunology*, 43 (12): 3167–3174. doi:10.1002/EJI.201343752.

van Lookeren Campagne, M., Wiesmann, C. and Brown, E.J. (2007) Macrophage complement receptors and pathogen clearance. *Cellular Microbiology*, 9 (9): 2095–2102. doi:10.1111/J.1462-5822.2007.00981.X.

Lucchini, A.C., Gachanja, N.N., Rossi, A.G., et al. (2021) Epithelial Cells and Inflammation in Pulmonary Wound Repair. *Cells*, 10 (2): 1–19. doi:10.3390/CELLS10020339.

Lugg, S. (2020) *DEVELOPING STRATEGIES FOR THE PREVENTION OF POSTOPERATIVE PULMONARY COMPLICATIONS AFTER LUNG CANCER SURGERY*. University of Birmingham.

Lugg, S.T., Scott, A., Parekh, D., et al. (2022) Cigarette smoke exposure and alveolar macrophages: mechanisms for lung disease. *Thorax*, 77 (1): 94–101. doi:10.1136/THORAXJNL-2020-216296.

Luks, A.M., Swenson, E.R. and Bärtsch, P. (2017) Acute high-altitude sickness. *European Respiratory Review*, 26 (143). doi:10.1183/16000617.0096-2016.

Lyons-Cohen, M.R., Nakano, H., Thomas, S.Y., et al. (2018) Imaging precision cut lung slices to visualize leukocyte localization and trafficking. *Methods in molecular biology (Clifton, N.J.)*, 1799: 237. doi:10.1007/978-1-4939-7896-0_18.

MA, R., B, M., H, B., et al. (2006) Hypoxia reduces the output of matrix metalloproteinase-9 (MMP-9) in monocytes by inhibiting its secretion and elevating membranal association. *Journal of leukocyte biology*, 79 (4): 706–718. doi:10.1189/JLB.0605302.

Maher, T.M., Evans, I.C., Bottoms, S.E., et al. (2012) Diminished Prostaglandin E2 Contributes to the Apoptosis Paradox in Idiopathic Pulmonary Fibrosis. *https://doi.org/10.1164/rccm.200905-0674OC*, 182 (1): 73–82. doi:10.1164/RCCM.200905-0674OC.

Maher, T.M., Wells, A.U. and Laurent, G.J. (2007) Idiopathic pulmonary fibrosis: multiple causes and multiple mechanisms? *European Respiratory Journal*, 30 (5): 835–839. doi:10.1183/09031936.00069307.

Mahida, R.Y., Scott, A., Parekh, D., et al. (2021a) Acute respiratory distress syndrome is associated with impaired alveolar macrophage efferocytosis. *The European respiratory journal*, 58 (3). doi:10.1183/13993003.00829-2021.

Mahida, R.Y., Scott, A., Parekh, D., et al. (2021b) Assessment of Alveolar Macrophage Dysfunction Using an in vitro Model of Acute Respiratory Distress Syndrome. *Frontiers in Medicine*, 8: 1669. doi:10.3389/FMED.2021.737859/BIBTEX.

Majmundar, A.J., Wong, W.J. and Simon, M.C. (2010) Hypoxia-inducible factors and the response to hypoxic stress. *Molecular cell*, 40 (2): 294–309. doi:10.1016/J.MOLCEL.2010.09.022.

Makled, S., Boraie, N. and Nafee, N. (2021) Nanoparticle-mediated macrophage targeting-a new inhalation therapy tackling tuberculosis. *Drug delivery and translational research*, 11 (3): 1037–1055. doi:10.1007/S13346-020-00815-3.

Mantell, L.L., Kazzaz, J.A., Xu, J., et al. (1997) Unscheduled apoptosis during acute inflammatory lung injury. *Cell death and differentiation*, 4 (7): 600–607. doi:10.1038/SJ.CDD.4400278.

Marijic, P., Schwarzkopf, L., Schwettmann, L., et al. (2021) Pirfenidone vs. nintedanib in patients with idiopathic pulmonary fibrosis: a retrospective cohort study. *Respiratory Research*, 22 (1): 1–11. doi:10.1186/S12931-021-01857-Y/TABLES/2.

Marinković, A., Liu, F. and Tschumperlin, D.J. (2013) Matrices of Physiologic Stiffness Potently Inactivate Idiopathic Pulmonary Fibrosis Fibroblasts. *American Journal of Respiratory Cell and Molecular Biology*, 48 (4): 422. doi:10.1165/RCMB.2012-0335OC.

Marshansky, V. and Futai, M. (2008) The V-type H+-ATPase in vesicular trafficking: targeting, regulation and function. *Current Opinion in Cell Biology*, 20 (4): 415–426. doi:10.1016/J.CEB.2008.03.015.

Martinet, Y., Rom, W.N., Grotendorst, G.R., et al. (1987) Exaggerated Spontaneous Release of Platelet-Derived Growth Factor by Alveolar Macrophages from Patients with Idiopathic Pulmonary Fibrosis. *New England Journal of Medicine*, 317 (4): 202–209. doi:10.1056/NEJM198707233170404.

Martinez-Pomares, L., Linehan, S.A., Taylor, P.R., et al. (2001) Binding Properties of the Mannose Receptor. *Immunobiology*, 204 (5): 527–535. doi:10.1078/0171-2985-00089.

Maurya, P., Saklani, R., Singh, S., et al. (2022) Appraisal of fluoroquinolone-loaded carubinose-linked hybrid nanoparticles for glycotargeting to alveolar macrophages. *Drug Delivery and Translational Research*, 12 (7): 1640–1658. doi:10.1007/S13346-021-01055-9/TABLES/3.

May, R.C., Caron, E., Hall, A., et al. (2000) Involvement of the Arp2/3 complex in phagocytosis mediated by FcγR or CR3. *Nature Cell Biology 2000 2:4*, 2 (4): 246–248. doi:10.1038/35008673.

McGovern, N.N., Cowburn, A.S., Porter, L., et al. (2011) Hypoxia Selectively Inhibits Respiratory Burst Activity and Killing of Staphylococcus aureus in Human Neutrophils. *Journal of immunology (Baltimore, Md. : 1950)*, 186 (1): 453. doi:10.4049/JIMMUNOL.1002213.

McKeown, S., Richter, A.G., O'Kane, C., et al. (2009) MMP expression and abnormal lung permeability are important determinants of outcome in IPF. *European Respiratory Journal*, 33 (1): 77–84. doi:10.1183/09031936.00060708.

Mcmurtrey, R.J. (2016) Analytic Models of Oxygen and Nutrient Diffusion, Metabolism Dynamics, and Architecture Optimization in Three-Dimensional Tissue Constructs with Applications and Insights in Cerebral Organoids. *TISSUE ENGINEERING*, 22 (3). doi:10.1089/ten.tec.2015.0375.

McQuattie-Pimentel, A.C., Ren, Z., Joshi, N., et al. (2021) The lung microenvironment shapes a dysfunctional response of alveolar macrophages in aging. *The Journal of clinical investigation*, 131 (4). doi:10.1172/JCI140299.

Medeiros, A.I., Serezani, C.H., Lee, S.P., et al. (2009) Efferocytosis impairs pulmonary macrophage and lung antibacterial function via PGE2/EP2 signaling. *Journal of Experimental Medicine*, 206 (1): 61–68. doi:10.1084/JEM.20082058.

Medina, C.B. and Ravichandran, K.S. (2016) Do not let death do us part: 'find-me' signals in communication between dying cells and the phagocytes. *Cell Death & Differentiation 2016 23:6*, 23 (6): 979–989. doi:10.1038/cdd.2016.13.

van der Meer, J.H.M., van der Poll, T. and Van't Veer, C. (2014) TAM receptors, Gas6, and protein S: roles in inflammation and hemostasis. *Blood*, 123 (16): 2460–2469. doi:10.1182/BLOOD-2013-09-528752.

Mercer, P.F., Woodcock, H. v., Eley, J.D., et al. (2016) Exploration of a potent PI3 kinase/mTOR inhibitor as a novel anti-fibrotic agent in IPF. *Thorax*, 71 (8): 701–711. doi:10.1136/THORAXJNL-2015-207429.

Metzen, E., Wolff, M., Fandrey, J., et al. (1995) Pericellular PO2 and O2 consumption in monolayer cell cultures. *Respiration Physiology*, 100 (2): 101–106. doi:10.1016/0034-5687(94)00125-J.

Meyer, K.C., Cardoni, A. and Xiang, Z.Z. (2000) Vascular endothelial growth factor in bronchoalveolar lavage from normal subjects and patients with diffuse parenchymal lung disease. *Journal of Laboratory and Clinical Medicine*, 135 (4): 332–338. doi:10.1067/MLC.2000.105618.

Meyer, K.C., Raghu, G., Baughman, R.P., et al. (2012) An official American Thoracic Society clinical practice guideline: the clinical utility of bronchoalveolar lavage cellular analysis in interstitial lung disease. *American journal of respiratory and critical care medicine*, 185 (9): 1004–1014. doi:10.1164/RCCM.201202-0320ST.

Meziani, L., Mondini, M., Petit, B., et al. (2018) CSF1R inhibition prevents radiation pulmonary fibrosis by depletion of interstitial macrophages. *The European respiratory journal*, 51 (3). doi:10.1183/13993003.02120-2017.

Michalski, J.E. and Schwartz, D.A. (2020) Genetic Risk Factors for Idiopathic Pulmonary Fibrosis: Insights into Immunopathogenesis. *Journal of Inflammation Research*, 13: 1305. doi:10.2147/JIR.S280958.

Miller, G.W., Mugler, J.P., Altes, T.A., et al. (2010) A short-breath-hold technique for lung pO2 mapping with 3He MRI. *Magnetic resonance in medicine*, 63 (1): 127–136. doi:10.1002/MRM.22181.

Minakami, R. and Sumimoto, H. (2006) Phagocytosis-coupled activation of the superoxide-producing phagocyte oxidase, a member of the NADPH oxidase (Nox) family. *International Journal of Hematology*, 84 (3): 193–198. doi:10.1532/IJH97.06133/METRICS.

Misharin, A. v., Morales-Nebreda, L., Mutlu, G.M., et al. (2013) Flow cytometric analysis of macrophages and dendritic cell subsets in the mouse lung. *American Journal of Respiratory Cell and Molecular Biology*, 49 (4): 503–510. doi:10.1165/RCMB.2013-0086MA/SUPPL_FILE/DISCLOSURES.PDF.

Misharin, A. V., Morales-Nebreda, L., Reyfman, P.A., et al. (2017) Monocyte-derived alveolar macrophages drive lung fibrosis and persist in the lung over the life span. *Journal of Experimental Medicine*, 214 (8): 2387–2404. doi:10.1084/JEM.20162152.

Mitsi, E., Kamng'ona, R., Rylance, J., et al. (2018) Human alveolar macrophages predominately express combined classical M1 and M2 surface markers in steady state. *Respiratory research*, 19 (1). doi:10.1186/S12931-018-0777-0.

Mitzner, W. and Wagner, E.M. (2004) Vascular remodeling in the circulations of the lung. *https://doi.org/10.1152/japplphysiol.00473.2004*, 97 (5): 1999–2004. doi:10.1152/JAPPLPHYSIOL.00473.2004.

Miyazono, K. and Heldin, C.H. (1989) Role for carbohydrate structures in TGF-beta 1 latency. *Nature*, 338 (6211): 158–160. doi:10.1038/338158A0.

Mizuno, S., Bogaard, H.J., Voelkel, N.F., et al. (2009) Hypoxia regulates human lung fibroblast proliferation via p53-dependent and -independent pathways. *Respiratory Research*, 10 (1): 1–12. doi:10.1186/1465-9921-10-17/FIGURES/7_731.

Molyneaux, P.L., Cox, M.J., Willis-Owen, S.A.G., et al. (2014) The role of bacteria in the pathogenesis and progression of idiopathic pulmonary fibrosis. *American Journal of Respiratory and Critical Care Medicine*, 190 (8): 906–913. doi:10.1164/RCCM.201403-0541OC.

Moore, B.B., Lawson, W.E., Oury, T.D., et al. (2013) Animal models of fibrotic lung disease. *American Journal of Respiratory Cell and Molecular Biology*, 49 (2): 167–179. doi:10.1165/RCMB.2013-0094TR/SUPPL_FILE/DISCLOSURES.PDF.

Moore, C.E.J., Mikolajek, H., Mota, S.R. da, et al. (2015) Elongation Factor 2 Kinase Is Regulated by Proline Hydroxylation and Protects Cells during Hypoxia. *Molecular and Cellular Biology*, 35 (10): 1788. doi:10.1128/MCB.01457-14.

Mora, A.L., Torres-González, E., Rojas, M., et al. (2006) Activation of Alveolar Macrophages via the Alternative Pathway in Herpesvirus-Induced Lung Fibrosis. *American Journal of Respiratory Cell and Molecular Biology*, 35 (4): 466. doi:10.1165/RCMB.2006-0121OC.

Morales-Nebreda, L., Misharin, A. v., Perlman, H., et al. (2015) The heterogeneity of lung macrophages in the susceptibility to disease. *European respiratory review : an official journal of the European Respiratory Society*, 24 (137): 505–509. doi:10.1183/16000617.0031-2015.

Morimoto, K., Janssen, W.J. and Terada, M. (2012) Defective efferocytosis by alveolar macrophages in IPF patients. *Respiratory Medicine*, 106 (12): 1800–1803.

doi:10.1016/J.RMED.2012.08.020/ATTACHMENT/2865C4FB-EF01-4D78-8151-3149B45C044A/MMC1.DOCX.

Morioka, S., Perry, J.S.A., Raymond, M.H., et al. (2018) Efferocytosis induces a novel SLC program to promote glucose uptake and lactate release. *Nature*, 563 (7733): 714–718. doi:10.1038/S41586-018-0735-5.

Mostafaei, S., Sayad, B., Azar, M.E.F., et al. (2021) The role of viral and bacterial infections in the pathogenesis of IPF: a systematic review and meta-analysis. *Respiratory Research*, 22 (1): 1–14. doi:10.1186/S12931-021-01650-X/FIGURES/6.

Mould, K.J., Barthel, L., Mohning, M.P., et al. (2017) Cell origin dictates programming of resident versus recruited macrophages during acute lung injury. *American Journal of Respiratory Cell and Molecular Biology*, 57 (3): 294–306. doi:10.1165/RCMB.2017-0061OC/SUPPL_FILE/DISCLOSURES.PDF.

Mould, K.J., Jackson, N.D., Henson, P.M., et al. (2019) Single cell RNA sequencing identifies unique inflammatory airspace macrophage subsets. *JCI Insight*, 4 (5). doi:10.1172/JCI.INSIGHT.126556.

Mould, K.J., Moore, C.M., McManus, S.A., et al. (2021) Airspace macrophages and monocytes exist in transcriptionally distinct subsets in healthy adults. *American Journal of Respiratory and Critical Care Medicine*, 203 (8): 946–956. doi:10.1164/RCCM.202005-1989OC/SUPPL_FILE/DISCLOSURES.PDF.

Muckenthaler, M.U., Rivella, S., Hentze, M.W., et al. (2017) A Red Carpet for Iron Metabolism. *Cell*, 168 (3): 344–361. doi:10.1016/J.CELL.2016.12.034.

Mukundan, L., Odegaard, J.I., Morel, C.R., et al. (2009) PPAR-delta senses and orchestrates clearance of apoptotic cells to promote tolerance. *Nature medicine*, 15 (11): 1266–1272. doi:10.1038/NM.2048.

Murray, J.K., Balan, C., Allgeier, A.M., et al. (2010) Dipeptidyl-quinolone derivatives inhibit hypoxia inducible factor-1α prolyl hydroxylases-1, -2, and -3 with altered selectivity. *Journal of Combinatorial Chemistry*, 12 (5): 676–686. doi:10.1021/CC100073A/SUPPL_FILE/CC100073A_SI_001.PDF.

Murray, L.A., Chen, Q., Kramer, M.S., et al. (2011) TGF-beta driven lung fibrosis is macrophage dependent and blocked by Serum amyloid P. *The international journal of biochemistry & cell biology*, 43 (1): 154–162. doi:10.1016/J.BIOCEL.2010.10.013.

Murray, L.A., Habiel, D.M., Hohmann, M., et al. (2017) Antifibrotic role of vascular endothelial growth factor in pulmonary fibrosis. *JCI Insight*, 2 (16). doi:10.1172/JCI.INSIGHT.92192.

Murray, P.J., Allen, J.E., Biswas, S.K., et al. (2014) Macrophage Activation and Polarization: Nomenclature and Experimental Guidelines. *Immunity*, 41 (1): 14–20. doi:10.1016/j.immuni.2014.06.008.

Myall, K., Martinovic, J., Wu, Z., et al. (2022) "Nocturnal hypoxaemia is associated with mortality in patients with fibrotic interstitial lung diseas." In *European Respiratory Society International Congress*. Barcelona, 2022.

Nagai, S., Aung, H., Takeuchi, M., et al. (1991) IL-1 and IL-1 Inhibitory Activity in the Culture Supernatants of Alveolar Macrophages from Patients with Interstitial Lung Diseases*. *Chest*, 99 (3): 674–680. doi:10.1378/CHEST.99.3.674.

Nagata, S. (2018) Apoptosis and Clearance of Apoptotic Cells. *Annual review of immunology*, 36: 489–517. doi:10.1146/ANNUREV-IMMUNOL-042617-053010.

Naik, P.K. and Moore, B.B. (2014) Viral infection and aging as cofactors for the development of pulmonary fibrosis. *http://dx.doi.org/10.1586/ers.10.73*, 4 (6): 759–771. doi:10.1586/ERS.10.73.

Nakagome, K., Dohi, M., Okunishi, K., et al. (2006) In vivo IL-10 gene delivery attenuates bleomycin induced pulmonary fibrosis by inhibiting the production and activation of TGF-β in the lung. *Thorax*, 61 (10): 886–894. doi:10.1136/THX.2005.056317.

Nalysnyk, L., Cid-Ruzafa, J., Rotella, P., et al. (2012) Incidence and prevalence of idiopathic pulmonary fibrosis: review of the literature. *European Respiratory Review*, 21 (126): 355–361. doi:10.1183/09059180.00002512.

Nanduri, J., Wang, N., Yuan, G., et al. (2009) Intermittent hypoxia degrades HIF-2alpha via calpains resulting in oxidative stress: implications for recurrent apnea-induced morbidities. *Proceedings of the National Academy of Sciences of the United States of America*, 106 (4): 1199–1204. doi:10.1073/PNAS.0811018106.

Narita, T., Yin, S., Gelin, C.F., et al. (2009) Identification of a novel small molecule HIF-1alpha translation inhibitor. *Clinical cancer research : an official journal of the American Association for Cancer Research*, 15 (19): 6128–6136. doi:10.1158/1078-0432.CCR-08-3180.

Nayak, A., Dodagatta-Marri, E., Tsolaki, A.G., et al. (2012) An Insight into the Diverse Roles of Surfactant Proteins, SP-A and SP-D in Innate and Adaptive Immunity. *Frontiers in immunology*, 3 (JUN). doi:10.3389/FIMMU.2012.00131.

Nayak, D.K., Mendez, O., Bowen, S., et al. (2018) Isolation and In Vitro Culture of Murine and Human Alveolar Macrophages. *Journal of Visualized Experiments : JoVE*, 2018 (134): 57287. doi:10.3791/57287.

Neuhaus, V., Schaudien, D., Golovina, T., et al. (2017) Assessment of long-term cultivated human precision-cut lung slices as an ex vivo system for evaluation of chronic cytotoxicity and functionality. *Journal of Occupational Medicine and Toxicology*, 12 (1): 1–8. doi:10.1186/S12995-017-0158-5/FIGURES/5.

NICE (2018) Pirfenidone for treating Idiopathic Pulmonary Fibrosis. *National Institute for Health and Care Excellence*, (April): 1–69. Available at: www.nice.org.uk/guidance/ta504.

Nimmerjahn, F. and Ravetch, J. v. (2006) Fcγ Receptors: Old Friends and New Family Members. *Immunity*, 24 (1): 19–28. doi:10.1016/J.IMMUNI.2005.11.010.

Nishi, Y., Sano, H., Kawashima, T., et al. (2007) Role of galectin-3 in human pulmonary fibrosis. *Allergology international : official journal of the Japanese Society of Allergology*, 56 (1): 57–65. doi:10.2332/ALLERGOLINT.O-06-449.

Nizamoglu, M., de Hilster, R.H.J., Zhao, F., et al. (2022) An in vitro model of fibrosis using crosslinked native extracellular matrix-derived hydrogels to modulate biomechanics without changing composition. *Acta Biomaterialia*, 147: 50–62. doi:10.1016/J.ACTBIO.2022.05.031.

Norris, P.C., Libreros, S. and Serhan, C.N. (2019) Resolution metabolomes activated by hypoxic environment. *Science Advances*, 5 (10): 4895–4918. doi:10.1126/SCIADV.AAX4895/SUPPL_FILE/AAX4895_SM.PDF.

Noth, I., Zhang, Y., Ma, S.F., et al. (2013) Genetic variants associated with idiopathic pulmonary fibrosis susceptibility and mortality: a genome-wide association study. *The Lancet. Respiratory medicine*, 1 (4): 309–317. doi:10.1016/S2213-2600(13)70045-6.

Novak, C.M., Sethuraman, S., Luikart, K.L., et al. (2023) Alveolar macrophages drive lung fibroblast function during idiopathic pulmonary fibrosis. *American Journal of Physiology-Lung Cellular and Molecular Physiology*. doi:10.1152/AJPLUNG.00263.2022.

Ó Maoldomhnaigh, C., Cox, D.J., Phelan, J.J., et al. (2021) Lactate Alters Metabolism in Human Macrophages and Improves Their Ability to Kill Mycobacterium tuberculosis. *Frontiers in Immunology*, 12: 1. doi:10.3389/FIMMU.2021.663695/FULL.

O'Driscoll, B.R., Howard, L.S., Earis, J., et al. (2017) BTS guideline for oxygen use in adults in healthcare and emergency settings. *Thorax*, 72 (Suppl 1): ii1–ii90. doi:10.1136/THORAXJNL-2016-209729.

Oida, T. and Weiner, H.L. (2010) Depletion of TGF-β from fetal bovine serum. *Journal of immunological methods*, 362 (1–2): 195. doi:10.1016/J.JIM.2010.09.008.

Olazabal, I.M., Caron, E., May, R.C., et al. (2002) Rho-Kinase and Myosin-II Control Phagocytic Cup Formation during CR, but Not FcγR, Phagocytosis. *Current Biology*, 12 (16): 1413–1418. doi:10.1016/S0960-9822(02)01069-2.

Oldenborg, P.A., Zheleznyak, A., Fang, Y.F., et al. (2000) Role of CD47 as a marker of self on red blood cells. *Science*, 288 (5473): 2051–2054. doi:10.1126/SCIENCE.288.5473.2051/ASSET/119CF8ED-AA9E-446B-847B-A999FD87BD29/ASSETS/GRAPHIC/SE2208601004.JPEG.

Otto, N.A., Pereverzeva, L., Leopold, V., et al. (2021) Hypoxia-Inducible Factor-1α in Macrophages, but Not in Neutrophils, Is Important for Host Defense during Klebsiella pneumoniae-Induced Pneumosepsis. *Mediators of Inflammation*, 2021. doi:10.1155/2021/9958281.

Palayoor, S.T., Mitchell, J.B., Cerna, D., et al. (2008) PX-478, an inhibitor of hypoxia-inducible factor-1alpha, enhances radiosensitivity of prostate carcinoma cells. *International journal of cancer*, 123 (10): 2430–2437. doi:10.1002/IJC.23807.

Palsson-Mcdermott, E.M., Curtis, A.M., Goel, G., et al. (2015) Pyruvate kinase M2 regulates Hif-1α activity and IL-1β induction and is a critical determinant of the warburg effect in LPS-activated macrophages. *Cell metabolism*, 21 (1): 65–80. doi:10.1016/J.CMET.2014.12.005.

Park, D., Han, C.Z., Elliott, M.R., et al. (2011) Continued clearance of apoptotic cells critically depends on the phagocyte Ucp2 protein. *Nature 2011 477:7363*, 477 (7363): 220–224. doi:10.1038/nature10340.

Park, D., Hochreiter-Hufford, A. and Ravichandran, K.S. (2009) The Phosphatidylserine Receptor TIM-4 Does Not Mediate Direct Signaling. *Current Biology*, 19 (4): 346–351. doi:10.1016/J.CUB.2009.01.042.

Park, H. and Cox, D. (2009) Cdc42 regulates Fcγ receptor-mediated phagocytosis through the activation and phosphorylation of Wiskott-Aldrich syndrome protein (WASP) and neural-WASP. *Molecular Biology of the Cell*, 20 (21): 4500–4508. doi:10.1091/MBC.E09-03-0230/ASSET/IMAGES/LARGE/ZMK0210992290007.JPEG.

Park, Y., Ahn, C. and Kim, T.H. (2021) Occupational and environmental risk factors of idiopathic pulmonary fibrosis: a systematic review and meta-analyses. *Scientific Reports 2021 11:1*, 11 (1): 1–10. doi:10.1038/s41598-021-81591-z.

Pashover-Schallinger, E., Aswad, M., Schif-Zuck, S., et al. (2012) The atypical chemokine receptor D6 controls macrophage efferocytosis and cytokine secretion during the resolution of inflammation. *The FASEB Journal*, 26 (9): 3891–3900. doi:10.1096/FJ.11-194894.

Pattle, R.E. (1955) Properties, Function and Origin of the Alveolar Lining Layer. *Nature 1955 175:4469*, 175 (4469): 1125–1126. doi:10.1038/1751125b0.

Pavlacky, J. and Polak, J. (2020) Technical Feasibility and Physiological Relevance of Hypoxic Cell Culture Models. *Frontiers in Endocrinology*, 11: 57. doi:10.3389/FENDO.2020.00057/BIBTEX.

Pechkovsky, D. v., Prasse, A., Kollert, F., et al. (2010) Alternatively activated alveolar macrophages in pulmonary fibrosis-mediator production and intracellular signal transduction. *Clinical immunology (Orlando, Fla.)*, 137 (1): 89–101. doi:10.1016/J.CLIM.2010.06.017.

Peiser, L., Gough, P.J., Kodama, T., et al. (2000) Macrophage class A scavenger receptor-mediated phagocytosis of Escherichia coli: Role of cell heterogeneity, microbial strain, and culture conditions in vitro. *Infection and Immunity*, 68 (4): 1953–1963. doi:10.1128/IAI.68.4.1953-1963.2000/ASSET/9E548E60-DBC0-4439-9702-A6EB684FAB87/ASSETS/GRAPHIC/II0401454009.JPEG.

Peljto, A.L., Zhang, Y., Fingerlin, T.E., et al. (2013) Association Between the MUC5B Promoter Polymorphism and Survival in Patients With Idiopathic Pulmonary Fibrosis. *JAMA*, 309 (21): 2232–2239. doi:10.1001/JAMA.2013.5827.

Peng, R., Sridhar, S., Tyagi, G., et al. (2013) Bleomycin induces molecular changes directly relevant to idiopathic pulmonary fibrosis: a model for “active” disease. *PloS one*, 8 (4). doi:10.1371/JOURNAL.PONE.0059348.

Pereverzeva, L., van Linge, C.C.A., Schuurman, A.R., et al. (2022) Human alveolar macrophages do not rely on glucose metabolism upon activation by lipopolysaccharide. *Biochimica et Biophysica Acta (BBA) - Molecular Basis of Disease*, 1868 (10): 166488. doi:10.1016/J.BBADIS.2022.166488.

Pesce, J.T., Ramalingam, T.R., Mentink-Kane, M.M., et al. (2009) Arginase-1-expressing macrophages suppress Th2 cytokine-driven inflammation and fibrosis. *PLoS pathogens*, 5 (4). doi:10.1371/JOURNAL.PPAT.1000371.

Phan, T.H.G., Paliogiannis, P., Nasrallah, G.K., et al. (2020) Emerging cellular and molecular determinants of idiopathic pulmonary fibrosis. *Cellular and Molecular Life Sciences 2020 78:5*, 78 (5): 2031–2057. doi:10.1007/S00018-020-03693-7.

Place, T.L., Domann, F.E. and Case, A.J. (2017) Limitations of oxygen delivery to cells in culture: An underappreciated problem in basic and translational research. *Free Radical Biology and Medicine*, 113: 311–322. doi:10.1016/J.FREERADBIOMED.2017.10.003.

Porter, J.C., Win, T., Erlandsson, K., et al. (2021) Measurement of hypoxia in the lung in idiopathic pulmonary fibrosis: an F-MISO PET/CT study. *The European respiratory journal*, 58 (4). doi:10.1183/13993003.04584-2020.

Prasse, A., Pechkovsky, D. v., Toews, G.B., et al. (2006) A vicious circle of alveolar macrophages and fibroblasts perpetuates pulmonary fibrosis via CCL18. *American journal of respiratory and critical care medicine*, 173 (7): 781–792. doi:10.1164/RCCM.200509-1518OC.

Proulx-Bonneau, S., Guezguez, A. and Annabi, B. (2011) A Concerted HIF-1α/MT1-MMP Signalling Axis Regulates the Expression of the 3BP2 Adaptor Protein in Hypoxic Mesenchymal Stromal Cells. *PLOS ONE*, 6 (6): e21511. doi:10.1371/JOURNAL.PONE.0021511.

Puttur, F., Gregory, L.G., Lloyd, C.M., et al. (2019) Airway macrophages as the guardians of tissue repair in the lung. *Immunology and Cell Biology*, 97 (3): 246–257. doi:10.1111/IMCB.12235.

Puxeddu, E., Comandini, A., Cavalli, F., et al. (2014) Iron laden macrophages in idiopathic pulmonary fibrosis: The telltale of occult alveolar hemorrhage? *Pulmonary Pharmacology & Therapeutics*, 28 (1): 35–40. doi:10.1016/J.PUPT.2013.12.002.

Qie, J., Liu, Y., Wang, Y., et al. (2022) Integrated proteomic and transcriptomic landscape of macrophages in mouse tissues. *Nature communications*, 13 (1): 7389. doi:10.1038/S41467-022-35095-7.

Raggi, F., Pelassa, S., Pierobon, D., et al. (2017) Regulation of human Macrophage M1-M2 Polarization Balance by hypoxia and the Triggering receptor expressed on Myeloid cells-1. *Frontiers in Immunology*, 8 (SEP): 1097. doi:10.3389/FIMMU.2017.01097/BIBTEX.

Raghu, G., Brown, K.K., Costabel, U., et al. (2008) Treatment of idiopathic pulmonary fibrosis with etanercept: an exploratory, placebo-controlled trial. *American journal of respiratory and critical care medicine*, 178 (9): 948–955. doi:10.1164/RCCM.200709-1446OC.

Raghu, G., Chen, S.Y., Yeh, W.S., et al. (2014) Idiopathic pulmonary fibrosis in US Medicare beneficiaries aged 65 years and older: incidence, prevalence, and survival, 2001-11. *The Lancet. Respiratory medicine*, 2 (7): 566–572. doi:10.1016/S2213-2600(14)70101-8.

Raghu, G., Collard, H.R., Egan, J.J., et al. (2011) An official ATS/ERS/JRS/ALAT statement: idiopathic pulmonary fibrosis: evidence-based guidelines for diagnosis and management. *American journal of respiratory and critical care medicine*, 183 (6): 788–824. doi:10.1164/RCCM.2009-040GL.

Raghu, G., Remy-Jardin, M., Myers, J.L., et al. (2018) AMERICAN THORACIC SOCIETY DOCUMENTS Diagnosis of Idiopathic Pulmonary Fibrosis An Official ATS/ERS/JRS/ALAT Clinical Practice Guideline. *JAPANESE RESPIRATORY SOCIETY*. doi:10.1164/rccm.201807-1255ST.

Raghu, G., Remy-Jardin, M., Richeldi, L., et al. (2022) Idiopathic Pulmonary Fibrosis (an Update) and Progressive Pulmonary Fibrosis in Adults: An Official ATS/ERS/JRS/ALAT Clinical Practice Guideline. *https://doi.org/10.1164/rccm.202202-0399ST*, 205 (9): E18–E47. doi:10.1164/RCCM.202202-0399ST.

Raleigh, J.A. and Koch, C.J. (1990) Importance of thiols in the reductive binding of 2-nitroimidazoles to macromolecules. *Biochemical pharmacology*, 40 (11): 2457–2464. doi:10.1016/0006-2952(90)90086-Z.

Ramirez-Moral, I., Ferreira, B.L., Butler, J.M., et al. (2022) HIF-1α Stabilization in Flagellin-Stimulated Human Bronchial Cells Impairs Barrier Function. *Cells*, 11 (3). doi:10.3390/CELLS11030391/S1.

Rauschmeier, R., Gustafsson, C., Reinhardt, A., et al. (2019) Bhlhe40 and Bhlhe41 transcription factors regulate alveolar macrophage self-renewal and identity. *The EMBO journal*, 38 (19). doi:10.15252/EMBJ.2018101233.

Recalcati, S. and Cairo, G. (2021) Macrophages and Iron: A Special Relationship. *Biomedicines*, 9 (11). doi:10.3390/BIOMEDICINES9111585.

Reinert, T., Baldotto, C.S. da R., Nunes, F.A.P., et al. (2013) Bleomycin-Induced Lung Injury. *Journal of Cancer Research*, 2013: 1–9. doi:10.1155/2013/480608.

Del Rey, M.J., Valín, Á., Usategui, A., et al. (2017) Hif-1α Knockdown Reduces Glycolytic Metabolism and Induces Cell Death of Human Synovial Fibroblasts Under Normoxic Conditions. *Scientific Reports 2017 7:1*, 7 (1): 1–10. doi:10.1038/s41598-017-03921-4.

Rink, J., Ghigo, E., Kalaidzidis, Y., et al. (2005) Rab Conversion as a Mechanism of Progression from Early to Late Endosomes. *Cell*, 122 (5): 735–749. doi:10.1016/J.CELL.2005.06.043.

Rius, J., Guma, M., Schachtrup, C., et al. (2008) NF-κB links innate immunity to the hypoxic response through transcriptional regulation of HIF-1α. *Nature 2008 453:7196*, 453 (7196): 807–811. doi:10.1038/nature06905.

Robinson, C.M., Neary, R., Levendale, A., et al. (2012) Hypoxia-induced DNA hypermethylation in human pulmonary fibroblasts is associated with Thy-1 promoter methylation and the development of a pro-fibrotic phenotype. *Respiratory Research*, 13 (1): 1–9. doi:10.1186/1465-9921-13-74/FIGURES/5.

Rogers, C., Fernandes-Alnemri, T., Mayes, L., et al. (2017) Cleavage of DFNA5 by caspase-3 during apoptosis mediates progression to secondary necrotic/pyroptotic cell death. *Nature Communications 2017 8:1*, 8 (1): 1–14. doi:10.1038/ncomms14128.

Romero, F., Shah, D., Duong, M., et al. (2015) A pneumocyte-macrophage paracrine lipid axis drives the lung toward fibrosis. *American Journal of Respiratory Cell and Molecular Biology*, 53 (1): 74–86. doi:10.1165/RCMB.2014-0343OC/SUPPL_FILE/DISCLOSURES.PDF.

Rosales, C. (2007) Fc receptor and integrin signaling in phagocytes. *Signal Transduction*, 7 (5–6): 386–401. doi:10.1002/SITA.200700141.

Rosales, C. and Uribe-Querol, E. (2013) Fc receptors: Cell activators of antibody functions. *Advances in Bioscience and Biotechnology*, 2013 (04): 21–33. doi:10.4236/ABB.2013.44A004.

Rőszer, T., Menéndez-Gutiérrez, M.P., Lefterova, M.I., et al. (2011) Autoimmune kidney disease and impaired engulfment of apoptotic cells in mice with macrophage peroxisome proliferator-activated receptor gamma or retinoid X receptor alpha deficiency. *Journal of immunology (Baltimore, Md. : 1950)*, 186 (1): 621–631. doi:10.4049/JIMMUNOL.1002230.

Rubio, K., Singh, I., Dobersch, S., et al. (2019) Inactivation of nuclear histone deacetylases by EP300 disrupts the MiCEE complex in idiopathic pulmonary fibrosis. *Nature Communications 2019 10:1*, 10 (1): 1–16. doi:10.1038/s41467-019-10066-7.

Sabha, N., Aitken, K., Lorenzo, A.J., et al. (2006) Matrix metalloproteinase-7 and epidermal growth factor receptor mediate hypoxia-induced extracellular signal-regulated kinase 1/2 mitogen-activated protein kinase activation and subsequent proliferation in bladder smooth muscle cells. *In Vitro Cellular and Developmental Biology - Animal*, 42 (5–6): 124–133. doi:10.1290/0510070.1/METRICS.

Saito, A., Horie, M. and Nagase, T. (2018) TGF-β Signaling in Lung Health and Disease. *International Journal of Molecular Sciences 2018, Vol. 19, Page 2460*, 19 (8): 2460. doi:10.3390/IJMS19082460.

Saleh, K.S., Hewawasam, R., Šerbedžija, P., et al. (2022) Engineering Hybrid-Hydrogels Comprised of Healthy or Diseased Decellularized Extracellular Matrix to Study Pulmonary Fibrosis. *Cellular and Molecular Bioengineering*, 15 (5): 505–519. doi:10.1007/S12195-022-00726-Y/FIGURES/5.

Sang, N., Stiehl, D.P., Bohensky, J., et al. (2003) MAPK signaling up-regulates the activity of hypoxia-inducible factors by its effects on p300. *The Journal of biological chemistry*, 278 (16): 14013–14019. doi:10.1074/JBC.M209702200.

Savill, J., Hogg, N., Ren, Y., et al. (1992) Thrombospondin cooperates with CD36 and the vitronectin receptor in macrophage recognition of neutrophils undergoing apoptosis. *The Journal of clinical investigation*, 90 (4): 1513–1522. doi:10.1172/JCI116019.

Schaer, D.J., Alayash, A.I. and Buehler, P.W. (2007) Gating the radical hemoglobin to macrophages: The anti-inflammatory role of CD163, a scavenger receptor. *Antioxidants and Redox Signaling*, 9 (7): 991–999. doi:10.1089/ars.2007.1576.

Scheuermann, T.H., Li, Q., Ma, H.W., et al. (2013) Allosteric inhibition of hypoxia inducible factor-2 with small molecules. *Nature chemical biology*, 9 (4): 271–276. doi:10.1038/NCHEMBIO.1185.

Schiff, D.E., Kline, L., Soldau, K., et al. (1997) Phagocytosis of Gram-negative bacteria by a unique CD14-dependent mechanism. *Journal of Leukocyte Biology*, 62 (6): 786–794. doi:10.1002/JLB.62.6.786.

Schilperoort, M., Ngai, D., Katerelos, M., et al. (2023) PFKFB2-mediated glycolysis promotes lactate-driven continual efferocytosis by macrophages. *Nature Metabolism 2023*, pp. 1–14. doi:10.1038/s42255-023-00736-8.

Scholz, C.C., Cavadas, M.A.S., Tambuwala, M.M., et al. (2013) Regulation of IL-1β-induced NF-κB by hydroxylases links key hypoxic and inflammatory signaling pathways. *Proceedings of the National Academy of Sciences of the United States of America*, 110 (46): 18490–18495. doi:10.1073/PNAS.1309718110.

Schupp, J.C., Binder, H., Jäger, B., et al. (2015) Macrophage activation in acute exacerbation of idiopathic pulmonary fibrosis. *PloS one*, 10 (1). doi:10.1371/JOURNAL.PONE.0116775.

Schyns, J., Bai, Q., Ruscitti, C., et al. (2019) Non-classical tissue monocytes and two functionally distinct populations of interstitial macrophages populate the mouse lung. *Nature Communications 2019 10:1*, 10 (1): 1–16. doi:10.1038/s41467-019-11843-0.

Segawa, K., Kurata, S., Yanagihashi, Y., et al. (2014) Caspase-mediated cleavage of phospholipid flippase for apoptotic phosphatidylserine exposure. *Science (New York, N.Y.)*, 344 (6188): 1164–1168. doi:10.1126/SCIENCE.1252809.

Seibold, M.A., Wise, A.L., Speer, M.C., et al. (2011) A Common MUC5B Promoter Polymorphism and Pulmonary Fibrosis. *The New England Journal of Medicine*, 364 (16): 1503. doi:10.1056/NEJMOA1013660.

Selman, M., Ruiz, V., Cabrera, S., et al. (2000) TIMP-1, -2, -3, and -4 in idiopathic pulmonary fibrosis. A prevailing nondegradative lung microenvironment? *American journal of physiology. Lung cellular and molecular physiology*, 279 (3). doi:10.1152/AJPLUNG.2000.279.3.L562.

Semba, H., Takeda, N., Isagawa, T., et al. (2016) HIF-1α-PDK1 axis-induced active glycolysis plays an essential role in macrophage migratory capacity. *Nature Communications 2016 7:1*, 7 (1): 1–10. doi:10.1038/ncomms11635.

Senavirathna, L.K., Huang, C., Yang, X., et al. (2018) Hypoxia induces pulmonary fibroblast proliferation through NFAT signaling. *Scientific Reports 2018 8:1*, 8 (1): 1–16. doi:10.1038/s41598-018-21073-x.

Sha, X., Dai, Y., Chong, L., et al. (2022) Pro-efferocytic macrophage membrane biomimetic nanoparticles for the synergistic treatment of atherosclerosis via competition effect. *Journal of Nanobiotechnology*, 20 (1): 1–22. doi:10.1186/S12951-022-01720-2/FIGURES/8.

Shaykhiev, R., Krause, A., Salit, J., et al. (2009) Smoking-dependent reprogramming of alveolar macrophage polarization: implication for pathogenesis of chronic obstructive pulmonary disease. *Journal of immunology (Baltimore, Md. : 1950)*, 183 (4): 2867–2883. doi:10.4049/JIMMUNOL.0900473.

Sheng, G., Chen, P., Wei, Y., et al. (2020) Viral Infection Increases the Risk of Idiopathic Pulmonary Fibrosis: A Meta-Analysis. *Chest*, 157 (5): 1175–1187. doi:10.1016/j.chest.2019.10.032.

Shi, M., Zhu, J., Wang, R., et al. (2011) Latent TGF-β structure and activation. *Nature 2011 474:7351*, 474 (7351): 343–349. doi:10.1038/nature10152.

Shi, Z., Xu, L., Xie, H., et al. (2020) Attenuation of intermittent hypoxia-induced apoptosis and fibrosis in pulmonary tissues via suppression of ER stress activation. *BMC Pulmonary Medicine*, 20 (1): 1–11. doi:10.1186/S12890-020-1123-0/FIGURES/6.

Shin, D.H., Dier, U., Melendez, J.A., et al. (2015) Regulation of MMP-1 expression in response to hypoxia is dependent on the intracellular redox status of metastatic bladder cancer cells. *Biochimica et biophysica acta*, 1852 (12): 2593. doi:10.1016/J.BBADIS.2015.09.001.

Simler, N.R., Brenchley, P.E., Horrocks, A.W., et al. (2004) Angiogenic cytokines in patients with idiopathic interstitial pneumonia. *Thorax*, 59 (7): 581–585. doi:10.1136/THX.2003.009860.

Singh, A., Chakraborty, S., Wong, S.W., et al. (2022) Nanoparticle targeting of de novo profibrotic macrophages mitigates lung fibrosis. *Proceedings of the National Academy of Sciences of the United States of America*, 119 (15). doi:10.1073/PNAS.2121098119/-/DCSUPPLEMENTAL.

Skold, C.M., Hed, J. and Eklund, A. (1992) Smoking Cessation Rapidly Reduces Cell Recovery in Bronchoalveolar Lavage Fluid, While Alveolar Macrophage Fluorescence Remains High. *Chest*, 101 (4): 989–995. doi:10.1378/CHEST.101.4.989.

Snell, N., Strachan, D., Hubbard, R., et al. (2016) P272 Epidemiology of idiopathic pulmonary fibrosis in the uk: findings from the british lung foundation's 'respiratory health of the nation' project. *Thorax*, 71 (Suppl 3): A236–A236. doi:10.1136/THORAXJNL-2016-209333.415.

Song, C., Li, H., Li, Y., et al. (2019) NETs promote ALI/ARDS inflammation by regulating alveolar macrophage polarization. *Experimental Cell Research*, 382 (2): 111486. doi:10.1016/J.YEXCR.2019.06.031.

Soroosh, P., Doherty, T.A., Duan, W., et al. (2013) Lung-resident tissue macrophages generate Foxp3+ regulatory T cells and promote airway tolerance. *Journal of Experimental Medicine*, 210 (4): 775–788. doi:10.1084/JEM.20121849.

Soucie, E.L., Weng, Z., Geirsdóttir, L., et al. (2016) Lineage-specific enhancers activate self-renewal genes in macrophages and embryonic stem cells. *Science (New York, N.Y.)*, 351 (6274): aad5510. doi:10.1126/SCIENCE.AAD5510.

Spek, C.A. and Duitman, J.W. (2019) Is idiopathic pulmonary fibrosis a cancer-like disease? Transcriptome analysis to fuel the debate. *ERJ Open Research*, 5 (1). doi:10.1183/23120541.00157-2018.

Spira, A., Beane, J., Shah, V., et al. (2004) Effects of cigarette smoke on the human airway epithelial cell transcriptome. *Proceedings of the National Academy of Sciences of the United States of America*, 101 (27): 10143–10148. doi:10.1073/PNAS.0401422101.

Stegmayr, J., Alsafadi, H.N., Lindstedt, S., et al. (2021) Human precision-cut lung slices generated from excess donor lungs as a model for IPF and drug screening. *ERJ Open Research*, 7 (suppl 6): 106. doi:10.1183/23120541.LSC-2021.106.

Stijn, W., Verleden Stijn, E., Vanaudenaerde Bart, M., et al. (2013) Multiplex protein profiling of bronchoalveolar lavage in idiopathic pulmonary fibrosis and hypersensitivity pneumonitis. *Annals of Thoracic Medicine*, 8 (1): 38. doi:10.4103/1817-1737.105718.

Stout-Delgado, H.W., Cho, S.J., Chu, S.G., et al. (2016) Age-Dependent Susceptibility to Pulmonary Fibrosis Is Associated with NLRP3 Inflammasome Activation. *American journal of respiratory cell and molecular biology*, 55 (2): 252–263. doi:10.1165/RCMB.2015-0222OC.

Strieter, R.M., Keeley, E.C., Hughes, M.A., et al. (2009) The role of circulating mesenchymal progenitor cells (fibrocytes) in the pathogenesis of pulmonary fibrosis. *Journal of Leukocyte Biology*, 86 (5): 1111–1118. doi:10.1189/JLB.0309132.

Strikoudis, A., Cieślak, A., Loffredo, L., et al. (2019) Modeling of Fibrotic Lung Disease Using 3D Organoids Derived from Human Pluripotent Stem Cells. *Cell Reports*, 27 (12): 3709-3723.e5. doi:10.1016/j.celrep.2019.05.077.

Subramanian, S., Busch, C.J.L., Molawi, K., et al. (2022a) Long-term culture-expanded alveolar macrophages restore their full epigenetic identity after transfer in vivo. *Nature Immunology 2022 23:3*, 23 (3): 458–468. doi:10.1038/s41590-022-01146-w.

Subramanian, S., Busch, C.J.L., Molawi, K., et al. (2022b) Long-term culture-expanded alveolar macrophages restore their full epigenetic identity after transfer in vivo. *Nature Immunology 2022 23:3*, 23 (3): 458–468. doi:10.1038/s41590-022-01146-w.

Surolia, R., Li, F.J., Wang, Z., et al. (2017) 3D pulmospheres serve as a personalized and predictive multicellular model for assessment of antifibrotic drugs. *JCI Insight*, 2 (2). doi:10.1172/jci.insight.91377.

Suryadevara, V., Ramchandran, R., Kamp, D.W., et al. (2020) Lipid Mediators Regulate Pulmonary Fibrosis: Potential Mechanisms and Signaling Pathways. *International journal of molecular sciences*, 21 (12): 1–46. doi:10.3390/IJMS21124257.

Svedberg, F.R., Brown, S.L., Krauss, M.Z., et al. (2019a) The lung environment controls alveolar macrophage metabolism and responsiveness in type 2 inflammation. *Nature immunology*, 20 (5): 571–580. doi:10.1038/S41590-019-0352-Y.

Svedberg, F.R., Brown, S.L., Krauss, M.Z., et al. (2019b) The lung environment controls alveolar macrophage metabolism and responsiveness in type 2 inflammation. *Nature immunology*, 20 (5): 571–580. doi:10.1038/S41590-019-0352-Y.

Swanson, J.A., Johnson, M.T., Beningo, K., et al. (1999) A contractile activity that closes phagosomes in macrophages. *Journal of Cell Science*, 112 (3): 307–316. doi:10.1242/JCS.112.3.307.

Syrjä, P., Heikkilä, H.P., Lilja-Maula, L., et al. (2013) The Histopathology of Idiopathic Pulmonary Fibrosis in West Highland White Terriers Shares Features of Both Non-specific Interstitial Pneumonia and Usual Interstitial Pneumonia in Man. *Journal of Comparative Pathology*, 149 (2–3): 303–313. doi:10.1016/J.JCPA.2013.03.006.

Takeda, N., O'Dea, E.L., Doedens, A., et al. (2010) Differential activation and antagonistic function of HIF-{alpha} isoforms in macrophages are essential for NO homeostasis. *Genes & development*, 24 (5): 491–501. doi:10.1101/GAD.1881410.

Talla, U., Bozonet, S.M., Parker, H.A., et al. (2019) Prolonged exposure to hypoxia induces an autophagy-like cell survival program in human neutrophils. *Journal of Leukocyte Biology*, 106 (6): 1367–1379. doi:10.1002/JLB.4A0319-079RR.

Tan, S.Y.S. and Krasnow, M.A. (2016) Developmental origin of lung macrophage diversity. *Development (Cambridge)*, 143 (8): 1318–1327. doi:10.1242/DEV.129122/-/DC1.

Tan, Z., Xue, H., Sun, Y., et al. (2021) The Role of Tumor Inflammatory Microenvironment in Lung Cancer. *Frontiers in Pharmacology*, 12. doi:10.3389/FPHAR.2021.688625.

Tandel, S., Brazil, D., Schroeder, G., et al. (2022) S74 The effect of hypoxia on MMP-1 production in M. avium lung disease. *Thorax*, 77 (Suppl 1): A46–A47. doi:10.1136/THORAX-2022-BTSABSTRACTS.80.

Tanguy, J., Goirand, F., Bouchard, A., et al. (2021) [18F]FMISO PET/CT imaging of hypoxia as a non-invasive biomarker of disease progression and therapy efficacy in a preclinical model of pulmonary fibrosis: comparison with the [18F]FDG PET/CT approach. *European journal of nuclear medicine and molecular imaging*, 48 (10): 3058–3074. doi:10.1007/S00259-021-05209-2.

Tannenbaum, J. and Bennett, B.T. (2015) Russell and Burch's 3Rs Then and Now: The Need for Clarity in Definition and Purpose. *Journal of the American Association for Laboratory Animal Science : JAALAS*, 54 (2): 120. Available at: /pmc/articles/PMC4382615/ (Accessed: 30 December 2022).

Tashiro, J., Rubio, G.A., Limper, A.H., et al. (2017) Exploring Animal Models That Resemble Idiopathic Pulmonary Fibrosis. *Frontiers in Medicine*, 4 (JUL): 1. doi:10.3389/FMED.2017.00118.

Tatler, A.L., Barnes, J., Habgood, A., et al. (2016) Caffeine inhibits TGFβ activation in epithelial cells, interrupts fibroblast responses to TGFβ, and reduces established fibrosis in ex vivo precision-cut lung slices. *Thorax*, 71 (6): 565–567. doi:10.1136/THORAXJNL-2015-208215.

Tazzyman, S., Murdoch, C., Yeomans, J., et al. (2014) Macrophage-mediated response to hypoxia in disease. *Hypoxia*, 2: 185. doi:10.2147/HP.S49717.

Thienpont, B., Steinbacher, J., Zhao, H., et al. (2016) Tumour hypoxia causes DNA hypermethylation by reducing TET activity. *Nature 2016 537:7618*, 537 (7618): 63–68. doi:10.1038/nature19081.

Thimmulappa, R.K., Chattopadhyay, I. and Rajasekaran, S. (2019) Oxidative stress mechanisms in the pathogenesis of environmental lung diseases. *Oxidative Stress in Lung Diseases*, 2: 103–137. doi:10.1007/978-981-32-9366-3_5/FIGURES/2.

Tigges, J., Eggerbauer, F., Worek, F., et al. (2021) Optimization of long-term cold storage of rat precision-cut lung slices with a tissue preservation solution. *American Journal of Physiology - Lung Cellular and Molecular Physiology*, 321 (6): L1023–L1035. doi:10.1152/AJPLUNG.00076.2021/ASSET/IMAGES/LARGE/AJPLUNG.00076.2021_F008.JPEG.

Tobin, R.W., Pope, C.E., Pellegrini, C.A., et al. (2012) Increased Prevalence of Gastroesophageal Reflux in Patients with Idiopathic Pulmonary Fibrosis. *https://doi.org/10.1164/ajrccm.158.6.9804105*, 158 (6): 1804–1808. doi:10.1164/AJRCCM.158.6.9804105.

Tohyama, Y. and Yamamura, H. (2006) Complement-mediated phagocytosis - the role of Syk. *IUBMB Life*, 58 (5–6): 304–308. doi:10.1080/15216540600746377.

Tolosano, E., Fagoonee, S., Morello, N., et al. (2010) Heme scavenging and the other facets of hemopexin. *Antioxidants & redox signaling*, 12 (2): 305–320. doi:10.1089/ARS.2009.2787.

Torres-Soria, A.K., Romero, Y., Balderas-Martínez, Y.I., et al. (2022) Functional Repercussions of Hypoxia-Inducible Factor-2α in Idiopathic Pulmonary Fibrosis. *Cells 2022, Vol. 11, Page 2938*, 11 (19): 2938. doi:10.3390/CELLS11192938.

Travaglini, K.J., Nabhan, A.N., Penland, L., et al. (2020) A molecular cell atlas of the human lung from single-cell RNA sequencing. *Nature 2020 587:7835*, 587 (7835): 619–625. doi:10.1038/s41586-020-2922-4.

Travis, W.D., Costabel, U., Hansell, D.M., et al. (2013) An Official American Thoracic Society/European Respiratory Society Statement: Update of the International Multidisciplinary Classification of the Idiopathic Interstitial Pneumonias. *American Journal of Respiratory and Critical Care Medicine*, 188 (6): 733. doi:10.1164/RCCM.201308-1483ST.

Travis, W.D., King, T.E., Bateman, E.D., et al. (2012) American Thoracic Society/European Respiratory Society International Multidisciplinary Consensus Classification of the Idiopathic Interstitial Pneumonias. *https://doi.org/10.1164/ajrccm.165.2.ats01*, 165 (2): 277–304. doi:10.1164/AJRCCM.165.2.ATS01.

Tsitoura, E., Trachalaki, A., Vasarmidi, E., et al. (2021) Collagen 1a1 Expression by Airway Macrophages Increases In Fibrotic ILDs and Is Associated With FVC Decline and Increased Mortality. *Frontiers in Immunology*, 12: 1. doi:10.3389/FIMMU.2021.645548/FULL.

Tsitoura, E., Vasarmidi, E., Bibaki, E., et al. (2019) Accumulation of damaged mitochondria in alveolar macrophages with reduced OXPHOS related gene expression in IPF. *Respiratory Research*, 20 (1): 1–16. doi:10.1186/S12931-019-1196-6/FIGURES/7.

Tuder, R.M., Lara, A.R. and Thannickal, V.J. (2012) Lactate, a Novel Trigger of Transforming Growth Factor-β Activation in Idiopathic Pulmonary Fibrosis. *https://doi.org/10.1164/rccm.201208-1491ED*, 186 (8): 701–703. doi:10.1164/RCCM.201208-1491ED.

Uchida, T., Rossignol, F., Matthay, M.A., et al. (2004) Prolonged hypoxia differentially regulates hypoxia-inducible factor (HIF)-1alpha and HIF-2alpha expression in lung epithelial cells: implication of natural antisense HIF-1alpha. *The Journal of biological chemistry*, 279 (15): 14871–14878. doi:10.1074/JBC.M400461200.

Ural, B.B., Yeung, S.T., Damani-Yokota, P., et al. (2020) Identification of a nerve-associated, lung-resident interstitial macrophage subset with distinct localization and immunoregulatory properties. *Science Immunology*, 5 (45): 8756. doi:10.1126/SCIIMMUNOL.AAX8756/SUPPL_FILE/AAX8756_TABLE_S6.XLSX.

Uribe-Querol, E. and Rosales, C. (2020) Phagocytosis: Our Current Understanding of a Universal Biological Process. *Frontiers in Immunology*, 11: 1066. doi:10.3389/FIMMU.2020.01066/BIBTEX.

Vancheri, C. (2013) Common pathways in idiopathic pulmonary fibrosis and cancer. *European Respiratory Review*, 22 (129): 265–272. doi:10.1183/09059180.00003613.

Vasarmidi, E., Bibaki, E., Koutoulaki, C., et al. (2019) Evaluation of CD163 expression on alveolar macrophages from BAL of patients with Fibrotic Lung Diseases. *European Respiratory Journal*, 54 (suppl 63): PA4694. doi:10.1183/13993003.CONGRESS-2019.PA4694.

Veit, T., Barnikel, M., Crispin, A., et al. (2020) Variability of forced vital capacity in progressive interstitial lung disease: a prospective observational study. *Respiratory Research*, 21 (1). doi:10.1186/S12931-020-01524-8.

Vieira, O. v., Bucci, C., Harrison, R.E., et al. (2003) Modulation of Rab5 and Rab7 Recruitment to Phagosomes by Phosphatidylinositol 3-Kinase. *Molecular and Cellular Biology*, 23 (7): 2501–2514. doi:10.1128/MCB.23.7.2501-2514.2003/ASSET/7AD6E26F-3287-4271-B006-47229BCE9288/ASSETS/GRAPHIC/MB0731306010.JPEG.

di Vincenzo, S., Ninaber, D.K., Cipollina, C., et al. (2022) Cigarette Smoke Impairs Airway Epithelial Wound Repair: Role of Modulation of Epithelial-Mesenchymal Transition Processes and Notch-1 Signaling. *Antioxidants 2022, Vol. 11, Page 2018*, 11 (10): 2018. doi:10.3390/ANTIOX11102018.

Visca, D., Mori, L., Tsipouri, V., et al. (2018) Effect of ambulatory oxygen on quality of life for patients with fibrotic lung disease (AmbOx): a prospective, open-label, mixed-method, crossover randomised controlled trial. *The Lancet. Respiratory medicine*, 6 (10): 759–770. doi:10.1016/S2213-2600(18)30289-3.

Visscher, D.W. and Myers, J.L. (2006) Histologic spectrum of idiopathic interstitial pneumonias. *Proceedings of the American Thoracic Society*, 3 (4): 322–329. doi:10.1513/PATS.200602-019TK.

Vitale, I., Manic, G., Coussens, L.M., et al. (2019) Macrophages and Metabolism in the Tumor Microenvironment. *Cell metabolism*, 30 (1): 36–50. doi:10.1016/J.CMET.2019.06.001.

Vohwinkel, C.U., Hoegl, S. and Eltzschig, H.K. (2015) Hypoxia signaling during acute lung injury. *Journal of Applied Physiology*, 119 (10): 1157–1163. doi:10.1152/JAPPLPHYSIOL.00226.2015/ASSET/IMAGES/LARGE/ZDG9991514800004.JPEG.

Walmsley, S.R., Print, C., Farahi, N., et al. (2005) Hypoxia-induced neutrophil survival is mediated by HIF-1α–dependent NF-κB activity. *The Journal of Experimental Medicine*, 201 (1): 105. doi:10.1084/JEM.20040624.

Wang, X.T., Cheng, K. and Zhu, L. (2021) Hypoxia Accelerate β-actin Expression through Transcriptional Activation of ACTB by Nuclear Respiratory Factor-1. *Molecular Biology*, 55 (3): 398–404. doi:10.1134/S0026893321020011/FIGURES/3.

Wang, Y.-T., Trzeciak, A.J., Rojas, W.S., et al. (2022) Metabolic adaptation supports enhanced macrophage efferocytosis in limited-oxygen environments. *Cell metabolism*. doi:10.1016/J.CMET.2022.12.005.

Warheit-Niemi, H.I., Edwards, S.J., SenGupta, S., et al. (2022) Fibrotic lung disease inhibits immune responses to staphylococcal pneumonia via impaired neutrophil and macrophage function. *JCI Insight*, 7 (4). doi:10.1172/JCI.INSIGHT.152690.

Watson, A., Madsen, J. and Clark, H.W. (2021) SP-A and SP-D: Dual Functioning Immune Molecules With Antiviral and Immunomodulatory Properties. *Frontiers in Immunology*, 11: 3692. doi:10.3389/FIMMU.2020.622598/BIBTEX.

Watson, A., Phipps, M.J.S., Clark, H.W., et al. (2019) Surfactant Proteins A and D: Trimerized Innate Immunity Proteins with an Affinity for Viral Fusion Proteins. *Journal of innate immunity*, 11 (1): 13–28. doi:10.1159/000492974.

Webb, J.D., Coleman, M.L. and Pugh, C.W. (2009) Hypoxia, hypoxia-inducible factors (HIF), HIF hydroxylases and oxygen sensing. *Cellular and Molecular Life Sciences*, 66 (22): 3539–3554. doi:10.1007/S00018-009-0147-7/FIGURES/3.

Wei, Y., Dong, W., Jackson, J., et al. (2021) Blocking LOXL2 and TGFβ1 signaling induces collagen I turnover in precision-cut lung slices derived from Idiopathic Pulmonary Fibrosis patients. *Thorax*, 76 (7): 729. doi:10.1136/THORAXJNL-2020-215745.

White, C., Yuan, X., Schmidt, P.J., et al. (2013) HRG1 is essential for heme transport from the phagolysosome of macrophages during erythrophagocytosis. *Cell metabolism*, 17 (2): 261. doi:10.1016/J.CMET.2013.01.005.

Wild, J.M., Fichele, S., Woodhouse, N., et al. (2005) 3D volume-localized pO2 measurement in the human lung with 3He MRI. *Magnetic Resonance in Medicine*, 53 (5): 1055–1064. doi:10.1002/MRM.20423.

Williams, K.J., Robinson, N.E., Lim, A., et al. (2013) Experimental induction of pulmonary fibrosis in horses with the gammaherpesvirus equine herpesvirus 5. *PloS one*, 8 (10). doi:10.1371/JOURNAL.PONE.0077754.

Wilson, M.S., Madala, S.K., Ramalingam, T.R., et al. (2010) Bleomycin and IL-1β–mediated pulmonary fibrosis is IL-17A dependent. *Journal of Experimental Medicine*, 207 (3): 535–552. doi:10.1084/JEM.20092121.

Woo, Y.D., Jeong, D. and Chung, D.H. (2021) Development and Functions of Alveolar Macrophages. *Molecules and Cells*, 44 (5): 292. doi:10.14348/MOLCELLS.2021.0058.

Woods, P.S., Kimmig, L.M., Meliton, A.Y., et al. (2020) Tissue-Resident Alveolar Macrophages Do Not Rely on Glycolysis for LPS-induced Inflammation. *American journal of respiratory cell and molecular biology*, 62 (2): 243–255. doi:10.1165/RCMB.2019-0244OC.

Woods, P.S., Kimmig, L.M., Sun, K.A., et al. (2022) HIF-1α induces glycolytic reprograming in tissue-resident alveolar macrophages to promote cell survival during acute lung injury. *eLife*, 11. doi:10.7554/ELIFE.77457.

Wu, G., Lee, Y.Y., Gulla, E.M., et al. (2021) Short-term exposure to intermittent hypoxia leads to changes in gene expression seen in chronic pulmonary disease. *eLife*, 10: 1–27. doi:10.7554/ELIFE.63003.

Wu, G., Xu, G., Chen, D.W., et al. (2018) Hypoxia exacerbates inflammatory acute lung injury via the toll-like receptor 4 signaling pathway. *Frontiers in Immunology*, 9 (JUL): 1667. doi:10.3389/FIMMU.2018.01667/BIBTEX.

Wu, T.T., Chen, T.L. and Chen, R.M. (2009) Lipopolysaccharide triggers macrophage activation of inflammatory cytokine expression, chemotaxis, phagocytosis, and oxidative ability via a toll-like receptor 4-dependent pathway: Validated by RNA interference. *Toxicology Letters*, 191 (2–3): 195–202. doi:10.1016/J.TOXLET.2009.08.025.

Xie, N., Cui, H., Ge, J., et al. (2017) Metabolic characterization and RNA profiling reveal glycolytic dependence of profibrotic phenotype of alveolar macrophages in lung fibrosis. *American journal of physiology. Lung cellular and molecular physiology*, 313 (5): L834–L844. doi:10.1152/AJPLUNG.00235.2017.

Xie, N., Tan, Z., Banerjee, S., et al. (2015) Glycolytic reprogramming in myofibroblast differentiation and lung fibrosis. *American Journal of Respiratory and Critical Care Medicine*, 192 (12): 1462–1474. doi:10.1164/RCCM.201504-0780OC/SUPPL_FILE/DISCLOSURES.PDF.

Xiong, M., Zhao, Y., Mo, H., et al. (2021) Intermittent hypoxia increases ROS/HIF-1α 'related oxidative stress and inflammation and worsens bleomycin-induced pulmonary fibrosis in adult male C57BL/6J mice. *International Immunopharmacology*, 100: 108165. doi:10.1016/J.INTIMP.2021.108165.

Xue, J., Schmidt, S. v., Sander, J., et al. (2014) Transcriptome-based network analysis reveals a spectrum model of human macrophage activation. *Immunity*, 40 (2): 274–288. doi:10.1016/J.IMMUNI.2014.01.006.

Yamashita, C.M., Dolgonos, L., Zemans, R.L., et al. (2011) Matrix Metalloproteinase 3 Is a Mediator of Pulmonary Fibrosis. *The American Journal of Pathology*, 179 (4): 1733. doi:10.1016/J.AJPATH.2011.06.041.

Yan, M., Collins, R.F., Grinstein, S., et al. (2005) Coronin-1 function is required for phagosome formation. *Molecular Biology of the Cell*, 16 (7): 3077–3087. doi:10.1091/MBC.E04-11-0989/ASSET/IMAGES/LARGE/ZMK0070571940008.JPEG.

Yanagihara, T., Chong, S.G., Vierhout, M., et al. (2020) Current models of pulmonary fibrosis for future drug discovery efforts. *Expert opinion on drug discovery*, 15 (8): 931–941. doi:10.1080/17460441.2020.1755252.

Yang, I. v., Fingerlin, T.E., Evans, C.M., et al. (2015) MUC5B and idiopathic pulmonary fibrosis. *Annals of the American Thoracic Society*, 12 (Suppl 2): S193–S199. doi:10.1513/ANNALSATS.201503-110AW/SUPPL_FILE/DISCLOSURES.PDF.

Yao, Y., Liu, Q., Adrianto, I., et al. (2020) Histone deacetylase 3 controls lung alveolar macrophage development and homeostasis. *Nature Communications 2020 11:1*, 11 (1): 1–15. doi:10.1038/s41467-020-17630-6.

Yasuda, K., Sato, A., Nishimura, K., et al. (1994) Phospholipid analysis of alveolar macrophages and bronchoalveolar lavage fluid following bleomycin administration to rabbits. *Lung*, 172 (2): 91–102. doi:10.1007/BF00185080.

Yin, C. and Heit, B. (2021) Cellular Responses to the Efferocytosis of Apoptotic Cells. *Frontiers in Immunology*, 12. doi:10.3389/FIMMU.2021.631714.

Yin, C., Kim, Y., Argintaru, D., et al. (2016) Rab17 mediates differential antigen sorting following efferocytosis and phagocytosis. *Cell Death & Disease 2016 7:12*, 7 (12): e2529–e2529. doi:10.1038/cddis.2016.431.

Yoshida, M., Ikegami, M., Reed, J.A., et al. (2001) Gm-csf regulates protein and lipid catabolism by alveolar macrophages. *American Journal of Physiology - Lung Cellular and Molecular Physiology*, 280 (3 24-3). doi:10.1152/AJPLUNG.2001.280.3.L379/ASSET/IMAGES/LARGE/H50310273009.JPEG.

Yoshida, M., Korfhagen, T.R. and Whitsett, J.A. (2001) Surfactant Protein D Regulates NF-κB and Matrix Metalloproteinase Production in Alveolar Macrophages via Oxidant-Sensitive Pathways. *The Journal of Immunology*, 166 (12): 7514–7519. doi:10.4049/JIMMUNOL.166.12.7514.

Yu, X., Buttgereit, A., Lelios, I., et al. (2017) The Cytokine TGF-β Promotes the Development and Homeostasis of Alveolar Macrophages. *Immunity*, 47 (5): 903-912.e4. doi:10.1016/J.IMMUNI.2017.10.007.

Yuan, G., Nanduri, J., Khan, S., et al. (2008) Induction of HIF-1α expression by intermittent hypoxia: Involvement of NADPH oxidase, Ca2+ signaling, prolyl hydroxylases, and mTOR. *Journal of Cellular Physiology*, 217 (3): 674–685. doi:10.1002/jcp.21537.

Yuan, Y., Li, Y., Qiao, G., et al. (2021) Hyperbaric Oxygen Ameliorates Bleomycin-Induced Pulmonary Fibrosis in Mice. *Frontiers in Molecular Biosciences*, 8: 425. doi:10.3389/FMOLB.2021.675437/XML/NLM.

Yurdagul, A., Subramanian, M., Wang, X., et al. (2020) Macrophage Metabolism of Apoptotic Cell-Derived Arginine Promotes Continual Efferocytosis and Resolution of Injury. *Cell metabolism*, 31 (3): 518-533.e10. doi:10.1016/J.CMET.2020.01.001.

Zhang, F., Wang, H., Wang, X., et al. (2016) TGF-β induces M2-like macrophage polarization via SNAIL-mediated suppression of a pro-inflammatory phenotype. *Oncotarget*, 7 (32): 52294. doi:10.18632/ONCOTARGET.10561.

Zhang, K., Xu, L. and Cong, Y.S. (2021) Telomere Dysfunction in Idiopathic Pulmonary Fibrosis. *Frontiers in Medicine*, 8: 739810. doi:10.3389/FMED.2021.739810.

Zhang, S., Weinberg, S., DeBerge, M., et al. (2019) Efferocytosis Fuels Requirements of Fatty Acid Oxidation and the Electron Transport Chain to Polarize Macrophages for Tissue Repair. *Cell Metabolism*, 29 (2): 443-456.e5. doi:10.1016/J.CMET.2018.12.004.

Zhang, Y.E. (2008) Non-Smad pathways in TGF-β signaling. *Cell Research 2009 19:1*, 19 (1): 128–139. doi:10.1038/cr.2008.328.

Zhang, Z., Garron, T.M., Li, X.J., et al. (2009) Recombinant human decorin inhibits TGF-beta1-induced contraction of collagen lattice by hypertrophic scar fibroblasts. *Burns : journal of the International Society for Burn Injuries*, 35 (4): 527–537. doi:10.1016/J.BURNS.2008.08.021.

Zhang, Z., Yao, L., Yang, J., et al. (2018) PI3K/Akt and HIF-1 signaling pathway in hypoxia-ischemia. *Molecular Medicine Reports*, 18 (4): 3547. doi:10.3892/MMR.2018.9375.

Zhou, W., Wang, C., Liu, Z., et al. (2022) Hypoxia-Activated Prodrugs with Dual COX-2/CA Inhibitory Effects on Attenuating Cardiac Inflammation under Hypoxia. *Journal of Medicinal Chemistry*, 65 (19): 13436–13451. doi:10.1021/ACS.JMEDCHEM.2C01355/SUPPL_FILE/JM2C01355_SI_001.CSV.

Zhou, Y., Peng, H., Sun, H., et al. (2014) Chitinase 3–like 1 Suppresses Injury and Promotes Fibroproliferative Responses in Mammalian Lung Fibrosis. *Science translational medicine*, 6 (240): 240ra76. doi:10.1126/SCITRANSLMED.3007096.

Ziehr, D.R., Leahy, K.J., Varon, J., et al. (2022) Lactate Transport Inhibition Therapeutically Reprograms Fibroblast Metabolism in Experimental Pulmonary Fibrosis. *American Thoracic Society International Conference Meetings Abstracts American Thoracic Society International Conference Meetings Abstracts*, (2): A5062–A5062. doi:10.1164/AJRCCM-CONFERENCE.2022.205.1_MEETINGABSTRACTS.A5062.

Zieseniss, A. (2014) Hypoxia and the modulation of the actin cytoskeleton – emerging interrelations. *Hypoxia*, 2: 11. doi:10.2147/HP.S53575.

Zizzo, G., Hilliard, B.A., Monestier, M., et al. (2012) Efficient clearance of early apoptotic cells by human macrophages requires M2c polarization and MerTK induction. *Journal of immunology (Baltimore, Md. : 1950)*, 189 (7): 3508–3520. doi:10.4049/JIMMUNOL.1200662.

Zuo, F., Kaminski, N., Eugui, E., et al. (2002) Gene expression analysis reveals matrilysin as a key regulator of pulmonary fibrosis in mice and humans. *Proceedings of the National Academy of Sciences of the United States of America*, 99 (9): 6292–6297. doi:10.1073/PNAS.092134099/SUPPL_FILE/1340FIG6LEGEND.HTML.